Dissertation zur Erlangung des Doktorgrades

der Fakultät für Chemie und Pharmazie

der Ludwig-Maximilians-Universität München

- NANOPARTICLES FOR RNA INTERFERENCE -
NOVEL PRECLINICAL FORMULATIONS FOR SIRNA MEDIATED GENE THERAPY

vorgelegt von

Stephan Johannes Baptist Schultes

aus Dachau (Altomünster)

2009

Erklärung

Diese Dissertation wurde im Sinne von § 13 Abs. 3 der Promotionsordnung vom 29. Januar 1998 von Herrn Prof. Dr. Gerhard Winter und Herrn Dr. Conrad Coester als Tutor betreut. Mit Erteilung der Lehrbefugnis wurde die Betreuung ab Februar 2009 von Herrn PD Dr. Conrad Coester übernommen.

Ehrenwörtliche Versicherung

Diese Dissertation wurde selbständig, ohne unerlaubte Hilfe erarbeitet.

München, am 20.10.2009

………………………………
(Stephan Schultes)

Dissertation eingereicht am: 20.10.2009

1. Gutachter: PD Dr. Conrad Coester

2. Gutachter: Prof. Dr. Gerhard Winter

Mündliche Prüfung am: 10.11.2009

IV

Für Juliane

Acknowledgements

Table of Contents

X

List of Abbreviations

AF4	Asymmetric flow field-flow fractionation
aGNP	Acetylated gelatin nanoparticles
AIA	Antigen induced arthritis
AMD	Age related macular degeneration
AMVn	Automated microviscosimetry
bFGF	Basic fibroblast growth factor
BSA	Bovine serum albumin
CDD-GNP	Cholamine-DEAE-dextran gelatin nanoparticles
C-GNP	Cholamine gelatin nanoparticles
CLSM	Confocal laser scanning microscopy
CMRA	Cell Tracker Orange
DD-GNP	DEAE-dextran gelatin nanoparticles
DEAE	Di-ethyl-amino-ethanol
DLS	Dynamic light scattering
DMEM	Dulbecco's modified eagle medium
DMF	Dimethylformamide
DMMAn	Dimethylmaleic anhydride
DMSO	Dimethylsulfoxide
DNA	Desoxyribonucleic acid
DOPC	1,2-dioleoyl-sn-glycero-3-phosphocholine
DOTAP	1,2-dioleoyl-3-trimethylammonium-propane
ds	Double-stranded
EDC	1-ethyl-3-(3-dimethyl-aminopropyl) carbodiimide hydrochloride
EDTA	Ethylene-diamino-tetraacetic acid

EIAV	Equine infectious anaemia virus
eNOS	Endothelial nitric oxide synthase
EPR	Enhanced permeability and retention (effect)
FACS	Fluorescence-activated cell sorting
FCS	Fetal calf serum
FDA	U.S. Food and Drug Administration
FFF	Field-flow fractionation
FGF	Fibroblast growth factor
FIV	Feline immunodeficiency virus
FITC	Fluoresceine-isothiocyanate
FT-IR	Fourier-transformation infrared spectroscopy
GNP	Gelatin nanoparticles
HMW	High molecular weight
HBG	HEPES buffered glucose
HEPES	2-(4-(2-Hydroxyethyl)-1-piperazinyl)-ethansulfonic-acid
HPLC	High performance liquid chromatography
HSA	Human serum albumin
ICAMm	Inter-cellular adhesion molecule
IEP	Isoelectric point
Ig	Immunoglobulin
IVIVC	*In-vitro in-vivo* correlation
LMW	Low molecular weight
LPS	Lipopolysaccharide
MA Gelatin	Dodecenylsuccinylated gelatin prototype
MALS	Multi angle light scattering
MCP-1	Monocyte chemotactic protein
mGNP	Methylated gelatin nanoparticles

MMP	Matrix metalloproteinase
MPS	Mononuclear phagocytosis system
mRNA	Messenger RNA
MS Gelatin	Succinylated gelatin prototype
MTT	3-(4,5-Dimethylthiazol-2-yl)-2,5-diphenyltetrazolium bromide
N-GNP	Neutral (unmodified) gelatin nanoparticles
NRP-1	Neuropilin-1
PBCA	Polybutylcyanoacrylate
PBS	Phosphate-buffered saline
PCS	Photon correlation spectroscopy
PDGF	Platelet derived growth factor
pDNA	Plasmid DNA
PDI	Polydispersity index
PEG	Polyethylenglycol
PEI	Polyethylene imine
PET	Positron emission tomography
PLGA	Poly (lactic-co-glycolic acid)
PLL	Poly-L-lysine
RI	Refractive index
RISC	RNA induced silencing complex
RNA	Ribonucleic acid
RNAi	RNA interference
RSV	Respiratory syncytial virus
SARS	Severe acute respiratory syndrome
SE-HPLC	Size exclusion high performance liquid chromatography
SEM	Scanning electron microscopy
SICON	siRNA containing gelatin nanoparticles

siRNA	Small interfering ribonucleic acid
SLN	Solid lipid nanoparticles
SLS	Static light scattering
SPA-mPEG	Succinimidyl propionate monomethoxy polyethylene glycol
SPECT	Single photon emission computed tomography
SPDP	Succinimidyl 3-(2-pyridyldithio) propionate
ss	Single-stranded
TBE	Tris / borate / EDTA buffer
TGF	Transforming growth factor
TMS	Tetramethylsilane
TPP	Tripolyphosphate
TRIS	Tris (hydroxymethyl) aminomethane
UV	Ultraviolet
VCAM	Vascular cell adhesion molecule
VEGF	Vascular endothelial growth factor

Abstract

Efficient and safe protein nanoparticles for the targeted delivery of small molecule, protein and oligonucleotide based drugs will play a key role in the field of science in the upcoming years. Whereas viral and liposomal formulations have been extensively tested throughout the last two decades, their inherent and in the case of viruses sometimes even fatal obstacles not seldom seem impossible to conquer. The time for the development of a new therapeutic option in form of an advanced drug delivery system within pharmaceutical technology, biopharmacy and clinical studies has come. In our eyes gelatin based nanoparticles with polysaccharide and peptide modifications are an optimum to fulfil this need and will therefore be the center of the research presented in this work.

Basically, nanoparticles with a size from 150 to 300 nm were prepared by desolvating a clear solution of gelatin through dropwise addition of an organic anti-solvent under heavy stirring. A subsequent destabilization of the water soluble protein chains resulted in round particles with a homogenous size distribution and an even surface.

Initially, the polymers used for the formulation of the nanoparticles were characterized by such methods like asymmetric flow field-flow fractionation and nuclear magnetic resonance spectroscopy. Furthermore, established measurement and calculation algorithms were revised into state-of-the-art technology and applied as so called automatic microviscosimetry for in-depth protein analysis. The development of novel nanoparticle formulations based on these polymers was done in a second step using diethyl-amino-ethanol-dextran, polysorbate and polyethylene glycol, as well as methylation and acetylation chemistry. While the modified dextran mainly increased the zeta potential of the nanoparticles, the other modifications were intended to change the pharmacokinetic distribution patterns towards *e.g.* prolonged circulation times.

In novel nanoparticle cytology science the use of a flow chamber device for cell cultivation allowed us to study the interaction patterns of nanoparticles with adherent cells under near to physiological conditions simulating blood vessels, junctions and shear stress. This *in-vitro* model can be used for online preclinical and high-throughput screenings of new nanoparticle and protein formulations with cell monolayers. The hindrances in traditional static cell culture

models were shown to be overcome by comparing several nanoparticle formulations in a static and in a flow model.

Proper nanoparticle formulations were tested further in innovative preclinical *in-vivo* models like the hamster dorsal skin fold chamber and the mouse cremaster model to elucidate their body distribution and targeting properties with a focus on kinetics, blood cell interaction and novel fluorescence detection techniques. In addition, the potential of gelatin nanoparticles as therapeutic options in a model for antigen induced arthritis was demonstrated.

Finally, hybrid (sandwich) nanoparticles were formulated by combining gelatin nanoparticle preformulations with the endosomolytic peptide Melittin from bee venom and loading them with small interfering RNA molecules against $VEGFR_2$ and luciferase. The novel hybrid carriers were extensively tested in cell cultures towards their efficiency to induce a protein knock-down based on RNA interference. With these results the door for further, more profound *in-vivo* studies in the field of oncology might be opened.

Keywords: Gelatin nanoparticle, drug delivery, RNA interference, siRNA technology, proteomics, oncology therapy, preclinical kinetic modelling, multifunctional nanocarriers

1 General Introduction

1.1 Endothelial related diseases

What Robert Langer almost 20 years ago so anticipatorily called an explosion in research output has now become a downright supernova aimed at creating new drug delivery systems [Langer, R. 1990]. Especially in those many new therapeutic fields related to angiogenesis, including cancer, and vessel related diseases, new unthought-of options are being explored and more and more room is given to nanotechnology and its preclinical research. With a simulation and a better understanding of their kinetics, nanoparticles as drug carriers may revolutionize therapy. Excessive angiogenesis, which is understood as the formation of new blood vessels from pre-existing ones [Rubanyi, G. M. 2000; Wikipedia 2009], correlates with a multitude of poorly treatable diseases, of which many can be solely found in western industrial nations. Among these are for example rheumatoid arthritis, arteriosclerosis, multiple sclerosis and psoriasis [Folkman, J. et al. 1987; Harris, E. D. 1990; Folkman, J. 1995]. Also, age related macular degeneration, where a local expansion of blood vessels may interfere with the physiological conditions, belongs into this field of therapeutic needs. Even in cancer, angiogenesis is postulated to be part of a central process in supplying tumor cells with nutrients and oxygen, and to foster metastasis [Uyttendaele, H. et al. 1996; Risau, W. 1997; Wissmann, C. et al. 2006; Baluk, P. et al. 2008]. Where traditional medications are either not an option or fail to ameliorate a disease, gene silencing by a mechanism called RNA interference (RNAi) offers new opportunities as the treatment of lung diseases such as lung cancer, cystic fibrosis, respiratory syncytial virus (RSV) and severe acute respiratory syndrome (SARS) has already shown. Hence for fighting such diseases, characterized by either poor or abnormal vascularization, combining the target "angiogenesis" with the rather futuristic but real principle of RNA interference is the right way to go.

The modern clinical application of angiogenesis can be divided into pro-angiogenic therapy and anti-angiogenic therapy; reviewed in [Carmeliet, P. 2005; DeWitt, N. 2005; Ferrara, N. et al. 2005; Greenberg, D. A. et al. 2005]. While pro-angiogenic therapies are being investigated as options to treat cardiovascular diseases, anti-angiogenesis is the process where our approach based on RNAi plays the vital part. From a molecular point of view, the targets for

anti-angiogenic therapy are in many cases proteins, *e.g.* tubulin [Rothmeier, A. S. et al. 2009], including several growth factors of which an overview is shown in **Table 1.1**

Table 1.1

List of stimulators of angiogenesis as potential targets for anti-angiogenic therapy

Stimulator	Mechanism
FGF	Promotes proliferation & differentiation of endothelial cells, smooth muscle cells and fibroblasts
VEGF	Affects permeability
VEGFR and NRP-1	Integrates survival signals
Ang1 and Tie2	Stabilizes vessels
PDGF (BB-homodimer) and PDGFR	Recruits smooth muscle cells
TGF-β, Endoglin and TGF-β receptors	Increases the extracellular matrix production
MCP-1	Unknown
Integrins αVβ3, αVβ5 and α5β1	Binds matrix macromolecules and proteinases
VE-cadherin and CD31	Endothelial junctional molecules
Ephrin	Determines the formation of arteries or veins
Plasminogen activators	Remodels extracellular matrix, releases and activates growth factors
Plasminogen activator inhibitor-1	Stabilizes nearby vessels

Of these growth factors, VEGF and its receptor $VEGFR_2$ have been identified as major contributors to angiogenesis by increasing the number of capillaries in the vascular network [Goto, F. et al. 1993]. In the presence of VEGF endothelial cells will more likely proliferate and show signs of tube-like structures that resemble capillaries [Prior, B. M. et al. 2004]. Eventually binding of VEGF to $VEGFR_2$ draws a cascade of reactions after it, starting from tyrosine kinase activation to the production of eNOS, bfGF, ICAMMs, VCAMs and matrix metalloproteinases (MMPs) (**Figure 1.1**). As a consequence, this depicted complexity has to be taken into close consideration for any $VEGFR_2$ related targeting.
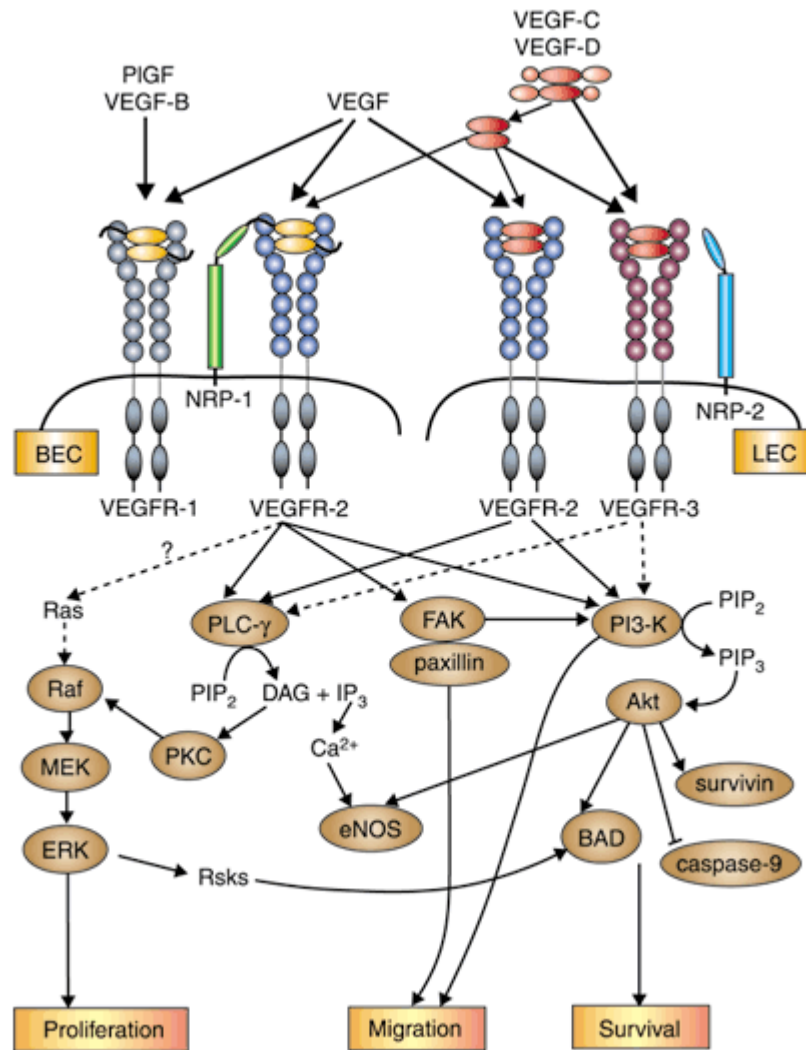
Figure 1.1

The VEGF family of ligands and their respective binding patterns to the VEGFRs are shown at the top. VEGFR-1 and neuropilin-1 (NRP-1) are mainly expressed in blood vascular endothelial cells (ECs), VEGFR-3 and NRP-2 in lymphatic ECs, and VEGFR-2 occurs in both cell lineages. VEGFR-2 is thought to be the main signal transducing receptor, as it activates several downstream signalling molecules (circles), and induces responses such as cell proliferation, migration and survival. VEGFR-1 signalling is not fully understood. The protein kinase C (PKC)-mediated MEK/ERK pathway mainly produces proliferation signals, in contrast to activation of the PI3-kinase/Akt pathway, which is important in regulating cell survival. Focal adhesion kinase (FAK) and PI3-kinase have also been implicated in cell migration by stimulating the reorganization of actin and recruitment of actin-anchoring proteins to the focal adhesions. VEGF-C and VEGF-D are ligands for VEGFR-3, and they can induce LEC survival, migration and growth via activation of the MEK/ERK and PI3-kinase/Akt pathways. Adopted from [Karkkainen, M. J. et al. 2002]

Endothelial cells form the inner monolayer of blood and lymphatic vessels throughout the entire circulatory system. Besides their above described function in angiogenesis, endothelial

cells play a role in inflammation, arteriosclerosis, blood clotting and vasoconstriction. At present, the most advanced targets of anti-angiogenic molecules are those growth factors and their receptors that drive vessel development. However, these factors also play crucial physiological roles and their inhibition can lead to heavy side effects, raising the need for more specific targets [Di Paolo, D. et al. 2008]. Either way, the expenditures for endothelial or angiogenic related diseases if not treated appropriately with new biopharmaceutics will have a strong macroeconomic impact as shown in a study from the Milken Institute (Santa Monica, USA) and raise the demand of society for cost-effective, efficient products with a short time to market (**Figure 1.2**).
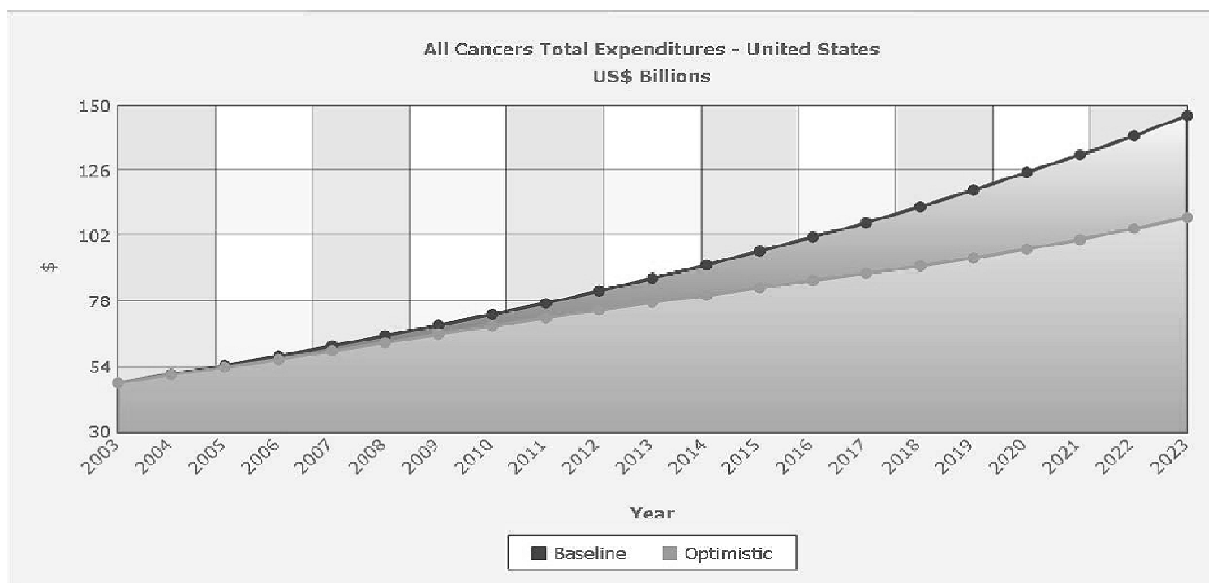
Figure 1.2

Treatment expenditures (direct costs) in cancer for both the baseline and optimistic scenarios through 2023 in the United States. The baseline course is the path we are currently on and the optimistic course is possible if moderate changes toward prevention and screening are made. Adopted from *http://www.chronicdiseaseimpact.com/ebcd.taf?cat=disease*

Fortunate enough, over 100 years ago early pioneers of endothelial related research observed that the growth of tumors is often related to an increased vascularity. In this context the vasculature in the whole cancer area is part of the central disease principle (reviewed in [Ferrara, N. 2002]). In 1971, scientists hypothesized that the idea of antiangiogenesis would be effective to treat cancer and an active search for angiogenesis inhibitors began [Folkman, J. 1971]. In 2004, the US Food and Drug Administration (FDA) approved Bevacizumab, a

humanized anti-VEGF-A monoclonal antibody, for the treatment of metastatic colorectal cancer in combination with 5-fluorouracil-based chemotherapy regimens [Hurwitz, H. et al. 2004]. This followed from a phase III study showing a significant survival benefit. Also in 2004, the FDA approved Pegaptinib, an aptamer that blocks the 165 amino-acid isoform of VEGF-A, for the treatment of the wet (neovascular) form of age-related macular degeneration (AMD) [Gragoudas, E. S. et al. 2004].

Delian and Eichhorn then summarized, that an anti-vascular treatment regimen for clinical use, including both anti-angiogenesis and vascular targeting, has the following theoretical advantages compared to conventional cytotoxic chemotherapy directed against malignant tumor cells [Eichhorn, M. E. et al. 2004]:

(a) It is not restricted to a certain histologic tumor entity as all solid tumors depend on angiogenesis.

(b) The tumor microvasculature is well accessible to systemic treatment. In contrast to chemotherapy no endothelial barrier has to be crossed by the therapeutic substances.

(c) In contrast to the blood supply in organs every single tumor microvessel has to supply up to hundreds of critically dependent tumor cell layers. For that reason, anti-vascular therapy is potentially very effective.

(d) Angiogenesis in adult organisms is only induced under certain physiologic conditions, *e.g.* during the reproductive ovarian cycle or wound healing. An antagonism of angiogenesis is therefore a highly selective therapy promising less serious side effects.

(e) The endothelial cell as a target is genetically stable and therefore suggested to be less prone to the development of drug resistance.

While antiangiogenic therapies have been evaluated in the clinic for over 8 years and the first clinical phase III studies have already been completed in the year 2003, there is in comparison to cytotoxic drugs very little clinical experience with combinations of vascular targeting agents like nanoparticles and the novel therapeutic mechanism of RNAi.

1.2 siRNA and the principle of RNA interference

RNA interference as a novel mechanism in biomolecular science

RNA interference is the process whereby doublestranded RNA (dsRNA) induces the sequence-specific targeting and degradation of homologous messenger RNA. The decisive factor in this case is the interaction with a protein termed the RNA-induced silencing complex (RISC) [Chiu, Y.-L. et al. 2004]. The dsRNA applied for RNAi is called siRNA and is composed of 21-23 nucleotides (nt) [Hammond, S. M. et al. 2001; McManus, M. T. et al. 2002].

When exposed to foreign genetic material (*e.g.* RNA or DNA), many organisms mount highly specific counter attacks to silence the invading nucleic-acid sequences before these can integrate into the host genome or subvert cellular processes. At the heart of these immunity mechanisms is the double-stranded RNA. Interestingly, dsRNA does more than helping to defend cells against foreign nucleic acids – it also guides endogenous developmental gene regulation, and can even control the modification of cellular DNA and associated chromatin. In some organisms, RNA interference (RNAi) signals are transmitted horizontally between cells and, in certain cases, vertically through the germ line from one generation to the next [Mello, C. C. et al. 2004]. The breakthrough observation by [Fire, A. et al. 1998] that dsRNA is a potent trigger for RNAi in the nematode Caenorhabditis elegans was important because it immediately suggested a simple approach for efficient induction of gene silencing, and accelerated the discovery of a unifying mechanism that underlies a host of cellular and developmental pathways.

In the above mentioned studies and many more that followed, dsRNA proved to be an extremely potent activator of RNAi – at least 10-fold and perhaps 100-fold more effective than purified preparations of singlestranded RNA. Those mentioned effects of siRNA are transmitted through a genetically conserved pathway [Denli, A. M. et al. 2003].

Figure 1.3

The 2006 Nobel Prize winners Craig Mello (left) and Andrew Fire (right) *"for their discovery of RNA interference - gene silencing by double-stranded RNA"*

In a short period of time and augmented by the Nobel Prize in 2006 (**Figure 1.3**), RNAi has become a popular tool to knock out specific genes in many species and even in mammalian cells [Novina, C. D. et al. 2004]. The discovery that synthetic double-stranded RNA sequences (siRNA) of 21-23 nucleotides can surrogate in this process and have the potential to specifically downregulate gene function in cultured mammalian cells has now opened the gateway to applications of the RNAi concept in functional genomics programs and in many therapeutic applications [Elbashir, S. M. et al. 2001].

To invoke RNAi-mediated gene silencing in human cells, duplex siRNA first needs to be transfected into cells. Once inside the cell, siRNA duplexes undergo 5' phosphorylation, are unwound, and associate with the RNA-induced silencing complex (RISC) [Nykänen, A. et al. 2001; Chiu, Y.-L. et al. 2002]. Activated RISC (RISC*) and the unwound antisense strand which is complementary to the target mRNA, then interact with the target mRNA (**Figure 1.4**). Single site-specific cleavage of the target mRNA then occurs, with the cut position defined with reference to the 5' end of the siRNA antisense strand [Hammond, S. M. et al. 2000]. Once cleavage has occurred, target mRNA is degraded and RISC is recycled for another cleavage reaction [Hutvagner, G. et al. 2002]. Therefore a particularly fascinating aspect of RNAi is its extraordinary efficiency [Kennerdell, J. R. et al. 1998]. Conversion of the long trigger dsRNA into many 21 to 23 nt siRNA fragments would itself provide a high degree of amplification. Another plausible explanation for the potency of interference is that the RISC* is a multiple-turnover enzyme, which can catalytically perform the targeting and cleavage activity [Chiu, Y.-L. et al. 2002].

siRNA Synthesis	RNA Interference

DNA

siRNA designed to be specific for gene target

Gene target

siRNA

RISC

mRNA

RISC

Target mRNA

Single strand of siRNA

mRNA degradation

siRNA is targeted to a specific gene. This can occur through a natural process or be designed through chemical synthesis.

Within cells, siRNA unwinds and is incorporated into RISC, a stable protein-RNA complex.

siRNA is directed to a targeted mRNA that is known to be involved in a disease pathway.

This mRNA is cleaved and undergoes degradation, thereby interrupting the protein synthesis of the targeted gene.

Figure 1.4

siRNA synthesis and RNA interference mechanism adopted from *http://www.alnylam.com*

Because of its effectiveness in silencing specifically targeted genes, RNAi is a mechanism that is being exploited for a variety of laboratory applications and from the recent point of view also for future clinical therapeutics. Due to the broad potential applications of RNAi in biology and medicine, it is important to understand the mechanisms of RNAi well and to develop new solutions for a successful delivery of siRNA to the target cells.

Similarities and differences between antisense oligonucleotides and siRNA

Before the discovery of RNA interference, antisense oligonucleotides were the primary tools for targeted gene silencing; however, they have been shown to cause significant non-specific effects [Stein, C. A. 1995; Cho, Y. S. et al. 2001; Fisher, A. A. et al. 2002]. In particular, their affinity for cellular proteins has been shown to cause significant complications in interpreting gene silencing effects [Brukner, I. et al. 2000]. Even though such complications are theoretically possible with siRNA either, little evidence can be found in the literature.

In a growing number of scientific studies siRNA has been proposed and already even been used as a future agent and alternative to antisense oligonucleotides for the treatment of numerous diseases such as cancer and other disorders, some of which are even based on genetic dysfunction [Kim, S. H. et al. 2006]. Synthetic siRNA and antisense oligonucleotides share many common features but there are also important differences that become relevant in the technological formulation process development (**Table 1.2**). For instance siRNA has gained greater acceptance in two years than traditional antisense oligonucleotides achieved in twenty because it is relatively easy to apply the technique successfully once a delivery vehicle has been found.

Another reason for the rapid adoption of siRNA is that research aimed at optimizing traditional antisense oligonucleotides has already solved many important problems. For example, cellular uptake of oligonucleotides is a major obstacle for the efficient gene inhibition inside cells and difficulties in tranfecting cells with antisense oligonucleotides seriously threatened the field [Hogrefe, R. I. 1999]. However, by the time siRNA appeared, a wide variety of efficient delivery systems for nucleic acids had been developed and was commercially available. In addition, researchers using traditional antisense oligonucleotides had already described potential pitfalls and developed criteria for the essential control experiments needed to produce convincing results [Crooke, S. T. 2000]. While from a theoretical point of view a lot of know-how is available for antisense technology, the real advantages of double-stranded siRNA come along with delivery, loading of carriers, endosomal release and preclinical *in-vitro* and *in-vivo* studies.

Table 1.2

Similarities and differences of siRNA vs. antisense oligonucleotides

Similarities	Differences
Short (~20 bases) nucleic acids	Two strands for siRNA, one strand for antisense oligonucleotides
Common methods for delivery to cultured cells	Unmodified duplex RNA is more stable than unmodified single-stranded RNA or DNA
Induce post-transcriptional gene silencing by targeting mRNA	Effects of siRNA mediated by the RISC complex
siRNA and many antisense oligonucleotides cause mRNA cleavage	Antisense oligonucleotides act by activation of RNAse H or steric inhibition
Similar biodistribution profiles	
Properties can be altered by introducing modified bases	Rapid and widespread adoption of siRNA among biomedical researchers [Paroo, Z. et al. 2004]

siRNA chemistry and modifications

Unlike single-stranded RNA, duplex RNA is quite stable and does not require chemical modifications to achieve a satisfactory half-life in cell culture media [Braasch, D. A. et al. 2003]. In addition, reduced need for chemical modifications lowers toxicity to cells [Hough, S. R. et al. 2003]. The structural integrity of siRNA duplex highly affects RNAi-mediated gene silencing efficiency [Braasch, D. A. et al. 2003; Prakash, T. P. et al. 2005]. It was reported that chemical modification of siRNA reduced the corresponding RNAi activity from 10 % to 50 % depending on where it was structurally altered and also elicited cellular toxicity to some extent [Amarzguioui, M. et al. 2003; Kim, S. H. et al. 2006].

For pharmaceutical technological developments based on siRNA it is important to notice that, in contrast to pDNA, siRNA cannot condense into particles of nanometric dimensions, being already a small subnanometric nucleic acid [Spagnou, S. et al. 2004]. Therefore,

electrostatic interactions between siRNA and a cationic particle pose two potential problems: (1) a relatively uncontrolled interaction process leading to particles of excessive size and poor stability and (2) incomplete encapsulation of siRNA molecules, which thereby exposes siRNA to potential enzymatic or physical degradation prior to delivery to cells. Further research indicates that nanoparticular transfected siRNA is located distinctly perinuclear and does not leave this compartment [Chiu, Y.-L. et al. 2004], which is a key factor for high efficiency and has a to be taken into consideration during formulation development.

Expectations put into this new mechanism in the therapeutic field

In 2001, Tuschl and co-workers demonstrated sequence-specific repression of target-gene expression using synthetic siRNA duplexes in mammalian cells, causing rapid adoption of the technology by researchers [Elbashir, S. M. et al. 2001]. From that point on, it became the distinct goal to develop RNAi from the laboratory bench to the patient's bedside.

1.3 RNA interference in research and therapy

Virtually any messenger RNA (mRNA) for whatever protein linked to a certain disease can be silenced using the right siRNA sequence. However, one of the greatest challenges today remains finding a way for the successful *in-vivo* delivery. A transition of theory from the laboratory into clinical trials is hence still far from near. Only a number of approaches for delivering siRNA have recently been explored: one approach was to deliver DNA or RNA templates encoding siRNA sequences to cells that can then be transcribed to express siRNA [Shi, Y. 2003]. These DNA- and RNA-based methods of siRNA expression rely on plasmid or viral vectors for delivery and require a transfection, a stable vector integration, and selection for maintenance of expression through generations [Lee, N. S. et al. 2002; Paddison, P. J. et al. 2002; Paul, C. P. et al. 2002; Shen, C. et al. 2003].

Other successful methods focus on the direct delivery of siRNA into cells, whereby fidelity in cellular uptake of siRNA is the key to successful RNAi using this approach. Currently, the most often used method for siRNA delivery is Lipofectamine[®] transfection [Dalby, B. et al. 2004]. However this strategy is limited to specific cell types, and this procedure - with properly designed and reviewed studies still missing - could be toxic to cells and animals

[Ohki, E. C. et al. 2001]. Newer strategies include experiments to deliver siRNA using a TAT-peptide as an uptake-enhancer [Chiu, Y.-L. et al. 2004] or sophisticated viral or non-viral carriers. In summary, research on the delivery of siRNA is itself at a quite preliminary level. For instance, despite the widespread use of cationic liposomes/lipid systems to deliver plasmid DNA and oligodinucleotides to cells, there has been very little reported in the literature concerning the formulation of siRNA in such vehicles [Spagnou, S. et al. 2004]. To say it with the words of Steve Dowdy, Ph.D., investigator at Howard Hughes Medical Institute, and professor at the Department of Cellular and Molecular Medicine at the University of California, San Diego (UCSD):

"The beauty of the siRNA is that you can knock down multiple targets at the same time. So, it looks quite promising," he adds. In addition, he believes that, in the next five years, there will be a much wider variety of delivery approaches because one delivery approach won't solve the problem for every disease. "RNAi has great potential - more potential than any drug regimen we have come up with." [Flanagan, N. 2009]

Evidently there is not much doubt that RNAi has quickly advanced from the initial discovery to a key tool in today's research, and by the same time become one of the most promising therapeutics with the potential to change the future of medicine. Within in Big Pharma's recent purchasing activities is GlaxoSmithKline to sign a $600 million collaboration with Regulus. Alnylam has milestone deals from $700 million to more than $1 billion with Novartis and Roche. Merck bought Sirna Therapeutics for $1.1 billion. Nothing can reflect the faith into this new technology better than such transactions [Flanagan, N. 2009].

1.4 Viral and non-viral gene delivery

The primary challenge in gene therapy is to develop a method that delivers a therapeutic gene to selected cells where proper gene expression can be achieved. An ideal gene delivery method needs to meet three major criteria: first it should protect the transgene (RNA or DNA) against degradation by nucleases in intercellular matrices, secondly it should bring the transgene across the plasma membrane and into the nucleus of target cells, and thirdly it should have no detrimental effects on the cell viability [Gao, X. et al. 2007].

Viral gene vectors

Viral vectors that have found clinical interest are either retrovirus (*e.g.* HIV, FIV or EIAV) or adenovirus based. The whole family of retroviruses is a class of enveloped viruses, the genome of which is contained in a single stranded RNA molecule of 10 kb. After penetrating into the cell, its genome is reversely transcribed into dsDNA and integrated into the host genome. Unfortunately, transgene expression has been reported to be reduced by inflammatory interferons [Ghazizadeh, S. et al. 1997]. Furthermore, retroviruses are inactivated to an extent by two elements in human sera *in-vivo*, the c1 complement protein and an anti-alpha galactosyl epitope antibody, the latter thought to provide a species barrier for the horizontal transmission of retrovirus [Rollins, S. A. et al. 1996]. Notably, lentiviral vectors, a species within the retroviridae family, represent an efficient system for both somatic and germ-line transduction because of their ability to transduce non-dividing cells, because they can pass through the intact membrane of the nucleus of the target cell. Furthermore immune responses to lentiviruses have not yet been reported. A major advantage of the lentiviral gene delivery system is also that transgenes expressed from lentiviruses are not silenced during development and can be used to generate transgenic animals through infection of embryonic stem cells or embryos [David, P. 1998; Janas, J. et al. 2006; Morris, K. V. et al. 2006]. Adenoviruses finally are among the most commonly used vectors for gene therapy, second only to retroviruses.

The acute immune response, immunogenicity, and insertion mutagenesis uncovered in gene therapy clinical trials have raised serious safety concerns about some commonly used viral vectors [Monahan, P. E. et al. 2002]. The limitation in the size of the transgene that recombinant viruses can carry and issues related to the production of viral vectors present additional practical challenges.

Non-viral gene vectors

With non-viral transgene delivery vehicles scientists seek to bypass the virus related hurdles. Non-viral vectors include cationic lipids, polymers, dendrimers, and peptides. Recently, gas filled lipidic monolayer bubbles called microbubbles have stepped in, offering another promising and efficient new way of gene transfer [Bekeredjian, R. et al. 2007; Tinkov, S. et al. 2009]. These gene delivery vectors do not have the typical limitations in the

size of the genetic material as viral vectors. Also, in contrast to viral delivery systems, non-viral carriers do not have the inherent selectivity of cell surface binding and internalization (called tropism) and in addition the intracellular route of the transgene is more efficiently directed [Amiji, M. 2004]. In general, non-viral systems have been investigated even more intensively since a lethal complication occurred in a virus-based gene therapy trial and leukaemia incidents after gene therapy of children with X-linked severe combined immune deficiency using a retroviral gene therapy vector [Ferber, D. 2001; Kohn, D. B. et al. 2003].

So in fact, there are serious unsolved problems related to gene therapy. Besides the effective integration of the therapeutic genes into the genome, reducing the risk of an undesired immune response, inflammatory response, toxicity and oncogenesis related to the viral vectors is a vital part in the upcoming research. Apparently there is also another serious obstacle that the injection of a single gene may not be sufficient in diseases caused by variations in many genes like high blood pressure or heart disease. Nanoparticles, and therefore non-viral gene carriers as shown in this thesis, shall be presented as a safe and efficient solution to those above mentioned obstacles.

1.5 Nanoparticles: definitions, history and current state of knowledge

Nanoparticles were initially meant to be used as carriers for vaccines and anticancer drugs but also for diagnostic purposes [Marty, J. J. et al. 1978; Couvreur, P. et al. 1979]. Later on, in order to enhance the tumor drug uptake, the strategy of drug targeting with nanoparticles – as suggested by Paul Ehrlich a century ago – came in handy, with a first focus on the development of methods for reducing the uptake of the nanoparticles by the cells of the mononuclear phagocytosis system (MPS) [Illum, L. et al. 1987]. Nanoparticles can be formulated from inorganic materials like TiO_2 [Sugimoto, T. et al. 2003] and gold [Paciotti, G. F. et al. 2004] or from organic polymers either from a synthetic, semi-synthetic or natural origin. Many early studies used human serum albumin and poly-lactic-co-glycolic acid as materials for nano- and microparticle formulation [Tomlinson, E. et al. 1987; Gupta, P. K. et al. 1989; Allémann, E. et al. 1993]. Gelatin nanoparticles proposed and developed by Marty et al. [Marty, J. J. et al. 1978] and Kreuter et al. [Kreuter, J. 1983] and later improved by our research team [Coester, C. J. et al. 2000; Zillies, J. et al. 2004; Zwiorek, K. et al. 2004]

16

indicated a milestone in the formulation of widely applicable biodegradable nanoparticles for drug delivery. These nanoparticles possess certain advantages over the hitherto prevalent liposomal delivery systems, such as a greater stability during storage, stability *in-vivo* and ease of scale-up during manufacture. Non-biodegradable matrices are possibly ideal for mechanistic studies in *in-vivo* models but might hardly get regulatory approval for *in-vivo* use in humans other than for diagnostic purposes because of unclear side-effects due to tissue persistence and formulation complexity. By now, one can already find studies on the controlled release from nanoparticles and targeting with promising results [Wan, W. K. et al. 2007] that are summarized and highlighted in two seminal reviews from Kim Park [Park, K. 2007] and Patrick Couvreur et al. [Brigger, I. et al. 2002].

The evolutionary stage at which nano-formulations are at the moment is reflected in an excerpt from the clinical studies database at the Food and Drug Agency (FDA) (**Table 1.3**). With Doxil® liposomes and Abraxane® nanoparticles being the first colloidal formulations to gain approval for ovarian and various other cancers there are also cyclodextrin, further liposomal and gold based formulations in the pipeline of clinical phases one and two of pharmaceutical companies.

Table 1.3

Excerpt overview of nanoscaled formulations currently in clinical phases at the FDA

Product	Type of Nanoparticle/ Drug	Indication	FDA	Company
Doxil	PEGylated liposome/doxorubicin hydrochloride	Ovarian cancer	Approved 11/17/1995 FDA50718	Ortholliotech
Abraxane	Nanoparticulate albumin/paclitaxel	Various cancers	Approved 1/7/2005 FDA21660	American Pharmaceutical Partners
Cyclosert	Cyclodextrin nanoparticle	Solid tumors	Phase I	Insert Therapeutics
Megace ES	Nanocrystal/megestrol acetate	Breast cancer	Approved 7/5/2005 FDA21778	Par Pharmaceutical Companies
INGN-401	Liposomal/FUS1	Lung cancer	Phase I	Introgen
Combidex	Iron oxide	Tumor imaging	Phase III	Advanced Magnetics
Aurimune	Colloidal gold/TNF	Solid tumors	Phase II	Cytimmune Sciences
SGT-53	Liposome Tf antibody/p53 gene	Solid tumors	Phase I	SynerGene Therapeutics

Source: http://www.accessdata.fda.gov/scripts/cder/drugsatfda/

1.6 Gelatin based nanoparticles as colloidal drug delivery vectors

With a similar background in research as albumin from Abraxane[®], gelatin has so far not been adopted by pharmaceutical companies for clinical trials. In close cooperation with Medigene AG (Martinsried) gelatin based nanoparticles shall be introduced into preclinical evaluation as siRNA delivery systems. Gelatin is a widely spread protein in food and in pharmaceutical preparations. Gelatin can be produced by two different processes which comprise either an acid hydrolysis or a base hydrolysis of porcine or bovine skin bulk. The properties of the final gelatin depend on exactly this manufacturing method, its origin (bovine or pig), the type and quantity of amino acids, and the molecular weight. With its inherent properties, gelatin can be seen as advantageous to other biopolymers available for nanoparticle formulation. Besides being abundantly available, gelatin also reflects a relatively tolerable antigenicity [Schwick, H. G. et al. 1969] and formulation scientists already provide over a significant experience in the use of gelatin in parenteral formulations [Hässig, A. et al. 1969]. The preparation of gelatin nanoparticles by desolvation was first described in 1978 [Marty, J. J. et al. 1978]. However, his method turned out to be rather unsatisfactory for routine nanoparticle formulations due to aggregation and other colloidal instability issues. Truong-Le et al. in an attempt to formulate gelatin/DNA complexes employed sodium sulphate as a desolvating reagent to facilitate phase separation by influencing the degree of hydration of the two ionic species (DNA and gelatin) and thus increasing the degree of inter- and intracoulombic forces between the ion pairs [Truong-Le, V. L. et al. 1999]. Various methods, including nanoencapsulation [Li, J. K. et al. 1998] and coacervation-phase separation [Yeh, T. K. et al. 2005], have been used to prepare gelatin nanoparticles. Other authors [Bajpai, A. et al. 2006] suggested a simple solvent evaporation technique following a publication of Cascone et al. [Cascone, M. G. et al. 2002]. Gelatin nanoparticles prepared by these methods were found to be large in size and have a high polydispersity index due to heterogeneity in molecular weight of the gelatin polymer compared to the two-step method where heterogeneous gelatin was in a way standardized to a narrow molecular weight fraction and thus enabling gelatin nanoparticles to be formulated reproducibly for preclinical studies. The first really stable nanoparticles made from gelatin by using this desolvation technique were described by Coester et al. [Coester, C. J. et al. 2000; Coester, C. et al. 2006]. In these studies a new two-step desolvation method for manufacturing gelatin nanoparticles was established which will be the basis for further optimization within this thesis. Until now,

gelatin nanoparticles formulated accordingly have been extensively studied *in-vitro* and *in-vivo* for antisense therapy of HIV [Coester, C. 2000] and the delivery of CpG oligonucleotides to lymph nodes for anti-tumor immunization [Bourquin, C. et al. 2008; Zwiorek, K. et al. 2008]. The results in these studies reflect the potential of gelatin nanoparticles and at the same time demand further studies.

1.7 Body distribution of nanoparticles

Peppas et al. [Owens, D. et al. 2006] stated in their review that the study of nanoparticles and their opsonization is a very active and developing area of research. Even though the proteins and blood components involved in this process are roughly known, the mechanism by which they activate specific cellular responses and interact with nanoparticles is not fully understood. Additionally, multiple cell lines and animal models need to be studied to better understand these mechanisms and propose realistic solutions. Systemically administered nanoparticles are rapidly cleared from the blood by a complex process of opsonization and elimination, which is started by complement activation and a preferred uptake of the nanoparticles by the macrophages of the mononuclear phagocyte system (MPS) and its respective main organs, the liver and the spleen. In a review article, Moghimi et al. [Moghimi, S. M. et al. 2001] have extensively discussed the development and applications of especially long-circulating and target-specific nanoparticles.

There are various factors that influence the degree of long circulation. These include the nature of the polymer used, the length of the hydrophobic anchor, the polymer molecular weight (energy of molecular motion), and the amount of the protective polymers on the particle surface [Kommareddy, S. et al. 2007]. One heavily examined and often employed aspect to alter the body distribution and circulation of nanoparticles and liposomes is the use of polyethylenglycol (PEG) chains to shield the nanocarriers with a hydrophilic surface from interaction with blood proteins and blood cells and prevent a fast blood clearance [Kommareddy, S. et al. 2007]. While some researchers demonstrated pegylation of thiolated gelatin nanoparticles to significantly enhance the circulation time, critical scientists have found contradicting arguments to the PEG-effect, which they called ABC (activated blood clearance) phenomenon [Ishida, T. et al. 2006]. In this case pegylated liposomes were cleared

from the circulation very fast through IgM and C3 complement opsonization leaving the implementation of PEG as a general solution to body distribution problems questionable.

Surfactant coatings of polymeric nanoparticles showed reasonable results in influencing the localization of nanoparticles and prolonging the circulation half-life [Illum, L. et al. 1984]. This approach was adopted in our research and used in nanoparticle kinetic investigations *in-vivo*. In addition to plasma protein adsorption studies done in our group [Zillies, J. C. 2008] the nanoparticle cell interaction *in-vivo* shall be studied and related to the various nanoparticle modifications described above. All this effort is necessary to determine the body distribution patterns of our nanocarrier systems that are mainly influenced by particle size and surface properties such as charge and hydrophilicity [Crommelin, D. J. et al. 1994; Kreuter, J. 1994]. While it was our goal to keep the nanoparticle formulation as simple as possible for reasons of scaling up and regulatory approval, adding functionality to nanoparticle surfaces plays an important role in experimental science and especially when the need demands for it.

1.8 Nanoparticle modifications

Surface modifications made to GNP

In terms of surface modification towards a cationic charge needed for drug loading, cholamine was one of the best established molecules used by our group. Based on the research and optimization done by Coester [Coester, C. 2003] and Zwiorek [Zwiorek, K. et al. 2004] 1-ethyl-3-(3-dimethyl-aminopropyl) carbodiimide hydrochloride (EDC) is used in this method to activate the free carboxylic groups of the gelatin molecules for the covalent attachment of cholamine in the following step. This method allows for sufficiently high zeta potentials of the nanoparticles for oligonucleotide loading [Zwiorek, K. et al. 2004] but not for siRNA [Zillies, J. et al. 2004]. Besides the load binding, nanoparticle integrity, colloidal stability and cross-linking are factors where such modification is pivotal.

Core modifications made to GNP

For these reasons and based on research by Cortesi [Cortesi, R. et al. 1999] and Dhaneshwar [Dhaneshwar, S. et al. 2006], diethylaminoethanol modified dextran (DEAE-dextran) as a

permanent cationic polysaccharide came into the focus of our research. Not so much in terms of crosslinking the gelatin to microspheres as Cortesi or Brannon-Peppas [Kosmala, J. D. et al. 2000] did, but as a means of cationizing the gelatin nanoparticles above the level of cholamine. The idea was picked up by Gref et al. [Gref, R. et al. 2006] who formulated nanogels between dextran and cyclodextrin using an alkyl chain based "lock mechanism". Besides this cationic charge, DEAE-dextran modification allows our nanoparticles to potentially escape the intense capture by macrophages due to a postulated dense, brush-like structure preventing opsonization. They should circulate in the blood stream for a longer period of time [Grislain, L. et al. 1983; Passirani, C. et al. 1998], which becomes relevant in nanoparticle *in-vivo* experiments.

Other biomaterials for nanoparticles

Albumin

Nanoparticles prepared by desolvation and subsequent crosslinking of human serum albumin (HSA) also represent promising carriers for drug delivery and were therefore part of this thesis. A method for the preparation of bovine serum albumin nanoparticles in the sub-200 nm range was described by Müller et al. [Mueller, B. G. et al. 1996]. In 1993, Lin et al. [Lin, W. et al. 1999] described the preparation of human serum albumin nanoparticles of diameter around 100 nm using a surfactant-free pH-coacervation method. Langer et al. [Langer, K. et al. 2003] did extensive research on the development of a desolvation procedure for the preparation of human serum albumin based nanoparticles under the aspect of a controllable particle size between 100 and 300 nm in combination with a narrow size distribution. The pH value of the human serum albumin solution prior to the desolvation procedure was identified as the major factor determining particle size. The study is based on an earlier work, describing a desolvation method for human serum albumin particle preparation and their characterization with respect to size, zeta potential and the number of available amino groups on their surface [Weber, C. et al. 2000]. Further studies on the synthesis, cationization and loading have been done in the works of Wartlick [Wartlick, H. et al. 2004]. Arnedo et al. [Arnedo, A. et al. 2002] adsorbed and incorporated 21-mer oligonucleotides on BSA-nanoparticles crosslinked with glutaraldehyde.

Chitosan

Chitosan is the most common, naturally occurring, positively charged polymer in pharmaceutical use. It is a polysaccharide composed of copolymers of glucosamine and N-acetylglucosamine. Chitosan is produced by partial deacetylation of chitin isolated from crustacean shells. The term chitosan is used to describe a series of chitosan polymers with different molecular weights, viscosities, and degrees of deacetylation (40-98 %) [Illum, L. 1998]. Also interestingly enough, chitosan is considered to lack a toxicity response [Arai, K. et al. 1968; Aspden, T. et al. 1997]. Chitosan nanoparticles are produced by either an emulsification crosslinking process or by use of complexation between oppositely charge macromolecules. Ohya et al. [Ohya, Y. et al. 1994] were the first to present data involving chitosan nanospheres for drug delivery applications. Using a water-in-oil (W/O) emulsion method followed by glutaraldehyde crosslinking of the chitosan amino groups, the group produced nanospheres which contained 5-fluorouracil as an anti-cancer drug.

Aside from its complexation with negatively charged polymers an interesting property of cationic chitosan is its ability to gel on contact with specific polyanions. This gelation process is due to the formation of inter- and intramolecular crosslinks, mediated by these polyanions. Bodmeier et al. [Bodmeier, R. et al. 1989] first reported the ionotropic gelation of chitosan with tripolyphosphate (TPP) for drug encapsulation.

Mumper et al. [Mumper, R. J. et al. 1998] were then the first to propose chitosan as a gene delivery system. The employed method generated chitosan-DNA particulate complexes. Since particle formation was elicited solely by the tropism of the two oppositely charged macromolecules for one another, these particles were termed "complexes". The simplicity of chitosan-DNA complexes is both an advantage and a drawback. Though such complexes are extremely easy to synthesize, the fact remains that their transfection efficacy is significantly below that of cationic liposomes *in-vitro* and viral vectors *in-vivo*.

To address this issue, gelatin nanoparticles with enhanced cationic charge as presented in this thesis were developed and examined in novel *in-vitro* and *in-vivo* models.

1.9 In-vitro and in-vivo models

The number of methods for the visualization of nanoparticles *in-vivo* is limited. A. Rolland was able to visualize indium-111 labeled nanoparticles and determine their kinetics, which in his case gave a first hint of generally very quick nanoparticle elimination from the blood stream in the range of 3-5 minutes [Rolland, A. 1989]. There are of course new fluorescence based methods with microscopic read-out systems [Schmitt-Sody, M. et al. 2003; Medarova, Z. et al. 2007] to localize nanoparticles beyond the blood stream, however with the drawback, that a monitoring can only be undertaken in certain, surgically difficult to prepare observation areas paired with a relative low sensitivity of the detection microscope. Positron emission tomography (PET) and single-photon emission computer tomography (SPECT) are among the newer nanoparticle tracking systems [Nahrendorf, M. et al. 2008]. For example, indirect computer tomography was performed, after subcutaneous injection of iodinated nanoparticles to swine, in order to detect cancerous lymph nodes in a cutaneous melanoma model [Wisner, R. et al. 1996]. In essence, for a detailed understanding of the nanoparticle fate, these tools are still unsatisfying and prompt the major drawback of heavily modifying the nanoparticle system with detection moieties towards, in many cases, totally different physicochemical properties [Gao, X. et al. 2004; Turner, J. L. et al. 2005]. Only with the new whole body imaging tools used in our study and described by Bartlett et al. [Bartlett, D. W. et al. 2007] many of the present obstacles seem conquerable, narrowing a gap in investigations of gelatin nanoparticle pharmacokinetics.

Nanoparticle cell interaction in a novel in-vitro flow model

The cultivation and microscopic analysis of cells has been stagnating for a long long time whereas the demands of high resolution fluorescence microscopy and high resolution nanoparticle analysis have risen drastically. Fluorescence correlation spectroscopy, fluorescence *in-situ* hybridisation and confocal laser scanning microscopy are just some of those modern methods that are widely used today. The traditional microscopic object plate cannot fulfil those demands anymore. New polymer based slides need to have high optical properties, be permeable for gas and show a good biocompatibility.

The new plastic flow chambers used for our nanoparticle studies unite those requirements and in addition do not disturb the optical measurements by meniscus forming and medium condensation phenomena [Horn, E. 2006]. As a preclinical evaluation tool for nanoparticles the flow channels when attached to a cell culture pump can even simulate human blood vessels [Raedler, U. et al. 2005] and will be used by us for this purpose.

Hamster dorsal skin fold

A real quantum leap in studying nanoparticles in an *in-vivo* setting compared to the also highly innovative flow-channel model described above is the so called hamster skin fold model. From its first description [Sandison, J. C. 1928] almost a century ago, the method of implanting a transparent glass cover on top of surgically opened tissue has been improved manifold to ensure reproducible and intact physiological conditions [Endrich, B. et al. 1980; Asaishi, K. et al. 1981]. With its medical background it is clear that the model has been mainly used for anatomical observations, vessel and blood cells analysis [Lehr, H. A. et al. 1993] but not for the observation of nanoparticles. Krasnici et al [Krasnici, S. et al. 2003] successfully employed the model for their studies of liposomes and demonstrated the different effects of surface charge on the endothelium targeting properties. The model allowed for a real-time analysis of fluorescent nanoparticles in a physiological milieu over sufficiently long time periods with a focus on blood cell and endothelium interaction.

Mouse cremaster

One of the most advanced ways to study nanoparticles in an *in-vivo* setting is by monitoring them at real-time and online from the time of application to incubation durations of several hours. Since we wanted to change our nanoparticles as less as possible and still be able to monitor their *in-vivo* fate from the point of injection we had to come up with a model that would allow us to study *e.g.* fluorescent labeled nanoparticles in a natural vessel environment and while the animal was still conscious. The model that fit most to these needs was the mouse cremaster model that was well established at the Walter-Brendel-Center in Munich for toxicological research but never before had been used to study polymeric nanoparticles *in-vivo*. Since the experiments with the hamster skin fold model was prone to accumulate a high percentage of nanoparticles in the lung and liver tissue before even one single signal could be detected, the advantages in the surgical and anatomical setup of the *musculus cremaster*

model was beneficial to our experiments. The first pass effect to the liver and lung are bypassed during the first circulation of the nanoparticles allowing for a fluorescence signal detection right after application of the sample into the blood flow and check for aggregation phenomena and endothelial cell membrane targeting.

Whole body imaging

In order to optimize our experimental treatment strategies, a method for non-invasive detection of fluorescent nanoparticles or fluorescent siRNA molecules had to be found. At present, reports of the *in-vivo* imaging of fluorescent gelatin nanoparticles loaded with siRNA in target tissue are limited and in most cases based only on *ex-vivo* studies. Based on technical reporting from Medarova et al. [Medarova, Z. et al. 2007] and in close cooperation with Professor Ernst Wagner, Ph.D. and Manfred Ogris, Ph.D. (LMU Munich), an *in-vivo* live imaging tool became available. Studies of the nanoparticle and siRNA distribution under normal physiological conditions over a long time period allow us to monitor the nanoparticle fate at an unprecedented resolution as reported in a review from Rao et al. [Rao, J. et al. 2007] Overall, this new approach could help in advancing the understanding of targeted siRNA delivery with nanoparticles towards therapy.

1.10 Barriers to gene transfer

Every biological level of organization presents a unique set of barriers to the delivery of therapeutic agents [Jabr-Milane, L. et al. 2008]. Considering these barriers, the traditional focus of drug delivery systems has been the optimization of pharmacokinetics and biodistribution [Ferrari, M. 2005]. With biological research progressing, new comprehensive strategies such as the use of nanoparticles have emerged. Due to their unique properties of nano-scale matter, the diversity of the materials and infinite design schemes, nanoparticles are the ideal platforms for achieving barrier bypassing. Whenever a viral or non-viral carrier system is employed for the delivery of genes to a cell it faces several levels of hindrances before reaching the cytoplasm or nucleus of choice with an intact payload. As learned above (refer to 1.3 RNA interference in research and therapy), in the case of RNAi there is no need for delivering the siRNA to the nucleus and overcoming the nucleic membrane because the mechanism takes place in the cytoplasm of the cell.

"The rate-limiting problem is how you get the small RNA into a cell. Some cells and tissues will readily take up the RNAs by endocytosis; most will not. The bigger problem is, how do you target deep tissues or circulating cells?" [Perkel, J. M. 2007].

Generally spoken, all carrier systems developed until today face one or more drawbacks in their application route that eventually leads to a decreased transfection efficiency. These barriers shall be described next and their impact on the transfection results will be evaluated. We will highlight those cases, where researchers have made a significant progress in overcoming these barriers successfully. The major difference of viral and non-viral carriers is that viral carriers in many cases already have the *perfect* toolkit to protect the load in the circulation and to enter many different cell types unhindered. Non-viral carriers only try to mimic this optimal behaviour at their best. Viral carriers are therefore much less susceptible to the following barriers than non-viral carriers like nanoparticles, liposomes or dendrimers. The series of barriers to efficient non-viral gene delivery includes (1) the physical and chemical stability of the DNA or siRNA and the delivery vehicle in the extracellular space, (2) cellular uptake by endocytosis, phagocytosis or – recently discovered – a caveolae mediated uptake, (3) escape from the endosomal compartments before lysosomal activation, (4) cytosolic transport and (5) for DNA nuclear localization of the plasmid for transcription [Wiethoff, C. et al. 2003]. These barriers are mainly of physical and chemical nature, whereas biological obstacles can be observed as well. Effective delivery of siRNA to the site of action is hindered by biological barriers *e.g.* bifurcations in the lung, mucociliary clearance, lung surfactant etc. [Thepen, T. et al. 1994; Jeffery, P. K. et al. 1997]. In morphological studies at electron microscopic level positively charged lipoplexes or polyplexes adsorbed to the negatively charged plasma membrane, followed by a clathrin-dependent endocytosis. Especially direct fusion with the cell membrane or fluid phase endocytosis may contribute to the uptake [Meyer, K. et al. 1997; Clark, P. R. et al. 1999]. Larger particles enter the cell by receptor- and clathrin-independent endocytosis while the smaller ones (< 200 nm) can be internalized via coated pits [Simoes, S. et al. 1999]. In the case of lipid based nanocarriers, regardless of the precise mechanism of membrane disruption, only few internalized lipoplexes reached the cytoplasm, while the rest was degraded within in the endo-lysosome [El Ouahabi, A. et al. 1997; Hasegawa, S. et al. 2001]. CpG containing DNA strands for example can induce an immune response, wanted or unwanted, and also the carrier itself can be responsible for an immunogenic reaction [Yew, N. S. et al. 1999; Scheule, R. K. 2000; Ruiz, F. E. et al. 2001].

26

An optimisation of the above mentioned points seems detrimental for any efficient gene delivery approach. When it comes to evaluating the extracellular stability of the loaded gene carrier one has to take into account on the one hand the susceptibility of DNA and RNA against all types of nucleases and on the other hand the physical and colloidal stability of the carrier. While the rapid nucleotide degradation can be overcome by choosing the right carrier with protective properties or by modifying the nucleotide towards a stealth nucleotide, which is less reactive with nucleases and passes underneath its radar of detection [Li, S. et al. 1999; Roger, C. A. et al. 1999; Yongsheng, Y. et al. 2001], recent findings also indicate that the colloidal stability of the non-viral vectors has been underestimated to a large extend. Though many carriers are used at an elevated cationic charge that would stabilize the system *in-vivo* some carriers have a neutral surface charge that will lead to colloidal instability. Such charge related effects are even stronger in the elevated ionic strength milieu inside a biological environment. The challenge for gene therapy with siRNA remains to pinpoint the rate limiting step(s) in the nanoparticle uptake and siRNA delivery – a highly complex process – and implement strategies to overcome these barriers [Lechardeur, D. et al. 2002].

1.11 Nanoparticles for siRNA mediated RNA interference

Hailed as the breakthrough of the year in 2002 by *Science* [Couzin, J. 2002] RNAi still holds promise as a powerful, novel therapeutic for a wide variety of diseases and viruses. Its capability to selectively silence whatever gene taunts scientists still struggling with substantial hurdles, including clinical transition, delivery, and safety. Experts agree that delivery remains the main obstacle, which is where most companies are currently focusing their efforts. It was reported the cationized-gelatin microspheres containing siRNA for VEGF could inhibit tumor growth in mice [Matsumoto, G. et al. 2006]. The concept of siRNA delivery to *in-vitro* cells was then adopted by [Katas, H. et al. 2006] who showed how chitosan nanoparticles could be loaded with siRNA and be used for temporary RNAi in cells. In an advanced study, the anti-VEGF siRNA sustained release from microparticles showed a suppressive effect of VEGF levels over one month *in-vitro* and was also effective *in-vivo* after intra-tumoral injection [Murata, N. et al. 2008]. Going one step further, real nanoparticles made of chitosan were used by Pillé et al. [Pillé, J. Y. et al. 2006] to deliver siRNA after *i.v.* administration for a successful therapy of breast cancer. Besides the other delivery systems for siRNA described in **Table 1.4**, gelatin nanoparticles have not been in the focus for siRNA delivery so far. Only

Zillies et al. [Zillies, J. et al. 2004] presented promising preliminary results on the loading capacities of siRNA molecules on cationic gelatin nanoparticles thus leaving a wide gap of knowledge and much research to be undertaken in this field.

Table 1.4

Delivery systems for siRNA for *in-vivo* application with detailed mechanism, target tissue and characteristics [Gao, K. et al. 2008]

Delivery system	Mechanism	Target tissue or model	Characteristics
Hydrodynamic *i.v.* or direct injection	High pressure contributes to penetration across the cell membrane	Rat brain, mouse[Dorn, G. et al. 2004] liver[Lewis, D. L. et al. 2007], mouse lung[Zhang, X. et al. 2004]	Relative simplicity of local administration
Cholesterol conjugation with siRNA	Promote distribution and cellular uptake via lipoprotein as a carrier	Dyslipidemia in mice[Soutschek, J. et al. 2004] and nonhuman primate[Wolfrum, C. et al. 2007]	Significantly decrease the complexity by conjugation with the sense strand
Liposomes and lipoplexes	Improve pharmacokinetic properties and reduce toxicity profiles	Dyslipidemia in monkeys[Geisbert, Thomas W. et al. 2006] pancreatic tumor xenografts in mice[Pirollo, K. F. et al. 2007], breast cancer in mice[Ge, Q. et al. 2004], prostate cancer xenografts in mice[McNamara, J. O. et al. 2006]	Similarity to commercial transfection agents
Polymers and peptide delivery systems for siRNA	Endosomal escape takes place because of proton sponge effect. Improve selectively and specifically deliver siRNA *in-vivo*	Ewing sarcoma in mice[Hu-Lieskovan, S. et al. 2005], mouse b rain[Kumar, P. et al. 2007], melanoma xenografts in mice[Song, E. et al. 2005]	Condensed nanoparticles with siRNA . Can be modified with a targeting element for receptor mediated uptake.
Surface modified LPD nanoparticles	siRNA condensed with protamine to form a core which is wrapped with cationic lipid membrane. Final PEGylation provides surface protection and targeting specificity.	Oncogenes in solid and metastatic tumors can be effectively silenced in mouse models[Shyh-Dar, L. I. et al. 2006; Li, W. et al. 2007; Li, S.-D. et al. 2008; Li, S.-D. et al. 2008]	Very high tumor uptake and low immunogenicity.

1.12 Goal of the thesis

Viral and lipid based gene therapy brings several obstacles and dead-end developments with it. From a humanitarian, economic and scientific point of view, our research group has seen the need to shift the focus in oncologic therapy, at a much faster pace than in the past, towards protein based nanoparticles. It is our strong belief, that colloidal nanocarriers formulated from biodegradable, non-toxic and abundant proteins can become the lead medication for the generations to come. While nanoparticles will be mainly used for diagnostic and delivery purposes, small interfering RNA molecules and the closely related RNA interference mechanism will definitely change the way we treat diseases today.

The goal of this thesis was to develop and technologically improve gelatin nanoparticles towards potent and safe siRNA delivery vehicles. Even though this topic is more or less completely untouched in literature so far, we see a great demand from industry and patient side for nanocarriers like ours. The presented research thus will stretch from initial polymer characterization over several nanoparticle development strategies and optimizations to an evaluation of their transfection and RNA interference efficiency. For the characterization of the polymers automatic microviscosimetry and asymmetric flow field-flow fractionation, as well as nuclear magnetic resonance spectroscopy are introduced as fast and reliable protein analysis tools. A deeper formulation focus will be put on the stable and efficient fluorescence labeling of either nanoparticle excipient materials or the final nanoparticles themselves. Homogenous and small nanoparticles shall be formulated through advancements in the formulation procedure while the goal of high zeta potentials on the nanoparticle surface demanded for the combination of more than one polymer in the reaction mixture. In order to use our novel formulations for RNA interference experiments further modifications to the nanoparticle structure with endosomolytic peptides will become essential. With the final formulation at hand, RNA interference will be tested in state-of-the-art *in-vitro* assays. In a first step, luciferase protein knock-down will be demonstrated, while a final therapeutic impact of the new formulation is assayed by means of VEGF-receptor interference quantity. From a preclinical research and developmental perspective a new *in-vitro* model for the new class of nanoparticles will be established and correlated to proof of principle studies in therapeutically relevant *in-vivo* models. The *in-vitro* model will comprise near to physiological blood flow simulations and endothelial cell adhesion studies in a transparent

flow-through chamber slide model. Apart from overcoming several of the drawbacks of static cell culture models, the flow model offers the broad applicability and depth of parameters needed for high-throughput studies. Last but not least, we will establish innovative preclinical *in-vivo* models like the mouse arthritic knee model, the hamster dorsal skin fold chamber model and the mouse cremaster model as body-distribution and endothelial cell wall targeting assays. In combination with the flow model we will examine similarities and differences in the *in-vitro* and *in-vivo* fate of nanoparticles along individual milestones (**Figure 1.5**).
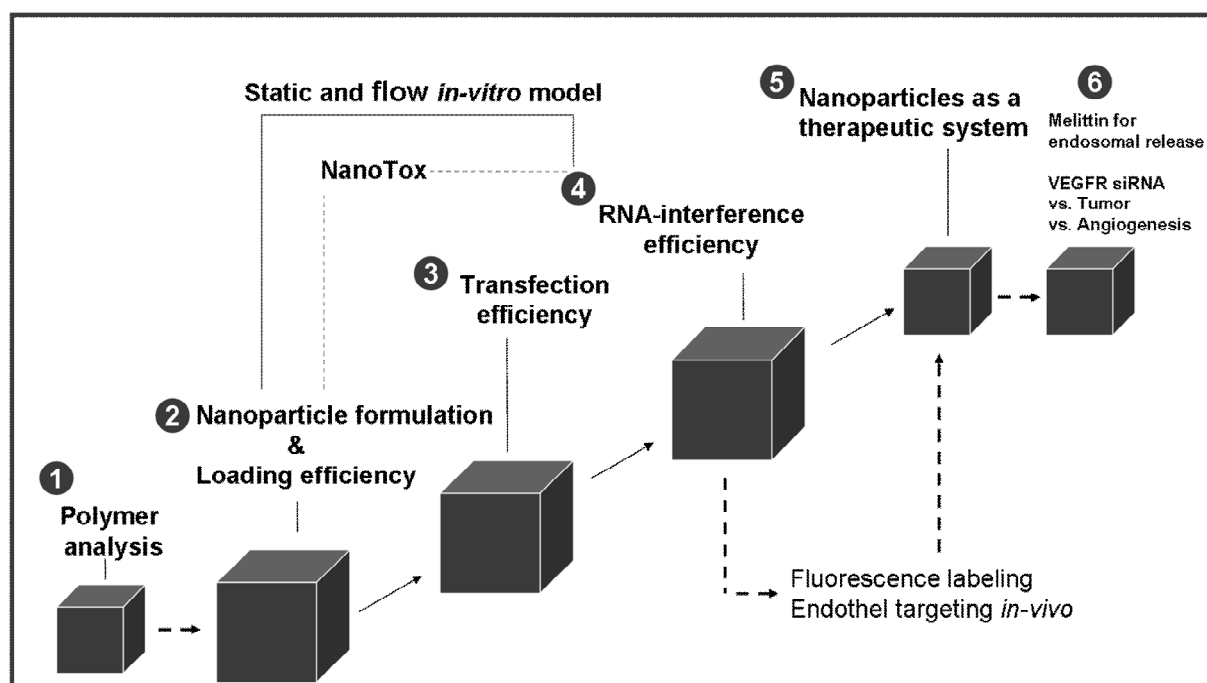
Figure 1.5

Schematic outline of the thesis milestones from initial polymer analysis (1) and nanoparticle formulation and siRNA loading studies (2) to analysis of the transfection efficiency (3) and RNA interference capabilities (4) of the newly developed formulations. Finally, the nanoparticle formulations shall be investigated on their therapeutic potential (5) with a focus on endosomal release functionality (6). Further projects will comprise first nanotoxicologic investigations of our formulations and the introduction of a novel cell culture flow chamber model for nanoparticle pre-clinical screenings.

2 Materials and Methods

2.1 Nanoparticle pre-formulation studies

Nanoparticle preparation was carried out under aseptic conditions in a laminar flow hood. Vials and flasks were heat sterilized and all solutions were sterile-filtered before use. All experiments including prolonged incubation steps were carried out under conditions avoiding microbial contaminations.

2.1.1 Chemicals and reagents

Reagent	Description	Supplier
1-Methyl-2-pyrrolidone	p.a.	Fluka (Buchs, Switzerland)
2-Iminothiolane	Traut's reagent	Sigma Aldrich (Wien, Austria)
Acetic anhydride	99 % (v/v)	Acros Organics (Morris Plains, USA)
Acetic acid	6% (v/v)	Acros Organics (Morris Plains, USA)
Acetone	p.a.	VWR International GmbH (Darmstadt Germany)
Chitosan	Low viscous	Sigma Aldrich (Wien, Austria)
Chitosan	Medium molecular weight	Sigma Aldrich (Wien, Austria)
Cholaminechloride hydrochloride	(2-aminoethyl)-trimethyl-ammoniumchloride hydrochloride 99 % (v/v)	Sigma Aldrich Inc. (St. Louis, USA)
Cyanoacrylat- Sico Met	Ethanol 96 % (v/v)	Sichel-Henkel (Hannover, Germany)
Di-ethyl-amino-ethyl modified dextran		Sigma Aldrich Inc. (St. Louis, USA)

Dimethylformamide	99.5 % (v/v)	Acros Organics (Morris Plains, USA)
D$_2$O 99 %		Euriso-Top (Gif-sur-Yvette, France)
Dulbeco's phosphate buffered saline	pH 7. (1x concentrate)	PAA Laboratories GmbH (Linz, Austria)
1-Ethyl-3-(3-dimethyl-aminopropyl) carbodiimide hydrochloride	EDC	Sigma Aldrich Inc. (St. Louis, USA)
Ethanol	99 % (v/v) + 1 % (v/v) Isohexane	Merck KGaA (Darmstadt, Germany)
Gelatin type A	175 Bloom, 8-80 mmoles free carboxyl groups per 100 g and a pI of 7-8.7.	Sigma Aldrich Inc. (St. Louis, USA)
Gelatin type MA	Dodecyl-succinate modified gelatin prototype	Gelita AG (Eberbach, Germany)
Gelatin type MS	Succinate modified gelatin prototype	Gelita AG (Eberbach, Germany)
Glutaraldehyde grade I	8,12, 25 % (v/v) aqueous solution	Sigma Aldrich Inc. (St. Louis, USA)
Guanidine HCl	2 M	Sigma Aldrich Inc. (St. Louis, USA)
Hydrochloric acid	2 N	VWR International GmbH (Darmstadt, Germany)
Iodine solution	1 mM	VWR International GmbH (Darmstadt, Germany)
Iodmethane	99 % (v/v), sterile	Acros Organics (Morris Plains, USA)
MilliQ highly purified electrolyte reduced water	Purelab Plus®, USF Elga Ionpure GmbH, Germany	Department of Pharmacy, University of Munich
Methoxy-poly-ethylene-glycol	13.000 Da	Iris Biotech (Marktredwitz, Germany)
Methoxy-poly-ethylene-glycol succinimidylester propionate	5.000 Da	Iris Biotech (Marktredwitz, Germany)

N-succinimidyl 3-(2-pyridyldithio) propionate		Sigma Aldrich Inc. (St. Louis, USA)
Poly-L-lysine	32.000 Da	Sigma Aldrich Inc. (St. Louis, USA)
Sodium hydroxide solution	1 N	VWR International GmbH (Darmstadt, Germany)
Sodium chloride	Puriss.	Riedel-de-Haen (Seelze, Germany)
Sodium nitrite		VWR International GmbH (Darmstadt, Germany)
Sulfo-NHS		Sigma Aldrich Inc. (St. Louis, USA)
Tripolyphosphate pentasodium hexahydrate		Sigma Aldrich Inc. (St. Louis, USA)
Tween® 80	Polysorbate 80, Ph. Eur.	Merck KGaA (Darmstadt, Germany)

2.1.2 Materials

Material	Description	Supplier
0.2 µm sterile filter	Cellulose acetate membrane	Acrodisc, Pall (Dreieich, Germany)
0.45 µm sterile filter	Cellulose acetate membrane	Acrodisc, Pall (Dreieich, Germany)
0.45 µm suction filter membrane	Cellulose acetate membrane	VWR International GmbH (Darmstadt, Germany)
5 µm sterile filter	Cellulose acetate membrane	Acrodisc, Pall (Dreieich, Germany)
26 G steel needle	Sterican	Braun (Emmenbruecke, Germany)
96-well plates		Greiner Bio-one GmbH (Frickenhausen, Germany)

Äkta Basic HPLC system		Amersham Biosciences (Freiburg, Germany)
Cation exchange column	MacroPrep High S; HR 10/10	BioRad (Munich, Germany)
Eppendorf safe-lock cap	1.5 ml, 2.0 ml	Eppendorf AG, Hamburg, Germany
Falcontubes	15.0 ml, 30.0 ml	Sarstedt (Nuernbrecht, Germany)
IKA stirring plate	IKA RT5	IKA Werke GmbH (Staufen, Germany)
Microslides/Vitrotubes	0.40 x 4.0 mm i.d.	Vitrocom (Mt Lakes, USA)
NMR tubes	178 mm, round bottom S-5-400-7	Norrell (Landisville, USA)
Peristaltic pump	Minipuls 3	Abimed Gilson (Langenfeld, Germany)
pH Meter		Mettler Toledo (Giessen, Germany)
Sephadex G-25 superfine HR 10/30 column		Pharmacia Biotech (Uppsala, Sweden)
Superdex 75 HR 10/30 column		Pharmacia Biotech (Uppsala, Sweden)
Sigma centrifuge	SIGMA 4K15	SIGMA GmbH (Osterode, Germany)
Spectra/Por® Float-A-Lyzer	MWCO 8,000 Volume 3ml	Spectrum Laboratories, Inc. (Rancho Dominguez, USA)
Vivaspin 2 ultrafiltration	MWCO 2000	Sartorius Vivascience AG (Hannover, Germany)
Zetasizer Nano ZS series folded capillary cells		Malvern Instruments (Worcestershire, England)

2.1.3 Formulation of unmodified gelatin nanoparticles

Nanoparticles were prepared from Sigma Aldrich gelatin based on the established two-step desolvation technique [Coester, C. J. et al. 2000]. In brief, a first desolvation step was performed to remove the low molecular weight fractions of gelatin which is important for a mono-modal size distribution of the nanoparticles. Therefore a 5 % (w/w) solution of gelatin type A in 0.2 μm filtered highly purified water (MilliQ) was prepared under constant stirring (500 rpm) at 50 °C on a temperature controlled stirring plate (IKA RT5, IKA Werke GmbH, Staufen, Germany) by dissolving 1.25 g gelatin in 25 g water. The solution was given 15 minutes time to equilibrate and to dissolve the gelatin completely. Now, 25.0 ml of acetone were quickly added to the stirred solution using a glass-burette to desolvate the high molecular weight fractions of gelatin and to separate them from the low molecular weight fraction. Right after addition of acetone, the beaker was removed from the stirring plate and desolvation was allowed to happen for a time period of 10 s after which the supernatant was quickly discarded. After resolution of the sediment with filtered highly purified water *ad* 25.0 g and pH adjustment with 110 μl 1 N HCl, the *in-situ* nanoparticles were formed by drop wise addition of 50.0 ml acetone at a pH of 2.5. The *in-situ* nanoparticles were then stabilized by crosslinking with glutaraldehyde solution 12 % (w/w) overnight under constant stirring. For further studies the stabilized nanoparticle dispersion was centrifuged at 8.000 g (SIGMA 4K15, SIGMA Laborzentrifugen GmbH, Osterode, Germany) and washed with highly purified water. This process was repeated two times at 16.000 g before the final dispersion was stored in aliquots at 4 °C. The basic formulation for all further nanoparticles was also formulated over 50 independently times for assessment with dynamic light scattering.

2.1.4 Formulation of cationic gelatin nanoparticles

One of the goals in nanoparticle formulation was, to achieve highly cationic nanoparticles with a sufficient residual surface charge before and after siRNA loading to allow for an efficient cell targeting, internalization and eventually intra-cellular therapeutic effect based on RNAi. In this context, covalent coupling of cholamine with its cationic trimethylammoniunchloride function was important. Cholamine cationized gelatin nanoparticles (C-GNP) were formulated as previously described by Coester [Coester, C.

2003] by adjusting the pH of the nanoparticle dispersion after the second desolvation step and purification to 4.5 and adding 50 mg ethylene-diamino-carbodiimide (EDC) and 50 mg cholamine under constant stirring. EDC was employed to activate the free carboxyl groups on the surface of the unmodified nanoparticles for the coupling with cholamine. The reaction was stopped after 3 hours by lowering the pH to 2.5 with 2 N HCl and the nanoparticles were purified as described above.

2.1.5 Formulation of diethyl-amino-ethanol-dextran and cholamine modified gelatin nanoparticles

DEAE-dextran nanoparticles (DD-GNP) from bovine gelatin and DEAE-dextran were prepared using a modified two-step desolvation technique. Again in brief, a first desolvation step was performed to remove the low molecular weight fractions. After resolution of the sediment, DEAE-dextran was added to the warm solution at different concentrations (**Table 2.1**) and under stirring (250 rpm).

Table 2.1

Representative DEAE-dextran concentrations for nanoparticle formulation. Percentage is expressed as (w/w) of total gelatin mass

DEAE-dextran concentrations % (w/w)		
0.04	0.08	0.2
0.3	0.4	0.8

After 10 minutes to allow for thorough intercalation of the DEAE-dextran chains with the gelatin molecules, nanoparticles were formed at pH 2.5 by drop wise addition of acetone. For a higher precision in the desolvation and to ensure a good size control, a peristaltic pump (Miniplus 3, Abimed Gilson, Langenfeld, Germany) was used and combined with an immersed needle for the first time (**Figure 2.1**) where the organic non-solvent was added via a 26 G steel needle (Sterican, Braun, Emmenbruecke, Germany) into the stirred solution at a flow rate of 5 ml/min.
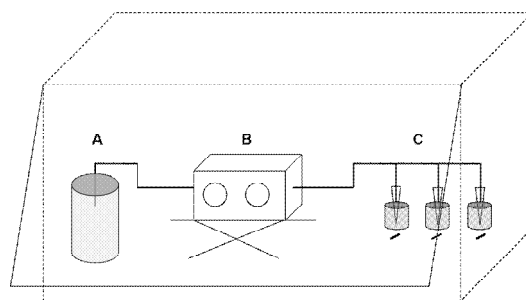
Figure 2.1

Schematic drawing of the aseptic nanoparticle formulation facility for large scale production with a good batch to batch reproducibility. **A)** Desolvating agent reservoir **B)** peristaltic pump with transparent and inert tubings **C)** nanoparticle birth and incubation vessels with external stirring unit and temperature controlled heating device

The *in-situ* nanoparticles were then stabilized by crosslinking with 110 µl glutaraldehyde 12 % (w/w) overnight. For further studies the nanoparticle dispersion was centrifuged at 8.000 g and washed with highly purified water. This process was repeated two times up to a final 16.000 g.

The Cholamine-DEAE-dextran GNP (CDD-GNP) were the most advanced cationic formulations within the project. We were able to formulate them by an additional modification step with cholamine onto the previously prepared DD-GNP. In detail, purified DD-GNP were transferred into a reaction beaker and adjusted to a concentration of 5 mg/ml in highly purified water. Again, the pH of the solution was adjusted to 4.8 before 50 mg of cholamine and 50 mg of EDC were added to the reaction. Slow stirring at room temperature was important for a successful and stable nanoparticle cationization. Also, aggregate formation could be suppressed this way. The reaction was stopped after 30 minutes by adding 200 µl of a 2 N HCl solution. Nanoparticles were purified as described above.

2.1.6 Formulation of human serum albumin nanoparticles

Nanoparticles from human serum albumin (HSA) were formulated by a desolvation method of the dissolved protein and a subsequent crosslinking as previously described by Weber [Weber, C. et al. 2000] and Marty [Marty, J. J. et al. 1978]. 250 mg HSA were dissolved in 2.5 ml highly purified water in a 250 ml Erlenmeyer beaker under constant stirring (500 rpm). The macromolecule was eventually dissolved by drop wise addition of 5 ml ethanol in total. The whole dispersion of freshly formed in-situ nanoparticles was incubated for 1 hour after which another 1 ml of ethanol was added to the dispersion to guarantee a maximum desolvation effect and hence a higher yield. Finally, the nanoparticles were crosslinked with 60 µl glutaraldehyde 8 % (w/w) over night. The nanoparticles were purified as described above by several centrifugation and washing steps.

2.1.7 Formulation of polybutylcyanoacrylate nanoparticles

Polybutylcyanoacrylate (PBCA) nanoparticles were formulated by a modified emulsion polymerisation reaction according to Gipps [Gipps, E. M. et al. 1987]. 50 ml of 0.1 N HCl and 450 mg of DEAE-dextran were given into a 100 ml beaker and stirred for 30 min until all DEAE-dextran was dissolved. Nanoparticles were formed by dropwise addition of 500 µl butylcyanoacrylate solution into the stirred solution. The whole reaction was allowed to incubate over night. Nanoparticle formation was indicated by a slight turbidity and a Tyndall effect-like light scattering. The final particle dispersion was filtered through a 5 µm and a 0.45 µm cellulose acetate filter to remove potentially larger agglomerates and was purified by 3-fold dialysis. For this reason 5 ml of PBCA nanoparticle dispersion were transferred into a Spectra/Por® Float-A-Lyzer dialysis tube and dialysed against 10 l highly purified water for 17 h. Within the first 5 h the 10 l dialysis medium were replaced every hour. The final nanoparticles were stored in 15 falcon tubes at 4 °C.

2.1.8 Formulation of chitosan nanoparticles

2.1.8.1 Preparation of low molecular weight chitosan

Low molecular weight chitosan as the basic material for the preparation of chitosan nanoparticles was prepared together with Claudia Vigl at the Institute of Pharmaceutical Technology at the University of Innsbruck, Austria, according to a method previously described by Bernkop-Schnuerch [Bernkop-Schnürch, A. et al. 2006]. In brief, 2 g of chitosan (medium molecular weight: 400 kDa) was dissolved in 100 ml of acetic acid 6 % (v/v). 80 mg of sodium nitrite were dissolved in 10 ml of highly purified water and added to reaction vessel. The reaction was allowed to stir for 1 h at ambient temperature, after which chitosan was precipitated by the addition of a 4 M solution of sodium hydroxide until pH 9 was reached. The pH was permanently controlled using a pH meter (Mettler Toledo, Giessen, Germany). The resulting precipitate was filtered through a 0.45 μm cellulose acetate suction filter membrane (VWR) and washed several times with cold acetone. Eventually the residue was resolubilized in 15 ml of 0.1 M acetic acid and dialysed exhaustively against demineralised water. The dialysate was concentrated partially under vacuum followed by lyophilization at -30 °C and 0.01 mbar (Benchtop 2K, VirTis, NY, USA).

2.1.8.2 Synthesis of thiobutylamidine and N-acetylcysteine modified chitosan

The thiobutylamidine chitosan was also prepared together with Claudia Vigl according to a method described previously by Roldo [Roldo, M. et al. 2004]. In short, 500 mg of the low molecular weight chitosan prepared as described above was dissolved in 50 ml of 1 % (v/v) acetic acid. 200 mg of 2-iminothiolane HCl was added to the solution after adjusting the pH to 6.5 with 1 N NaOH. The conjugation reaction was carried out for 12 h at room temperature under constant stirring. Dialysis of the conjugate was made two times against 5 mM HCl containing 1 % NaCl to quench any ionic interaction, against 5 mM HCl and last but not least against 0.4 mM HCl. As above, the polymer conjugate was freeze-dried at -30 °C and 0.01 mbar (Benchtop 2K, VirTis, NY, USA) and stored at 4 °C until further need.

The synthesis of chitosan-N-acetylcysteine was performed according to Loretz [Loretz, B. et al. 2007]. In brief, 1.0 g of low viscous chitosan was dissolved in 10 ml 0.1 mol HCl and diluted to 100 ml after which the pH was adjusted to 5.5. 2.0 g of N-acetylcysteine dissolved in 10 ml highly purified water and 0.5 g sulfo-NHS dissolved in 1 ml highly purified water were added to the chitosan solution. 1.0 g of 1-ethyl-3-(3-dimethylaminopropyl) carbodiimide hydrochloride (EDAC) was used to catalyse the reaction. After 14 h of continuous stirring, the thiolated chitosan solution was dialysed five times each for 12 h as described by Loretz [Loretz, B. et al. 2007].

2.1.8.3 Preparation of unmodified and thiolated chitosan nanoparticles

Nanoparticles from those modified low molecular chitosan were obtained by an ionic interaction mechanism using tripolyphosphate (TPP) in aqueous solution. The method was basically described by Calvo [Calvo, P. et al. 1997] and v.d. Lubben [van der Lubben, I. M. et al. 2001]. In brief, thiolated or unmodified low molecular weight chitosan were dissolved in 0.05 % (w/v) acetic acid solution to a final concentration of 0.25 % (w/v). Then the pH was adjusted to 5.5 by adding 0.5 % NaOH solution. The TPP solution was prepared at 0.2 % (w/v) in highly purified water and 1 ml was added dropwise to 3 ml of the respective chitosan solution which lead to the formation of chitosan nanoparticles. After incubation of the dispersion for 10 h instead of 3 h the particles were oxidized by the addition of 10 µl of 1 mM iodine solution and incubating the whole assay for 6 h. Thereafter the anions and oxidants were removed by dialysis against 0.1 M HCl over 12 h.

2.2 Post-formulation modification of nanoparticles

2.2.1 Methylation and acetylation

2.2.1.1 Methylation

Based on the protocol for the quaternisation of N-trimethylchitosanchloride [Polnok, A. et al. 2004] gelatin type A was methylated with methyl iodide as follows. A mixture of 2.0 g gelatin type A, 4.8 g sodium iodide and 10 ml of a 20 % (w/v) sodium hydroxide solution were dissolved in 40 ml 1-methyl-2-pyrrolidone. The mixture was stirred for 20 min on a

60 °C warm water bath before 1 ml of methyl iodide was slowly added to the solution and refluxed at 60 °C for another 2 h. The methylated gelatin was obtained by desolvation with ethanol 80°% (v/v) and subsequent centrifugation at 2800 g for 10 min. The sediment was washed with 20 ml diethyl ether and centrifugation at 2800 g was repeated for 10 min followed by another washing and centrifugation step with 20 ml of 1:1 diethyl ether:highly purified water. In order to exchange the iodide ions, 80 ml of a 5 % (w/v) solution of sodium chloride were added to the vessel and incubated for 60 min. The final methylated polymer was obtained by adding 100 ml ethanol:diethyl ether 1:1 to desolvate the polymer and a final filtration via a suction filter. At last the polymer was dried under vacuum for 16 h. and stored at 4 °C for further use to prepare nanoparticles thereof.

The nanoparticles were formulated from the freeze-dried methylated gelatin with a single-step desolvation method.

2.2.1.2 Acetylation

For the acetylation of gelatin type A, 3.0 g of gelatin were gently levigated in a mortar and transferred to a 50 ml reaction vial. The gelatin was covered with 10 ml acetic anhydride and dried for 2 h at 80 °C in a drying oven. After the reaction the acetylated polymer was washed and stored at 4 °C for further use.

The nanoparticles were formulated from the freeze-dried acetylated gelatin with a single-step desolvation method.

2.2.2 Fluorescence labeling

For fluorescence labeling of the nanoparticles, various fluorophores had to be used and tested due to the different physicochemical properties of the employed mono- and polymers. The used fluorophores (**Table 2.2**) were chosen based on their covalent binding properties with the functional groups of the polymers and also based on their relative molecular charge and lyophilicity behaviour, but always with the focus on maximum fluorescence emission intensity.

Table 2.2

List of the used fluorophores for nanoparticle labeling

Reagent	Description	Supplier	Excitation	Emission	Extinction
Alexa 488 succinimidyl ester	0.1 % (w/v)	Invitrogen Molecular Probes (Carlsbad, USA)	495 nm	519 nm	71000
Coumarine 6	98 % (w/v) 500 µg/ml, 1.43 mM	Acros Organics (Morris Plains, USA)	459 nm	505 nm	54000
FITC-dextran	50 µg/ml	Sigma Aldrich GmbH (Darmstadt, Germany)	490 nm	520 nm	52000
Lissamine Rhodamine B sulfonyl chloride	10 mg/ml	Invitrogen Molecular Probes (Carlsbad, USA)	575 nm	595 nm	62000
Oregon Green 514 carboxylic acid succinimidyl ester	5 mg/ml	Invitrogen Molecular Probes (Carlsbad, USA)	511 nm	530 nm	70000

Fluorescent neutral and cationic cholamine modified gelatin nanoparticles were formulated according to manufacturer's protocol. In brief, the pH of the gelatin solution after the first desolvation step with acetone was adjusted to pH 9.0 using 1 N NaOH. To this solution 300 µl Lissamine Rhodamine B sulfonyl chloride 10 mg/ml (**Figure 2.2**) were added and the solution was incubated under constant stirring and under the exclusion of light for 1 h. In the end, the pH of the labeled gelatin solution was lowered to pH 2.5 by the drop wise addition of 1 N HCl and nanoparticles were formulated as described earlier (refer to 2.1.3 Formulation of unmodified gelatin nanoparticles) with the restriction, that all steps handling steps were performed under the strict exclusion of light.
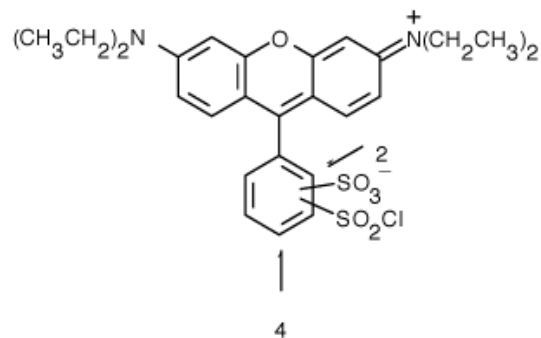
Figure 2.2

Lissamine Rhodamine B sulfonyl chloride

In case of DEAE-dextran modified gelatin nanoparticles, the fluorescent dye was also added to the gelatin solution right after the first desolvation step; however DEAE-dextran was added after the incubation time of 1 h.

FITC-dextran labeling of the gelatin nanoparticles was done by adding 100, 200 or 600 µl of a 5 mg/ml FITC-dextran solution to the fractionated gelatin solution at a temperature of 50 °C under constant stirring and the exclusion of light. Nanoparticles were formed as described above.

Gelatin nanoparticles were also labeled using a succinimidyl ester based coupling reaction with Oregon Green 514 carboxylic acid succinimidyl ester 5 mg/ml (**Figure 2.3**) and Alexa 488 succinimidyl ester. The pH of the desolvated gelatin solution was adjusted to pH 8.3 and a fluorophore amount of 100 µl was added to the stirred polymer solution. The incubation time amounted to 60 min.
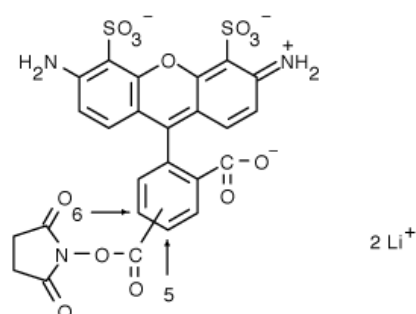
Figure 2.3

Alexa 488 Succinimidyl ester

Human serum albumin nanoparticles were labeled with Lissamine Rhodamine B sulfonyl chloride according to the process described above for gelatin nanoparticles.

In contrast to the above covalent linking of fluorescent dyes, hydrophobic acetylated gelatin nanoparticles were reacted with a fluorophore based on lipophilic molecular interactions. 3.5 ml of the dispersed aGNP (refer to 2.2.1.2 Acetylation) were incubated with 100 µl Coumarine 6 (500 µg/ml (w/w)) (**Figure 2.4**) for a time period of 1 h under the exclusion of light. Excessive Coumarine 6 was removed by 3-fold centrifugation and washing steps at 11000 g for 10 min with each time 3.5 ml highly purified water. Final nanoparticles were stored at 4 °C for further use.
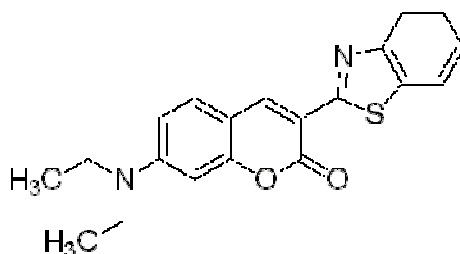
Figure 2.4

Coumarine 6

2.2.3 Polysorbate and polyethylene glycol modification

Coating of the gelatin nanoparticles with polysorbate 80 was performed as per a modified procedure formerly described for cyanoacrylate nanoparticles [Ramge, P. et al. 2000]. In short, gelatin nanoparticles were suspended in phosphate buffered saline at a concentration of 5 mg/ml under constant stirring. Polysorbate 80 was added to give a final dispersion of 1% polysorbate 80. After incubation for 60 minutes the nanoparticles were centrifuged once to remove any excess polysorbate from the disperion.

Pegylation of the gelatin nanoparticles with amine reactive mPEG-13,000 was conducted under permanent stirring of a 5 mg/ml nanoparticle suspension in highly purified water at a pH of 8.5. The nanoparticles were incubated for 120 minutes with the reagent on a

thermomixer (25 °C, 800 rounds per minute) and washed thoroughly afterwards with several centrifugation and redispersion steps. The determination of the amount of PEG bound to the GNP was described elsewhere [Zillies, J. C. et al. 2007].

2.2.4 Polyethylene imine modification

The gelatin PEI complex nanoparticles were formed by using our previously formulated CDD-GNP polysaccharide modified gelatin nanoparticles with cholamine coupling on its surface as the basic material. The nanoparticles were then loaded in a 96-well plate (Greiner Bio-one GmbH, Frickenhausen, Germany) with siRNA at concentrations of 5, 10, 20, 40, 80, 120, 160, and 200 : 1 in HBG buffer under ambient temperature and by intensive mixing with the pipette tip. Lastly, 0.5 μg PEI 25br was added to each well to allow for the final nanoparticle sandwich formation. All samples were immediately transferred to the cell culture wells for transfection.

2.2.5 Melittin modification

The PLL-PEG-DMMAn-Mel conjugate was synthesized in Prof. Wagner's lab according to a method described elsewhere [Meyer, M. et al. 2008]. In brief, PLL was PEGylated with mPEG-succinimidyl propionate (MW 5000). Therefore, PLL (1.25 μmol, 40 mg PLL hydrobromide corresponding to 25.7 mg PLL free base, MW 32 000) in 2 mL buffer (0.5 M NaCl, 20 mM HEPES, pH 7.4) was mixed with SPA-mPEG (1.6 μmol, 8 mg) dissolved in 400 μl dimethyl sulfoxide (DMSO). After 2 h at room temperature (RT) the reaction mixture containing modified PLL (PLL-PEG) was loaded on a cation-exchange column (MacroPrep High S; HR 10/10, BioRad, München, Germany) and fractionated with a salt gradient from 0.6 to 3.0M NaCl in 20 mM HEPES pH 7.4. The fractions containing PLL-PEG were pooled, dialyzed against water and lyophilized.

The PEGylated polycation was further modified with heterobifunctional N-succinimidyl 3-(2-pyridyldithio) propionate allowing subsequent coupling of DMMAn-Mel peptide via the N-terminal cysteine. PLL-PEG (0.313 μmol, containing 6.45 mg PLL) in 2 mL buffer (20 mM HEPES, pH 7.4) was mixed with SPDP (3.8 μmol, 1.19 mg) dissolved in 200 μl DMSO.

After 2 h at RT PLL-PEG with pyridyldithio-propionate-linkers (PLL-PEG-PDP) was purified by gel filtration using an Äkta Basic HPLC System (Amersham Biosciences, Freiburg, Germany) equipped with a Sephadex G-25 superfine HR 10/30 column (Pharmacia Biotech, Uppsala, Sweden) equilibrated in 0.5 M NaCl, 20 mM HEPES, pH 7.4; the flow rate was 1 mL/min. The fractions containing PLL-PEG-PDP were pooled, aliquots were snap frozen in liquid nitrogen and stored at -80 °C.

The PLL-PEG-PDP conjugate had a molar ratio of PLL/PEG/PDP of approximately 1/1/8.

Melittin peptide (1.38 μmol, 4 mg) (**Figure 2.5**) was dissolved in 400 μl of 100 mM HEPES and 125 mM NaOH and mixed with 1000μl ethanol containing 15.8 μmol (2 mg) DMMAn by rapid vortexing under argon for 0.5 h following concentration and purification via ultrafiltration (Vivascience, Vivaspin 2, MWCO 2000 HY). 1.38 μmol of the acylated Melittin was mixed under argon with 1.06 ml PLL-PEG-PDP (116 nmol PLL, 2.39 mg PLL, molar ratio of PLL/PEG/PDP of approximately 1/1/8) diluted in 2M guanidine hydrochloride, 0.5 M NaCl, 20 mM HEPES, pH 8. PLL-PEG-DMMAn-Mel conjugates were purified on the Äkta Basic HPLC System equipped with a Superdex 75 HR 10/30 column (Pharmacia Biotech, Uppsala, Sweden) equilibrated in 0.5M NaCl, 20 mM HEPES, pH 8. The flow rate was 0.5 mL/min. The void fractions containing PLL-PEG-DMMAn-Mel (molar ratio of PLL/PEG/DMMAn-Mel of approximately 1/1/8) were pooled and aliquots were snap frozen in liquid nitrogen and stored at -80 °C.
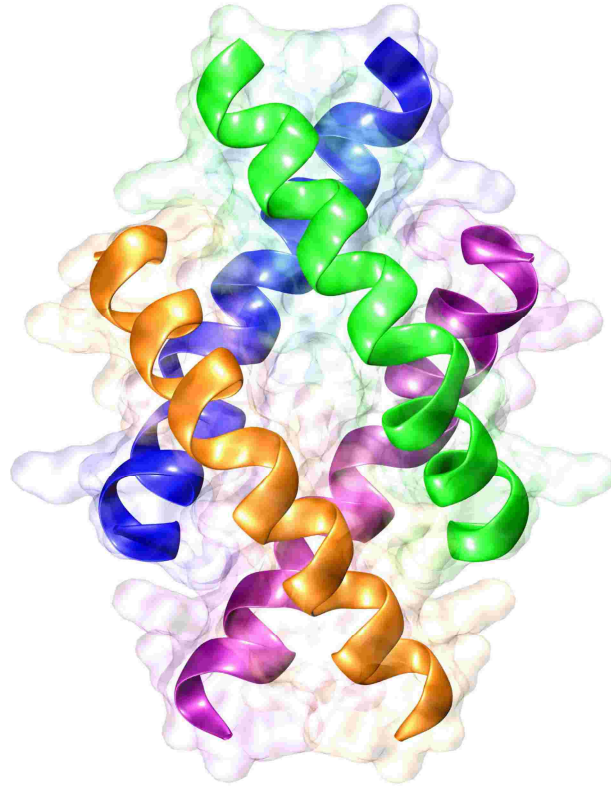
Figure 2.5

The 3-D tetrameric conformation of Melittin, courtesy of Fabrice David, SIB Geneva

From *http://www.uniprot.org/uniprot/P01501*

   The gelatin Melittin complex nanoparticles were also formed by using the previously formulated polysaccharide modified gelatin nanoparticles with cholamine coupling on its surface. The nanoparticles were loaded with siRNA at the same concentrations as for the PEI 25br assay (refer to 2.2.4 Polyethylene imine modification) in HBG buffer under ambient temperature and by intensive mixing with the pipette tip. Lastly, 0.5 µg PLL-PEG-DMMAn-Mel conjugate was added to each well to allow for the final nanoparticle sandwich formation. All samples were immediately transferred to the cell culture for transfection.

2.3 Analytics

2.3.1 Chemicals and reagents

Reagent	Description	Supplier
Acetic acid	6% (v/v)	Acros Organics (Morris Plains, USA)
Dimethylformamide		Acros Organics (Morris Plains, USA)
D_2O	99 % (v/v)	Euriso-Top (Gif-sur-Yvette, France)
Dulbeco's phosphate buffered saline	pH 7. (1x concentrate)	PAA Laboratories GmbH (Linz, Austria)
Ethanol	99 % + 1 % Isohexane	Merck KGaA (Darmstadt, Germany)
Ethidiumbromide		VWR International GmbH (Darmstadt Germany)
Hydrochloric acid	2 N	VWR International GmbH (Darmstadt, Germany)
$NaBH_4$		VWR International GmbH (Darmstadt Germany)
Sodium hydroxide	1 N	VWR International GmbH (Darmstadt Germany)
Starch	Soluble, p.a.	VWR International GmbH (Darmstadt Germany)
Tris buffer	Tris (hydroxymethyl) aminomethane	Merck KGaA (Darmstadt, Germany)
Tetramethylsilane	99.9 % (v/v)	VWR International GmbH (Darmstadt Germany)
Xylencyanol		AppliChem GmbH (Darmstadt, Germany)

2.3.2 Materials

Material	Description	Supplier
Cellulose	Regenerated (RC) MWCO 5 kDa	Postnova GmbH (Landsberg, Germany)
Cellulose	Regenerated (RC) MWCO 10 kDa	Postnova GmbH (Landsberg, Germany)
Glass capillary	1.6 μm i.d.	Anton Paar Inc (Ashland, USA)
Steel ball		Anton Paar Inc (Ashland, USA)

2.3.3 Asymmetric flow field-flow fractionation

2.3.3.1   Setup and function
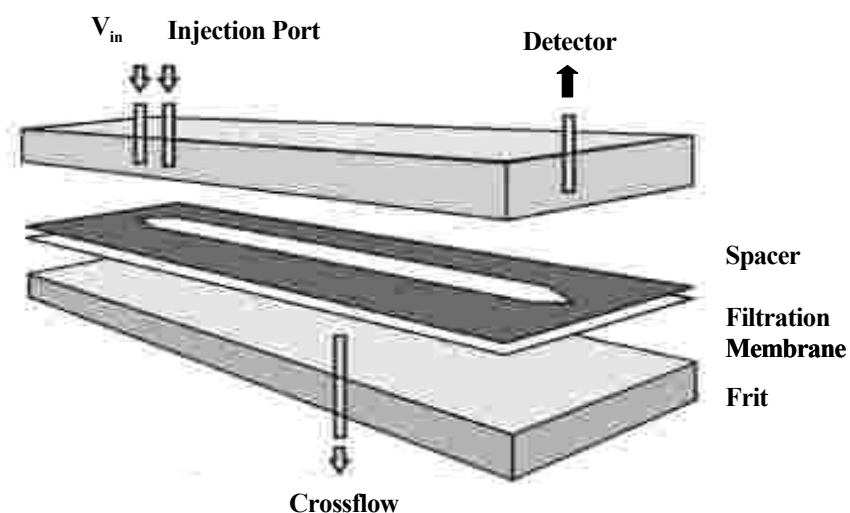
Figure 2.6

Exploded view into an AF4 separation channel. From top to bottom: upper non-permeable block, spacer (forming the channel, ultra-filtration membrane, solvent permeable frit inside the bottom block)

Figure 2.7

Basic setup of the used AF4 machine comprising from left to right: a computer unit, an autosampler with injection port, a degassing unit, the channel flow and cross flow pumps, the separation channel (in the front), RI, UV and MALS (not shown) detectors

In order to get a more detailed impression of the exact distribution of the gelatin molecules, which is important to guarantee uniform and therefore reproducibly transfecting nanoparticles, a modern separation technique like AF4 had to be used. The primary focus hence was to characterize the gelatin type A batch and to exclude suboptimal molar weight fractions that could potentially lead to extremely large and unstable nanoparticles. In a second analysis, the incorporation of DEAE-dextran into the nanoparticle matrix was examined by measuring a dextran and a nanoparticle sample and the final formulation.

The AF4 technique is based on a parabolic flow profile of the sample liquid inside a separation channel with an applied cross-flow to determine the retention time of the molecules. The general principle has been discussed and published elsewhere [Fraunhofer, W. et al. 2004].

2.3.3.2   Asymmetric flow field-flow fractionation of gelatins

The AF4 studies were performed using an AF1000-FOCUS system (Postnova, Landsberg am Lech, Germany) coupled with UV (UV100 Thermo Separation Products, Egelsbach, Germany) and refractive index (RI) detection (n-1000 WGE Dr. Bures, Germany) as well as a static light scattering (SLS) detector (Wyatt, Santa Barbara, USA) for molecular weight determination. The laser wavelength accounted for 690 nm, while slice collection was set to 1200. For molar mass determination the refractive index increment was set to 0.174 ml/g and the second virial coefficient was set to 0.

The separation was achieved using a PBS buffer pH 6.0 as mobile phase, a channel with 350 µm height and an ultra-filtration membrane consisting of regenerated cellulose with 5 kDa cut-off (Postnova). All proteins were dissolved in analysis buffer at a concentration of 2.5 %. The channel flow rate accounted for 1 ml/min, while the cross flow was adjusted to 0.05 ml/min over 10 minutes, and then reduced to 0 ml/min, which resulted in a total measurement period of 20 minutes.

Beside two hydrophobically modified gelatin prototypes (Gelita, Eberbach, Germany) called MS and MA, with succinate and dodecenylsuccinate residues, standard gelatin type A (Bloom ~175) from porcine skin (Sigma Aldrich, Munich, Germany) was analyzed in this

study. Hydrophobic succinylated (MS) and dodecenylsuccinylated (MA) gelatin samples used for comparison were kindly provided by Gelita AG (Germany).

2.3.3.3 Asymmetric flow field-flow fractionation of chitosans

The modification of the chitosan raw materials (Sigma) was conducted according to protocols described elsewhere [Bernkop-Schnuerch, A. B. et al. 2001; Bernkop-Schnuerch, A. B. et al. 2003]. Chitosan low viscosity modified with N-acetylcysteine (Sigma) (lyophilized), chitosan low viscosity modified with thiobutylamidine (Sigma) (lyophilized), chitosan low molecular weight modified with N-acetylcysteine (lyophilized), and chitosan low molecular-weight modified with thiobutylamidine (lyophilized) were investigated with the same AF4 hardware setup as for gelatin. The solvent for the chitosan samples as well as the running buffer were made of 0.3 M acetic acid, 0.2 M sodium acetate and sodium hydroxide / hydrochloric acid quantum satis. The pH was adjusted to 4.0 at a chitosan concentration of 0.1 %. A membrane consisting of regenerated cellulose with a cut-off of 10 kDa was used in a 350 μm separation channel. The detector's dn/dc was set to 0.163 ml/g and the second virial coefficient to 0. For chitosan the cross flow was set to 1.0 ml/min at a channel flow of 1.0 ml/min while the focus time amounted to 350 seconds. The complete measurement period was 25 minutes.

2.3.3.4 Molecular weight determination via AF4

In general, the determination of macromolecular size via AF4 is prone to several miscalculations due to the mathematical algorithms backing up the analysis software. For example, calculations, comparable to photon correlation spectroscopy, expect perfectly spherical molecules or particles for correct results. Furthermore, an overloading of the channel with sample or any interaction of the analytes with the membrane can lead to falsifications within the method. In case of charged analytes the factor of charge and charge related inter- and intra-molecular repulsion can also play a pivotal role. For those above reasons, one nowadays employs detectors that can determine the molecular weight directly, such as multi-angle light scattering detectors (MALS). Since theoretical descriptions of scattering phenomena of dissolved polymers and suspensions by Einstein [Einstein, A. 1910]

and Raman [Raman, C. V. 1928], light scattering has become the established method in polymer analytics. If the analyte is a macromolecule, the molecular weight can be extrapolated already with very few angles from the intensity at an angle of detection of $\theta=0°$. Very often the so called Zimm-equation [Wyatt, P. J. 1993] is used for this.

$$\frac{Kc}{R_\theta} = \frac{1}{M_w P_\theta} + 2A_2 c$$

Equation 1

With K being

$$K = \frac{4\pi^2 (dn/dc)^2 n_L^2}{N_A \lambda_0^4}$$

Equation 2

In most cases, the wavelength of the laser λ_0, the Avogadro number N_A and the refractive index of the solvent n_L should be easily available. The refractive index increment dn/dc is also known for many substances and can be determined before the measurement. The scattering function P_θ can also usually be disregarded for macromolecules, since below $\lambda_0/20$ the scattering is independent of the direction. A_2 as the second viral coefficient, defining the interaction between the solvent and the sample has of course to be determined before the actual measurement, but experience here shows that the value often is very small.

The intensity of the scattered light I_θ can hence be calculated with [Wyatt, P. J. 1993]:

$$R_\theta = \frac{(I_\theta - I_\theta^{LM}) \times r_{SD}^2}{I_0 \times V_S}$$

Equation 3

53

Here the scattering of the solvent I_θ has to subtracted, while further parameters are V_s as the scattering volume and r_{SD} as the distance between scattering volume and photo diode. Now in case of an angle dependent plotting of K_C/R_θ $1/M_W$ can be obtained on the ordinate, where M_W is the weight averaged molecular weight of the macromolecule. Since this M_W value represents only a fraction of the sample the M_W of the whole sample can be calculated according to Winter and Noll [Winter, R. et al. 1998] via the following formula:

$$M_N = \frac{\sum_i N_i M_i}{\sum_i N_i}$$

Equation 4

This formula can well be used to characterize disperse samples. After all, the channel of the AF4 is only relevant for the separation of the sample, while the determination of molecular weight and size is made with MALS and concentration detectors.

The relation between intrinsic viscosity [η] and molecular weight M_V is expressed in the so called Mark-Houwink-Kuhn-Sakurada (MHKS) equation [Berth, G. et al. 1998].

$$[\eta] = k_\alpha \times M_V^\alpha$$

Equation 5
Here k_α is the constant value and α is the exponent.

2.3.4 Lyophilization of chitosan nanoparticles

The solutions were deep-frozen and lyophilized, after adding 3.6 % (w/v) of trehalose as a lyoprotectant according to a method described by Loretz et al. [Loretz, B. et al. 2007].

2.3.5 Chitosan sulfhydryl-group and disulfide-bond quantification

The amount of sulfhydryl groups on thiolated chitosan was evaluated via an iodometric titration as described previously [Kast, C. E. et al. 2001]. In brief, 1 mg of the lyophilized thiomer was dissolved in 1 ml of highly purified water and the pH was adjusted to 1.5 by adding 1 M HCl. 150 µl of a 2 % solution of starch was added as the indicator. The solution was titrated by adding 9 µl of a 1 mM iodine solution until a persisting light blue color became visible. The sulfhydryl group content was calculated with the following equations: (**Equation 6, Equation 7**)

$$SH\ [\%] = \frac{V_{iodine} \times c_{iodine} \times M_r \times 2}{m_{thiomer}}$$

Equation 6

$$SH\ [\mu mol/g] = \frac{SH[\%]}{M_r} \times 10^4$$

Equation 7

The disulfide content was measured after reduction of the disulfide bonds with $NaBH_4$. 0.5 mg of thiomer were hydrated with 350 µl highly purified water in a 15 ml falcon tube for 30 min and then diluted with 150 µl of TRIS buffer. 1 ml of a 4 % $NaBH_4$ solution in highly purified water was added and the tube was incubated in an oscillating water bath at 37 °C for 1 h. The reaction was stopped by adding 200 µl 5 M HCl. Iodometric titration was performed as described above. Via subtraction of the result of the iodometric titration of the polymer itself from the result of the iodometric titration after reduction lead to the amount of disulfide bonds.

2.3.6 Automatic microviscosimetry

In a first step of the formulation process of uniform, small and stable nanoparticles, a detailed understanding of the viscosity of the used polymer solutions in respect to their inherent molecular weights plays an important role. Especially during the intercalation of gelatin and the polysaccharide DEAE-dextran molecules the success of the nanoparticle formation can depend on the correct viscosity of the final incubation mixture. In this context the microviscosimetry experiments were performed using an AMVn microviscosimeter (Anton-Paar, Ostfildern, Germany). In general the viscosity of a polymer liquid can be determined by examining the rolling time of a solid sphere under the influence of gravity in an inclined cylindrical tube filled with the sample liquid.
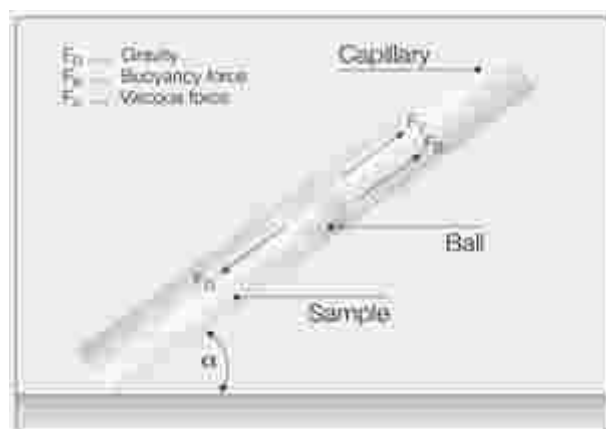
Figure 2.8

Principle of the viscosity measurement with the automatic microviscosimeter based on the principle of a rolling steel ball in an inclined capillary filled with the sample.

From *http://www.anton-paar.com/001/de/Web/Document/download/1648?clng=de*

A calibrated 1.6 µm glass capillary was used together with a 1.5 µm steel ball (**Figure 2.8**). At a reference temperature of 25 °C the steel ball density was determined with 7.6327 g/cm^3, while the internal system settings where a temperature adjusting time of 120 seconds (tolerance $\pm$ 0.03 K), a sample volume of 400 µl and a measurement length of 100 mm. To ensure a constant temperature within the samples a built-in peltier thermostat was used

throughout the measurements. All calibration and sample measurements were conducted using the Rheoplus/32 V3.21 software (Anton-Paar, Ostfildern, Germany) and repeated three times. The viscosity was then calculated using the laws of Stoke (**Equation 8**).

$$F_r = 3 \times \pi \times \eta \times d \times v$$

Equation 8

Here F_r is the frictional force, η the sample viscosity, d the capillary parameter and v the velocity of the steel ball within the sample over a given distance and inclination angle. The molecular weight was approximated (according to DIN 53015 and ISO 12058) with the *Mark-Houwink* or *Staudinger* equation. Here the molar mass was calculated as

$$M = (\frac{\eta}{K})^{\frac{1}{\alpha}}$$

Equation 9

with K being parameter K, η standing for viscosity and α for the *Staudinger* index. The needed relative viscosity η_r was calculated via

$$\eta_r = \frac{t}{t_0} \text{ and } \eta_r = \frac{\eta}{\eta_0}$$

Equation 10

For the quintessential K-value the following equation was used

$$K = 1000 \cdot \frac{b - 1 + \sqrt{1 + (\frac{2}{\beta_L} + 2 + b) \cdot b}}{150 + 300 \cdot \beta_i}$$

Equation 11
where $b = 1.5 \cdot \log(\eta_r)$

Using these formulas the molecular weight of gelatin type A and type B (for comparative reasons) was calculated, as well the viscosity of the employed DEAE-dextran. The polymers were measured at different concentrations according to their respective final concentrations during the manufacturing process of the nanoparticles. In short, gelatins were measured at 5.0 % (w/w), 2.5 % (w/w) and 0.25 % (w/w) while the highly viscous DEAE-dextran was measured at 0.25 % (w/w).

2.3.7 Photon correlation spectroscopy

The nanoparticle size was determined by dynamic light scattering using a Zetasizer Nanoseries Nano-ZS (Malvern Instruments Ltd., Worchestershire, UK) for backscatter measurements. The refractive index for the nanoparticles was set to 0.90, and the absorption index to 0.01, according to the established optical model. The refractive index for the dispersant was set to 1.333, corresponding to water. The Zetasizer device was equipped with a laser source operating at 405 nm wavelength.

2.3.8 Electrophoretic mobility measurements

The zeta potential of the nanoparticle formulations was determined by electrophoretic light scattering using a Zetasizer Nanoseries Nano-ZS (Malvern Instruments Ltd., Worchestershire, UK). For the measurements the dielectric constant (τ) was set to 78.48 (pure water at 25 °C). The optical parameters – refractive index and absorption index, for nanoparticles were set to correspondingly 0.90 and 0.01. The applied voltage value was set to 40 V and the monomodal analysis model was used. Measurements were carried out in triplicate for each sample. Data was processed using Dispersing Technology Software v.5.10 (Malvern Instruments Ltd., Worchestershire, UK). Disposable flow-through cells in highly purified water or phosphate buffered saline at a pH of 7.0 were used in order to get most valid results. To assess the general stability of the gelatin nanoparticle and dextran gelatin nanoparticle formulations, all samples were stored at room temperature and at 4 °C in 2 ml Eppendorf vials over a time period of 6 months with a temperature control on a daily basis. Samples were drawn from the storage at different time intervals and were analyzed visually for signs of sedimentation and

aggregation. The size distribution in this case was also analyzed by DLS as described above (refer to 2.3.7 Photon correlation spectroscopy).

2.3.9 Static light scattering spectroscopy

Laser diffraction measurements, also known as low angle light scattering, Fraunhofer diffraction or Mie scattering, were performed using a Partica LA-950 (Horiba Ltd., Kyoto, Japan), equipped with a blue LED laser source, operating at a wavelength of 405 nm, and a red laser source, operating at 650 nm. The measurement range of the device was from 40 nm up to 3 mm. The laser diffractometer was equipped with quartz cuvettes with volumes of 15 ml and 10 ml and a magnetic stirring facility. An optical model was produced and data processing was carried out using the software Horiba LA950 v.5.00. The iteration value was set to 15 for all measurements, a refractive index of 1.59 (i_{abs}=0.01) and highly purified water as the dispersion medium were used [Chu, B. et al. 2000]. The nanoparticle formulations were sampled immediately prior to measurements by addition of 20-100 µl undiluted nanoparticle dispersion into the dilution medium, highly purified water, under continuous stirring. Basically the static light scattering was used for verification of the DLS results and to monitor potential larger aggregates more detailed.

2.3.10   Nuclear magnetic resonance spectroscopy

Nuclear magnetic resonance is based on the interaction between the magnetic momentum of the atom nucleus and a homogeneous and static external magnetic field around the nucleus [Hesse, M. et al. 1984]. ^{1}H-NMR spectroscopy was performed using a JEOL JNM Eclipse 400 spectrometer (JEOL GmbH, Eching, Germany) ([1]H: 400 MHz). The chemical shift was given as σ values in ppm. Tetramethylsilane (TMS) was used as an internal standard (σ = 0.00 ppm) and all measurements were carried out at 50 °C in deutered water as the solvent.

For all ^{1}H-NMR measurements 1 g of sample was diluted in 5 ml 20 (w/w) or 100 (w/w) D_2O. Before filling, the NMR-tubes with prewarmed samples, the NMR tubes were tempered 1 h in the cabinet drier at 50°C and kept at 50°C during the filling process using a blow drier. The samples were measured directly after the filling process.

2.3.11   Scanning electron microscopy

The modified gelatin and chitosan nanoparticles were analyzed by SEM to characterize the surface morphology of dry, non-dispersed nanoparticles. The analysis was made with a field emission scanning electron microscope (JSM-6500 F, JEOLl, Ebersberg, Germany) at 5.0 kV and a working distance of 9.7 mm. For sample preparation nanoparticles were dispersed in acetone at a concentration of 20 µg/mL and applied on a specifically polished sample grid. The samples were vacuum-dried over 12 hours and finally metallized with a 2 nm gold layer before microscopical analysis.

2.3.12   siRNA loading determination via ultra-violet-absorption

For siRNA loading of the nanoparticles, the respective nanoparticle dispersion was adjusted to a certain concentration in different loading media. HEPES buffered glucose (HEPES) pH 7.0, PBS pH 7.0, PBS pH 7.5 and highly purified water were used for the loading studies. The nanoparticles were incubated with the respective amounts of siRNA and incubated on a thermomixer for 30 minutes at 26 °C. In order to quantify the amount of loaded siRNA the batches were centrifuged at 18.000 g for 1 hour and potential free siRNA was determined in the supernatant by UV-spectrometry. The weight to weight amount of loaded siRNA was calculated from unbound siRNA determined UV-spectrophotometrically at a wavelength of 260nm (UV1, Thermo Spectronic, Dreieich, Germany) in the supernatant of the reaction media after separating the nanoparticles by centrifugation for 50 min at 14000 g (neo lab 16/18, Hermle Labortechnik GmbH, Wehingen, Germany). In addition blanks of siRNA and gelatin nanoparticles alone were prepared accordingly.

2.3.13   siRNA loading determination via gel shift assay

For the quantification of the siRNA loading with the gel shift assay the siRNA was diluted to 0.25 µg/µl = 20 µM with siRNA buffer solution. Both siRNAs, the GL3 siRNA and the control siRNA, were checked on correct dilution with photometer read-out. Nanoparticles were dispersed in the correct amount of medium, siRNA was added and the dispersion was incubated on a thermomixer at 650 rpm and 26 °C for 30 minutes. Agarose gels were

prepared from 3.0 g agarose to 120 g TBE buffer one minute in the microwave when 4 µl ethidiumbromide (Sigma) 1:1000 was added. Sedimentation buffer was made from 0.5M EDTA (pH 8.0), Glycerine 100 %, MQ water (sterile) and xylencyanol and was added to each vial, which were then vortexed shortly. The vials were centrifuged and the whole content of all vials was inserted into the respective gel bags. To start the electrophoresis a voltage of 120 V was applied to the chamber for 40 minutes. Values are given as relative light units (RLU) per 10,000 seeded cells as mean +/- standard deviation of at least triplicates. 2 ng of luciferase corresponds to 10^7 light units.

2.3.14 Characterization of Melittin complexes

The size distribution and polydispersity of all nanoparticles was analyzed in aqueous dispersion by dynamic light scattering (refer to 2.3.7 Photon correlation spectroscopy). Each size value and the corresponding polydispersity index was the mean of 10 subruns. Static light scattering was used for verification of the DLS results. All experiments were conducted on a LA-950 laser diffractometer with a refractive index of 1.59 (i_{abs}=0.01) and highly purified water as the dispersion medium (refer to 2.3.9 Static light scattering spectroscopy). The zeta potential of the nanoparticles was measured with the Zetasizer Nano and flow through cells in highly purified water or phosphate buffered saline at a pH of 7.0 (refer to 2.3.8 Electrophoretic mobility measurements).

2.3.15 Confocal laser scanning microscopy

The cells and fluorescent nanoparticles were observed by fluorescence confocal laser-scanning microscopy using a Zeiss LSM 510 (Carl Zeiss Microimaging, Göttingen, Germany). A pinhole of 204 µm was exerted with a 63x oil-immersion objective producing optical slices of about 700 nm. The excitation and emission wavelengths used are represented in **Table 2.2**.

2.3.16   Endotoxin assay

The gelatin nanoparticles and modified gelatin nanoparticles tested in the *in-vitro* and *in-vivo* experiments were analyzed for their endotoxin content after the final formulation step. The samples were collected and sent to Lonza Verviers SPRL, Verviers, Belgium. The samples have been diluted 1/100 and 1/1000 and tested with the Limulus amebocyte lysate (LAL) kinetic chromogenic assay (method D described in the section 2.6.14 of the European Pharmacopoeia). The final results are expressed in endotoxin units per milliliter (EU/ml). Each sample is tested with a positive product control (PPC) of 0.5 EU/ml. If the endotoxin recovery is between 0.25 and 1.0 EU/ml (50-200 % of the PPC), the result is valid.

2.3.17   Determination of process yield

The process yield of gelatin nanoparticles was determined as the weight percentage of the final product after drying, with respect to the total amount of polymer and other materials used for the preparation.

2.3.18   Storage conditions during stability studies

To assess the general stability of the gelatin nanoparticle and dextran gelatin nanoparticle formulations all samples were stored at room temperature (RT) and 4 °C in 2 ml Eppendorf vials over a time period of 6 months. Samples were drawn from the storage at different time intervals and were analyzed visually for signs of sedimentation and aggregation. The size distribution was analyzed by DLS. In addition, the influence of the siRNA loading process on zeta potential and nanoparticle size increase were as well monitored by DLS and electrophoretic mobility measurements. Last but not least, the stability of the loaded siRNA molecules over time was examined. Finally for the loaded nanoparticles the colloidal stability of the formulations as well as the loading stability against changing electrolyte concentrations and different pH values was investigated.

2.4 In-vitro models

2.4.1 Cell culture

2.4.1.1   Chemicals and reagents

Reagent	Description	Supplier
Accutase		Invitrogen Inc. (Carlsbad, USA)
Cell Tracker™ Orange CMRA		Invitrogen Molecular Probes (Carlsbad, USA)
Dulbeco's modified eagle medium	pH 7.0-7.5	GIBCO/Invitrogen Ltd., (Paisley, England)
ECGM	Endothelial cell growth medium	GIBCO/Invitrogen Ltd., (Paisley, England)
Fetal calf serum		PAA Laboratories GmbH (Linz, Austria)
Formaldehyde solution	4 % (v/v)	VWR International GmbH (Darmstadt Germany)
Glutamine		Invitrogen Inc. (Carlsbad, USA)
Hoechst 33342 trihydrochloride trihydrate	10 mg/ml	Invitrogen Molecular Probes (Carlsbad, USA)
Lipofectamine		Invitrogen Inc. (Carlsbad, USA)
Optimem		Invitrogen Inc. (Carlsbad, USA)
Penicillin		Invitrogen Inc. (Carlsbad, USA)
scVEGF-Cy 5.5		Sibtech (Newington, USA)
Streptomycin		Invitrogen Inc. (Carlsbad, USA)

Trypan blue stain	0.4 % (v/v)	GIBCO/Invitrogen Ltd., (Paisley, England)
Trypsin-EDTA-solution	1x concentrate	PAA Laboratories GmbH (Linz, Austria)

2.4.1.2   Materials

Material	Description	Supplier
Cell culture flask	T75	Sigma Aldrich Inc. (St. Louis, USA)
ibiTreat µ-slides y-shaped		Ibidi GmbH (Munich, Germany)
ibiTreat µ-slides 8 well		Ibidi GmbH (Munich, Germany)

2.4.1.3 Cell lines

Cell Line	Specifications	Distributor	Source
Neuro2A-eGFPLuc	Mouse neuroblastoma stably expressing luciferase; (ATCC CCl-131)	Gift of Prof. Dr. E. Wagner, (University of Munich, Germany)	[Meyer, M. et al. 2008]
KDR/293	<u>Expressing transgene:</u> Full-length human VEGF receptor VEGFR-2 (KDR/Flk-1) <u>Derivatives of:</u> 293 Human kidney embryonic cells transformed with adenovirus 5 DNA (ATCC CRL-1573)	Sibtech Inc. (Newington, USA)	[Backer, M. V. et al. 2001]
HEK/293	Human adherent hypotriploid cells transformed with adenovirus 5 DNA	GIBCO/Invitrogen Ltd. (Paisley, England)	[zur Hausen, H. 1967]

2.4.1.4 Cultivation of cell lines

Cell culture media, antibiotics and fetal calf serum were purchased from Invitrogen Inc. (Carlsbad, USA). All cultured cells were grown at 37 °C in 5% CO_2 humidified atmosphere in sterile T75 cell culture flasks. Neuro2A-eGFPLuc cell line (mouse neuroblastoma stably expressing luciferase) were cultured in DMEM (1 g/L glucose) containing 10% fetal calf serum, 100 U/ml penicillin, 100 µg/ml streptomycin and 2mM glutamine. KDR/293 and HEK/293 cells were cultured in DMEM (1 g/L glucose) containing 10% fetal calf serum. Cells were split on a routinely basis every 3 days at a ratio of 1:10. Therefore the cells were washed three times with 10 ml sterile PBS (Invitrogen) and detached from the flask bottom by incubation with 1.5 ml trypsine-EDTA (Invitrogen) for 3 min. Trypsination was stopped by adding 9 ml DMEM + 10% FCS. Now, 1 ml of the cell suspension was transferred to a new cell culture flask and gently mixed with 9 ml fresh medium. Dead cells were distinguished under the microscope by staining with 0.4 mg/ml trypan blue while un-stained healthy cells were counted with a modified Neubauer chamber. The cell concentration was adjusted according to each experiment using the correct amount of DMEM.

2.4.1.5 Particle stability in cell culture medium

The influence of the ingredients of the cell culture medium on nanoparticle size and zeta potential and also on the aggregation and hence colloidal stability was measured using the Zetasizer Nano ZS (Malvern, UK) as described above (refer to "2.3.5 Photon correlation spectroscopy and 2.3.6 Electrophoretic mobility measurements"). For this purpose 50 µl of a 1.0 mg/ml nanoparticle dispersion was incubated with 1 ml of DMEM for 1, 5, 10, 20, 30 and 60 min. Measurements were conducted right after the respective end time points.

2.4.1.6 Metabolic activity of luciferase silenced cells

Cells were grown in 96-well plates and treated with different amounts of loaded nanoparticles as follows. The metabolic activity was determined using an MTT assay. To each well 10 µl of a 5 mg/ml solution of MTT in sterile PBS buffer were added. Cells were incubated at 37 °C for 2 h, the medium was removed and the samples were frozen at − 80 °C

for at least 2 h. 100 µl of DMSO was added and samples were incubated at 37 °C for 30 min under constant shaking. The optical absorbance of thiazolyl blue was measured at 590 nm (reference wavelength 630 nm) using a microplate plate reader (Spectrafluor Plus, Tecan Austria GmbH, Grödig, Austria) and cell viability was expressed as a percent relative to untreated control cells. The results are presented as means of n = 3.

2.4.1.7 Cytotoxicity via microscopic observations

After incubation with polymers or polyplexes, changes in morphology and detachment of cells from the well plate were observed using a Zeiss Axiovert 200 microscope (Carl Zeiss AG, Oberkochen, Germany).

2.4.2 Flow model

Establishing the in-vitro model

For the interaction studies with endothelial cells, we had to come up with a completely new system, allowing for **nea**r **to p**hysiological (**NEATOP**) cell growth and monitoring conditions. With the newly developed surface plasma treated ibidi slides (ibidi GmbH, Martinsried, Germany) such cell adhesion and growth under medium flow conditions was possible, while at the same time the material guaranteed optimal fluorescent analysis capabilities.
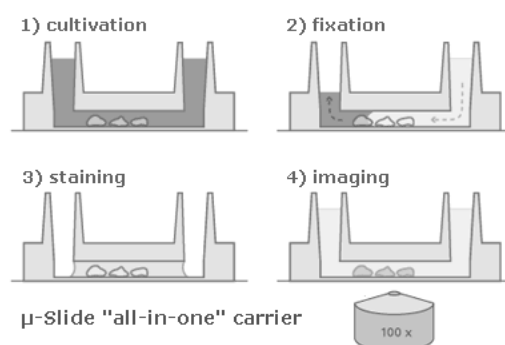
Figure 2.9

Adherent cells are cultivated inside the µ-slide under flow (1), fixed with formaldehyde (2), stained with fluorescent dyes (3) and analyzed in an inverted confocal laser scanning microscope
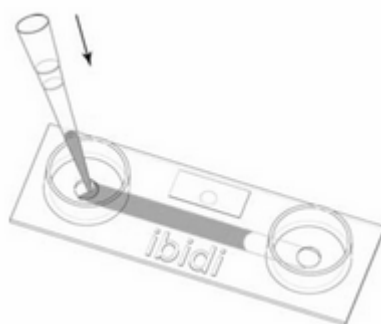
Figure 2.10

Filling of an ibidi µ-slide channel

For the experiments, 8.8 x 10^4 human umbilical vein cells (HUVECs) were seeded in a plasma surface treated y-shaped plastic µ-slide channel (IBIDI, Martinsried, Germany) (**Figure 2.9**, **Figure 2.10**). The height of the channel was given with 4.0 µm while the channel growth area was 2.8 cm². After five days of cultivation in Endothelial Cell Growth Medium (GIBCO, Karlsruhe, Germany) under permanent flow in an incubator (37°C, 5% CO_2) the cells were incubated with cationic and neutral nanoparticles for 60 minutes, with a media flow of 7 ml/min.
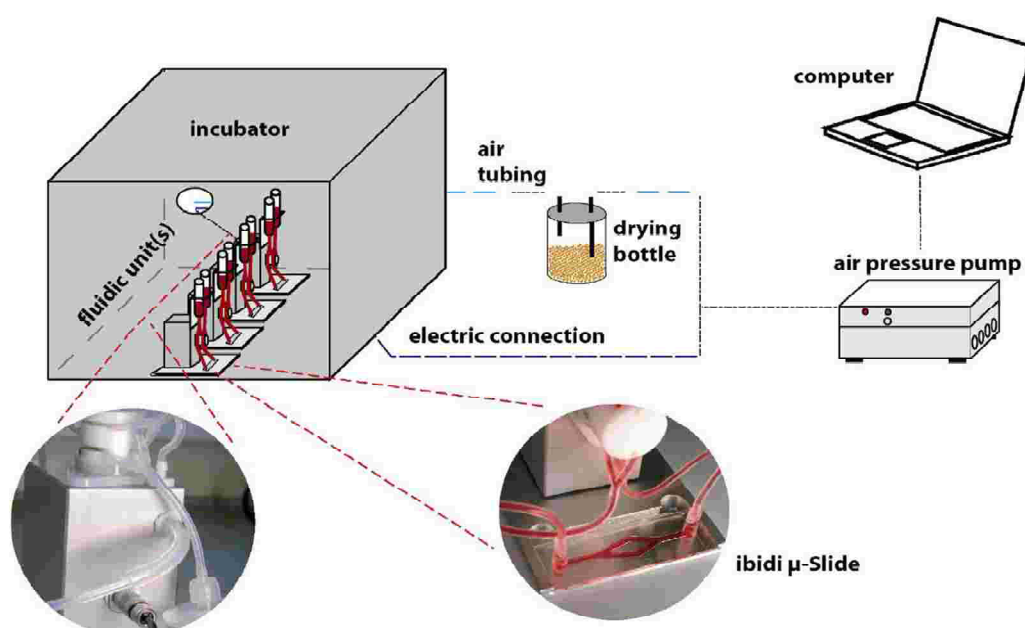
Figure 2.11

Exploded view of the nanoparticle cell flow system

The whole setup is depicted in **Figure 2.11**. With the computer software and a highly precise air pressure pump connected via sterile air tubings to the slides inside the CO_2 incubator the flow velocity and direction inside the ibidi μ-slide can be regulated.

Following fluorescent staining with Hoechst 33342 and Cell Tracker Orange CMRA (both Invitrogen, Karlsruhe, Germany) and two washing steps with buffer, the cells were analyzed with a confocal laser scanning microscope (Zeiss LSM 510, Göttingen, Germany). Image processing was done with Zeiss LSM Image Browser software 4.0. During the cell incubation, all chambers were analyzed microscopically to ensure that cells were in good health and did not show any aggregates, debris or other visible signs of contamination. The cell supernatants were tested for mycoplasmal contamination routinely, according to a standardized protocol at the Department of Pharmaceutical Biology, University of Munich, Germany.

Figure 2.12

The flow model was validated in order to determine the optimal operation conditions and to ensure reproducibility of the results.

2.4.3 Fluorescence activated cell sorting analysis of VEGFR expression

The 293 KDR cells for our experiments were meant to over-express the VEGF Receptor 2 (VEGFR$_2$) as a model cell monolayer for nanoparticle targeting and siRNA delivery against the VEGFR$_2$. VEGFR$_2$ [also known as KDR (kinase insert domain receptor) in humans or Flk-1(fetal liver kinase-1) in mice], is a member of the class III subfamily of receptor tyrosine kinases (RTKs) that also includes VEGFR$_1$ (Flt-1) and VEGFR$_3$ (Flt-4). All three receptors contain seven Ig-like repeats within their extracellular domains and kinase insert domains in their intracellular regions. The expression patterns of VEGFR$_1$, VEGFR$_2$, and VEGFR$_3$ are almost exclusively restricted to endothelial cells. These VEGF/VEGFR$_2$ signalling pathways play an important role in tumor angiogenesis and other diseases where "pathological angiogenesis" is involved. Inactivation of functional VEGFR$_2$ by a blocking antibody can disrupt angiogenesis and prevent tumor cell invasion [Skobe, M. et al. 1997; Brekken, R. A. et al. 2000]. Angiogenesis induced by the HIV-1 Tat protein is mediated by VEGFR$_2$ on vascular endothelial cells [Albini, A. et al. 1996]. Tat specifically binds and activates VEGFR$_2$. Tat-induced angiogenesis is blocked by agents that can block VEGFR$_2$.

FACS analysis was done in a FACSCalibur (Becton Dickinson, Franklin Lakes, USA). FACS analysis was conducted under assistance of Tanja Lange at Medigene AG (Munich, Germany). The quantification of VEGFR$_2$ was done by using single chain scVEGF-Cy5.5. For this reason HEK 293/KDR cells and HEK 293 control cells were plated at a number of 250.000 cells in DMEM cell culture medium in 75 cm² cell culture flasks and grown to 40 % confluence. The cells were detached with 3 ml accutase, set to a concentration of $5x10^5$ cells per FACS tube and incubated for another 60 minutes with scVEGF-Cy5.5 (1:100) before measuring 50,000 cells in FACS gate 4.

For a comparative study of the knock-down capacity of a lipid based "gold standard" transfection reagent, we consequently did a siRNA based transfection and FACS read-out using our VEGFR2 siRNA and Lipofectamine RANiMAX. For this experiment 250 µl of Opti-MEM reduced serum medium were pipetted into a sterile Eppendorf cap and mixed gently with 5 µl Lipofectamine RNAiMAX (Invitrogen?). 15 µl of a 30 pm siRNA solution were incubated with 250 µl Opti-MEM reduced serum medium and transferred to the

Eppendorf caps containing the Lipofectamine. To each well with cells 500 µl of the siRNA Lipofectamine RNAiMAX complex were added resulting in a final volume of 3 ml and a final RNA concentration of 10 nM. The cells were incubated for 24h, 48h and 72h at 37 °C in a CO_2 incubator until ready to assay for gene knockdown. At the respective time points the cells were detached with 3 ml accutase, set to a concentration of $5x10^5$ cells per FACS tube and incubated for another 60 minutes with scVEGF-Cy5.5 (1:100) before measuring 50.000 cells in FACS gate 4.

2.4.4 Coulter counter analysis of blood cells

The concentration of different blood cells after nanoparticle application was measured with a Beckman Coulter counter (A°T-Series, Beckman, Krefeld, Germany). Samples were drawn directly through a catheter at different time points from 0 to 90 minutes after nanoparticle infusion. In detail, white blood cells and thrombocytes and haemoglobin (photometrically) were assayed with this method. Again, all measurements were conducted in triplicate.

2.5 In-vivo models

2.5.1 Chemicals and reagents

Reagent	Description	Supplier
Cutasept®	72% (v/v) ethanol	Bode Chemie (Hamburg, Germany)
Ketavet®	Ketamine hydrochloride	Pharmacia GmbH (Karlsruhe, Germany)
Pilca® med Cream		Asid Bonz GmbH (Bieblingen, Germany)
Rompun®	Xylazine hydrochloride	Bayer (Leverkusen, Germany)

2.5.2 Hamster dorsal skin fold chamber model

The surgical work demonstrated in this section was undertaken under the scientific supervision of Dr. med. Martin Eichhorn (Walter-Brendel-Center, Munich, Germany) and Siiri Lüdemann (Walter-Brendel-Center, Munich, Germany).

Animal model

The animals for these experiments were Syrian gold hamster from Charles River Laboratories (Sulzfeld, Germany). A maximum of 3 animals were hosted in a cage with free access to water and standard laboratory animal chow (Sniff, Soest, Germany) at an ambient temperature of 24 °C and a relative air humidity of 50 % (v/v). The artificial light cycles consisted of 12 h light/dark intervals. The median body weight of the animals was 60 g (55-65 g) for the hamster dorsal skin fold chamber model. During the experiments the animals were kept in single animal cages under the same surrounding conditions as mentioned before. After surgical implantation of the hamster skin fold chamber, the animals were temporarily held in an intensive care incubator (Model 7510, Drägerwerk AG, Lübeck, Germany) at 32 °C and a relative air humidity of 70 % (v/v).

Surgical preparation

In order to judge the nanoparticle accumulation and microcirculation within the tumor and within the endothelial vessel regions, a transparent dorsal skin fold chamber as developed by [Endrich, B. et al. 1980; Asaishi, K. et al. 1981] was implanted into the hamsters.

In detail, a laterally inversed titanium frame with a central circular opening for reasons of observation was used for this purpose and implanted in the double folded dorsal skin area of the hamster (**Figure 2.13**). One side of the skin was completely removed by surgical means allowing visual access to the vessel bearing tissue region. Therefore the animals were anaesthetized by intraperitoneal injection of 100 mg/kg ketamine hydrochloride and 10 mg/kg xylazine hydrochloride and the dorsal hair was removed through manual and chemical depilation using razor blades and Pilca®-med cream. The now hair-free dorsal skin was cleaned with 72 % (v/v) ethanol and knitted to the top of the titanium frame. In the following

surgical step the complete dermis and subcutaneous connective tissue were removed with micro-surgical instruments giving view to the contra-lateral side with skin muscle and supplying vessels. The circular opening again was covered with a coverslip (diameter 11.8 mm, thickness 1 mm) (Edgar Hefele Medizintechnik, Munich, Germany) and fixed with a ferrule. Distance nuts were used at an offset of 4 mm to avoid any compression of the folded tissue. The chamber halves were fixed to the skin of the hamster with screws and stitches.
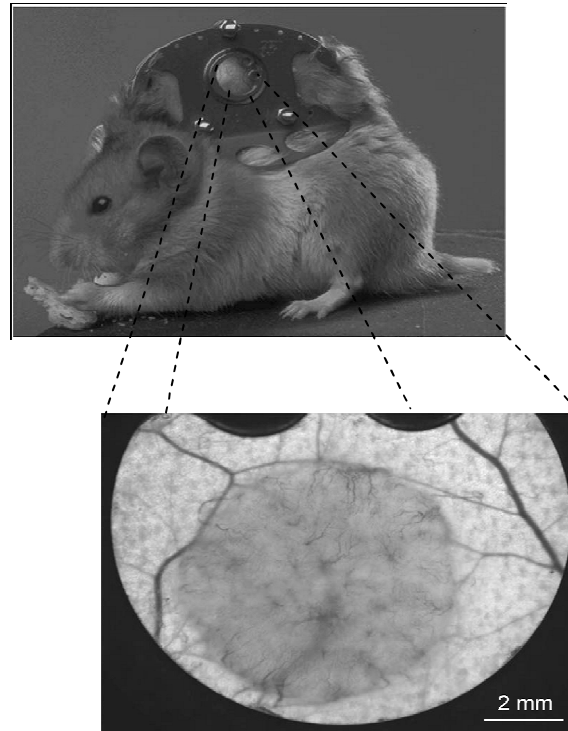
Figure 2.13

Anatomical model of a prepared hamster skin fold chamber (top); microscopic view of the chamber window with an inoculated, well vascularized tumor (bottom); pictures kindly provided by Claudia Nussbaum [Nussbaum, C. 2008]

Criterion for exclusion

The animals tolerated the dorsal skin fold chamber after a two to three day phase of reconstitution very well and did not show any signs of behavioural anomalies. Animals however, that lacked species-like normal behaviour, showed loss in weight or a lack of reaction on external stimuli were excluded from further studies.

The chambers were examined macroscopically and microscopically and in case of traumata, air inclusion or general signs of inflammation, edema, another criterion for exclusion was fulfilled.

Venous access

One day before the nanoparticle injection the animals received a catheter into the right *vena jugularis interna*. Therefore the animals were anesthetized as described above and after cranial ligation of the vessel with silk (Perma Handseide, Ethicon, Nordstedt, Germany) and incision a polyethylene catheter (PE 10, 0.28 mm ID, Portex, Hythe, UK) was inserted and fixed. Until the day of the experiment, the distal end of the catheter was rolled up and secured with Leukosilk (3M Health Care, Neuss, Germany).

2.5.3 Mouse cremaster model

The following experiments at the mouse *musculus cremaster* (*m. cremaster*) were conducted under supervision of Professor Fritz Krombach, Ph.D. (Walter-Brendel-Center, Munich). The surgical preparation of the *m. cremaster* was kindly done in close cooperation with Peter Bihary (Walter-Brendel-Center, Munich).

The mouse cremaster model is a well established model within the international scientific literature for the investigation of the microcirculation [Thorlacius, H. et al. 1997]. From an anatomical point of view the *m. cremaster* is embedded in the *fascia cremasteria* and part of the lower part of the *m. obliquus internus abdominis* and the *m. transverses abdominis*. For our experiments the micro-surgical preparation the *m. cremaster* was done according to the first time description of Baez [Baez, S. 1973] with some slight modifications. The advantages of the *m. cremaster* model are its characteristic morphology. An almost two-dimensional vessel architecture combined with a high vessel density when analyzed with modern intra-vital microscopic techniques allows for the non-overlapping imaging of anatomical structures, blood flow and even single cells [Reichel, C. A. 2008].

Animal models

For the intra-vital studies of nanoparticle flow and interaction behaviour within the mouse *musculus cremaster*, male wild type (WT) C57BL/6 mice (Charles River, Sulzfeld, German) were used. The mice had an average body weight 25 to 35 g and were housed under controlled day and night light cycles in groups of 3 to 5 animals in Makrolon cages. They had free access to war and standard laboratory mice chow (Sniff Spezialdiäten, Soest, Germany).

Narcotisation

During spontaneous breathing the animals were anaesthetized with ketamine and xylazin. In detail, the narcotization was initiated by intra-abdominal injection of a mixture of ketamin (100 mg/kg) and xylazin (10 mg/kg) and was kept pending during he whole examination with repeating injections of ketamin (100 mg/kg). The body temperature of the animals during surgical preparation and during the experiments was kept constantly at 37 °C by fixation on a medical heating plate.

Surgical preparation of the musculus cremaster

The surgical preparation of the *m. cremaster* was exercised under a surgeon microscope (Leitz, Wetzlar, Germany) using a 5 − 42x magnification and with slight modifications to the first time description of Baez [Baez, S. 1973]. In brief, after initiation of the anaesthetization, and insertion of a cannula into the *arteria femoralis* with a polypropylene-catheter (ID 0.28 mm, Portex, Lythe, United Kingdom), the right testicle was exposed by ventral incision of the scrotum (**Figure 2.14**). Now, using an electro-cauther the *m. cremaster* was carefully ventrally opened in a region of low blood vessel density and strapped over a special stage. The testicles themselves were separated from the *m. cremaster* and put back into the abdominal cavity. During this whole process, the muscle was superfunded with warm buffered saline solution.
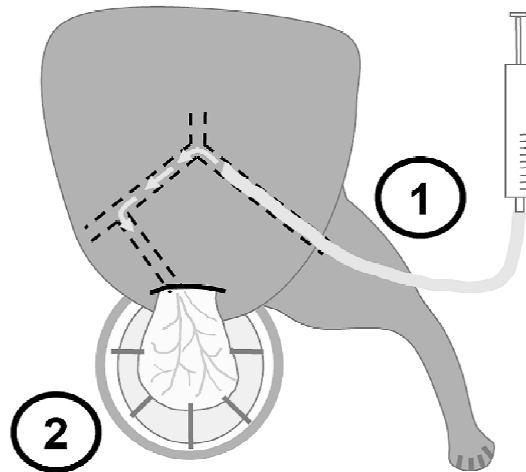
Figure 2.14

Simplified view of the preparation of the *m. cremaster* in the mouse: (1) canuled left *arteria femoralis*, (2) stretched *m. cremaster* within the superfusate [Reichel, C. A. 2008]

Intravital microscopy

All intravital microscopic examinations were done on an Olympus BX 50 microscope (Olympus, Hamburg, Germany). The light source was a 75 W xenon lamp equipped with a fluoresceine-isothiocyanate filter-block that consisted of dichroic filters and emission filters (DCLP 500, LP515, Olympus, Hamburg, Germany). Special care was put on setting the light exposure times as low as possible in order to minimize phototoxic effects during the fluorescence microscopy [Steinbauer, M. et al. 2000].

For the nanoparticle experiments, at first, cationic gelatin nanoparticles labeled with 0.1 mg/ml Alexa 488 and dispersed in 10.5 % trehalose solution were prepared. A second mouse was treated with 1:10 of the same batch and a volume of 200 µl over a time period of 20 seconds. In a second approach neutral gelatin nanoparticles labeled with rhodamin lissamine in PBS/Tween (5 % w/w) were tested. Furthermore two cremaster models received a total of 800 µl of a 5 mg/ml nanoparticle dispersion. Neutral gelatin nanoparticles labeled with Alexa 488 suspended in PBS/Tween (5% w/w) were applied to a cremaster mouse. The particles were diluted 1:10 to a final concentration of 0.5 mg/ml of which 100 µl were injected i.a.

2.5.4 Mouse arthritic knee model

Antigen-induced arthritis (AIA) in mice is histologically and immunologically well characterized and is one of the most useful models in the understanding of rheumatoid arthritis (RA) [Brahn, E. 1991]. AIA permits an exactly defined time course of arthritis in the affected joint (typically the knee joint; **Figure 2.15**), with inflammation characterized by hyperplasia of the synovial lining layer and cell infiltration. These abnormalities reach a maximum on day 7 [Simon, J. et al. 2001], the time point which was therefore chosen for imaging. Although it is impossible to determine a disease-specific antigen expressed in joints only in the context of arthritis, macrophages are believed to play an essential pathophysiologic role at a local level, with presentation of antigens and production of tissue-degrading enzymes and mediators of inflammation [Berg van den, W. B. et al. 1996; Hansch, A. et al. 1996; Bresnihan, B. 1999; Kinne, R. W. et al. 2000].
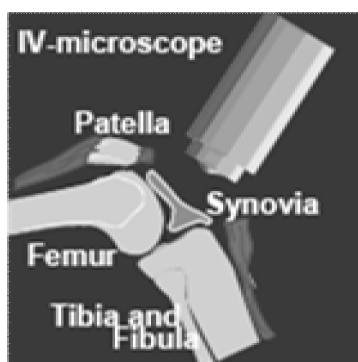
Figure 2.15

Analysis of the prepared knee joint tissue with an intra vital microscopic set up

Therefore, the aim of the present study was to visualize arthritic joints with fluorochrome dyed nanoparticle probes in the vis range by targeting macrophages and inflamed tissue with fluorochrome-labeled gelatin nanoparticles. For comparative reasons chitosan nanoparticles and DOTAP liposomes were used.

In detail, besides our liposomal formulations (not shown) the following nanoparticle samples were transferred to the animal model:

Table 2.3

GNP-1-0.1-VEGF	Gelatine nanoparticles red	+ siRNA
GNP-1-0.1-Block	Gelatine nanoparticles	+ siRNA red
Chitosan-1-0-1-VEGF	Chitosan nanoparticles red	+ siRNA
Chitosan-1-0.1-Block	Chitosan nanoparticles	+ siRNA red

After *i.v.* application of the nanoparticle samples the knee was monitored via an intra-vital fluorescent microscope. In addition tissue samples of the knee were fixed in 4 % (v/v) formaldehyde (pH 7.4) and embedded in paraffin to be cut with a microtome. These histological cuts of ~ 6 μm thickness were stained according to various histochemical and immohistochemical protocols for further analysis.

2.5.5 Mouse whole body imaging

The non-invasive *in-vivo* analysis of the body distribution of protein and respectively gelatin nanoparticles today is limited due to the lack of appropriate tools and methods. Recently, fluorescent whole body imaging has been introduced to measure nanoparticle distribution under live conditions without changing the nanoparticle surface characteristics at large.
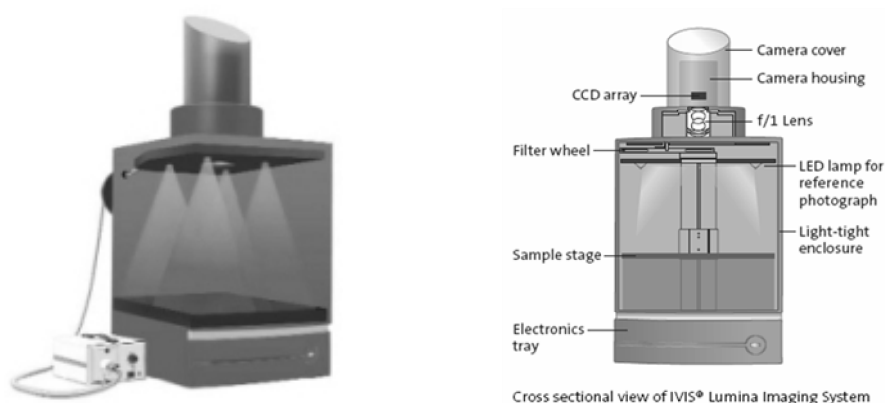
Figure 2.16

Display of the IVIS® Lumina Imaging system: photography chamber (left); cross section (right); the mice are placed (from http://www.caliperls.com/products/ivis-lumina.htm)

For the *in-vivo* studies, female young nude mice with an average body weight of 27.1 g were used. The animals received 150 µl injections of the nanoparticle formulations at different concentrations in HEPES buffered glucose (HBG) through the tail vein. Recording of the whole body images was done using the IVIS Lumina CCD whole body camera system equipped with an ICG filter set. Living Image® software Version 2.6.1 from Xenogen Corporation (California, USA) was used for picture analysis. The animal house was well ventilated and the animals were maintained on a 12:12 h light/dark cycle in large spacious cages throughout the experimental period. The animals were provided with food and water ad libitum. All efforts were made to minimize animals suffering and to reduce the number of animals for the study.

All animal procedures were approved and controlled by the local ethics committee and carried out according to the guidelines of the German law of protection of animal life.

2.5.6 Pharmcokinetic studies

The concentration of different blood cells during nanoparticle application was measured with a Beckman Coulter counter (A^{c}T-Series, Beckman, Krefeld, Germany). Samples were drawn directly through a catheter inserted in the carotid artery at different time points from 0 to 90 minutes after *i.v.* nanoparticle infusion. In detail, white blood cells, thrombocyte count and hemoglobin concentration were assayed. Again, all measurements were conducted in triplicate.

For the nanoparticle kinetic data, blood samples (100 µl) were drawn from the animals at different time points via a catheter inserted into the carotid artery. The samples were transferred directly into microslides and fluorescence intensity was quantified by means of a photomultiplier tube (PMT P30A-11, Electron Tubes Limited, Middlesex, UK) coupled to a fluorescence microscope (modified Zeiss Axiotech microscope, Zeiss, Goettingen, Germany). Epiilumination using a specific fluorescence filter set (excitation: BP 546/12 nm; emission: 575-640 nm) was performed by a 100W mercury lamp (FluoArc, Zeiss, Goettingen, Germany).

2.6 siRNA mediated gene silencing and protein knock-down

2.6.1 Chemicals and reagents

Ready to use siRNA duplexes were purchased from MWG-Biotech (Ebersberg, Germany). The GL3 luciferase-siRNA sequence was 5´-UUACGCUGAGUACUUCG (dTdT)-3´, and the non-specific control siRNA sequence was 5´-AUUGUAUGCGAUCGCAGC (dTdT)-3´. Ethylene-carbodiimide (EDC) and cholamine were purchased from Sigma Aldrich (Munich, Germany). Gelatin and diethylamino-ethanol-dextran were also obtained from Sigma Aldrich (Munich, Germany). Glutaraldehyde was obtained from Sigma. Branched polyethylene imine (PEI; average MW = 25kDa; cataloge number 40,872-7; lot number 07112DF, polydispersity index 3.4), Poly-L-lysine-HBr (PLL; degree of polymerization = 153, MW = 32000; cataloge number P2636, lot number 085K5100, polydispersity index 1.2), succinimidyl 3-(2-pyridyldithio) propionate (SPDP), 2,3-dimethylmaleicanhydride (DMMAn) and succinicanhydride (Succ) were obtained from Sigma-Aldrich (Munich, Germany). Cysteine modified Melittin (Mel) was obtained from IRIS Biotech GmbH (Marktredwitz, Germany) and had the sequence CIGA VLKV LTTG LPAL ISWI KRKR QQ (all-(*D*) configuration). All-(*D*) stereochemistry was used because it is non immunogenic while being as lytic as the natural peptide. Succinimidyl propionate monomethoxy polyethylene glycol (SPA-mPEG, molecular weight 5000, cataloge number 85969, lot number 071049/1) was purchased from Fluka (Buchs, Switzerland). Cell culture media, antibiotics, and fetal calf serum were purchased from Invitrogen (Karlsruhe, Germany). Formulations for nucleic acid delivery were prepared in HBG (HEPES-buffered glucose solution; 20mM HEPES, 5% glucose, pH 7.4).

The PLL-PEG-DMMAn-Mel conjugate was synthesized according to a method described elsewhere [Meyer, M. et al. 2008]. In brief, PLL (hydrobromide, MW 32 000) was PEGylated with mPEG-succinimidyl propionate (MW 5000). The PEGylated polycation was further modified with heterobifunctional *N*-succinimidyl 3-(2-pyridyldithio)propionate allowing subsequent coupling of DMMAn-Mel peptide via the N-terminal cysteine. The resulting conjugates had molar ratios of approximately 1/1/8 for PLL/PEG/DMMAn-Mel.

All other solvents and reagents were either of HPLC grade or of the American Chemical Society reagent grade.

2.6.2 Biological activity of nanoparticles

siRNA delivery efficiency of the loaded nanoparticles was examined with the Neuro2A-eGFPLuc cells. Luciferase siRNA was loaded onto the nanoparticles in a HBG pH 7.0 solution. Cells were seeded in 96-well plates (TPP, Trasadingen, Switzerland) using 5000 cells per well 24 h prior to gene silencing. The experiments were carried out with each nanoparticle formulation loaded with 500 ng luciferase siRNA at different ratios. 48 hours after initial transfection, the cells were lysed and assayed for luciferase expression. In parallel, complexes with a control siRNA sequence were applied. If luciferase expression decreases upon transfection with control siRNA, knockdown is mainly due to carrier toxicity and can hereby be distinguished from a real siRNA knockdown effect.

Luciferase activity was measured using a Lumat LB9507 instrument (Berthold, Bad Wildbad, Germany). Luciferase light units were recorded from a 25 µl aliquot of 50 µl cell lysate with 10 s integration time after automatic injection of freshly prepared luciferin using the Luciferase Assay System (Promega, Mannheim, Germany). Knock-down efficiency was evaluated as relative light units (RLU) per number of seeded cells. Two nanogram of recombinant luciferase (Promega, Mannheim, Germany) corresponded to 107 light units.

3 Results and Discussion

Goal of the present thesis was to develop and modify novel nanoparticles based on gelatin towards an efficient siRNA carrier for cellular RNA interference and expression silencing. Throughout the course of formulation development, different gelatins as well as different cationization approaches were evaluated for their potential to link negative nucleic acids to the nanoparticle surface. Early stage *in-vitro* evaluation was carried out in cell cultures by incubation with nanoparticles in static and flow through conditions. The cell interaction and uptake profiling were thereby monitored. Accent was put on culture studies under flow-shear conditions in order to evaluate the contact and adhesion between cultured cells and nanoparticles. This innovative approach holds the chance to more closely simulate *in-vivo* conditions especially in the field of nanotechnology and to allow *in-vitro/in-vivo* correlations.

The *in-vivo* experiments were then used to transport the cellular observations to a real life setting with the purpose to overcome the static model for nanoparticle studies. Finally, a new type of endosomolytic gelatin nanoparticles was developed by utilizing the strong cationic polysaccharide DEAE-dextran and the lytic Melittin peptide. Those newly developed nanoparticles were used to transport and deliver siRNA molecules to cells and stably knock-down the inherent target protein levels.

3.1 Nanoparticle formulation

Generally, for the delivery of negative siRNA molecules under near to physiological conditions, under the presence of serum and flow-shear conditions, a sophisticated cationic nanoparticle design is needed. Negatively charged RNA molecules can be electrostatically attached to nanoparticles when their positive surface charge prevails strong enough in physiological ionic surrounding. The same interaction as with siRNA can of course be undergone with other nucleic acids like shorter oligonucleotides or long double stranded DNA. Several authors have already shown the delivery of oligonucleotides and DNA with nanoparticulate systems [Mao, H.-Q. et al. 2001; Zwiorek, K. et al. 2004; Cui, Z. et al. 2006; Remaut, K. et al. 2006]. However, it has to be mentioned that in most cases, the interaction of carrier or carrier polymer was facilitated by DNA condensation and compaction process due

to its length [Porschke, D. 1991]. Since siRNA cannot be condensed, an intercalation with the polymer chains of the carrier becomes unrealistic and a new way of siRNA binding had to be developed. The ionic interaction on the surface of the nanoparticles has the potential to fulfil this role with the restriction though, that the nanoparticles' positive charge will be reduced by a large extent, which has consequences for the colloidal stability. It was therefore mandatory to develop highly cationic nanoparticles which can remain with a sufficient residual positive charge after siRNA loading to stabilize the nanoparticle colloidal conformity.

All nanoparticle formulations were examined for their distinctive size distribution using 173° angle dynamic light scattering and static light scattering. The static light scattering allowed for screening of larger particle agglomerates while the dynamic light scattering was accurate in the lower size range.
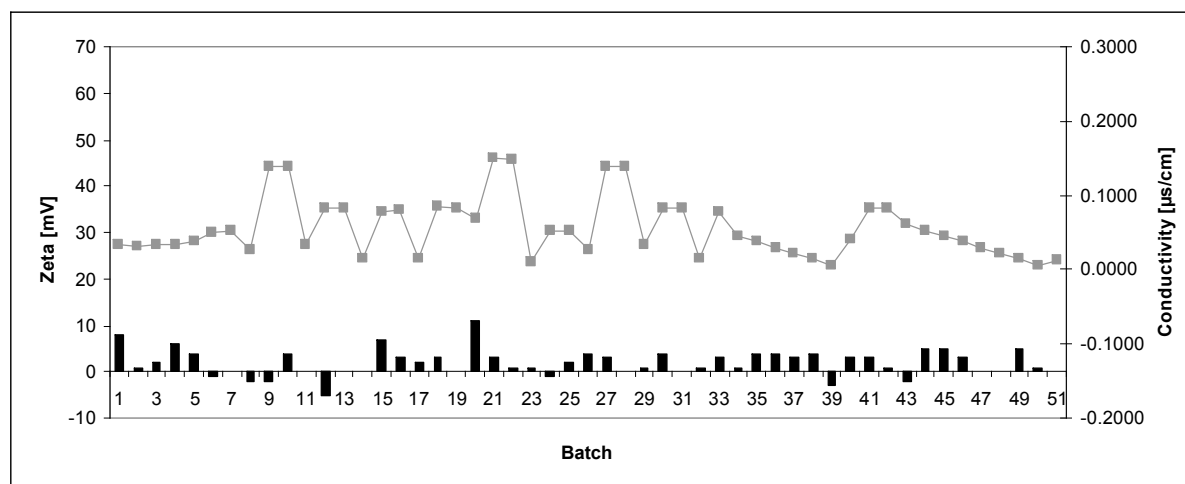
Unmodified gelatin nanoparticles

Homogenous and small nanoparticles were prepared with the given formulation conditions by Coester et al. [Coester, C. J. et al. 2000]. These nanoparticles were used as reference in the loading, *in-vitro* and *in-vivo* experiments and will be further referred to as "unmodified" nanoparticles with a zeta potential close to the neutral. Since no cationization was made to these batches, the nanoparticles were not suitable for the loading and delivery of siRNA. The charge of unmodified nanoparticles was only determined by the available surface primary amino and carboxy groups. **Figure 3.1** shows the average size range of unmodified nanoparticles reflecting an overall very narrow size distribution within our chosen formulation approach and very good interday and inter-batch reproducibility. The nanoparticle size ranged from 172 nm to 256 nm over 50 separately and independently formulated GNP batches with an overall size and standard deviation of 214 nm $\pm$ 26.04 nm. The increased homogeneity compared to previous work *e.g.* [Zwiorek, K. 2006] was attributed to our development of a standardized formulation protocol and the use of standardized equipment like *e.g.* low-protein adsorptive glass stirring beads and a pump and needle based apparatus for precise dosage of desolvation agent. The small standard deviation was especially remarkable, since gelatin is a polymer from biological origin and heterogeneity in its medium molecular weight is inherent to it. Again in comparison to early stage studies of our group but also compared to other types of today's nanoparticle [Lutsiak, M. E. C. et al. 2002] the size reproducibility in the lower size range was further optimized.
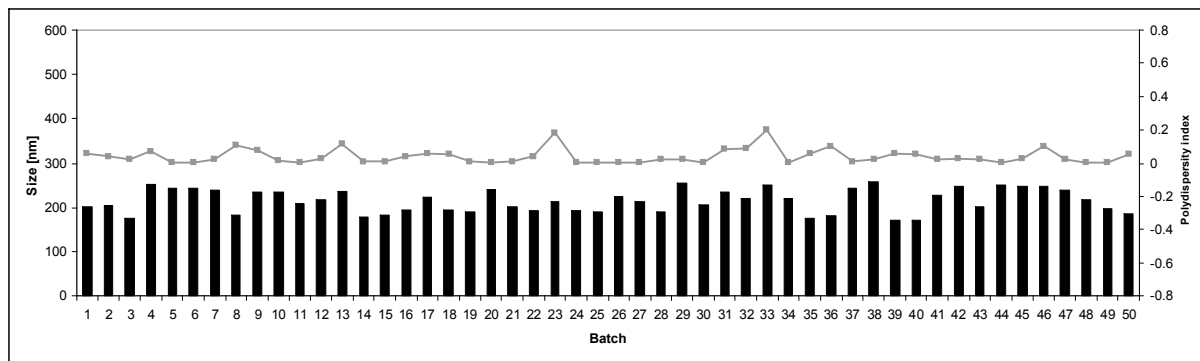
Figure 3.1

Size distribution determined by DLS of gelatin nanoparticles (bars) and PDI (dotted line) within 50 formulations showed a good batch-to-batch reproducibility in a size range from 172 nm to 256 nm.

Yet it was not the size of the nanoparticles that should be relevant for the later siRNA loading process but their charge represented by the zeta potential. **Figure 3.2** shows how the zeta potential of unmodified nanoparticles stays at a very low level ranging from -5 mV to +5 mV (SD 2.87 mV) in highly purified water (**Figure 3.2**). It has to be noted at that point, that the presence of ions in the measurement media dramatically influenced the zeta potential due to their shielding of the electronic cloud around the nanoparticles. For this reason all zeta potential measurements were conducted in freshly prepared highly purified water at the same conductivity if not stated otherwise. A comparison of the zeta potential in the different media was made for the modified nanoparticles in particular and is discussed in detail later (refer to 3.10.1.2 Medium influence). The close to neutral charge can lead to the aggregation over time if the system is not otherwise stabilized [Hsu, J.-P. et al. 1999]. Surprisingly, neutral GNP remained well dispersed in low ionic water as well as in phosphate buffered saline (PBS). This allows for the assumption, that their colloidal state is not only stabilized via charge based repulsive forces but also via lack of physical interaction, thereby resembling a simpler occurrence of the highly complex stealth systems known from liposomes [Deol, P. et al. 1997].

Figure 3.2

Zeta potential (black bars) of unmodified gelatin nanoparticles over a range of 50 independently prepared formulations

Single cationized gelatin nanoparticles

For a cationization of the gelatin nanoparticles the method of covalently coupling cholamine moieties to the carboxy functional groups of the final nanoparticles was used. The chemical reaction behind this modification required a pH adjustment and the addition of a catalyst like EDC as described in 2.1.4 Formulation of cationic gelatin nanoparticles. The formulation of nanoparticles using this method required exact amounts of the catalyst in order not to cross-bridge the nanoparticles and create agglomerates.

As shown previously by other members of our research group, the size of cholamine cationized gelatin nanoparticles was 205 nm $\pm$ 24 nm S.D. respectively [Zwiorek, K. et al. 2004]. We confirmed this size range in over 200 independently cross batch measurements throughout the course of 3 years. More importantly the zeta potential of the single cationized GNP ranged between 25 and 30 mV $\pm$ 4 mV S.D. before siRNA loading in highly purified water and dropped by more than 60 % for siRNA loaded GNPs which leaves the need for the further enhancement of the cationization process.

Highly cationic DEAE-dextran modified gelatin nanoparticles

After the above experiments with cholamine modification of the GNP DEAE-dextran incorporation into the gelatin matrix was thought to be the more potent cationization step. Therefore a matrix of several formulation approaches was developed and the potential outcome of nanoparticles was evaluated. According to the assay layout in **Table 3.1** it turned out that DEAE-dextran at concentrations as low as 0.05 % (w/w) was able to cationize the gelatin nanoparticles significantly (+5 - +40 mV) above the level of the above nanoparticles. On the contrary, DEAE-dextran as a polysaccharide at concentrations above 1 % (w/w) increased the viscosity of the gelatin solution so much that the formation of uniform nanoparticles was not possible. Hence the optimum range for polysaccharide modifications was found to be in between 0.04 % (w/w) and 0.5 % (w/w). The static light scattering results revealed aggregates with a size of 800 nm – 5 μm for those formulations with more than 1 % (w/w) and to up 10 % (w/w) DEAE-dextran.

It was beneficial for the nanoparticle preparation to set the temperature for the protein/polysaccharide solution to 30° C $\pm$ 2 °C in order to receive the smallest and most homogenous nanoparticles (n=3), (**Figure 3.3**). One possible explanation is that at this temperature an optimal equilibrium between medium viscosity and Brownian molecular movement of the macromolecule chains exists. The viscosity of the medium and the thermodynamic influences on polymer nanoparticles has so far not been studied in literature. Our data suggests that low viscosities and thereby a fast molecular kinetic movement were beneficial for the formation of nanoparticles. These results in general demand further studies in the field of protein nanoparticle thermodynamics while later on in the thesis such considerations will become important again when nanoparticles were studied *in-vitro* under flow conditions and at elevated temperatures.

Table 3.1

Nanoparticle formulation and DLS size results for different DEAE-dextran concentrations and temperatures between 25 °C and 50 °C

DEAE-dextran [%]	pH	ΔT [°C]	Size [nm] ± S.D.	PDI	Aggregates
0.04	2.5	25	210 ± 2	0.022	No
0.04	2.5	30	198 ± 4	0.054	No
0.04	2.5	35	208 ± 7	0.076	No
0.04	2.5	40	173 ± 12	0.020	No
0.04	2.5	50	251 ± 4	0.046	No
0.08	2.5	25	198 ± 11	0.013	No
0.08	2.5	30	215 ± 2	0.070	No
0.08	2.5	35	143 ± 4	0.147	No
0.08	2.5	40	198 ± 1	0.106	No
0.08	2.5	50	270 ± 4	0.083	No
0.2	2.5	25	205 ± 7	0.061	No
0.2	2.5	30	199 ± 2	0.003	No
0.2	2.5	35	253 ± 7	0.040	No
0.2	2.5	40	233 ± 6	0.146	No
0.2	2.5	50	301 ± 1	0.100	No
0.3	2.5	25	238 ± 5	0.051	No
0.3	2.5	30	229 ± 1	0.010	No
0.3	2.5	35	231 ± 4	0.009	No
0.3	2.5	40	247 ± 8	0.035	No
0.3	2.5	50	318 ± 22	0.204	No
0.4	2.5	25	240 ± 31	0.081	No
0.4	2.5	30	240 ± 4	0.004	No
0.4	2.5	35	202 ± 12	0.002	No
0.4	2.5	40	237 ± 13	0.077	No
0.4	2.5	50	299 ± 11	0.080	No
0.8	2.5	25	316 ± 15	0.049	No
0.8	2.5	30	301 ± 4	0.104	No
0.8	2.5	35	288 ± 6	0.151	No
0.8	2.5	40	333 ± 41	0.017	**Yes**
0.8	2.5	50	346 ± 8	0.096	**Yes**
1.0	2.5	25	441 ± 5	0.091	**Yes**
1.0	2.5	30	322 ± 4	0.096	**Yes**
1.0	2.5	35	551 ± 16	0.180	**Yes**
1.0	2.5	40	304 ± 8	0.199	**Yes**
1.0	2.5	50	589 ± 4	0.444	**Yes**

The temperature effect on DD-GNP was studied from 25 to 55 °C (**Figure 3.3**) and showed that at 30 – 35 °C the smallest nanoparticles could be formulated. The more viscous the

gelatin solution became the harder it was to formulate small nanoparticles whereas the PDI could be maintained.
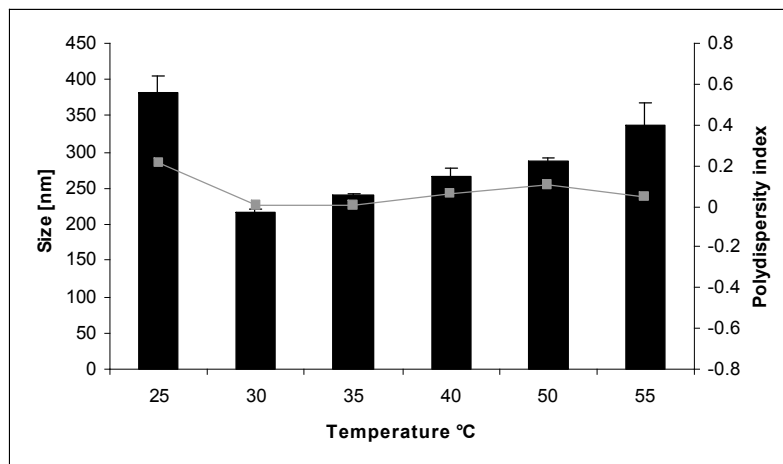
Figure 3.3

Determination of the optimum temperature conditions for the formation of small DEAE-dextran GNP (bars = size, line = PDI)

Also in contrast to the formulation of pure GNP, the stirring speed played a more critical role in nanoparticle formulation. While Zwiorek [Zwiorek, K. 2006] was able to formulate GNP at a stirring speed of 400 rpm, DEAE-dextran modified GNP required a slower speed of 200-250 rpm in order to form the smallest nanoparticles possible (**Figure 3.4**). This can be explained by a higher intercalation probability of the polymer chains at higher stirring rates.
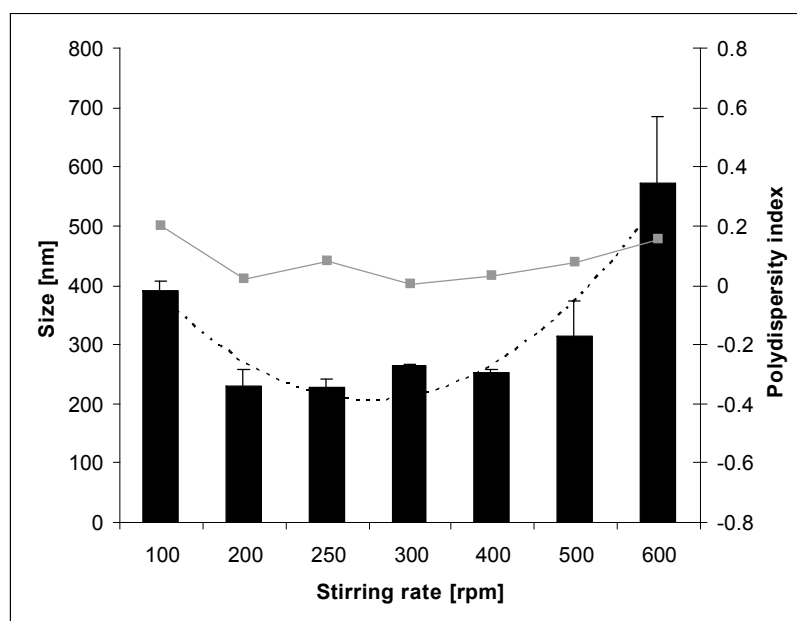
Figure 3.4

Determination of the optimum stirring rate for the formation of small DEAE-dextran GNP (n=5) (bars = stirring rate, line = PDI, dotted line = trend)

*Human serum albumin nanoparticles*

Human serum albumin nanoparticles were successfully formulated as described above (refer to 2.1.6 Formulation of human serum albumin nanoparticles). It turned out that the nanoparticles could be formulated almost in the same way as the GNP but possessed a lower colloidal stability over the time period of 14 days. In detail, human serum albumin nanoparticles with an average size of 248 nm $\pm$ 12 nm S.D. and an average PDI of 0.08 nm grew by 8 % in size after 3 days and by 12 % after 14 days. After all, HSA nanoparticles were formulated to compare their formulation feasibility and *in-vitro* potential as another biocompatible, biodegradable polymer to that of GNP.

Polybutylcyanoacrylate nanoparticles

Formulated by an emulsion polymerization reaction in acidic pH, the polybutylcyanoacrylate (PBCA) nanoparticles had to be dialysed after the preparation to remove any toxic monomers [Evans, C. E. et al. 1999]. In addition, several washing and centrifugation steps were made to ensure the lowest possible monomer contamination. The

size of the final formulation was 352 nm $\pm$ 8 nm S.D. with an average PDI of 0.292. While GNP formulations were well stable over a long period of time and also throughout several changes of medium [Zwiorek, K. 2006] the PBCA nanoparticles showed a tendency of agglomeration after changing the medium from highly purified water to PBS, HEPES or DMEM [Broermann, P. et al. 2008], which was in accordance to findings of Sommerfeld et al. [Sommerfeld, P. et al. 2000]. In addition we found out that at 4 °C PBCA NP were well stable while at 37 °C as a model temperature for our cell culture studies the PBCA NP showed signs of growth or aggregation by increasing from 372 nm $\pm$ 7 nm S.D. to 427 nm $\pm$ 12 nm S.D. after 240 hours (**Figure 3.5**).

In summary, PBCA NP served as a negative reference standard that, besides our comparative studies, will not be investigated further due to the mentioned stability issues and proposed incorporation problems of biological drugs during the harsh formulation conditions.
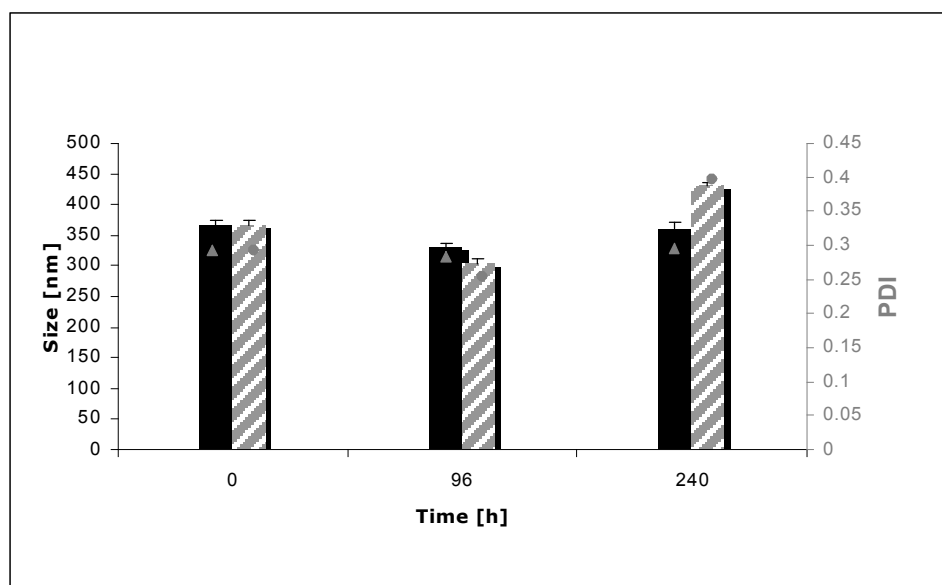
Figure 3.5

Size distribution and PDI of PBCA nanoparticles measured by DLS over a time span of 240 hours at two different storage conditions: Size at 4 °C (black column), Size at 37° C (grey column), PDI (- / •)

Chitosan nanoparticles

The other polymer that was studied was chitosan and its modified thiomers. Here small and uniform chitosan nanoparticles can be as easily generated the lower the molecular weight of the excipient polymer is [Bernkop-Schnürch, A. et al. 2006]. By chemically "cracking" the chitosan (refer to 2.1.8.1 Preparation of low molecular weight chitosan) down to a molecular weight of approximately 10 kDa, nanoparticles from thiolated chitosan in the low nanometer range could be formed. When lyophilized the thiolated chitosans showed a fibrous and white yellow color. In **Table 3.2** we compared cationic GNP and GNP formulated from more hydrophobic prototype gelatins (MS and MA) with chitosan and thiomer nanoparticles. C-GNP had a zeta potential of +27 mV $\pm$ 4 mV S.D. and therefore a comparable cationic surface charge as nanoparticles from low molecular weight chitosan with the sizes of 213 nm and 290 nm providing a small but significant advantage in favor to C-GNP. For the other thiomers nanoparticles were also formulated with a cationic charge, but interestingly in most cases with a comparatively high PDI value leaving chitosan an unfavorable material to formulate nanoparticles for *in-vivo i.v.* use. Chitosan-NAC-low-viscosity for instance formed the most cationic thiomer nanoparticles with +32 mV $\pm$ 12 mV S.D. and a PDI of 0.432. The MS and MA nanoparticles due to their surface modified gelatin matrix prompted negative nanoparticle surface charges with -36 mV and – 13 mV respectively and sizes with 362 nm and 193 nm.

Table 3.2

Size distribution and zeta potential of the cationic gelatin nanoparticles and chitosan nanoparticles measured by DLS, SLS and electrophoretic mobility (n=3)

Batch	Zeta [mV]	Size [nm] $\pm$ S.D.	PDI	SLS [nm]	Span
C-GNP	+27 ± 4	213 ± 22	0.005	215	0.422
MS-NP	-36 ± 8	362 ± 45	0.053	380	0.523
MA-NP	-13 ± 2	193 ± 18	0.107	198	0.721
Chitosan–low viscosity	+21 ± 2	272 ± 19	0.103	273	0.881
Chitosan–low molecular weight	+27 ± 9	290 ± 24	0.140	335	0.923
Chitosan–TBA–low viscosity	+12 ± 4	412 ± 37	0.231	812	0.786
Chitosan–NAC–low viscosity	+32 ± 12	304 ± 5	0.432	621	0.699

The used ionic crosslinking of nanoparticles allowed us to quickly formulate nanoparticles in the desired size range with the only disadvantage of time consuming dialysis processes to harden the particles. The additional covalent disulfide crosslinking resulted in slightly larger nanoparticles due to less bridges formed between the intercalated polymer chains compared to ionic crosslinking. For other *in-vivo* studies the disulfide bonds are important not only for the stability of the chitosan nanoparticles but also for the muco-adhesive and permeation enhancing properties [Roldo, M. et al. 2004]. The molecular interaction between the single chitosan chains is shown in **Figure 3.6**.
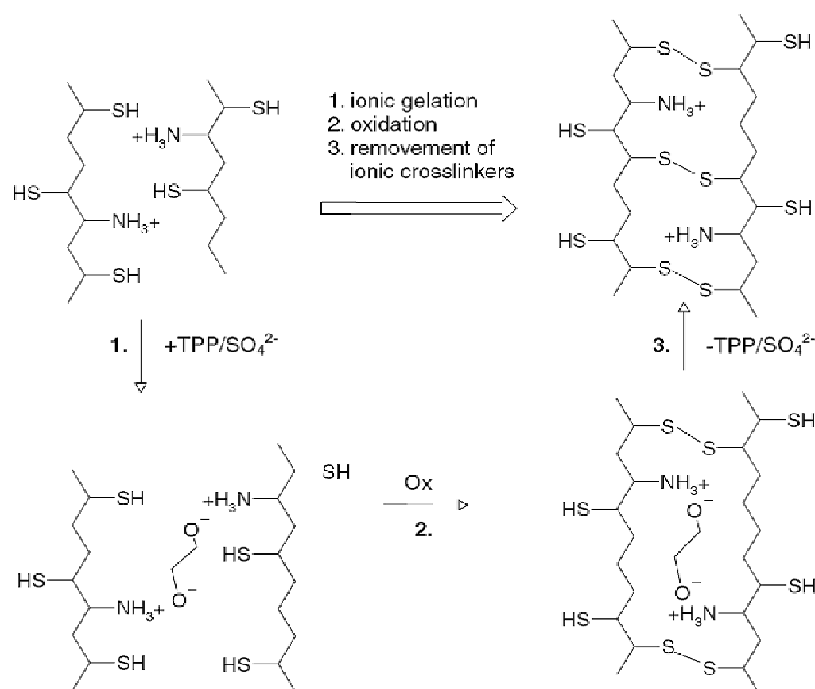
Figure 3.6

Molecular interpretation of the ionic and oxidative crosslinking process of thiomers to thiomer nanoparticles; (SH = sulfhydryl group, Ox = oxidation, TPP = tripolyphosphate) [Bernkop-Schnürch, A. et al. 2006]

It turned out that choosing the right amount of crosslinker concentration and incubation time were the decisive factors for a reproducible nanoparticle formulation. The formulation developed by Bernkop-Schnürch could be improved by increasing the oxidation time from 3 h to 10 h and thereby generating nanoparticles with a lower PDI. As seen in **Table 3.5** crosslinking with TPP resulted in nanoparticles of size from 170 nm $\pm$ 16 nm to 348 $\pm$ 36 nm. A threefold increase of the crosslinker amount from 0.25 0.75 % (w/v) lead to a median size

of 174 nm $\pm$ 5 nm indicating overall very small nanoparticles. For later assays nanoparticles in the medium size range of GNP were used to exclude size related biological side-effects.

3.2 Nanoparticle fluorescence labeling

The fluorescence labeling was a critical part in our studies and had to be optimized not only for the *in-vitro* studies but also first-time tested for the later *in-vivo* studies. While all fluorophores were successfully coupled to the nanoparticles as indicated by fluorimetric data, the fluorophore concentration, coupling conditions, incubation time, nanoparticle concentration, fluorimeter excitation and emission slit as well as the detector voltage were tested. Measurement of the fluorescence by fluorimetry turned out to be insufficient for a quantitative approach due to quenching and noise effects through the particle based light scattering even within rather diluted samples. In general the scatter from the dispersed nanoparticles made it impossible to determine the net fluorescence of the final formulations (**Figure 3.7**). **Figure 3.8** reveals how even increased slit width in the fluorimeter would not increase the signal sensitivity against the particle scatter. Therefore a work-around using subtractive calculations of free fluorophore in the supernatant compared to a 100 % (w/w) solution had to be used in order to determine the fluorescence yield (9.85 % - 19.5% (w/w)).
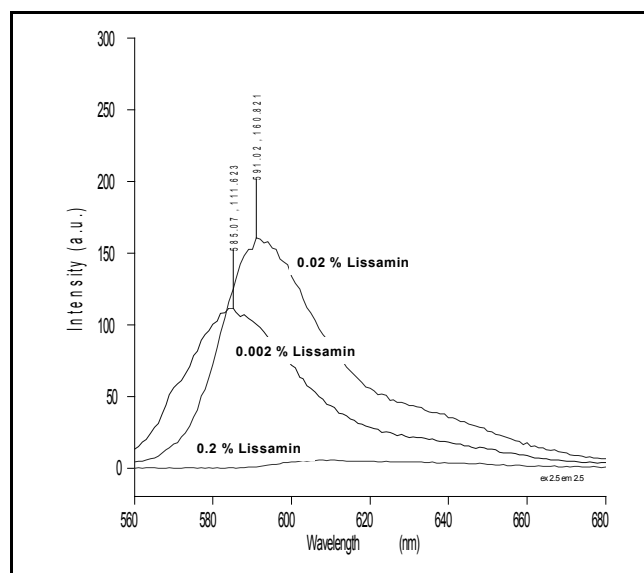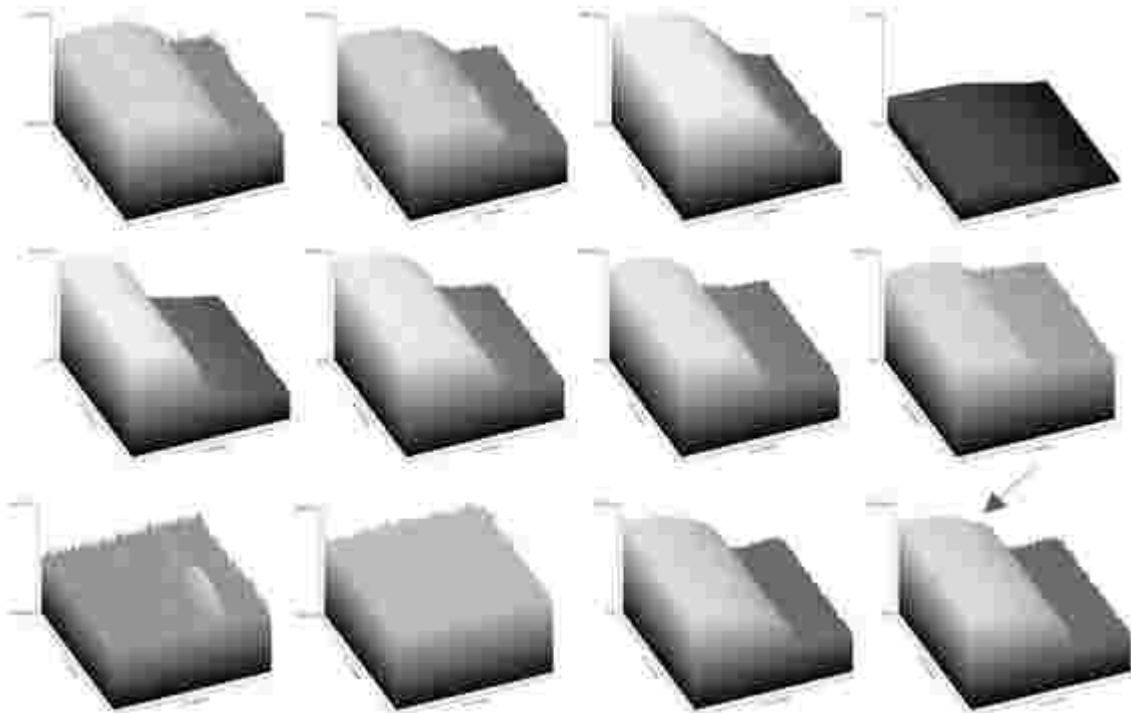

Figure 3.7

Observed quenching for fluorescently labeled GNP at an increased fluorophore concentration of 0.2 % (w/w) compared to 0.02 % (w/w) and 0.002 % (w/w) lissamine
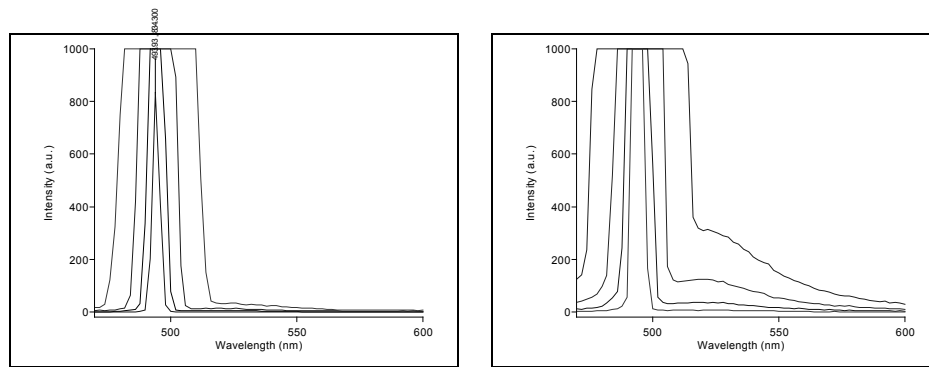
Figure 3.8

Fluorescence emission recording is disturbed for GNP at a concentration of 0.01 mg/ml (left, excitation slit 2.5, emission slits 2.5, 5, 10, 20 from bottom to top) and 0.1 mg/ml (right, excitation slit 2.5, emission slits 2.5, 5, 10, 20 from bottom to top) measured in PBS

Because the intention of the fluorescence measurements initially was to determine the emission in the same fluorescence detection setup that was used for the *in-vitro* and *in-vivo* experiments a comparative study was conducted in microslides.

Figure 3.9

Fluorescence measurements of labeled nanoparticles in a microslide recorded by a fluorescent camera; 1. FITC-dextran 100 μl, 200 μl, 600 μl labeled N-GNP, FITC-dextran labeled PBCA-NP; 2. Oregon Green labeled N-GNP, diluted 1:1, 3:7, 1:9; 3. Coumarine 6 labeled aGNP, Lissamine Rhodamine B labeled C-GNP, HSA-NP; the arrow indicates the nanoparticle dispersion inside the slide

Figure 3.9 shows the fluorescence plots of several fluorescence labeled nanoparticle formulations, quantitatively demonstrating the intensity fluctuations of the used fluorophores as measured with the fluorescence microscope. Here a labeling of N-GNP and C-GNP with FITC-dextran 600 µl and lissamine rhodamine B depicted the highest fluorescence intensities next to Oregon green and was therefore used for the *in-vitro* and *in-vivo* studies. FITC-dextran labeling of PBCA-NP on the contrary was rather low, and so was the coumarine 6 labeling of aGNP. For Oregon Green dilutions an almost linear reduction in fluorescence emission was recorded, showing a signal even at a dilution of 1:9 and therefore enough for *in-vivo* experiments. With this data the quantitative results from the fluorimeter studies could be linked to a qualitative result which is directly relevant for the *in-vivo* studies.

## 3.3 Nanoparticle advancements with DEAE-dextran

DEAE-dextran has the potential of complexing nucleic acids due to its polymeric and permanent cationic nature. Several authors have shown that transfection with DEAE-dextran is not only possible but besides being a standard method in biotechnology, it has however major drawbacks like decreased cell viability and lack of complex stability [Kosmala, J. D. et al. 2000]. DEAE-dextran (**Figure 3.10**) is basically a polycationic derivative of dextran and is commercially produced by binding diethylaminoethyl chloride with dextran. In a novel combination with gelatin nanoparticles as proposed in this thesis, DEAE-dextran can prove to be of great interest, because of the combination of the complexing and transfecting properties of the polysaccharide with the inherent positive properties of gelatin nanoparticles. We also propose a thin polymer brush like surface of the DEAE-dextran gelatin nanoparticles allowing for an increased siRNA binding capacity due to a better intercalation of the tiny, uncondensed nucleic acids. The combination of the characteristics of a nano-sphere and a polyplex to form something that could be called a SPHEROPLEX (**Figure 3.11**) might bring forward several synergistic effects in drug delivery and RNAi where until now no solution could be found.

The modification of the gelatin nanoparticles with DEAE-dextran resulted in slightly larger particles with a broader size distribution and higher standard deviations as shown in **Table 3.3**. The rise in size was nearly linear to the amount of added DEAE-dextran.
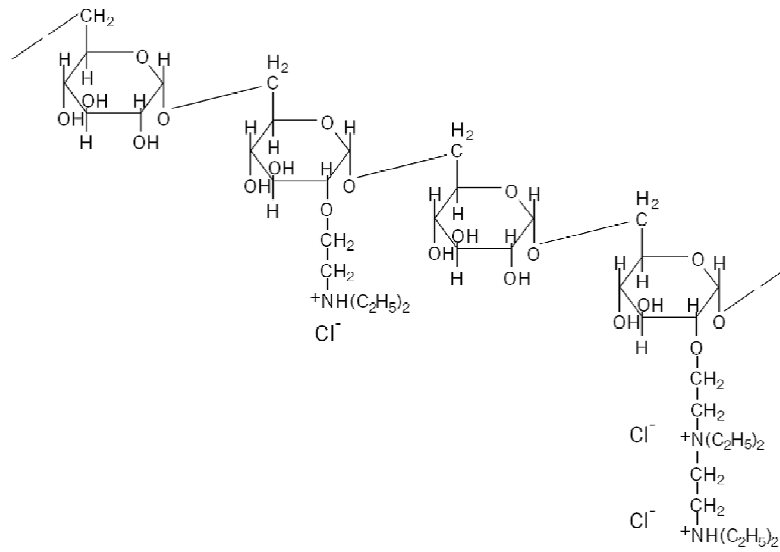
Figure 3.10
Molecular formula of DEAE-dextran
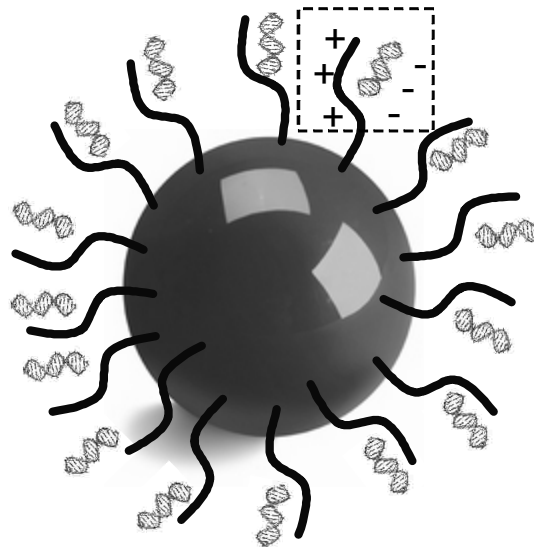
Figure 3.11

Theoretical visualization of a gelatin-DEAE-dextran spheroplex with oligonucleotides

Table 3.3

Influence of different DEAE-dextran amounts on the size single modified GNP and additionally cholamine modified GNP

DEAE-dextran [mg]	0	5	10	20	30	50	75	100
N-GNP Size	190	#	#	#	#	#	#	#
PDI	0.001	#	#	#	#	#	#	#
SD	6	#	#	#	#	#	#	#
DD-GNP Size	175	198	209	218	227	291	322	343
PDI	0.001	0.002	0.004	0.01	0.008	0.029	0.034	0.038
SD	17	9	10	6	4	12	18	23
N-GNP + Cholamine Size	205	#	#	#	#	#	#	#
PDI	0.01	#	#	#	#	#	#	#
SD	9	#	#	#	#	#	#	#
CDD-GNP Size	199	185	226	253	280	301	390	398
PDI	0.005	0.03	0.04	0.04	0.05	0.08	0.06	0.09
SD	16	5	7	7	37	14	22	27

It was further observed that the post-formulation modification of the DEAE-dextran nanoparticles with cholamine again increased the nanoparticle size but with the tendency of a steeper slope at higher DEAE-dextran concentrations. N-GNP could be formulated at 190 nm (PDI 0.001) whereas for DD-GNP with 5 mg of DEAE-dextran an increase in size to 198 nm (PDI 0.02) was determined (n=3). For the following amounts of DEAE-dextran the size of the nanoparticles increased to a final 343 nm (PDI 0.038) indicating the successful incorporation of the polysaccharide into the gelatin while the PDI remained low. A second step cholamine modification of these nanoparticles increased the nanoparticle size and PDI only a little bit further to 398 nm (PDI 0.09).

The zeta potential results for this formulation are shown in **Figure 3.12**. The optical model used here for our measurements was interpreted by the method of Smoluchowski in which the F(Ka) value was set to 1.5. Compared to neutral gelatin nanoparticles the cholamine modification led to sufficient cationic charged nanoparticles. However, if these nanoparticles were loaded with siRNA molecules, they lost much of their cationic surface potential, while a

combination of DEAE-dextran and cholamine has proven beneficial in this context (refer to 3.6 siRNA containing gelatin nanoparticles (SICONs)).
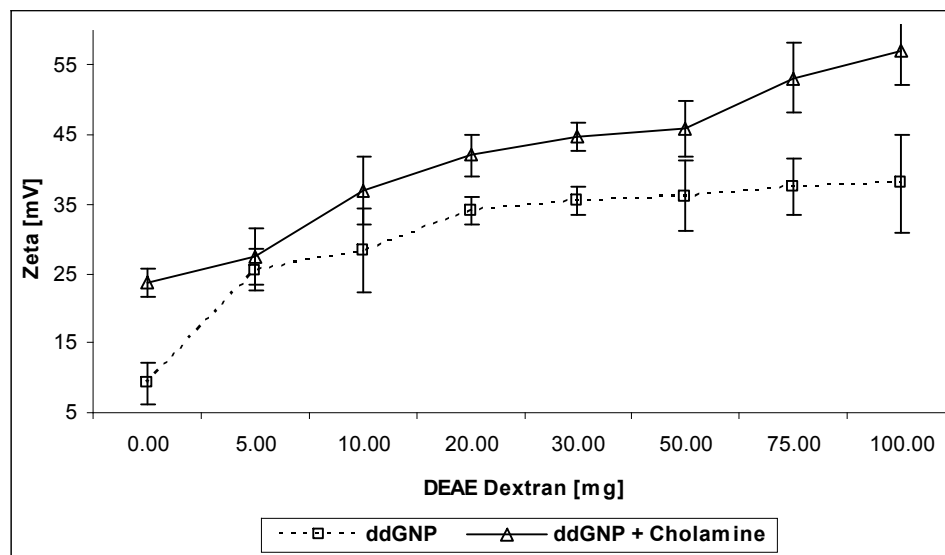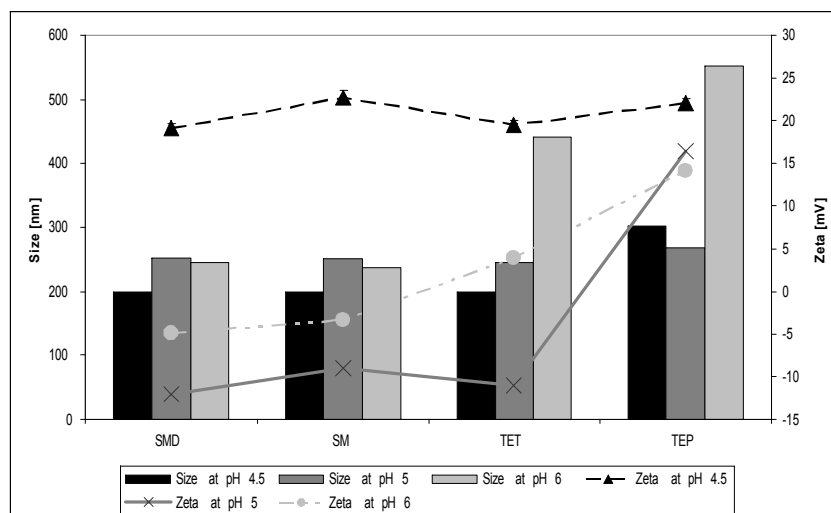

Figure 3.12

Zeta potential of DEAE-dextran modified GNP and cholamine (constant) cationized DEAE-dextran modified GNP over DEAE-dextran amounts from 0 to 100 mg (n=3)

Depending on the amount of DEAE-dextran used for the nanoparticle formulation increasing zeta potentials were measured. The increase was almost linear with a plateau reached at 100.0 mg where an increased viscosity prevented a reproducible nanoparticle formation. DD-GNP had an initial zeta potential of 24.5 mV with the 5 mg DEAE-dextran modification, approaching a maximum between 33 and 37 mV with 100 mg. With a combination of cholamine and DEAE-dextran an increase of cationic zeta potential by ~37 % to 55 mV + 17 mV could be achieved which was an increase of 55 % compared to unmodified C-GNP and of 87 % compared to neutral GNP. In summary it was shown that nanoparticles modified with cholamine and DEAE-dextran had a much higher zeta potential than what was achievable with pure cholamine modification or pure DEAE-dextran modification, which in the further formulation steps was mandatory for loading with siRNA and other molecules.

3.4 Additional nanoparticle modifications

Besides the above described results in formulating cationic nanoparticles additional techniques were transferred from chemistry to nanoparticle science. It was a major concern to formulate new gelatin nanoparticles with either a very hydrophobic surface or a permanent cationic charge. The hydrophobisation was proposed to be of invaluable help in the *in-vivo* studies allowing for less interaction with blood proteins and hence an altered circulation profile [Ehrenberg, M. S. et al. 2009]. With the permanent cationic charge, we wanted to increase the chance of our nanoparticles to transfect cells. The hydrophobisation of the nanoparticles should be achieved through acetylation and the use of differently succinylated prototype gelatins while the cationization method was based on modification either with polyamines or aminomethylation with methyl groups. CLSM recordings of the modified nanoparticles after incubation with cells were used to elucidate the cellular interaction. And finally by comparing the particle attachment and uptake patterns on cell monolayers in our cell flow-system with a conventional static system we could bring forward the differences inherited in those new formulations and demonstrate the potential advantages of the flow-system itself.

At first we investigated formulations of nanoparticles modified with the oligoamines spermine, spermidine, TEPA and TETA (**Figure 3.13**). The size of for spermidine GNP was between 198 nm and 253 nm depending on the pH, for spermine sizes between 199 nm and 249 nm were achievable. TETA and TEPA modified GNP showed larger variations with sizes ranging from 198 nm to 441 nm and from 267 nm to 551 nm (n=3). In terms of zeta potential, only the TEPA modification with a permanently cationic charge over all examined pH values would be valuable for oligonucleotide or respectively siRNA loading. TEPA GNP had a zeta potential of ~14 mV - ~24 mV while the zeta potential for the other modifications was in all cases < 5 mV.

Figure 3.13

Size and zeta potential of spermidine, spermine, TET and TEP modified GNP, prepared at pH values of 4.5 and 6.0

Modified methylated and acetylated nanoparticles were formulated and the production process was standardized. As with all new formulations, the nanoparticles were thoroughly characterized by size, zeta and ^{1}H-NMR. The CLSM recordings showed the expected different targeting and aggregation patterns depending on the modification and the type of incubation. Further data and discussion on these special modifications will be made in 2.3.10 Nuclear magnetic resonance spectroscopy. An in-depth study of this particular project has been published as the Bachelor Thesis of Ms Pia Broermann, who did her work under the author's supervision in 2008.

3.5 Nanoparticle and polymer analytics

3.5.1 Automatic microviscosimetry

Gelatin type A showed slightly higher viscosities than gelatin type B, *e.g.* a solution of 2.5 % (w/w) of each polymer 2.5 mPas respectively 1.4 mPas (40 °C, n=20, σ=0.1). At 40 °C the viscosity of DEAE-dextran 0.25 % (w/w) as about the same as the for the gelatin type A 2.5 % (w/w) solution, which made the combination of these concentrations preferable for our later nanoparticle formulation. At a concentration of 0.25 % (w/w) gelatin type A was still

within the limit of detection for the chosen method, while 5.0 % (w/w) of gelatin type A was analyzed as the maximum gelatin concentration used for nanoparticle preparation. The viscosity for these samples was in the range of 3.3 – 3.6 mPas (40 °C, n=20, σ=0.1).
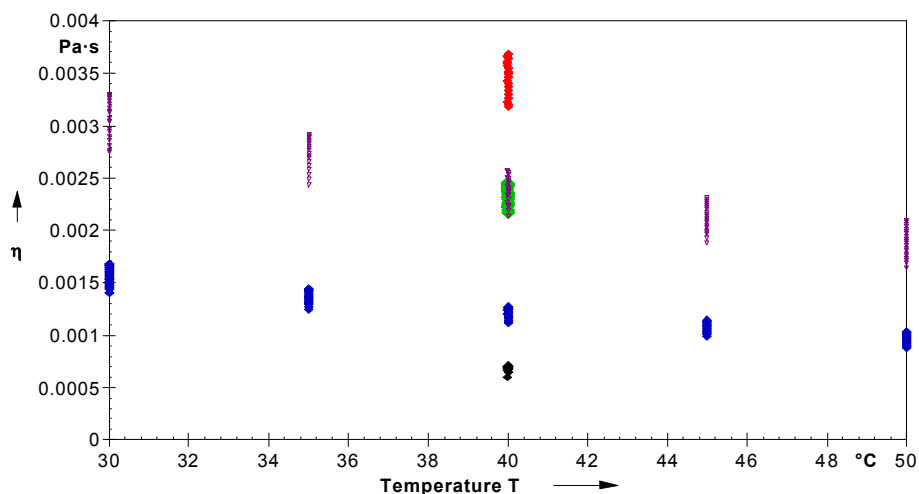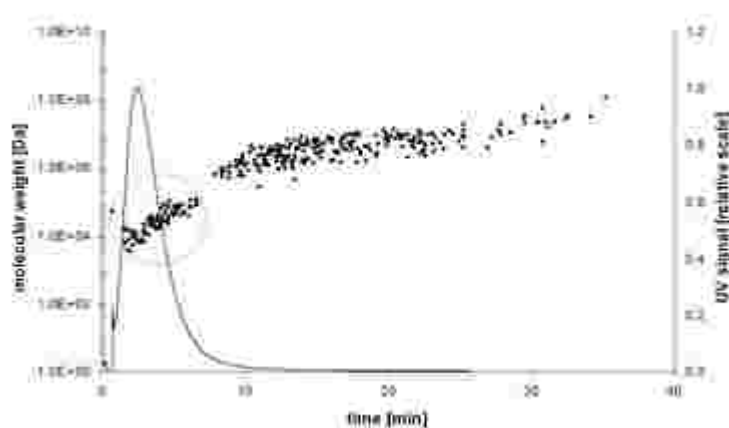

Figure 3.14

From top to bottom at 40 °C: gelatin type A 5.0 %, gelatin type A 2.5 % and DEAE-dextran 0.25 % (30-50°C), gelatin type B 2.5 % (30-50 °C), gelatin type A 0.25 %

We showed that our used gelatin solutions at concentrations of 0.25 % (w/w) to 5 % (w/w) could be analyzed with our chosen capillary set-up using automatic microviscosimetry. As shown for the nanoparticle characterization, a mixing of these two polymer solutions with respect to comparable viscosities resulted in homogenous and small nanoparticles with a low polydispersity index and a good colloidal stability. The fact that viscosity can influence the nanoparticle formulation process to a large extent has indirectly been examined by Coester and Zwiorek in their comparative studies with different gelatin types and different molecular weight gelatins [Zwiorek, K. 2006]. By introducing the combination with a polysaccharide like DEAE-dextran into the complex nanoparticle formulation process, we expand this theory towards two-factorial colloidal systems. In addition, the automatic microviscosimetry has been shown to be a fast and reliable tool for in-process control during nanoparticle development. In addition to the viscosity influences shown, the molecular weight analyzed by AF4 plays an important role in the polymeric nanoparticle formulation.

3.5.2 Asymmetric flow field-flow fractionation of gelatins

At first, gelatin bulk material from Sigma-Aldrich was analyzed to gain a benchmark for the following investigations of the modified samples. The gelatin molar mass distribution ranged from 10 kDa to above 10,000 kDa, which confirmed the data reported by Fraunhofer et al. [Fraunhofer, W. et al. 2004] and exceeded the findings from SE-HPLC/MALS analysis by more than one order of magnitude. The difference between data measured with SE-HPLC compared to AF4 reflects the fundamental differences between these two separation techniques. The separation process in SE-HPLC takes place in a packed column with high pressure applied to the sample; AF4 however has an open channel resulting in lower hydrostatic pressures and in conclusion lower shear force stress during analysis. Especially the high molecular weight specimen are inclined to degradation by increased shear forces and thus will only be detected in their native state if AF4 is used.

In a study by Zillies et al. (**Figure 3.15**) it had been demonstrated how the high molecular weight fractions of gelatin elute almost over the entire measurement cycle. Hence Zillies decided to only apply a weak separation force in order to expand the elution of the blend of molecules over a prolonged period and thereby visualizing the heterogeneous nature of gelatin.

Figure 3.15

UV signal (continuous line) and molecular weight (dots) calculated from respective UV and MALS data resulting from AF4 analysis of gelatin bulk material purchased from Sigma-Aldrich; the circle marks the low molecular weight fraction [Zillies, J. C. 2008]

As solely the high molecular weight fraction of Sigma gelatin can be used for the preparation of homogenous nanoparticles it generally has to be processed by two-step desolvation [Coester, C. J. et al. 2000]. Manufacturing experiments by Zillies [Zillies, J. C. 2008], conducted with two customized Gelita batches (VP306 / VP413-2) that possessed less than 20 % (w/w) peptides < 65 kDa resulted in successful one-step desolvation synthesis of gelatin nanoparticles exhibiting equivalent size and size distribution. These findings revealed the restriction that has especially to be made for the presence of low molecular weight portions in gelatin batches designated to one-step desolvation. The successful depletion of the low molecular weight fraction of gelatin is demonstrated in **Figure 3.16**.
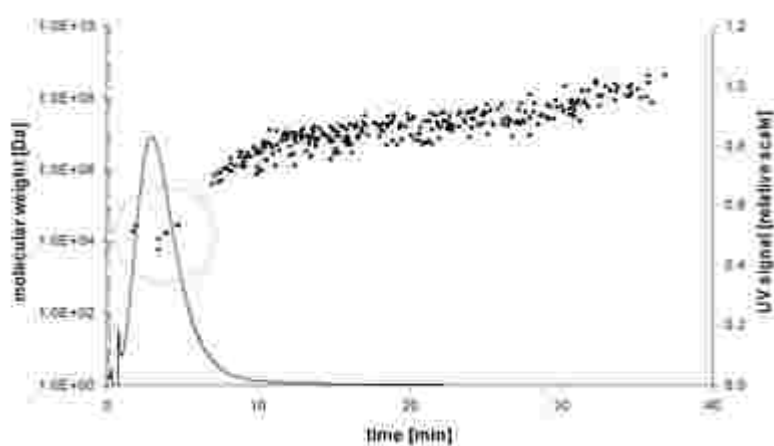
Figure 3.16

UV signal (continuous line) and molecular weight (dots) calculated from respective UV and MALS data resulting from AF4 analysis of gelatin bulk material VP413-2 developed and provided from Gelita; the circle marks the low molecular weight fraction [Zillies, J. C. 2008]

In addition, gelatin sediment obtained from two-step desolvation after the first desolvation step − as the result from fractionation and used for the preparation of nanoparticles − also underwent AF4 analysis. Data from these experiments and from gelatin bulk material are displayed as function of their mean molecular weight in **Figure 3.17.**
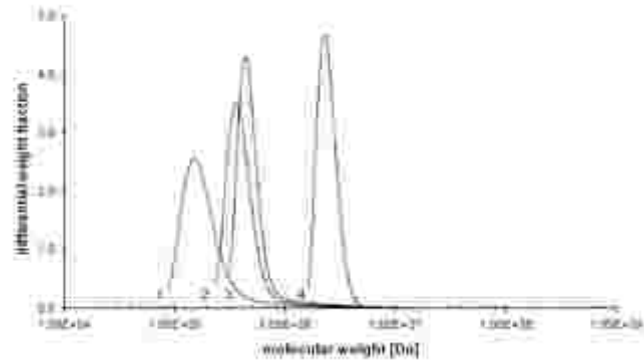
Figure 3.17

Mean molecular weight fractions calculated from respective UV and MALS data resulting from AF4 analysis of gelatin bulk material purchased from Sigma-Aldrich (1), of gelatin bulk material VP306 (2) and VP413-2 (3) developed and provided from Gelita, and of gelatin sediment obtained after the first desolvation step from the manufacturing process of the gelatin nanoparticles (4) [Zillies, J. C. 2008]

Interestingly the clear shift of the mean molecular weight of the gelatin sediment (4) by more than one order of magnitude compared to the bulk material (1) is not a prerequisite for a successful one-step desolvation. A mean molecular weight between 400 and 500 kDa determined for the Gelita batches VP306 and VP413-2 was already sufficient for the optimized one-step desolvation approach. Based on experiment findings the optimal molecular weight of gelatine for one-step desolvation manufacturing of gelatin nanoparticles is about 500 kDa with a concentration of low molecular weight fractions < 65 kDa of maximum 20 % (w/w). The mean molecular weight of gelatin sediment ranges clearly above the one of the Gelita batches, which may be attributed to even more reduced amounts of peptides < 65 kDa far below 20 %. Thus, the fractionation of gelatin bulk material during two-step desolvation supposedly led to an efficient fractionation and isolation of high-MW molecule fractions above 65 kDa.

As initially mentioned (refer to 3.4 Additional nanoparticle modifications) hydrophobisation could also be achieved by introducing succinyl (MS) - and dodecenylsuccinate (MA) groups into the gelatin resulting in novel prototype gelatins. These modifications were made by Gelita AG and were the basis for the following AF4 in-depth analysis of those prototypes before assessing their potential in gelatin nanoparticle formulation. In the initial process of

method development for the analysis of MA and MS gelatins, several ultra-filtration membrane types were tested due to an increased hydrophobic interaction potential of the prototype polymers. In particular, regenerated cellulose 5 kDa MWCO, regenerated cellulose 10 kDa MWCO and a nitrocellulose membrane also with 5 kDa MWCO were tested with focus on their recovery and repeatability (n=3). The results in terms of recovery rate, repeatability and signal quality are presented in **Table 3.4**. For regenerated cellulose (5 kDa) the recovery was determined with 92.3 % at a medium repeatability of 97.4 %. Regenerated cellulose (10 kDa) had 3.4 % higher recovery with 95.7 % and a repeatability of 98.5 %. Nitrocellulose finally showed the lowest recovery with only 86.5 % which could be attributed to a too strong interaction of the analyte with the membrane making nitrocellulose unfavorable for further analysis of our prototypes. After experiments with different materials and cut-off values regenerated cellulose with a cut-off of 10 kDa proved to be the most adequate. Regenerated cellulose is a very low protein binder and therefore ideally suited for analyses that require maximum sample recovery. In addition the membrane possesses a good solvent resistance with both aqueous and organic solvents, and is able to work over a wide pH range [Klein, T. 2008].

Table 3.4

Influence of the different membrane types on recovery rate and repeatability (defined as the intra day repeatability of a 100 % value in per cent of 6 replicates)

Membrane and cut-off	Recovery	Repeatability
Regenerated cellulose 5 kDa	92.3 %	97.4 %
Regenerated cellulose 10 kDa	95.7 %	98.5 %
Nitrocellulose 5 kDa	86.5 %	91.9 %

The derivated hydrophobic prototype gelatins showed a molar mass distribution from 140 to 10.000 kDa and 200 to 100.000 kDa for MS and MA, respectively. While the average molecular weight of MS was 218 kDa, MA showed an average molecular weight of 395 kDa. The molar mass distribution of standard gelatin was found to be between 140 to 1.000 kDa with an average molar mass of 158 kDa (**Figure 3.18**). This was in accordance with the prior studies, where even fractions up to 10.000 kDa were detected. The average recovery in this study was about 97.4%.

According to the data from Zillies and present studies it is possible to exert the hypothesis, that higher molecular weights in gelatin allow a better, more homogenous nanoparticle formulation. Prior to the present research it was still unknown whether this hypothesis was transferable to other gelatin types with in our case highly altered physiochemical properties.
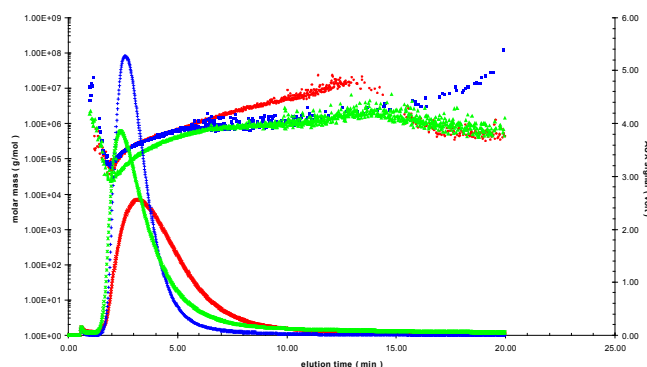
Figure 3.18

AF4 signals of the examined gelatin batches; MALS (dots) and UV signals (curves): Sigma gelatin (▲), MS gelatin (■) and MA gelatin (-)

But indeed we were able to formulate nanoparticles with the hydrophobic prototype gelatins although under completely new formulation settings. The results in size from DLS measurements are given in **Table 3.2**.
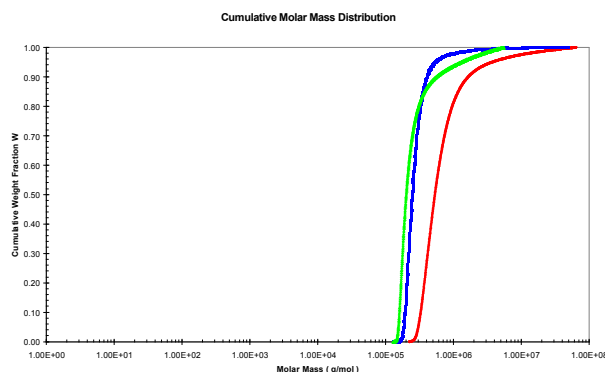
Figure 3.19

Cumulative molar mass distribution within the gelatin samples: Sigma gelatin (▲), MS gelatin (■) and MA gelatin (-)

We demonstrated the applicability of the hypothesis derived from the two-step desolvation theory of gelatin, namely the relevance of high molecular weight fractions and the absence of low molecular weight fractions for other gelatin types. Further we demonstrated that nanoparticles from hydrophobic gelatins could be formulated, making them a potential new nanotechnology platform for targeted drug delivery with either hydrophobic drugs or with the brain itself as the potential therapeutic target region [Fricker, G. et al. 2004]. The possibility of nanoparticles to pass the blood brain barrier resides at the margin of today's pharmaceutical research, yet it bears a great potential, leaving room for further in-depth studies with our newly developed GNP. Last but not least AF4 was introduced as a valuable pre-formulation tool for the formulation development of biological polymer based nanoparticles.

### 3.5.3 Asymmetric flow field-flow fractionation of chitosans

Next to the nanoparticles from gelatin, chitosan nanoparticles had to be developed and formulated. In this case however no background data on the molecular weight characteristics and their direct influence on nanoparticle size and stability were published besides some data from Bernkop-Schnuerch [Bernkop-Schnürch, A. et al. 2006] and Augsten [Augsten, C. 2008]. In the case of modified chitosans such as thiomers no literature was available making a thorough AF4 analysis of these samples in the nanoparticle pre-formulation process mandatory. The regenerated cellulose (10 kDa) membrane proved to be the right choice again with a medium recovery rate of 97 % for all chitosans. Unmodified chitosan NV (low viscosity) had a molecular weight from $1.0*10^6$ g/mol up to $2.0*10^7$ g/mol and chitosan (low molecular weight) ranged from $4.0*10^5$ to $3.0*10^7$. Chitosan NAC NV (low viscosity) had a MW range from $2.0*10^6$ g/mol – $7.0*10^7$ g/mol, chitosan TBA NV (low viscosity) had a MW of $2.0*10^6$ g/mol to $2.0*10^7$ g/mol, chitosan TBA (lower molecular weight) ranged from $3.0*10^5$ g/mol to $3.0*10^7$ g/mol.

For the sake of a better comparison with the gelatin samples the cumulative mass distribution was plotted during the analysis of chitosan (**Figure 3.20**). As seen in **Figure 3.21** the distribution of molecular weight fractions in chitosan was much broader than as for gelatin (**Figure 3.19**).
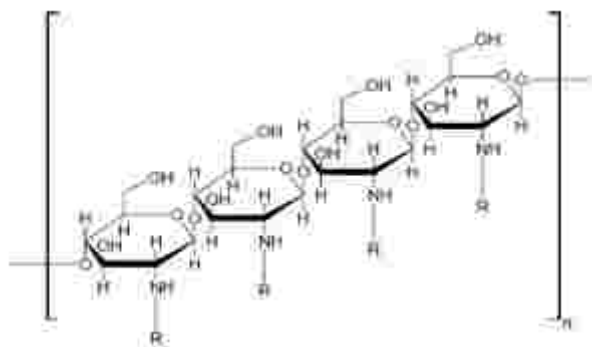
Figure 3.20

Chitosan molecular formula
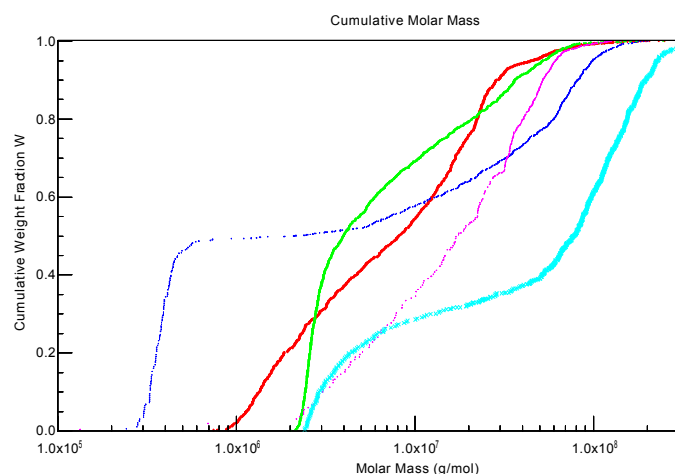
Figure 3.21

Cumulative weight fractions of chitosan samples, Chitosan–low viscosity (■), Chitosan–low molecular weight (■), Chitosan–TBA–low viscosity (■), Chitosan–TBA–low molecular weight (■), Chitosan–NAC–low viscosity (■)

Interestingly, chitosan LMW modified with thiobutylamidine as a potential nanoparticle crosslinker showed an increased amount of low molecular weight fractions compared to the unmodified chitosan LMW samples. (**Figure 3.21**) A polymer crosslinking throughout the small molecular weight range could have been the potential reason for this data. In contrast, the thiobutylamidine modification of low viscosity chitosan lead to higher molar mass profiles over the whole range, which might be based on the natural origin of chitosan and also on a partial depolymerisation during the sulfhydryl modification process.

3.5.4 Chitosan sulfhydryl-group and disulfide-bond quantification

Since the chitosan types discussed were modified with the sulfhydryl groups we compared the total amount of free sulfhydryl groups and the existing disulfide bonds to the calculated molar masses. In **Figure 3.22** these three parameters were correlated and it was shown, that a constant amount of disulfide bonds throughout the samples did not automatically account for higher molar masses of the polymers.
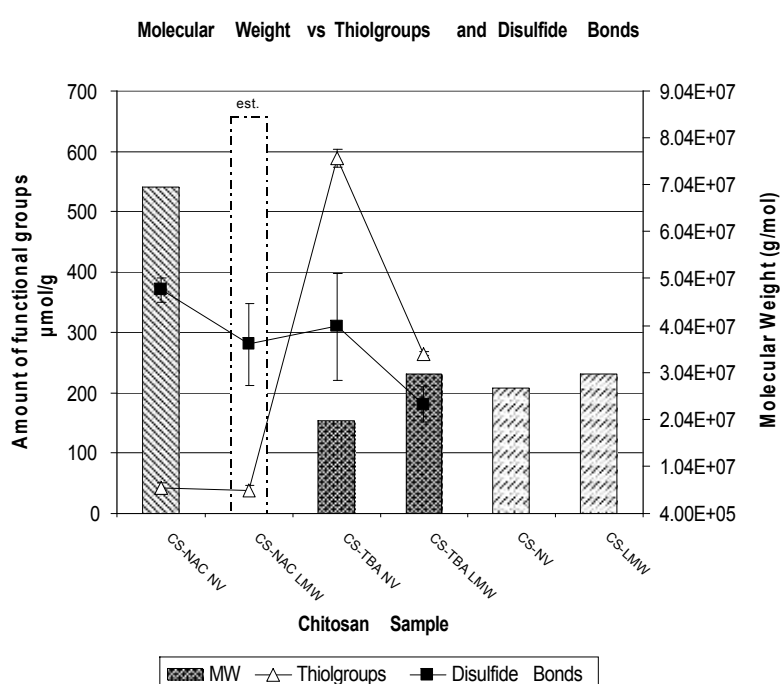
Figure 3.22

Comparison of the calculated molecular weights with disulfide bonds and free sulfhydryl groups in the chitosan samples. The CS-NAC low molecular weight sample was too viscous for analysis with AF4. Therefore an extrapolated value is shown (dotted line) under consideration of the factor that leads to a MW increase for CS-TBA-LMW.

Chitosan NAC (low viscosity) had 41 μmol/g in sulfhydryl groups and 370 μmol/g in disulfide-bonds, chitosan NAC (low molecular weight) had 38 μmol/g in sulfhydryl groups and 280 μmol/g in disulfide-bonds. The TBA modified chitosan acclaimed for 589 and 265 μmol/g in sulfhydryl groups and 310 and 180 μmol/g in disulfide-bonds for TBA chitosan (low viscosity) and TBA chitosan (low molecular weight) respectively.

110

The influence of these modifications was given exemplarily for the case of TBA modified chitosan in **Figure 3.23**. For the N-acetylcysteine modification of chitosan LMW, the viscosity was so high, that a molar mass calculation could not be made. In all other cases the molar separation and molecular weight calculation was successful and reproducible.
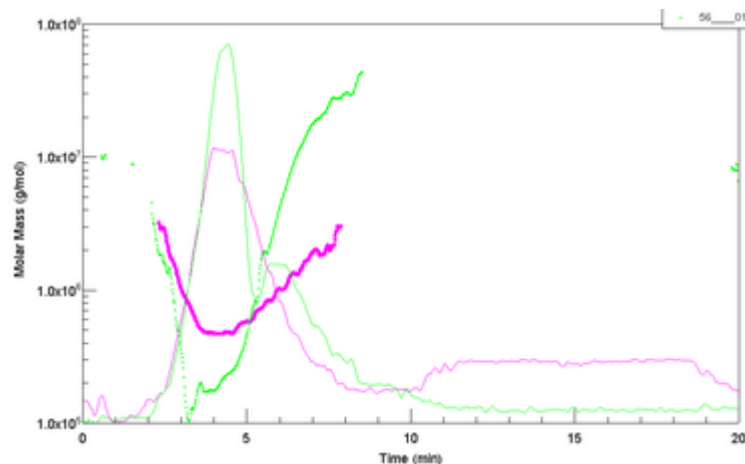
Figure 3.23

Molar mass signals of chitosan samples, chitosan–low molecular weight (■, top), chitosan–TBA–low molecular weight (■, bottom)

With the molecular weight of the thiomers determined we formulated nanoparticles from all unmodified and modified chitosans according to the described method (2.1.8 Formulation of chitosan nanoparticles) and determined the respective hydrodynamic sizes and polydispersity indices. (**Table 3.5**) It turned out that unmodified chitosans after all resulted in the smallest nanoparticles with a narrow size distribution indicated by a small PDI. The TBA chitosans with a large amount of sulfhydryl groups resulted in just slightly larger nanoparticles but with an increased colloidal stability over time. Last but not least, the NAC modulation of chitosan resulted in larger nanoparticles which was due to the high viscosity of the resulting polymer solution.

In conclusion, AF4 analysis was able to determine the molecular weight distribution of the chitosan samples and where modifications of the backbone lead to different retention behaviour to an increased post formulation molecular weight.

Table 3.5

Overview of molecular weight and size of chitosan samples

Chitosan	Avg. MW [g/mol]	SH-groups [µmol/g]	Size [nm]	PDI
C-NV	$1.0*10^6 - 2.7*10^7$	***	170 ± 16	0.04
C-LMW	$4.0*10^5 - 3.0*10^7$	***	190 ± 4	0.09
C-TBA-NV	$2.0*10^6 - 2.0*10^7$	589	220 ± 17	0.20
C-TBA-LMW	$3.0*10^5 - 3.0*10^7$	265	289 ± 23	0.08
C-NAC-NV	$2.0*10^6 - 7.0*10^7$	41	305 ± 8	0.40
C-NAC-LMW	***	38	348 ± 36	0.10

3.5.5 Asymmetric flow field-flow fractionation of DEAE-dextran

An analytical method for the analysis of free DEAE-dextran in presence of free gelatin and gelatin nanoparticles using the conventional AF4 technique had to be developed. Further the amount of free DEAE-dextran in DEAE-dextran modified gelatin nanoparticle preparations had to be quantified as a process quality-control, as a proof of concept and lastly as a means to determine the maximum loading capacity of this polysaccharide within the protein matrix. The analysis of dextran incorporation into gelatin nanoparticles with AF4 at the chosen conditions was quantitative. In the final nanoparticle formulation no free dextran could be detected.
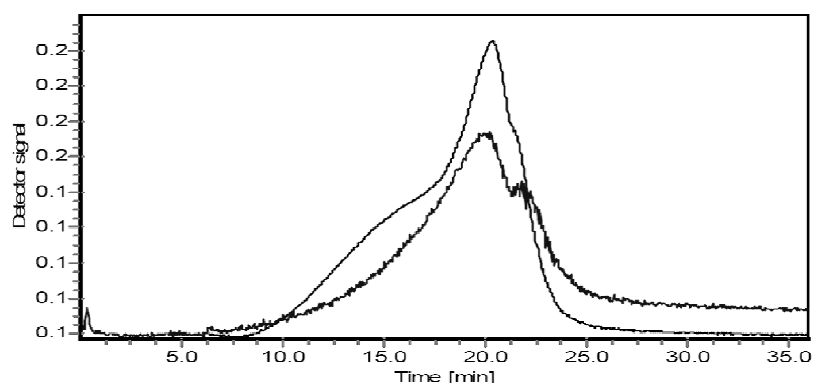
Figure 3.24

90° light scattering signals of unmodified dextran (top) and modified DEAE-dextran (bottom)

In the course of method development at first the signals of DEAE-dextran were correlated with those of a pure unmodified dextran (**Figure 3.24**). As a result no artefacts within the samples were detected as exemplarily shown in the RI signals.
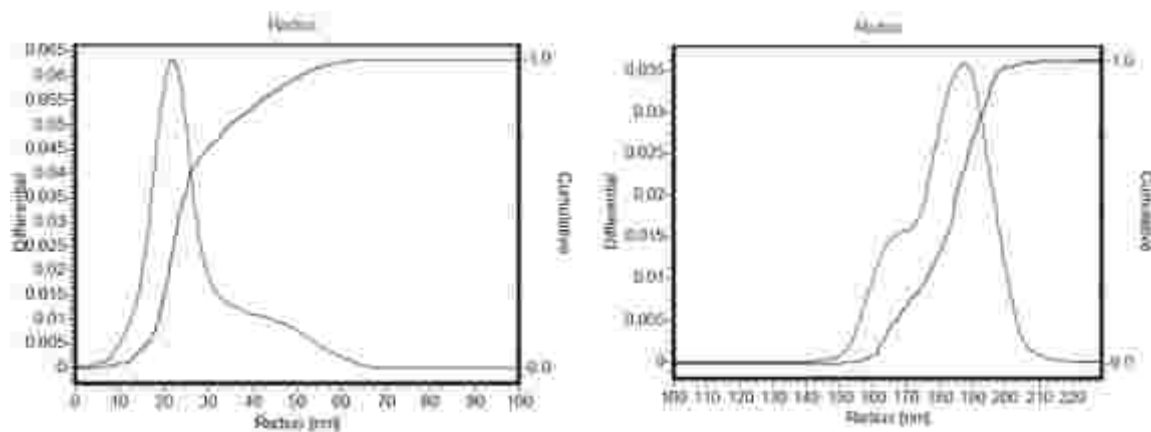
Figure 3.25

Differential and cumulative molar mass distribution plotted against the molecular radius of pure DEAE-dextran (left) compared to a sample of DEAE-dextran modified GNP (right)

Cumulative and differential analysis of the distribution of radii revealed, that the no free DEAE-dextran was present in the finished formulation (**Figure 3.25**). The radius with 182 nm and a shoulder at 165 nm was much larger than that of the free dextran control with 20 nm. With AF4 it could be shown that the used amounts of DEAE-dextran were fully incorporated into the gelatin nanoparticle matrix and that there was no polysaccharide leaking over time.

In addition to the above studies the mobile phases NaCl and $NaNO_3$ and two different membranes were evaluated. A RC 10 kDa membrane was compared to an amphiphilic YM10 membrane. Based on these results the optimum separation conditions were determined. We observed that the literature based $NaNO_3$ buffer had a negative effect on the DEAE-dextran samples since we could observe strong aggregation phenomena in the AF4 chromatograms as depicted by the presence of two peaks in the chromatogram (**Figure 3.26**).
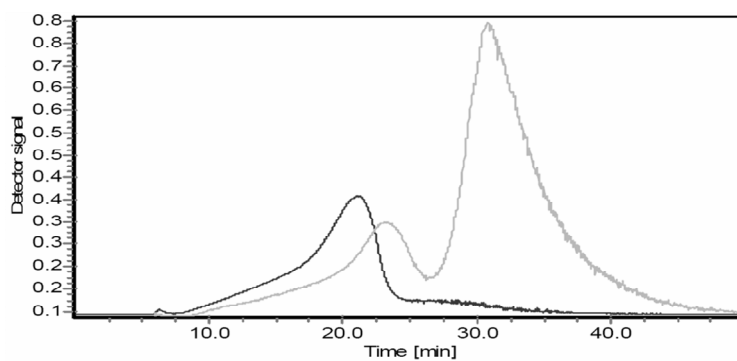
Figure 3.26

90° light scattering signals of DEAE-dextran in 0.1 M NaCl + 0.2 g/L NaN_3 and in 0.1 M $NaNO_3$ (two peaks)
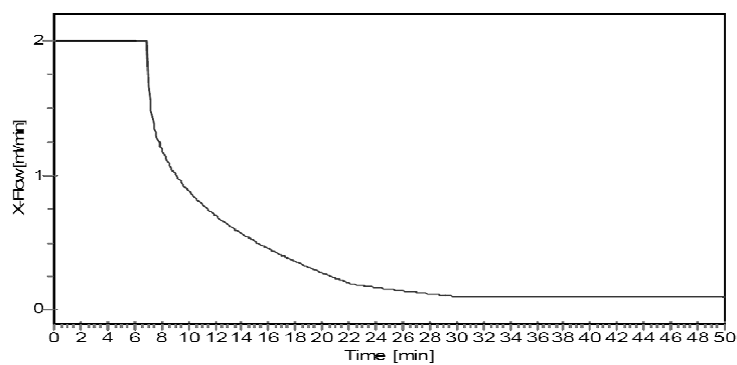
Figure 3.27

Cross-flow profile of the dextran runs from **Figure 3.26**

Concerning the differences in the membrane materials for DEAE-dextran samples no significant differences were detected, while gelatin was found to coat the RC10 membrane in $NaNO_3$ buffer. YM10 was much less susceptible to gelatin loading as confirmed by analysis of the 90° laser diffraction signals.

3.5.6 Nuclear magnetic resonance spectroscopy of modified gelatins

It was a major concern to formulate new gelatin nanoparticles with either a very hydrophobic surface or a permanent cationic charge.

Methylation

Methylation resulted in a pH dependent cationization of the amino groups of the gelatin and the respective nanoparticles formulated there from. This method of cationization was an alternative approach to cholamine and DEAE-dextran assays. Possibly advantageous in terms of a higher cationic charge is the fact, that besides amino modifications also hydroxy group methylations of some amino acids happened [Polnok, A. et al. 2004]. After several needful modifications to the protocol obtained from literature [Cafaggi, S. et al. 2007], methylation could be achieved while the solvent 1-methyl-2-pyrrolidon was not fully discarded, disturbing the signal quality. The solution was to change the desolvation agent from ethanol to an ethanol:diethylether mixture 1:1 (w/w) and to use acetone as the desolvation agent after ion exchange. The resulting modified gelatin was of a yellow shiny hue. NMR results of the probe showed the new methyl groups at δ [ppm] = 2.5 and at δ [ppm] = 2.7 when compared to unmodified gelatin (**Figure 3.28**).

Table 3.6

Zeta potential of mGNP at pH 5.7 (N-GNP 24 mV at this pH) and size

Batch	Zeta potential [mV]	Conductivity [µS/cm]	Size [nm]	PDI
Methylated GNP 1	29.8	0.319	380	0.100
Methylated GNP 2	28.1	0.480	405	0.085
Methylated GNP 3	32.6	0.420	377	0.043
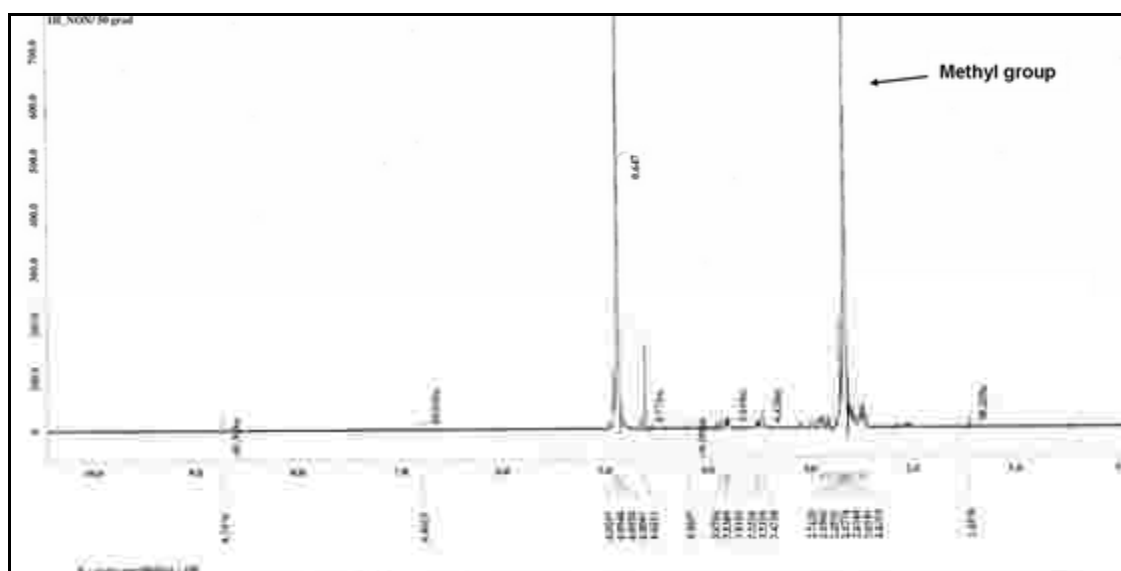
Figure 3.28

^{1}H-NMR spectrum of methylated gelatin in D_2O

Acetylation

It was the goal of the acetylation to formulate GNP with changed physicochemical properties and at first hand an increased hydrophobicity. This should then allow for different cell uptake and cell interaction patterns in the *in-vitro* and *in-vivo* studies with the long term goal of passing the blood-brain-barrier [Löffler, G. et al. 2007]. The reagent for this reaction was acetic anhydride which reacts with nucleophilic groups like amino groups, phenolic groups, aliphatic amino groups, sulfhydryl and imidazole groups. As a result, the number of pH-dependent positive amino groups decreased and the amount of neutral acetylic groups increased, thus reducing the positive charge of the potential nanoparticles. Furthermore did the electrostatic interactions between anionic carboxylic groups and cationic amino groups decrease [Glazer, A. N. et al. 1976].

Table 3.7

Zeta potential of aGNP at pH 5.7 (N-GNP 24 mV at this pH) and size

Batch	Zeta potential [mV]	Conductivity [µS/cm]	Size [nm]	PDI
Acetylated GNP 1	15.7	0.572	312	0.080
Acetylated GNP 2	16.3	0.577	318	0.062
Acetylated GNP 3	12.3	0.824	384	0.008

116

The color of the acetylation product was dark yellow with a tendency to grey. Compared to the unmodified gelatin, acetylated gelatin was hardly soluble in water, evidently indicating the success of the acetylation process. The acetylation was however not significantly detectable in the ^{1}H-NMR where only minor changes were detectable in an overlay of modified and unmodified gelatin (**Figure 3.29**). Nanoparticles formed from a 1:1 mixture of normal and modified gelatin resulted in GNP with a reduced zeta potential compared to that of normal neutral GNP (**Table 3.7**).
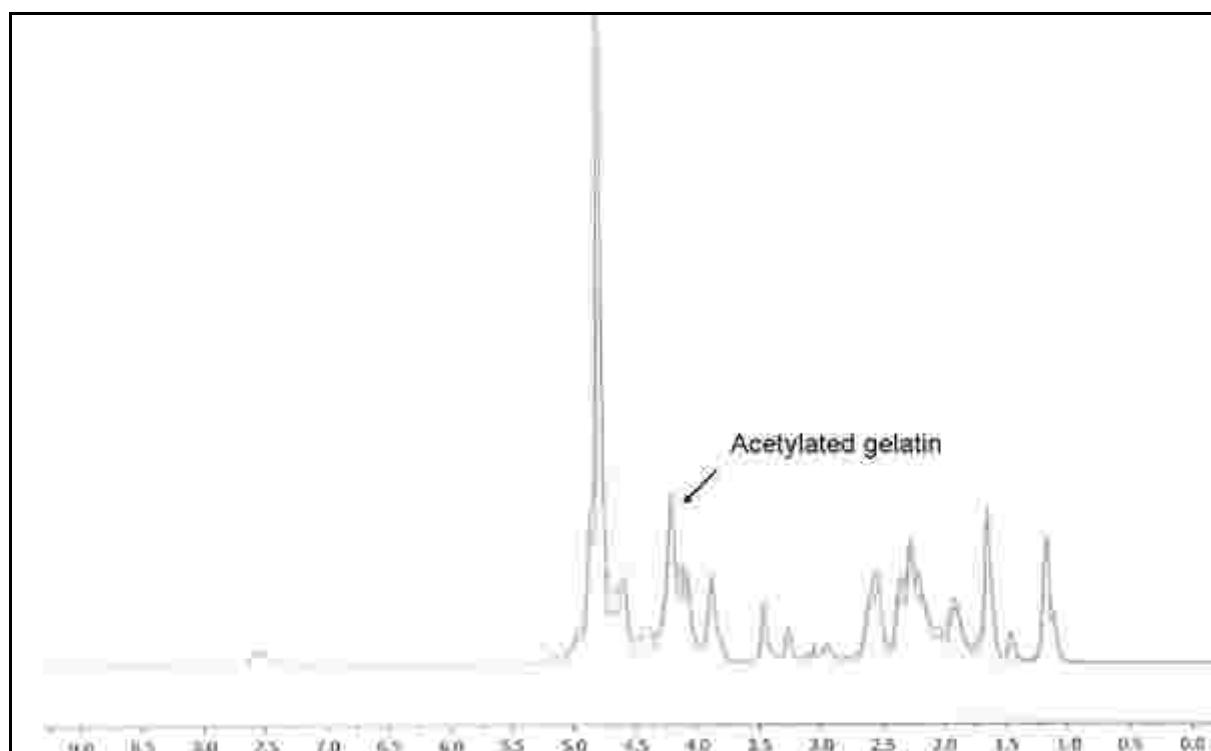
Figure 3.29

^{1}H-NMR spectrum of acetylated gelatin

3.6 siRNA containing gelatin nanoparticles (SICONs)

The zeta potential measurements of our modified nanoparticles revealed an interesting fact: Compared to neutral gelatin nanoparticles the cholamine modification lead to sufficient cationic charged nanoparticles. However, when loaded with siRNA molecules, these nanoparticles lost much of their cationic surface potential again. This effect was due to the ionic interaction of negatively charged siRNA molecules with the cationic amino groups of the nanoparticles. For example, a zeta potential of 25 mV was measured on common cholamine cationized GNP that was lowered to 2 mV after loading with 0.5 % siRNA. This raises the question how nanoparticles with a higher zeta potential can be formulated and secondly what the impact of siRNA loading on their surface would be. In contrast to the cationic cholamine gelatin nanoparticles, cholamine DEAE-dextran modified GNP showed a weaker influence of the incubation medium concerning the total amount of loaded siRNA. The enhanced cationic charge on the surface as well as the cationic polysaccharide backbone was found to be the reason for this phenomenon.

The weight to weight amount of loaded siRNA was calculated from unbound siRNA determined UV-spectrophotometrically at a wavelength of 260 nm (refer to 2.3.12 siRNA loading determination via ultra-violet-absorption). Here it was shown that nanoparticles with cholamine modification could hold up to 10 % (w/w) siRNA on its surface, again, with the amount of siRNA put into direct relation to the total amount of dry nanoparticle polymer.

For dose finding studies in the following transfection studies, the nanoparticles had to be analyzed first on any changes of zeta potential and size at different loading ratios Nanoparticles could be loaded with siRNA to a maximum of 2.5 % with siRNA without losing their positive zeta potential (**Figure 3.30**). Larger amounts of siRNA (above 5 % and up to 20 %) resulted in the zeta potential dropping beneath 0 mV. Cholamine DEAE-dextran gelatin nanoparticles were loaded to a maximum of 5% (w/w) before losing their positive charge. However any amounts above 2.5 % will not be needed for gene silencing studies due to the catalytic effect of the RNAi mechanism where already smallest amounts in the nanomole range were enough to induce a protein knock-down. More importantly these novel siRNA containing gelatin nanoparticles (**SICON**s) retained much of their initial cationic

surface charge after being loaded with siRNA molecules. In addition, covalently bound cholamine emphasized this effect even further.
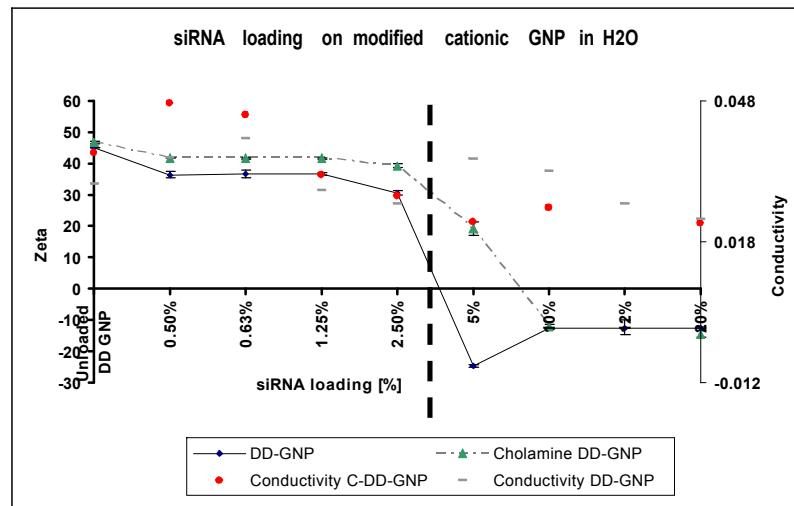
Figure 3.30

Zeta potential and conductivity of DD-GNP and cholamine modified DD-GNP at different siRNA loading ratios (w/w)

Additionally, **Figure 3.31** shows that the change in zeta potential from positive to negative was also reflected in aggregation phenomena of the nanoparticles as detected by size changes combined with an increase in the polydispersity index.
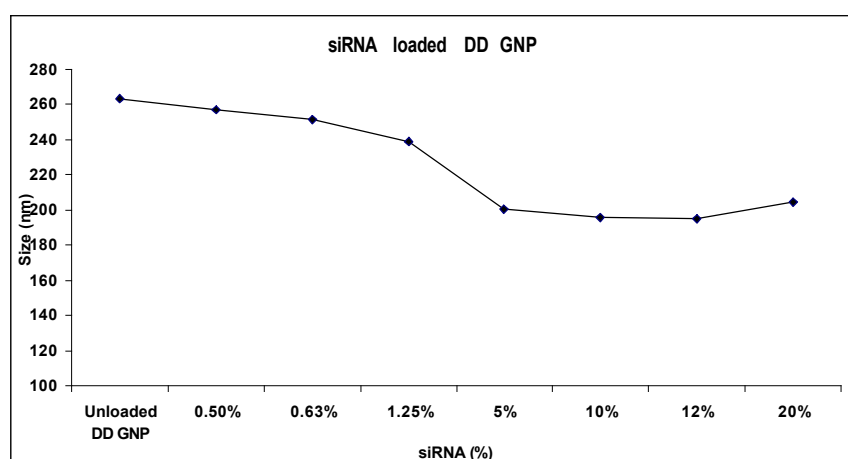
Figure 3.31

Size of siRNA loaded gelatin nanoparticles (+DEAE-dextran) at the following different loading ratios: 0.5, 0.63, 1.25, 5, 10, 12 and 20 %

In highly purified water and without any other stress factors siRNA stayed bound on the nanoparticles up to a minimum time span of 60 minutes. Before this time point no significant changes in size and zeta were observed. We were able to demonstrate that siRNA loaded nanoparticles did not aggregate after 72 hours of storage at 4 °C
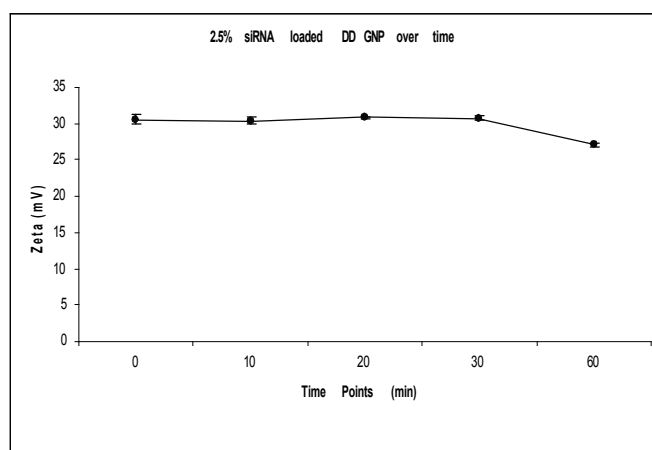
Figure 3.32

Zeta potential of siRNA loaded gelatin nanoparticles (+DEAE-dextran) over time (n=3)

3.7 Sandwich nanoparticle formulation with a Melittin construct

The basic idea of our novel sandwich nanoparticles is shown in **Figure 3.33**. At first, based on the DEAE-dextran and gelatin particle core the surface was further cationized with cholamine residues as described earlier (refer to 2.1.4 Formulation of cationic gelatin nanoparticles). The second step was the incubation with siRNA followed by the final PEG-PLL-DMMel surface coating to form the ready-to-use loaded nanoparticles. The sufficient and lasting binding of the siRNA was important for further formulation and gene silencing. The siRNA binding capacity and stability in the relevant media was therefore determined using quantitative gel electrophoresis for the following formulations: cholamine cationized gelatin nanoparticles, DEAE-dextran-GNP (DD-GNP) and cholamine cationized DEAE-dextran gelatin nanoparticles (CDD-GNP), all loaded with siRNA molecules at different weight to weight ratios. The screening of these different siRNA to gelatin ratios was conducted in the four different loading media that were HEPES buffered glucose, MQ water and PBS at two different pH values (7.0 and 7.4). The quantification was done by analyzing the gel-shift assay with ethidium bromide staining.
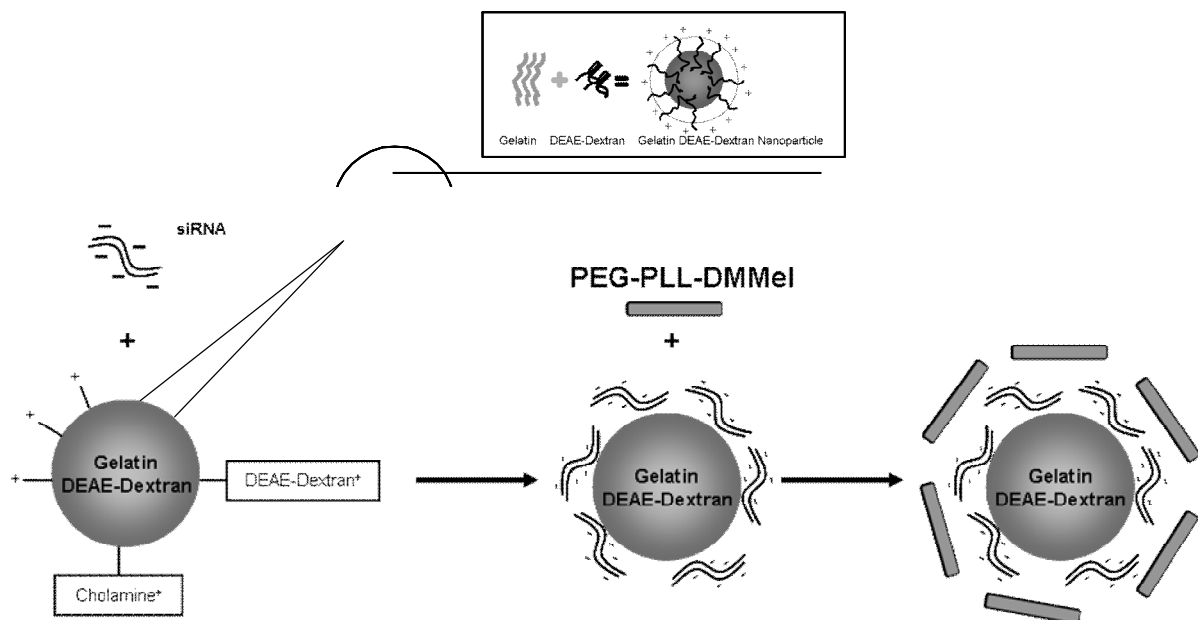
Figure 3.33

Schematic principle of siRNA loading onto cholamine modified DEAE-dextran GNP and consecutive formation of sandwich nanoparticles with PEG-PLL-DMMel

The chosen conditions worked well for our nanoparticle formulations and we were able to produce reproducible results over min. n=3 measurements. The gel shift analysis provided the more sensitive quantification method of the loading process compared to the conventional centrifugation procedure. It allowed for a broader loading screening with less time effort and has a higher resolution when used with modern picture analyzer software. The tested nanoparticles had the following characteristics:

Table 3.8

Overview of the used GNPs for the siRNA loading and gel-shift analysis

Sample Name	T (°C)	Z-Ave (d.nm)	Pdl
cGNP in PBS pH 7.4	25	194.1	0.05
cGNP in PBS pH 7.0 f	25	194.4	0.038
cGNP in MQ	25	243.3	0.03
cGNP in HBG	25	226.7	0.027

Over all cationic gelatin nanoparticle formulations loading capacities from 8.3 % (w/w) up to 25 % (w/w) could be achieved (**Figure 3.34**, **Figure 3.35**). An optimum loading ratio was found between 12:1 (w/w) and 8:1 (w/w) nanoparticle:siRNA. In HBG, siRNA was completely loaded onto the C-GNP nanoparticles at a nanoparticle to siRNA ratio of 8:1 (w/w). That was equivalent to a 12.5 % loading For the CDD-GNP loading ratios up to 4:1 could be reached which was equivalent to a 25 % loading. DD-GNP could also be loaded with siRNA however to a smaller extent which can be explained by the lower zeta potential of the nanoparticles. CDD-GNP showed a strong binding of the siRNA in the highly ionic media PBS with PBS at pH 7.4 allowing for a slightly better binding than PBS at pH 7.0 which however cannot be explained by the slightly decreased zeta potential but probably by the physicochemical characteristics of the siRNA. Compared to older loading studies [Zillies, J. et al. 2004] we could facilitate the loading process by changing the complexation temperature to lower temperatures (room temperature rather than +30 °C). Complexation was then completed within 20-30 minutes compared to the often published several hours time frame [Aouadi, M. et al. 2009]. Due to the lower kinetic energy of siRNA and the longer contact time with the nanoparticles this is reasonable due to the generally exothermic adsorption process. As expected, the loading capacities were always slightly higher in highly purified water due to the low ionic background.
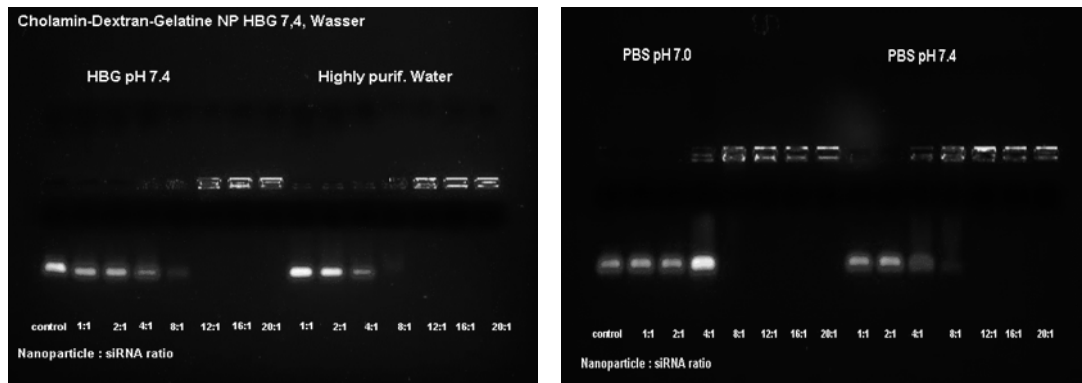
Figure 3.34

Agarose gel shift assay of cholamine modified DEAE-dextran GNP in HBG and HPW (left gel) and in PBS pH 7.0 and PBS pH 7.4 (right gel)
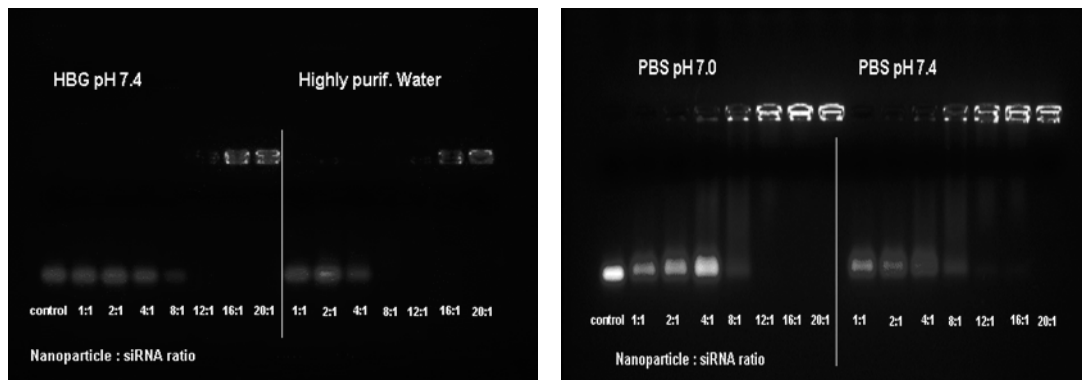
Figure 3.35

Agarose gel shift assay of cholamine modified GNP in HBG and HPW (left gel) and in PBS pH 7.0 and PBS pH 7.4 (right gel)

The gel-shift chromatograms were transferred to 3D projection for a better interpretation and quantification of the single signals (**Figure 3.36**, **Figure 3.37**). For the generated peaks, intensity values can be calculated for further mathematical comparison.

Concluding, we could successfully implement this method of loading quantification into our nanoparticle studies. The method proved to be quick and reliable in combination with the 3D-modelling with a high resolution, showing already small traces of leaking siRNA.
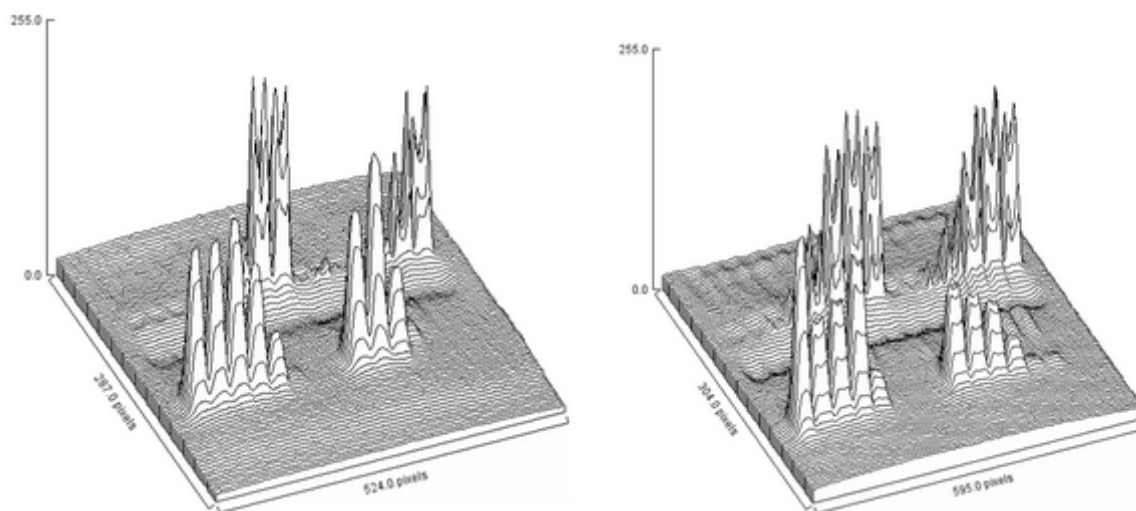
Figure 3.36

3D projection of **Figure 3.34**
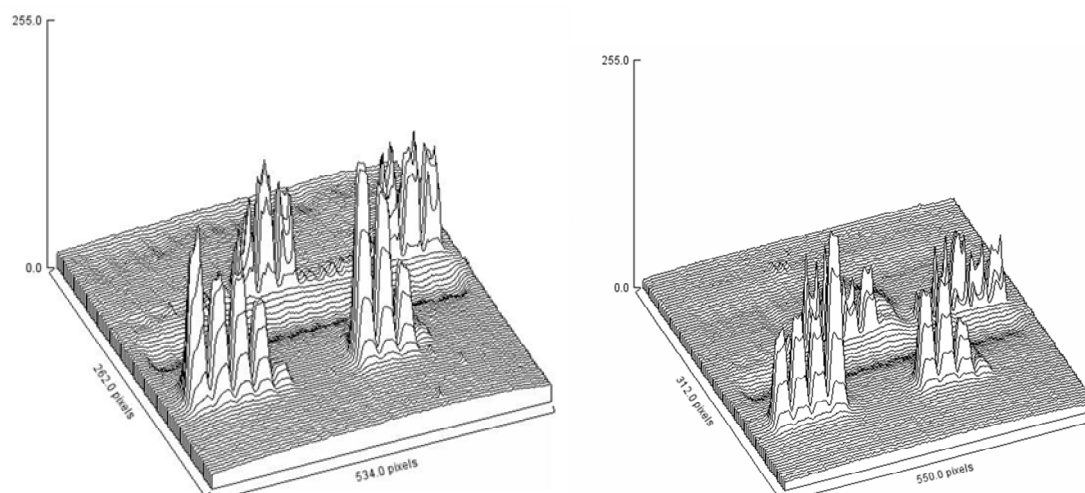
Figure 3.37

3D projection of **Figure 3.35**

Loading of new gelatin nanoparticles under stress:

Cholamine cationized gelatin nanoparticles, DEAE-dextran GNP and cholamine cationized DEAE-dextran gelatin nanoparticles (CDD-GNP) were loaded with siRNA molecules under modified conditions (FCS, DMEM) in order to simulate the conditions during the gene silencing. The determination of the loading efficiency was again done by gel-shift assay with ethidium bromide staining on agarose gel as previously described (refer to 2.3.13 siRNA

loading determination via gel shift assay). siRNA stability under stress conditions was examined as shown in **Figure 3.38**.

Figure 3.38

Agarose gel shift assay of siRNA loaded CDD-GNP in DMEM and FCS at loading ratios of 40:1 and 160:1 (w/w) as described in **Table 3.9**

Table 3.9

Description of the bands in the agarose gel shift assay in **Figure 3.38**

1	siRNA			
2	siRNA	+NP		
3	siRNA	+NP	+DMEM	40 : 1 (w/w)
4	siRNA	+NP	+FCS	
5	siRNA	+NP		
6	siRNA	+NP	+DMEM	160 : 1 (w/w)
7	siRNA	+NP	+FCS	

We found that lower temperatures were helpful for a higher siRNA loading. In terms of stability of the loaded siRNA in cell culture medium and FCS (fetal calf serum) we demonstrated that the siRNA was protected from degradation and dissociation when loaded on the nanoparticles. While free siRNA (band 1) would of course run from the origin in the center of the gel to the electrode, neither nanoparticles loaded with siRNA at a ratio of 40:1

nor at 160:1 showed a siRNA leaking. Instead, FCS and DMEM treatments of the samples did also not destabilize the load making those loaded nanoparticles suitable for *in-vitro* and *in-vivo* experiments. No free siRNA or smaller siRNA snippets could be detected. We think that this observed oligo-protective effect of our nanoparticles can be attributed to the sponge like structure and the brush-like chains from the DEAE-dextran. Our siRNA results were further underlined by earlier results with thiolated GNP and DNA, [Kommareddy, S. et al. 2007] where the positive effect of our whole formulation approach was confirmed, however only with DNA, and not with siRNA.

The confirmation of the successful formation of sandwich nanoparticles was done by photometric analysis and size measurements. PEG-PLL-DMMel and siRNA could not be centrifuged at the given conditions due to their small size that was found to be in a range of 40 nm in the case of complex formation and less for the single molecules, and were therefore measured in the supernatant (**Figure 3.39**).
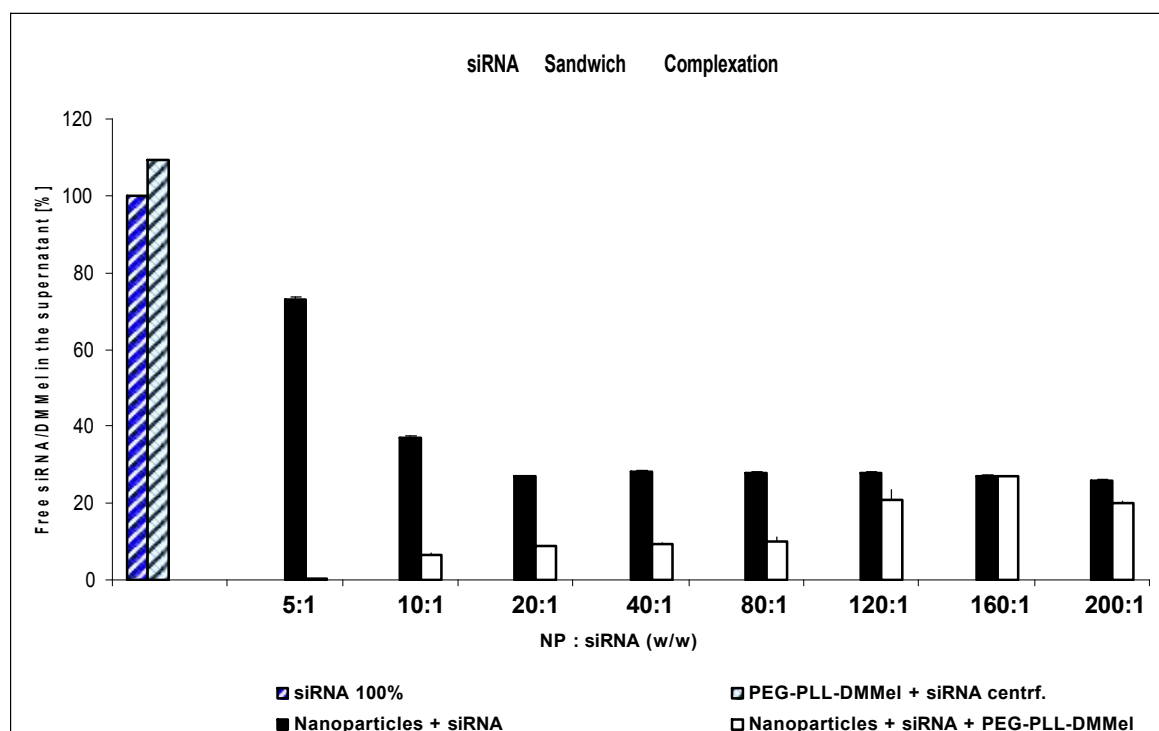
Figure 3.39

UV photometric characterization of the supernatant at 260 nm of nanoparticles (234 nm, PDI 0.01, +47 mV) loaded only with siRNA and nanoparticles loaded with siRNA and PEG-PLL-DMMel.

If SICONs now were incubated with PEG-PLL-DMMel however, the signal of free siRNA and PEG-PLL-DMMel in the supernatant was greatly reduced indicating the formation of sandwich nanoparticles by adsorption of PEG-PLL-DMMel and siRNA onto the nanoparticles. In this case the siRNA molecules as well as the bee peptide construct were bound onto the charged surface of the gelatin nanoparticles taken into account their different electrostatic interaction potential. Without this centrifugation and photometric analysis it was not clear whether the PEG-PLL-DMMel was effectively bound to the nanoparticle surface and whether there was no interaction between PEG-PLL-DMMel and the siRNA itself. The GNP loaded with siRNA alone strongly bound the available siRNA molecules in the dispersion. From 5:1 down to a ratio of 10:1 (w/w) NP:siRNA, free siRNA was unbound in the nanoparticle dispersion corresponding to the gel shift assay, while at a ratio of 20:1 (w/w) and higher most siRNA molecules were bound. Up to a tested ratio of 200:1 (w/w) the sandwich complexes could be formed.
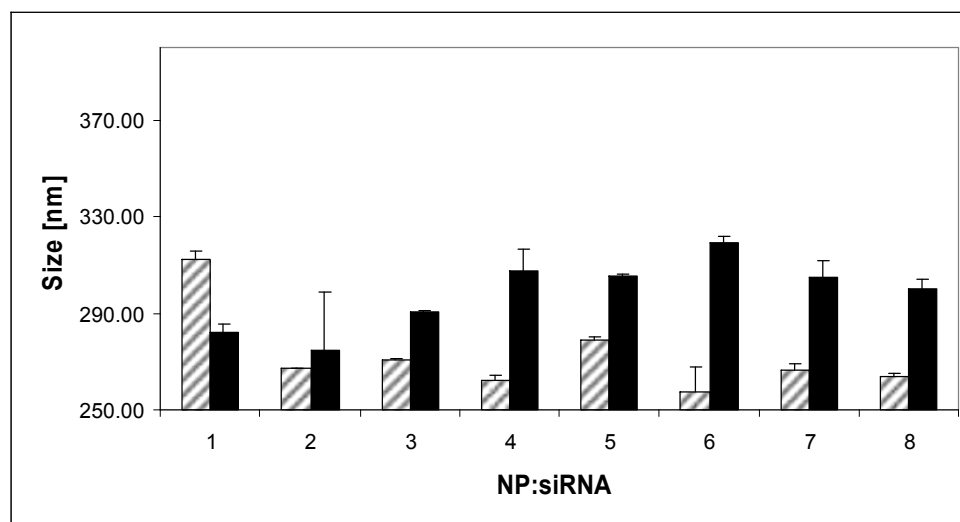
Figure 3.40

Size distribution of SICONs loaded with PEG-PLL-DMMel (■) and unloaded (▱)

In addition to the photometric assay, DLS based size analysis of the **SICON**s and the sandwich nanoparticles was performed (**Figure 3.40**). In all samples we detected a very narrow size distribution with sandwich nanoparticles being significantly larger by ~10 – 60 nm $\pm$ 2 nm S.D. than the uncoated nanoparticles indicating the layer formation around the **SICON**s.

Finally with our results we could show that a sandwich like loading of both siRNA and PEG-PLL-DMMel had taken part during the incubation time and that no siRNA was withdrawn from the nanoparticle surface by the cationic polymer construct. These findings ensured that the given cell targeting, endosomal escape and later knock-down results could be attributed to our novel nanoparticle system. The first report on electrostatically driven layer-by-layer assembly of colloidal particles was published by Iler [Iler, R. K. 1966]. He showed the interaction between oppositely charged silica and alumina particles to multilayer structures. The first layer-by-layer technique for biomacromolecules was then demonstrated by Decher et al. [Decher, G. et al. 1991]. From then on many groups worldwide have used this technique to formulate novel carriers in the micrometer and nanometer range. For gelatin nanoparticles layer-by-layer modifications were so far only shown by Shutava et al. [Shutava, T. G. et al. 2009] for the delivery of polyphenols making our study a seminal step forward in this field and pushing the potential of gelatin nanoparticles as a multifunctional carrier a little further.

3.8 Storage stability of unloaded and siRNA loaded gelatin nanoparticles

The presented data showed that all formulations did not decrease or increase significantly in size and PDI. Throughout the examined time span, no major changes in the zeta potential of the formulation could be observed.

For the relevant stability of the formulation it was mandatory to examine the novel formulations over a time period of four months both at room temperature and at 4 °C. By analyzing the zeta potential of the stored formulations, stability issues like surface adhesion, polymer interactions and changes in particle shape can be brought forward. An increase in particle size due to aggregation phenomena paired with larger polydispersity indices accounted for changes within the formulation. However we could demonstrate, that over the given storage conditions no significant changes within the formulation could be observed. This again demonstrates how a potential colloidal instability could be overcome by a controlled increase of the zeta potential of the nanoparticles. In detail, the measured size for t=0 for the final sandwich formulation (the same that as tested *in-vitro*) was 235 nm.

3.9 Endotoxin assay

Endotoxins are toxins derived from structural components of bacteria. Recent research has demonstrated how endotoxins can promote adhesive interactions between platelets and microvascular endothelium *in-vivo*. Studies in the mouse cremaster of C57BL/6 and C57BL/10J mice with lipopolysaccharide (LPS) and escherichia coli endotoxin showed enhanced rates of venular platelet thrombus formation. The time to microvessel occlusion was reduced by 50% (P<0.005) compared with saline treated animals [Rumbaut, R. E. et al. 2006]. Since these findings were highly relevant to our study with nanoparticles in the mouse cremaster model but also plays a pivotal role in any *in-vivo* application of nanoparticles we had to make sure that our nanoparticles from the first formulation step to the final dosage form was generated in an endotoxin free way. Gabrielsson and Vallhov from the Karolinska Institute in Stockholm support this notion that a high purity in the production of nanoparticles is essential in order not to interfere with the assessment of biological and medical effects [Vallhov, H. et al. 2006]. Therefore our nanoparticles were analyzed with LAL test (**Table 3.10**).

The final results expressed in endotoxin units per milliliter (EU/ml) are referred to as S1 for gelatin nanoparticles resulted in raw EU of <0.0544 and a recovery rate of 113 % for a dilution of 1:100 and EU of <0.005 and a valid recovery rate of 113 % for a dilution of 1:1000. The average incubation time was 4059 sec for the nanoparticles and 1293 sec for the positive product control. All samples were beneath the relevant limit of 5.00 EU/ml and are therefore regarded endotoxin free.

With this data we could exclude endotoxin related effects on the low fluorescent signals or thrombotic effects of the nanoparticles during our *in-vivo* experiments. Also the rare thrombotic effects after application of highly concentrated nanoparticle dispersions shall not be related to endotoxin contamination but to other effects explained later.

Table 3.10

LAL endotoxin assay

Analyst ID: SMARECHAL (VA)	BWI LAL Lot No	GL 168H	Exp: 18/06/2010	Time 16:51.34
Inhibition Enhancement Assay	Water Lot No	GL 1294	Exp: 07/05/2010	Date: 05/06/2008
Template: SM 05/06/08	Endotoxin Lot No	GL 1157	Exp: 04/10/2011	KQCL
Temp: N/A				S/N 1584
Linear Regression	CORR = -0.998	SLOPE = -0234	Y Int. = 3.054	
Reader Parameters	Delta t = 160	Meas. Filt. 405	Delta mOD = 200	Reads No = 40

			Nanoparticles			
						Rel. Limit: N/A
SAMPLES	**DILUTION**	**WELL**	**REACTION TIME (sec)**	**AVG. TIME**	**RAW EU**	**RESULTS (LR) EU/ml**
S2	100	C9	2187	2178	<0.0544	5.44
		C10	2168			
PPC	100	D9	1193	1197	0.620	
		D10	1200			
	PPC Value: 0.5	PPC % recovery	113%	PPC-Sample 1 Endotoxin Recovered: 0.566		

			Nanoparticles			
						Rel. Limit: N/A
SAMPLES	**DILUTION**	**WELL**	**REACTION TIME (sec)**	**AVG. TIME**	**RAW EU**	**RESULTS (LR) EU/ml**
S1	1000	G1	4071	4059	<0.005	<5.00
		G2	4056			
PPC	1000	H1	1290	1293	0.567	
		H2	1296			
	PPC Value: 0.5	PPC % recovery	113%	PPC-Sample 1 Endotoxin Recovered: 0.567		
	Comment LTS 4135					

Even though the endotoxin analysis was not conducted prior to all *in-vivo* experiments because of the high cost, the results of the given endotoxin analysis can be extrapolated since all nanoparticles were prepared with the same standardized preparation method. The simple and easy to scale-up preparation method of our nanoparticles in an acetone milieu can be seen as the key role for the low endotoxin contamination observed and eventually will play a role when regulatory [Carpenter, J. F. et al. 2009] and scaling issues come into discussion in the course of preclinical development.

3.10 In-vitro models

3.10.1 Traditional static conditions versus novel flow conditions cell culture model

Cells in their physiological surroundings are subject to shear stress from the blood flow. This force influences the cell morphology to a large extent and can also alter the cell metabolism, gene expression and gene differentiation. Thus, cultivating cells in a model with circulating medium and a persistent shear rate resembles more physiological conditions than doing so in a static cell culture system. The aim of the present study was to investigate the attachment and interaction of various nanoparticles with a cell monolayer under flow conditions. For cell cultivation various ibiTreat µ-slides were used. These were coated with a special surface coating called ibiTreat where plasma was used to modify the polymer so that cells will adhere to the slide in a strong way.

For our experiments 293/KDR epithelial cells and also HUVEC endothelial cells were cultivated for 18 h either under flow conditions in y shaped µ-slides or in static 8-well µ-slides (n=6; refer to 2.4.1.4 Cultivation of cell lines). Within 6 h the cells in the flow channel began to adjust themselves according to the flow direction and to take over a streamlined morphology. After 24 h the cells were grown to 80 % confluence and had a healthy and uniform appearance. Three different spots on the channel were chosen from where to monitor the cell population (**Figure 3.41**).
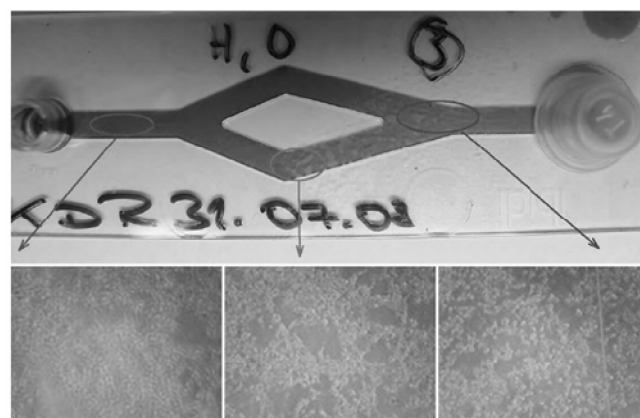
Figure 3.41

Overview (top) and detailed microscopic (bottom) pictures of ibidi y-shaped µ-slide channel incubated with KDR 293 cells

As a result the main channel had the most homogeneous cell growth, we also found cells directed along the flow in the side channels. The cell growth was deviating only at the split in the channel where tiny turbulences occurred. In contrast, the cells in the static chamber grew disordered with higher cell concentration in the corners of the wells, followed by a region of low cell growth and a maximum of confluence again in the very center of the well (**Figure 3.42**). In percent of the total amount of cells grown in one well the growth patterns were determined as 42 %, 8 % and 50 % (from distal to proximal) Furthermore we observed the formation of a meniscus of the medium inside the static well followed by a multi-layer cell growth. We conclude from this data that traditional static cell culture models might be well usable for overall biological assay like receptor analysis with antibodies but for reproducible results in the field of nanoparticle analysis the drawbacks of the model were too eminent to be overseen. In terms of critical discourse with many published nanoparticle *in-vitro* studies a critical review of many results is needed if the data was generated in a static cell culture. Our observations indicate that not only non-reproducible growth-patterns influenced nanoparticle-cell studies but many more factors that will be discussed next.
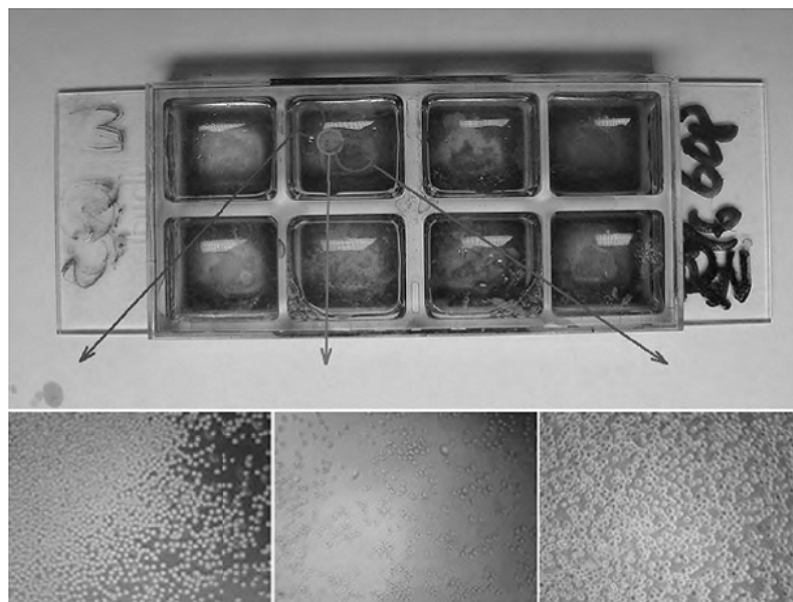
Figure 3.42

Overview and detailed microscopic pictures of ibidi 8 well static chamber incubated with KDR 293 cells

All nanoparticles when added to the flow model circulation were immediately taken up by the medium flow and moved away from the injection side towards the adherent cell monolayer. Thereby the nanoparticles undergo interaction with the medium components. We have demonstrated above (refer to 2.4.1.5 Particle stability in cell culture medium) that our nanoparticles whether unmodified or cationic were not prone to major increases in size due to adhesion of medium components or aggregation phenomena.
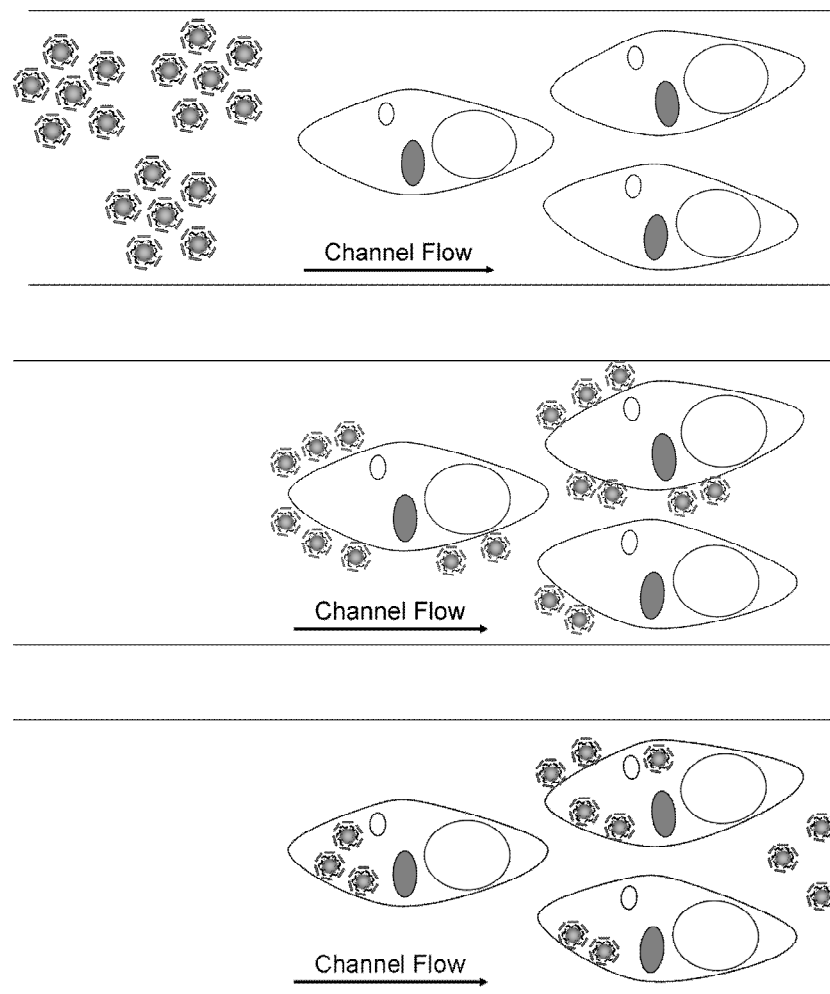
Figure 3.43

Nanoparticle cell interaction studies in the flow chamber model with applied flow and shear rate: top: nanoparticles were added to the confluent cell monolayer; middle: nanoparticles potentially interact with / attach to the cell membrane; bottom: some nanoparticles get internalized while others were floating by, entering another round of circulation.

During the time when the nanoparticles were pumped along the cell monolayer depending on their surface properties, charge and size respectively they interacted with the single cells and attach to their surface. The theoretic principle of nanoparticle interaction with and uptake into cells in our flow model is depicted in **Figure 3.43**.

The expected targeting pattern where nanoparticles would attach to a larger percentage from the flow-directed side was confirmed in confocal studies (**Figure 3.44**).

For a deeper understanding of the later *in-vivo* fate of a nanoparticle we primarily investigated GNP with different modifications in the new flow model. The results for this study where we particularly examined the cell interaction potential of GNP can be seen in **Table 3.11.**

Table 3.11

Type	Size [nm]	PDI	Zeta [mV]	NP/ 100 cells
N-GNP	179	0.004	+4.3	7
DD-GNP	210	0.016	+34.7	29
CDD-GNP	214	0.007	+43.0	71
CDD-GNP	234	0.019	+52.1	83
mGNP	380	0.100	+29.8	18
aGNP	312	0.080	+15.7	9
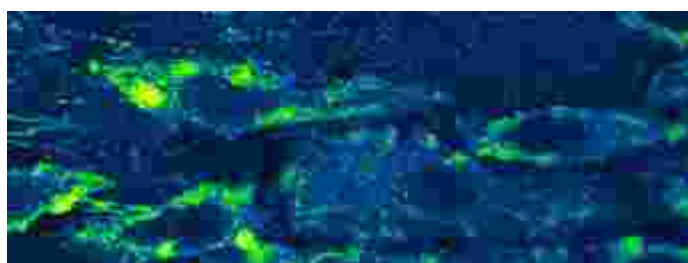
Figure 3.44

Flow directed cationic nanoparticle attachment on epithelial KDR 293 cells under flow (arrow = flow direction)

The most surprising results however were that it were the cationic nanoparticles that interacted with the cells in this very specific manner while the neutral nanoparticles did not show any sign of interaction with the cells in the flow model. They simply got washed away with the medium and even in the recirculation process never managed to give significant fluorescent signals from the cell membrane. A static model study with both neutral and cationic fluorescent GNP revealed that both nanoparticles interacted with the cell membrane leading the researcher totally in the wrong direction with those false positive results (refer to the bachelor thesis of Pia Broermann for detailed results). Of course, for any realistic and preclinical data, the flow of the blood and the homogenous monolayer of cells have to be taken into account for many if not all experiments. It has been shown, that shear stress lead to different protein patterns on the cell surface than when the cells were incubated in a static environment. At physiological shear stresses in the vasculature ranging from 0.5–0.75 dyn/cm^2 to several dyn/cm^2 in microvessels and 30 dyn/cm^2 in large vessels like arteries [Neumann, T. et al. 2003; Ueda, A. et al. 2004] different genes will be expressed than when no shear stress is applied [Dekker, R. J. et al. 2002; Ohura, N. et al. 2003]. Therefore, any interactions between nanocarriers and the cell membrane can vary depending on the flow rate. This aspect is not well documented in the field of non-viral gene delivery systems. To date, the only recent study that has been reported was done with cationic lipids/DNA complexes (lipoplexes) by Harris and Giorgio [Harris, S. S. et al. 2005]. Unfortunately, no statement was made on the type of lipid used, yet they predicted the influence of the flow rate on lipoplex delivery by theoretical calculations and experimental observations with ECV-304 cells and HeLa cells.

3.10.1.1 Toxicity screening

In terms of cell viability in the flow model compared to the static well plate incubation, significant differences could be observed for nanoparticle incubation. **Figure 3.45** shows cell morphology in the static model for C-GNP, PBCA-NP, aGNP and HSA-NP. The cationic GNP were well tolerated and even after 1 h of incubation did not change their morphology when in contact with our nanoparticles. The same accounted for acetylated GNP and methylated GNP (not shown). HSA NPs, due to their negative zeta potential, showed a rather diffuse interaction with the cell membrane that can most likely be attributed to sedimentation and unspecific interaction. HSA NPs however also did not change the morphology in this

experiment significantly however 20 % cell detachment compared to untreated cells was observed over a time period of 1 h.

A cGNPs (green)   B PBCA-NPs (green)   C aGNPs (green)   D HSA-NPs (red)
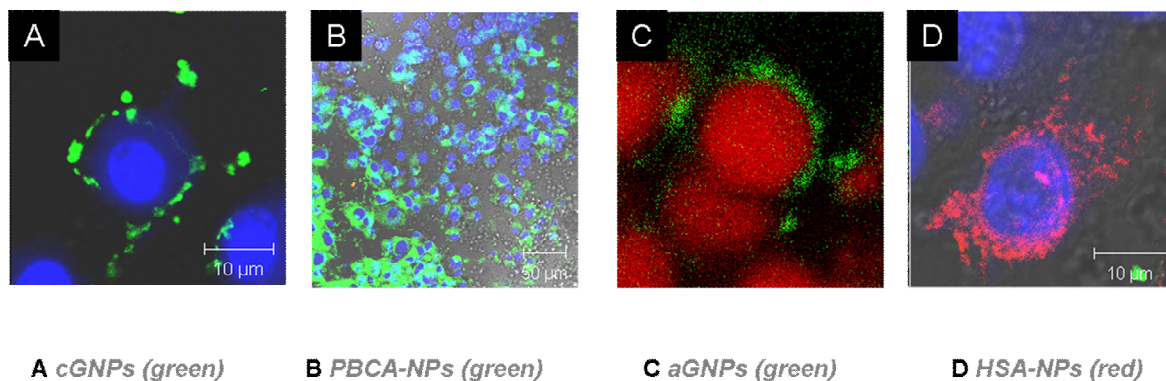
Figure 3.45

Toxicity influence of C-GNP, PBCA-NP, aGNP and HSA-NP on the cell morphology after incubation in a traditional static cell culture model

3.10.1.2 Medium influence

Because not only the above studies but also the gene silencing studies would be done in medium with serum and hence in an environment with different viscosity we had to examine the influence of the medium on the nanoparticle interaction patterns as well. In fact the quantity of serum had a negative effect on the binding capabilities of the cationic nanoparticles. While at 10 % serum a reduction of cell adhesion by 18 % $\pm$ 6 % S.D. was observed (n=3, ROI), 100 % serum lead to high medium viscosity that consequently reduced the nanoparticle sedimentation velocity and their trajectories, only allowed those nanoparticles to attach that were passing the cells closer. In number of cells in the ROI this accounted for a reduction of attached cells by 20 % compared to 10 % serum. Since the binding sites on the cells like proteoglycans could also be coated with serum components, an additional effect to hinder nanoparticle attachment at high serum concentration is possible.

3.10.1.3 Flow and shear stress influence
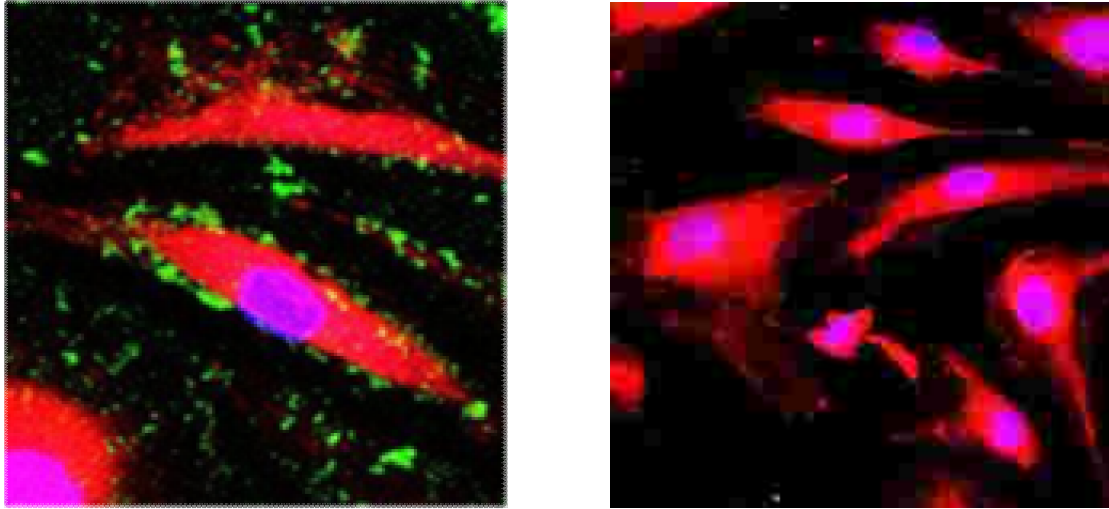
Figure 3.46

Fluorescent labeled cationic GNP (left) and fluorescent labeled unmodified cationic gelatin nanoparticles (right) incubated with HUVEC cells under flow conditions. The unmodified GNP could not target the cell membrane and got flushed away with the medium flow. Similar results were made for KDR 293 cells.

The present data does in fact differ from the results by Harris et al. [Harris, S. S. et al. 2005] by means that we a) used real nanoparticles for the first time for our studies b) employed a closed system for nanoparticle passage on adherent monolayer cells under constant flow conditions with recirculation c) put our focus on adherence rather than on uptake d) used different cell types and e) quantitatively evaluated the attached nanoparticles by using fixed regions of interest (ROIs) over the cells. While our results therefore cannot easily be compared to their study, we confirmed their results of shear stress induced carrier cell interaction and added the new component of nanoparticle and especially gelatin nanoparticles and their distinct different surface characteristics. Taken together with our data, these observations indicate that the shear stress influence both the binding and the uptake of nanoparticles.

3.10.2   VEGF – studies

3.10.2.1 FACS analysis of VEGFR$_2$ overexpression in HEK 293 / KDR cells

With respect to the initially mentioned important role of VEGF and its receptors in many therapeutical applications, VEGFR over-expressing cells were examined next. VEGFR$_2$ in this context plays a major role as a potential target for RNAi and their suitability for the *in-vitro* model had to be proven first. For this reason, human embryonic kidney (HEK) cells over expressing the VEGFR$_2$ (Sibtech, Inc., Newington, USA) were cultivated and tested on their levels of receptor expression compared to normal HEK cells. In order to elucidate the receptor expression a sensitive method using fluorescent single chain VEGF and FACS read-out. The resulting number of fluorescent events detected in the FACS was calculated from a fixed region of interested (gate) that was kept the same throughout all measurements.
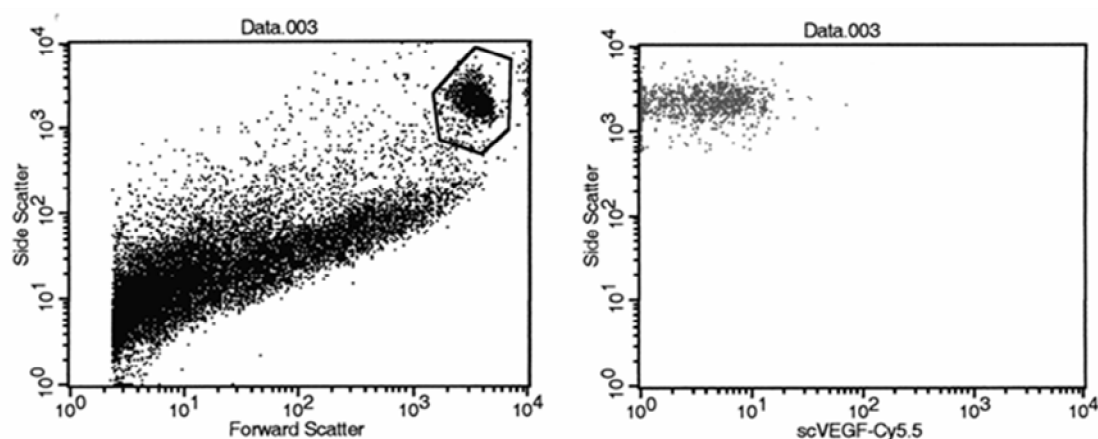
Figure 3.47

ROI (Region of interest) settings for FACS analysis for scVEGF-CY5.5 marked endothelial KDR 293

The unmodified HEK cells when unmodified with scVEGF showed a total of 4001 events in the gate and 130 events within the M1 marker. After 1 h of incubation with scVEGF 2092 were gated with 161 inside M1 (**Figure 3.48**). At the final 2 h measurement point 2395 events could be detected with 233 inside M1. In comparison to those values the HEK/KDR cells revealed the following values. While the unlabeled cells counted 2808 events total and 141

inside the M1 marker, after 1 h and scVEGF-Cy5.5 labeling 2367 events in total and now 816 events inside the M1 were detected (**Figure 3.49**). This amount rose even further after 2 h of incubation to a total of 2799 and 913 events inside M1. In respect to 100% of the gated events this accounted to 32.62 % $VEGFR_2$ expression and a 23 % higher receptor density than on the standard cells.
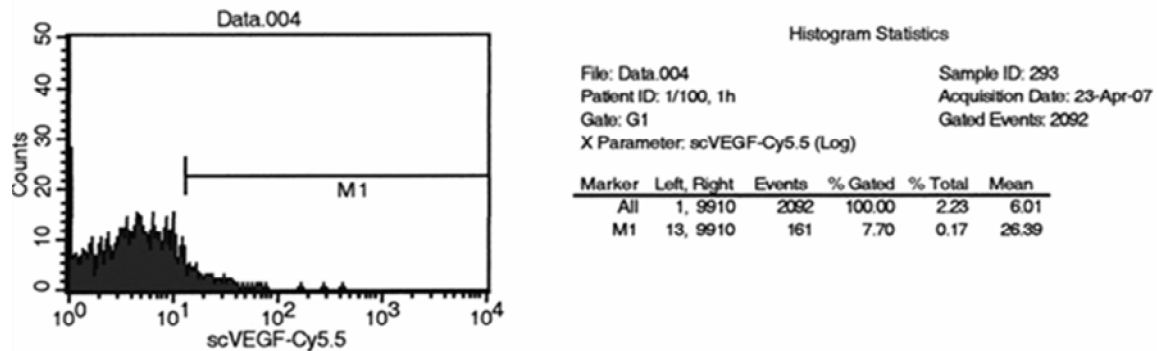
Figure 3.48

FACS histogram of scVEGF-Cy5.5 labeled 293 cells after 1 h incubation
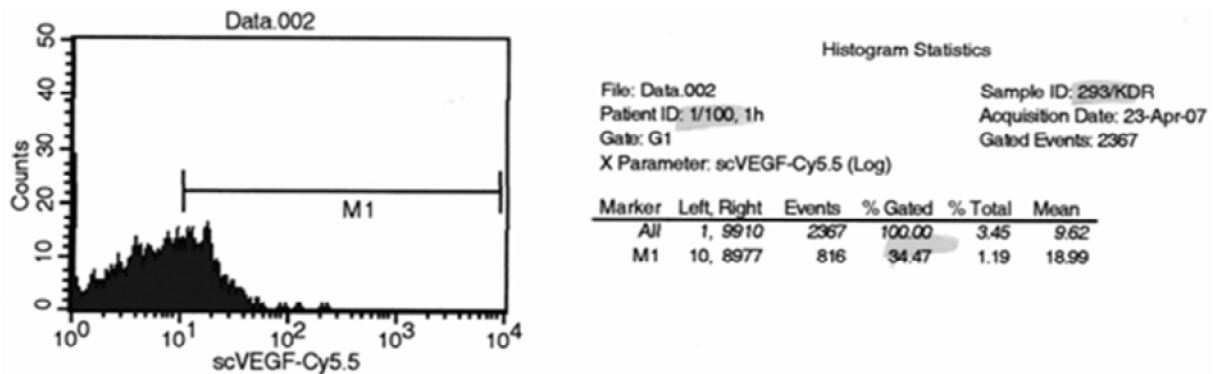
Figure 3.49

FACS histogram of scVEGF-Cy5.5 labeled 293 / KDR cells after 1 h incubation

In conclusion the cells used for our flow-model experiments were capable of expressing higher levels of VEGFR than unmodified KDR cells and were therefore better suitable for strong surface attachment under shear stress application and also for $VEGFR_2$ RNAi experiments with anti-$VEGFR_2$ siRNA.

3.11 In-vivo models

3.11.1   Hamster dorsal skin fold chamber model

In 1928, Sandison [Sandison, J. C. 1928] was the first to implant observation chambers into animals for intravital microscopy of living tissues. Since then, various chambers have been developed and implanted with the aim to investigate the microcirculation in mice, [Algire, G. H. 1943] hamsters, [Greenblatt, M. et al. 1967] rats, [Hobbs, J. B. et al. 1976] rabbits, [Clark, E. R. et al. 1930] and even in human subjects [Branemark, P. L. et al. 1964]. In a very central publication of Krasnici et al. [Krasnici, S. et al. 2003] the authors highlight the tumor targeting effects of their, as model nanocarriers used, cationic DOTAP liposomes in such a microcirculation model. Their results with liposomes were the basis for our further investigations with gelatin nanoparticles. The study revealed that neutral and anionic liposomes when applied intra venously showed a very diffuse and global distribution. Cationic liposomes accumulated within the tumor located inside the hamster skin fold chamber. In terms of fluorescence within normal tissue to tumor tissue ratio, 1.1 (neutral) -1.4 (anionic) : 1 were measured, whereas cationic liposomes showed a ratio of up to 30:1.
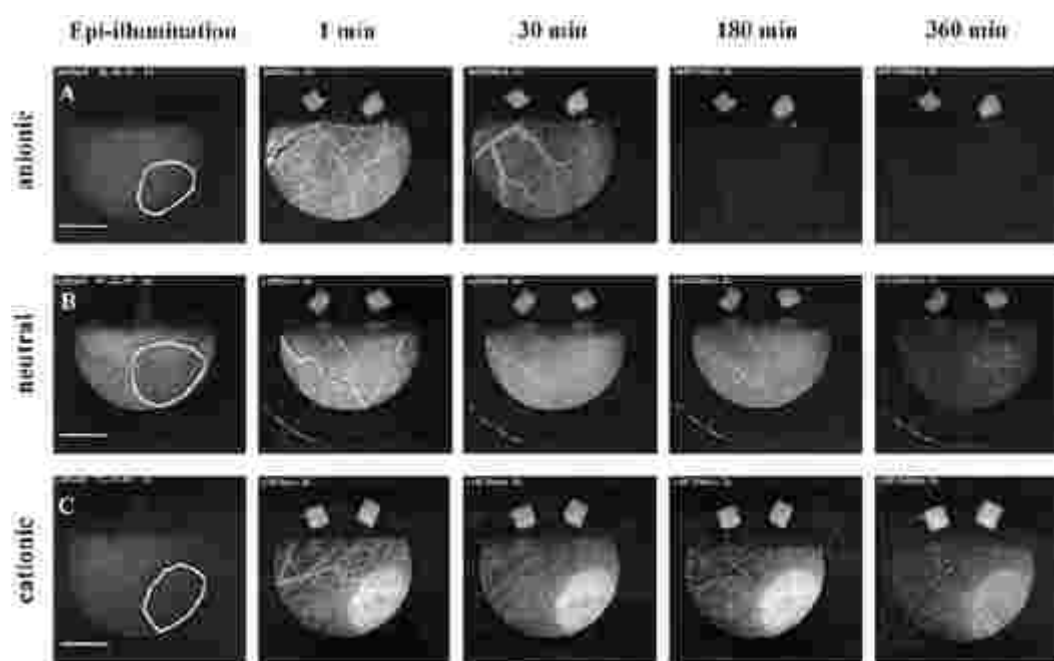
Figure 3.50

Fluorescent labeled anionic (top), neutral (middle), cationic (bottom) liposomes detected in the hamster skin fold chamber. Cationic liposomes persist over minimum 360 minutes.

It still remained hypothetical why these cationic charged liposomes selectively bound to angiogenic microvessel as demonstrated in the above results. Since neutral and anionic liposomes did not show this feature while revealing the same liposome size, the mechanism responsible for liposome binding to tumor endothelial cells is supposed to be charge related.
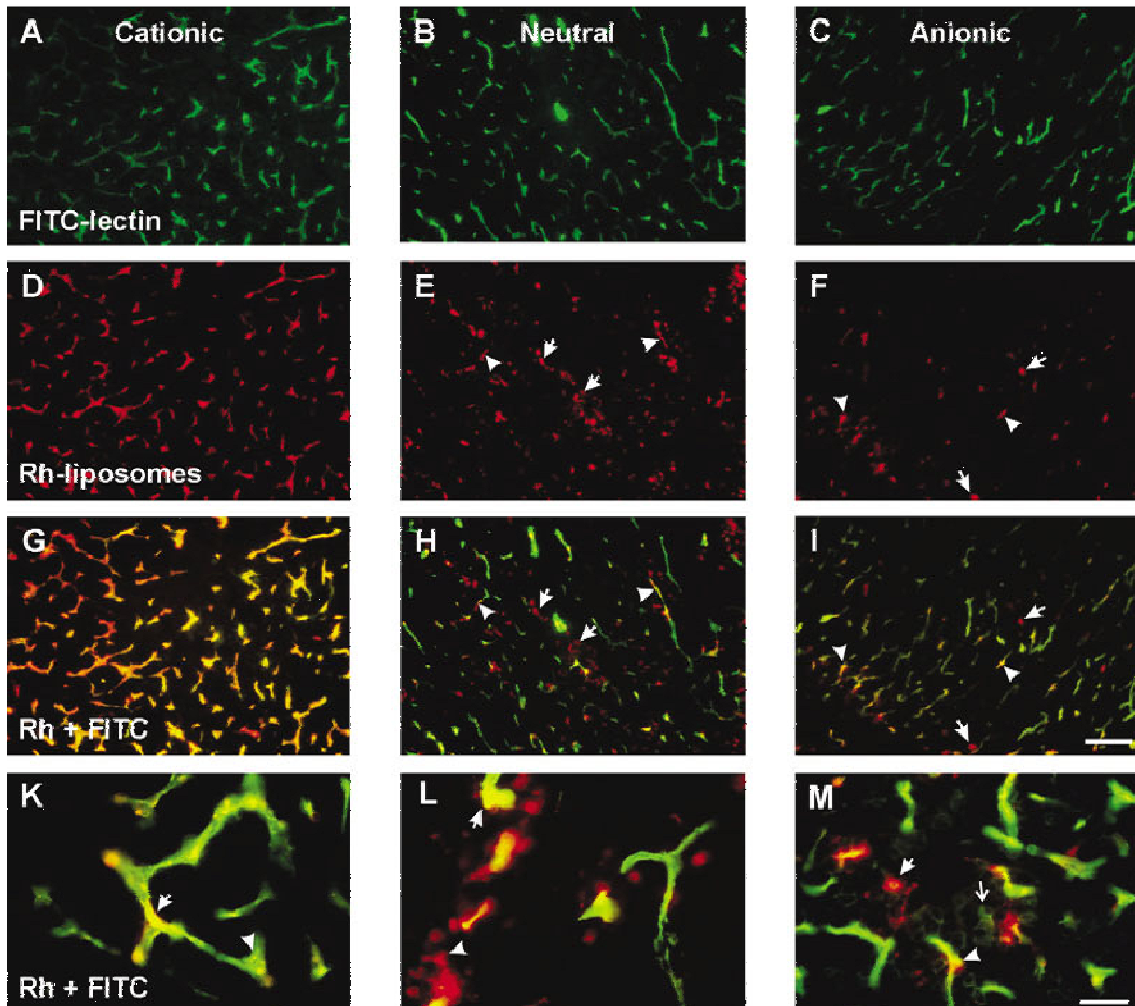
Figure 3.51
Distribution of cationic (d), neutral (e) and anionic (f) liposomes. The FITC-labeled lectin serves as a green vascular counterstain (a–c). Cationic liposomes exhibited a strong and specific accumulation at sites of FITC-lectin labeled endothelium (g,k) showing a fine punctuate (arrowhead) and a patchy (arrow) pattern. There was apparently no extravascular rhodamine fluorescence. Beneath minor vascular co-localization (arrowheads, e,h), neutral liposomes were mainly found within the tumor parenchyma outside of blood vessels (h,l). The anionic liposomes (f) accumulate moderately within the tumor. They co-localize sporadically with the tumor vessels (arrowheads) and exhibited clear leakage into the parenchyma (i,m). Scale bar a–i: 200 µm; scale bar k–m: 50 µm. From [Krasnici, S. et al. 2003]

Other studies have shown similar results [Lappalainen, K. et al. 1997; McLean, J. W. et al. 1997] suggesting that the positive charge on the liposomal surface interacts with a negative charge on the cell surface of angiogenic microvessels. Such endothelium of normal vessels is equipped with negatively charged glycocalyx [Vink, H. et al. 1996]. Given the fact that cationic liposomes bind preferentially to angiogenic endothelial cells due to charge related mechanisms, one has to hypothesize an enhanced presentation of cell surface molecules or negatively charged scavenger receptors on the surface of angiogenic endothelium in comparison to normal microvessels.

Using cationic liposomes from Medigene AG (Martinsried, Germany) as a primary model nanoparticle, we did distribution and tumor accumulation studies *in-vivo* (**Figure 3.52**). These cationic liposomes again preferably targeted the tumor inside the hamster skin fold chamber. Over a time period of 360 minutes the fluorescence signal increased in the tumor to a maximum about 45-120 minutes and then slowly decreased again.
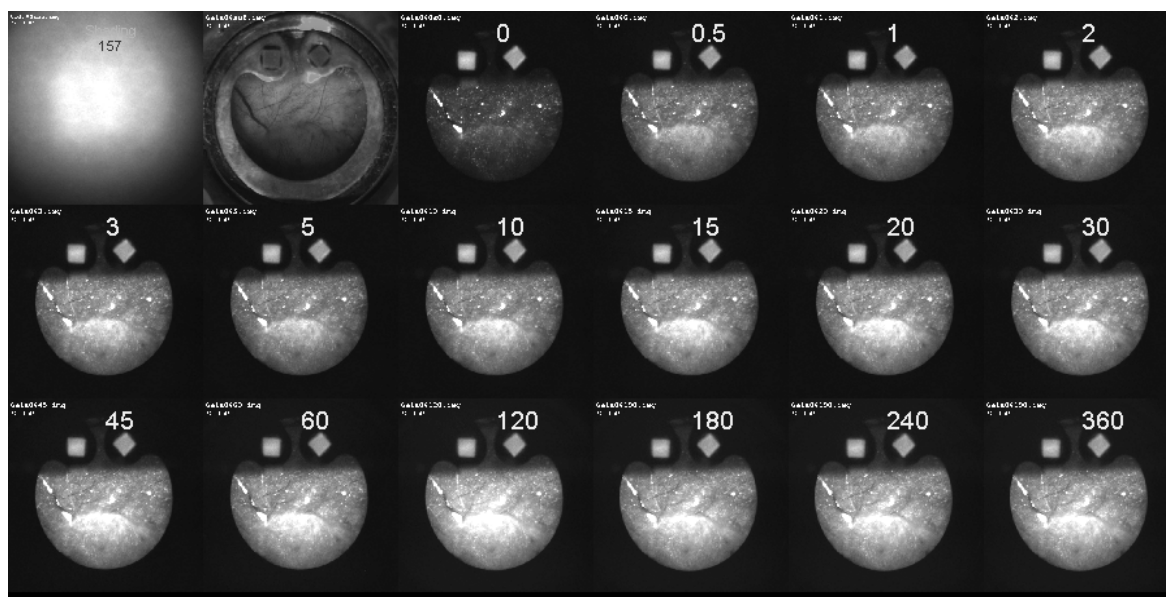
Figure 3.52

Cationic ENDOTAG® liposomes analyzed in the hamster dorsal skin fold chamber model

In comparison, neutral gelatin nanoparticles with a size of 226 nm (zeta potential +3 mV in highly purified water) when applied *i.v.* (n=6) over the same route as the liposomal formulation, did not show any fluorescent signal strong enough for microscopic read out.

At the tested concentrations ranging from 0.01 mg/ml to 5 mg/ml the hamsters tolerated the nanoparticles well throughout the whole experimental time. Fluorescence of the nanoparticles themselves was confirmed by fluorescence microscopy and macroscopic fluorescent scanning in microslides with the result that the nanoparticle fluorescence *ex-vivo* was sufficient for the used equipment (**Figure 3.53**).
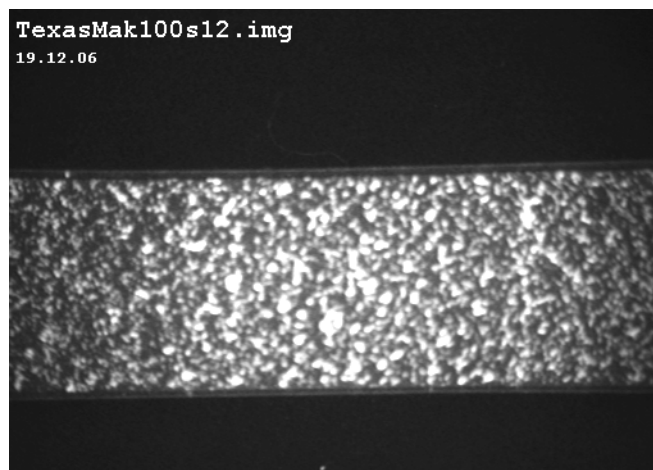
Figure 3.53

Cationic, fluorescent labeled gelatin nanoparticles in microslide

With regard to the *ex-vivo* results it was not clear why the nanoparticles were not be detectable *in-vivo*. Even at highest sensitivity neither initial signals nor a brightening over the time course of the experiment were detectable. These results lead to the hypothesis that either the detection setup for the *in-vivo* experiment was not sensitive enough for fluorescent nanoparticles when assayed in the *in-vivo* environment or secondly, that the nanoparticles were trapped in the lung right after application. Similar results were observed for cationic gelatin nanoparticles with a size of 340 nm and a zeta potential of 32 mV in highly purified water.
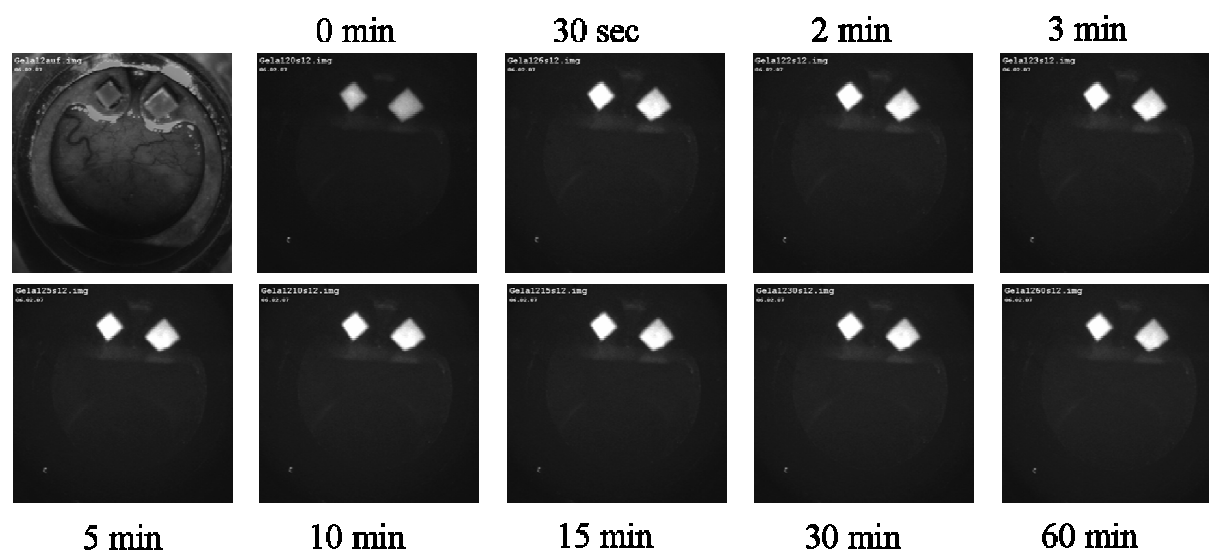
Figure 3.54

Neutral gelatin nanoparticles at a size of 226 nm (PDI 0.042) and a zeta potential of 6 mV in the hamster dorsal skin fold chamber model
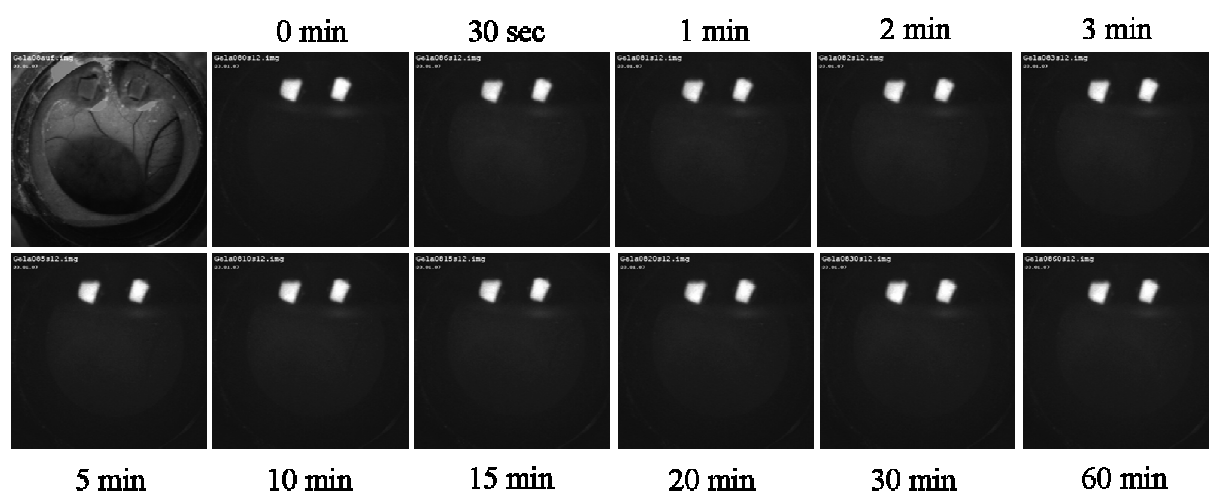
Figure 3.55

Cationic gelatin nanoparticles at a size of 340 nm (PDI 0.05) and a zeta potential of 33 mV in the hamster dorsal skin fold chamber model

With the low fluorescence signals of the nanoparticles we eventually decided to do a tissue analysis of the lung and the liver as the main filter organs for nanoscaled systems. Therefore the animals were sacrificed and cryocuts from these tissues were studied with fluorescent microscopy. As expected, strong fluorescent signals were observed in both organs (lung

sample shown in **Figure 3.56**). The cryocuts of the lung tissue revealed that both neutral and cationic charged gelatin nanoparticles accumulated to a large extent in the tissue.
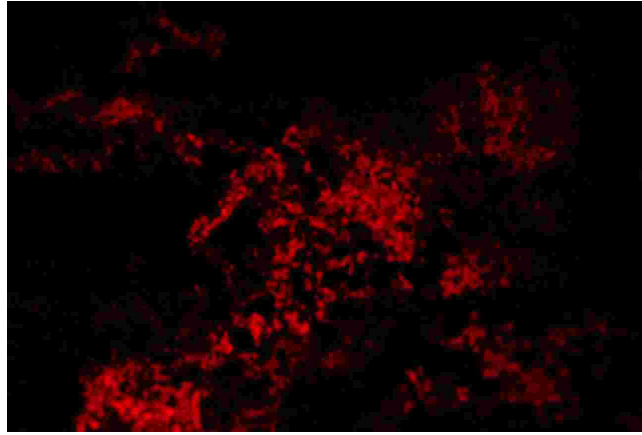
Neutral gelatin nanoparticles in lung tissue cryocut
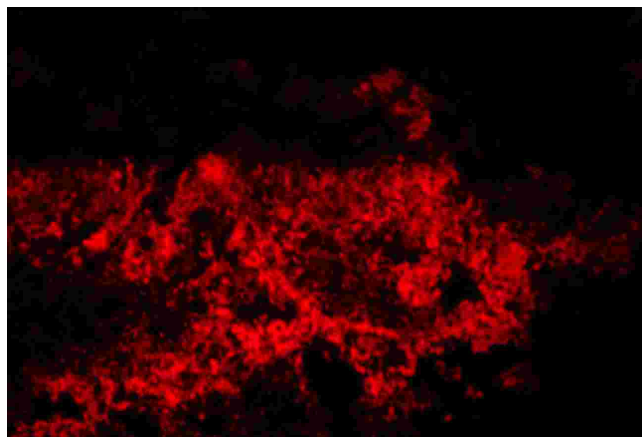
Figure 3.56

Cationic gelatin nanoparticles in lung tissue cryocut

Cationic gelatin nanoparticles as well as neutral gelatin nanoparticles showed a broad distribution throughout the whole liver and lung tissue while organs like spleen and kidney did not show strong signals at all.

In conclusion, the dorsal skin fold chamber model was not the model of choice for thorough nanoparticle analysis. Even though we were able to detect nanoparticle fluorescence within the chamber for both cationic and neutral nanoparticles, their local fluorescence was too low

to be recorded with the fluorescence camera. Also, the route of formulation application leads the nanoparticles through the lung and liver with a highly concentrated bolus effect which can lead to vessel clogging. We certainly tried to circumvent this side effect by applying the formulations via a long-time infusion but still they could not reach the capillary bed in the chamber. Of course the nanoparticles circulate within the main blood system as shown from interaction studies and whole body imaging later on (refer to 3.11.4 Pharmacokinetics and whole body imaging) yet an endothelium adsorption as in the *in-vitro* chamber simulation was not possible to demonstrate.

3.11.2   Mouse cremaster model

The choice of the animal model fell onto the mouse, since this species is immunological very well characterized. In general, a broad spectrum of antibodies and also a variety of differently genetically modified animals are available for investigations of the biological relevance of the nanoparticles and delivered siRNAs.

In this cooperation the analysis of gelatin nanoparticles in the mouse cremaster was on the main focus. In detail we wanted to find out whether there were any animal dependent differences reflected in the pharmacokinetic profiles compared to the information gained from the hamster skin fold studies. In addition we also wanted to analyze, if different optical detector setups (different microscopes, detection filters, and video software) allow for better nanoparticle monitoring. Last but not least, we investigated, whether the nanoparticle fluorescence available for our gelatin was sufficient for such a read-out system. The studies were completed by CLSM read-out and normal microscopic visualization of endothelium-targeting.

All nanoparticles were covalently labeled with fluorescent dyes and were examined in special microslides under a fluorescence microscope. In a second concern we wanted to get a better understanding of nanoparticle fate when applied via the arterial route from very low to very high concentrations. Again – like in the skin fold model– concentration of nanoparticles, viscosity, amount of applied volume and type of nanoparticle played a major part in the investigations. Last but not least, formulations of nanoparticles based on PLGA, HSA, DEAE-dextran gelatin and polybutylcyanoacrylate were tested in the cremaster model on their

pro-thrombic or non-thrombic effects. The nanoparticles were injected intravenously and monitored with intravital-microscopy on changes at the endothelial and vessel system. The expertise in the group of Prof. Krombach was used as a basis for these experiments.
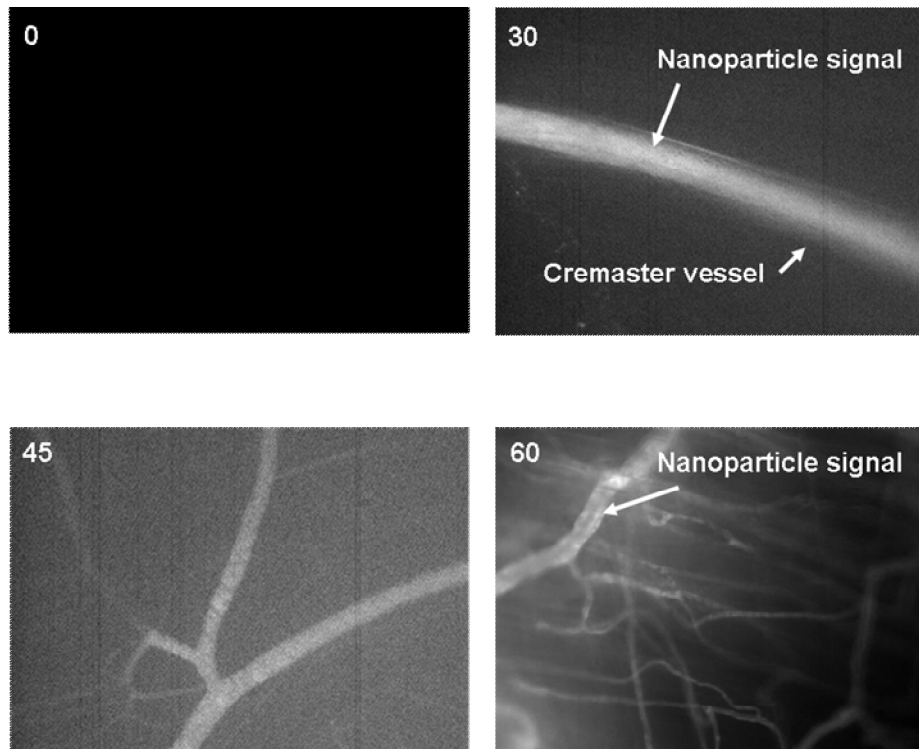
Figure 3.57

Cationic GNP monitored with a fluorescent microscope in the mouse cremaster model over 4 time points: 0, 30 (top), 45, 60 (bottom) minutes

We found out that when using nanoparticles at *in-vivo* tolerable concentrations the fluorescent signal of the nanoparticles was not detectable. In combination with the results obtained from our experiments together with Dr. Eichhorn (Walter-Brendel-Center), we can state, that a low fluorescent signal was the main factor for the false "low" *in-vivo* circulation time and not charge or overall intolerability of the particles. Nanoparticles were detectable at concentrations of 5 mg/ml which is equivalent to 25 mg/kg *b.w.*. However 80 % of the animals showed thrombogenic effects right after application and for a time period of 5-10 minutes. Nanoparticles applied in lower concentrations down to 0.005 mg/ml did not show these thrombogenic effects but were not detectable in the fluorescent microscope either. We

found out that optimum application concentrations of nanoparticles were in the range of 0.1 to 0.8 mg/ml when dispersed in PBS.
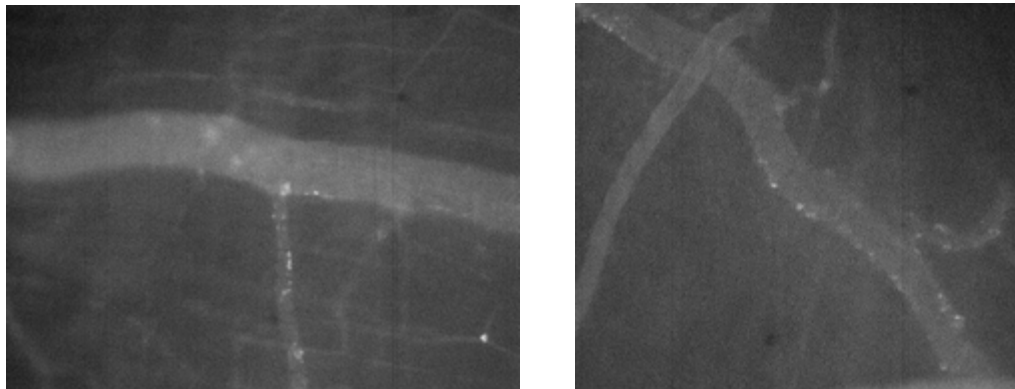
Figure 3.58

Cationic GNP targeting the slightly inflamed endothelium tissue in the cremaster model after 15 minutes post injection (vein), right (artery)

With this knowledge an optimum fluorescence or other label has to be found that is sufficient to monitor nanoparticle interactions with the cell membrane. HSA and DEAE-dextran gelatin nanoparticles were tested so far with a statistically relevant amount of animals (n>5). Interestingly the HSA nanoparticles did not show any pro-thrombic effect within the applied concentration range. DEAE-dextran nanoparticles however lead to small thrombic vessel clogging in the microcirculation. In particular we found out that *in-vivo* experiments with more or less solid nanoparticles have a very small concentration window in concerns of sufficient fluorescence signal and vessel thrombosis. Fluorescent nanoparticles when applied in concentrations low enough for no thrombic effects occurring, could not be detected anymore by *in-vivo* fluorescence imaging. It was most interesting that the thrombic effects were only temporarily. That means that nanoparticles at a certain concentration (high enough for fluorescence signalling > 25 mg/kg) induced vessel blockage for a certain time period and restore the original state after a few minutes if blockage was not too strong. Visualization of targeted fluorescent nanoparticles on excised tumor vessels would be the most promising step to monitor endothelium targeting. In cryocuts and CLSM picturing the fluorescent signals were detectable even at low concentrations of applied nanoparticles (refer to 3.11.1 Hamster dorsal skin fold chamber). An infusion of very small amounts of nanoparticles at several time

points could prevent thrombosis and allow for enough nanoparticles to be present in the circulation for a longer time.

The batches were injected into a cremaster mouse catheter with a volume of 200 µl *i.a.* over 10 seconds. After approximately 2 minutes the blood flow was drastically reduced within the cremaster window until final thrombostenosis. The reduction in blood flow was less in this case and did not occur instantaneously. In a second approach neutral gelatin nanoparticles labeled with rhodamin lissamine in PBS/Tween 5 % (w/w) were tested. Analysis of fluorescence in this case *ex-vivo* on a microscopy plate did not show any sufficient fluorescence for further *in-vivo* experiments. In two cremaster mouse models, which received a total of 800 µl of a 5 mg/ml nanoparticle dispersion a strong arterial signal was recorded, from which we concluded that labeling in all cases was sufficient. But even at this concentration a thrombus of nanoparticles was detected with the video setup, resulting in signal blockage towards the veins and the rest of the blood circulation. After 3 minutes the thrombus dissolved. Again a second animal received 5 mg/ml nanoparticle dispersion which again resulted in a severe slow-down of the blood flow. After 5 minutes the normal circulation speed was restored. Besides this the animal did not show any signs of intolerance of the applied nanoparticles.

In conclusion, besides a slight thrombogenic potential of highly concentrated cationic gelatin nanoparticles, for the first time a charge dependent *in-vivo* adhesion in the cremaster endothelium was demonstrated for gelatin nanoparticles. While the thrombogenic potential demands further investigations, the basic formulation remains with the potential to target endothelium specifically in slightly inflamed areas.

3.11.3   Mouse antigen induced arthritic knee model

Moving one step further and away from the kinetic and biodistribution profiling, the nanoparticles were investigated on their potential in a therapeutic model for antigen induced arthritis in the knee. Here the objective was to assess the targeting potential of cationic gelatin nanoparticles, chitosan nanoparticles and liposomal formulations either unloaded or complexed with fluorescent nonsense siRNA towards inflamed chronic arthritic knee tissue in mice. For our studies we used the so called CIA-MG5 model in cooperation with an American

Medigene laboratory. As a result the liposomal formulations of "siRNA-red" (fluorescent labeled siRNA) changed the biodistribution compared with free "siRNA-red". These cationic liposomes accumulated in the inflamed knee tissue prompting for a therapeutical application. As already known from earlier studies with liposomes [Krasnici, S. et al. 2003], they of course could also be found in the liver and in the lung which are both the major first passage organs.
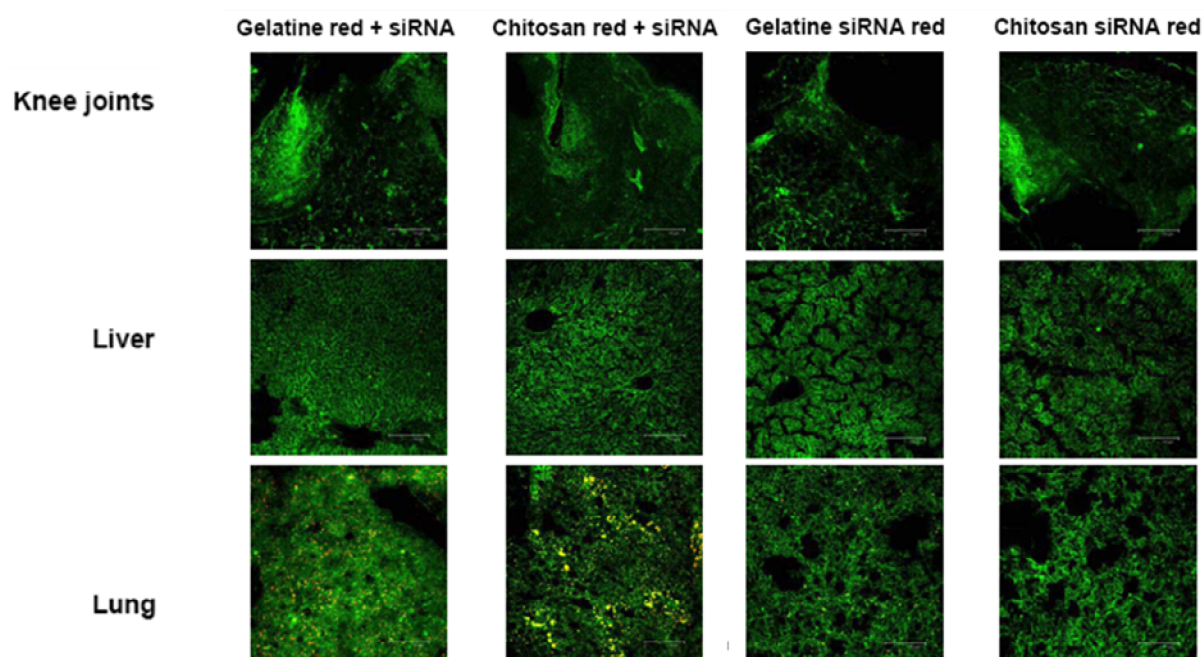
Figure 3.59

Cryocuts of knee-joint, synovial tissue, liver, and lung from "antigen induced arthritis" mice after treatment with GNP+siRNA and chitosan-NP+siRNA. Chitosan nanoparticle aggregates in the lung vs. a good homogenous and non-aggregated GNP distribution in the lung.

Unloaded cationic gelatin nanoparticles and formulations with siRNA seemed to be trapped in the lung which again strengthens a systemic depot theory (**Figure 3.59**). A signal of fluorescent siRNA delivered with GNP could be detected in the lung but no detectable signals were found in the arthritic knee joints and the liver. The chitosan nanoparticles compared with free siRNA did after all show no significant changes in terms of biodistribution of the siRNA. Also chitosan nano-polyplexes showed no trend of specific targeting compared to our GNP. In addition, when monitoring the *in-vivo* particle shape, a tendency of aggregation in tissues was higher with the chitosan nanoparticles than with the gelatin nanoparticles.

Hence we concluded a not sufficient capability of chitosan as a siRNA delivery tool within our animal models. Gelatin on the other hand did show positive results in terms of targeting, low aggregation and siRNA delivery. Due to the fact that the amount of fluorophore mounted onto the liposomal formulations was several folds higher than the theoretical labeling maximum of gelatin nanoparticles a final correlation between liposomal and particulate formulations could not be made. With respect to the high costs of the experiments however that prevented further experiments in this field, the distilled data still shows us a trend. Repetition would only make sense if strong fluorescent Quantum-dots, as proposed earlier [Broermann, P. et al. 2008], can be coupled on the nanoparticles. Studies with several fluorescent dyes and their influence on nanoparticle behaviour *in-vitro* have shown us however that even small amounts of fluorophore on the nanoparticle surface could change the nanoparticle properties extremely.

3.11.4 Pharmacokinetics and whole body imaging

Pharmacokinetics

We decided to monitor the kinetic profile of our nanoparticles with a fluorescent read out as this would allow a quantitative determination of free, non-endothelium-targeted nanoparticles at different time intervals with a high resolution detection system. While the read-out system had previously been used to monitor liposomal formulations it was not validated for fluorescent nanoparticle analysis. Therefore several validation steps with different fluorescent gelatin nanoparticles were conducted and the linear range of detection was determined (**Figure 3.60**).
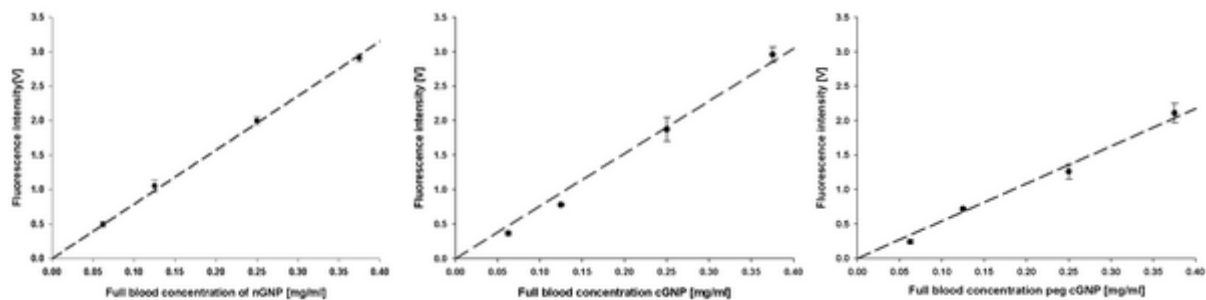
Figure 3.60

Validation with different nanoparticle batches for the full blood fluorescent analysis

First neutral gelatin nanoparticles were compared to cationic gelatin nanoparticles and pegylated cationic gelatin nanoparticles over a period of 60 minutes. The concentration of detectable nanoparticles is shown in **Figure 3.61**. All three nanoparticle batches showed a relatively fast elimination from the blood circulation stream. After 5 minutes, the concentration of N-GNP was reduced by about one fourth of the initial concentration, while approximately one fifth was detectable for at least 30 minutes. We measured an initial concentration of 0.07 mg/ml for the neutral GNP and 0.017 mg/ml for the cationic GNP. The cationic and the pegylated nanoparticles showed almost identical concentration curves where after a fast drop within the first 5 to 10 minutes the concentration remained at about one eighth of the concentration of the neutral nanoparticles. After 30 minutes a slight increase could be observed. In general the neutral nanoparticles had a longer half-life than cationic or pegylated nanoparticles.
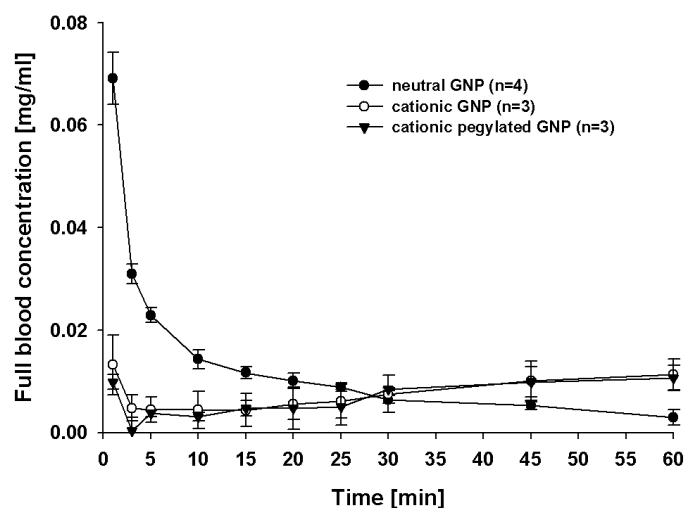
Figure 3.61

Full blood concentrations of neutral, cationic and pegylated cationic GNP after bolus *i.v.* administration to mice recorded over 60 minutes

The modification of the nanoparticle surface with polysorbate 80 (Tween) resulted in very different kinetic profiles for both neutral and cationic nanoparticles. As seen in **Figure 3.62,** Tween modification of the nanoparticles resulted in prolonged circulation times of both neutral and cationic nanoparticles. In the case of neutral nanoparticles a higher detectable signal right after injection could be detected. After approximately 5 minutes of circulation the

signal was reduced to one half of this initial value with Tween coating, while the concentration of uncoated nanoparticles was strongly reduced.
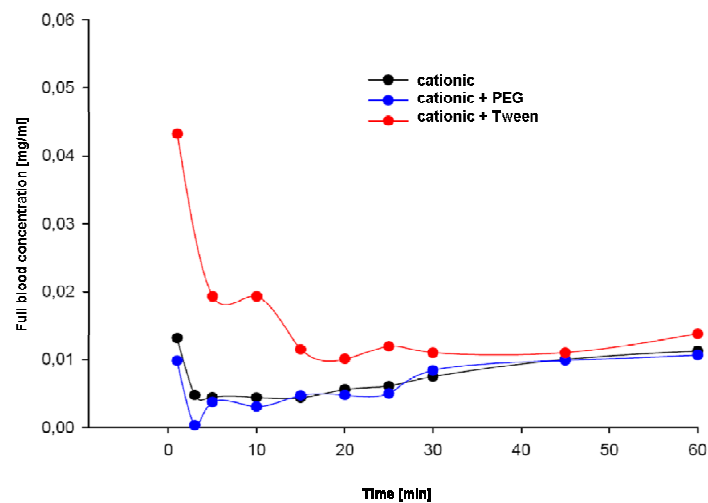
Figure 3.62

Full blood concentrations of pegylated (bottom), unmodified (middle) and Tween coated cationic DD-GNP after bolus *i.v.* administration to mice recorded over 60 minutes (n=3)

Another effect of the Tween modification can be seen in a small but reproducible secondary concentration peak after 10 minutes. **Figure 3.63** shows the same secondary peak for cationic Tween coated nanoparticles. Also only a marginal effect of PEG as used in our experiments on the half-life of the nanoparticles was seen.
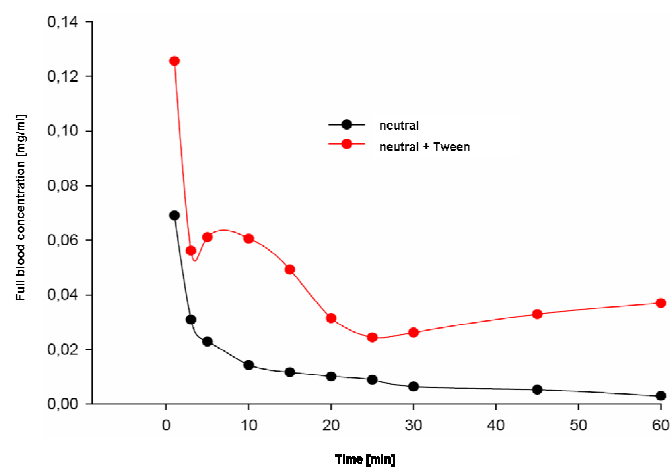
Figure 3.63

Full blood concentrations of unmodified and Tween coated neutral GNP after bolus *i.v.* administration to mice recorded over 60 minutes (n=3)

As expected, the cationic nanoparticles showed less circulatory potential within the full blood compared to neutral nanoparticles. Similar data was shown by Bowman et al. [Bowman, K. et al. 2006]. An interaction of the nanoparticles with negatively charged endothelium surface proteins but also with lung and liver tissue could be a potential explanation for this phenomenon. With the fast elimination of the nanoparticles from the circulatory system an increase of the nanoparticle concentration at specific organ sites was shown (refer to **Figure 3.68**). But not only DEAE-dextran modification and cholamine modification were examined, also a coating of these cationic nanoparticles with PEG was studied. Based on results from Amiji et al. [Kommareddy, S. et al. 2007] we expected a prolonged circulation time of PEG modified nanoparticles compared to unmodified nanoparticles. However, PEG did not have a significant effect in the formulation with our novel DEAE-dextran gelatin nanoparticles. This might be due to polysaccharide chains already sticking out of the smooth nanoparticle surface, potentially leaving the nanoparticle already with a postulated PEG-like brush-type surface as a protection against opsonization. Last but not least, Tween was used as a special coating onto the cationic nanoparticles based on studies by [Kreuter, J. 1983]. The increased circulation time of Tween coated nanoparticles described in the literature, could also be proven for our novel DEAE-dextran gelatin nanoparticles. With almost no loss in charge through the Tween coating, a longer circulating nanoparticle system was obtained. The complete mechanisms by which Tween prevents nanoparticles from aggregation and opsonization through blood molecules has yet not been discovered, but it can be postulated, that the surfactant properties on the phase transition gelatin – water play a pivotal role. The secondary concentration peak in (**Figure 3.62**, **Figure 3.63**) for the Tween modified nanoparticles can possibly be explained by a nanoparticle cell interaction within in the endothelial regions and the major organs combined with a following regeneration processes. An on and off type nanoparticle depot due to this cell interaction can also be an explanation. Such depots as described next could be potentially formed with white blood cells or other types of blood cells with which the nanoparticles come into contact after injection.

Blood cell interaction

Based on previous *in-vitro* studies and the above results with cationic nanoparticles taking a closer look on the cellular level of nanoparticle interaction became necessary to directly elucidate the nanoparticle fate. Since nanoparticles first come into contact with blood cells

when applied *i.v.*, the influence on these cells was extensively studied. We found that the strongest effect of nanoparticles on blood cells was obtained for white blood cells. All examined nanoparticle types and surface charges reduced the white blood cell concentration in full blood samples within 10 to 15 minutes by 70 to 80%. After that time a regeneration of the amount of white blood cells could be observed for all nanoparticle types. Within 60 minutes the starting value of white blood cells was restored for cationic nanoparticles, while the white blood cell concentration was slightly increased for pegylated nanoparticles and decreased for the neutral nanoparticles as seen in **Figure 3.64**. Similar charge related observations have been made by other research groups [Kuhn, S. H. et al. 1983; Mayer, A. et al. 2008] where however in contrast to our results the white blood cell counts took several hours to regenerate completely. In the field of liposomal and nanoparticle research temporary interaction with blood cells has so far been used to prolong the circulation time of the respective nanoparticle in the blood [Chambers, E. et al. 2007]. Unfortunately, so far this observed phenomenon cannot be pinpointed to one single causa and needs further experiments.
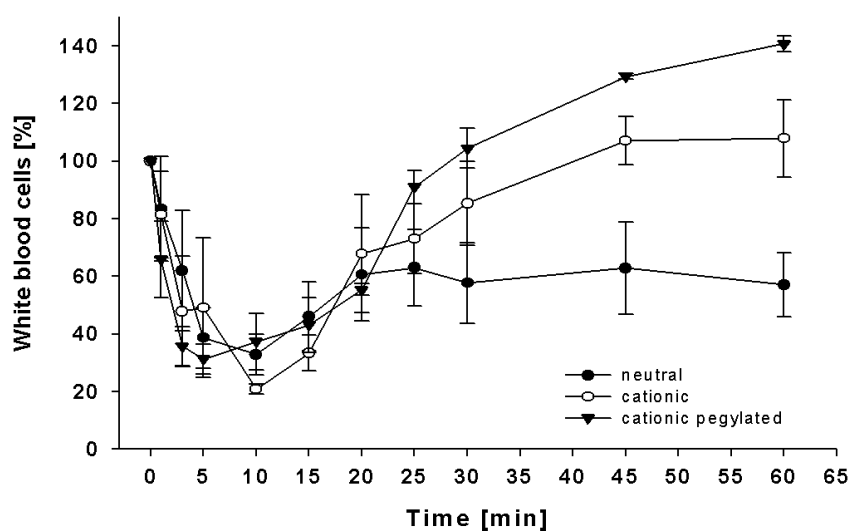
Figure 3.64

White blood cell concentration measured by Coulter counter for neutral, cationic and cationic pegylated GNP over a time period of 60 minutes (n=3)

The nanoparticle interaction with thrombocytes resulted in a drop of free thrombocytes in the full blood samples by more than 50 % of the initial value after a time span of 8-10 minutes. As seen in other studies [Anna, R. et al. 2005], a charge related interaction between the platelets and the nanoparticles is the most likely explanation for these results. For neutral and pegylated cationic nanoparticles these effects were not strong, leaving the thrombocyte count around placebo level Neutral nanoparticles in our studies did not seem to influence the concentration of thrombocytes at all (**Figure 3.65**). The high thrombocyte count at 60 minutes for cationic pegylated nanoparticles as an outlier shall not be taken into account for further interpretation.
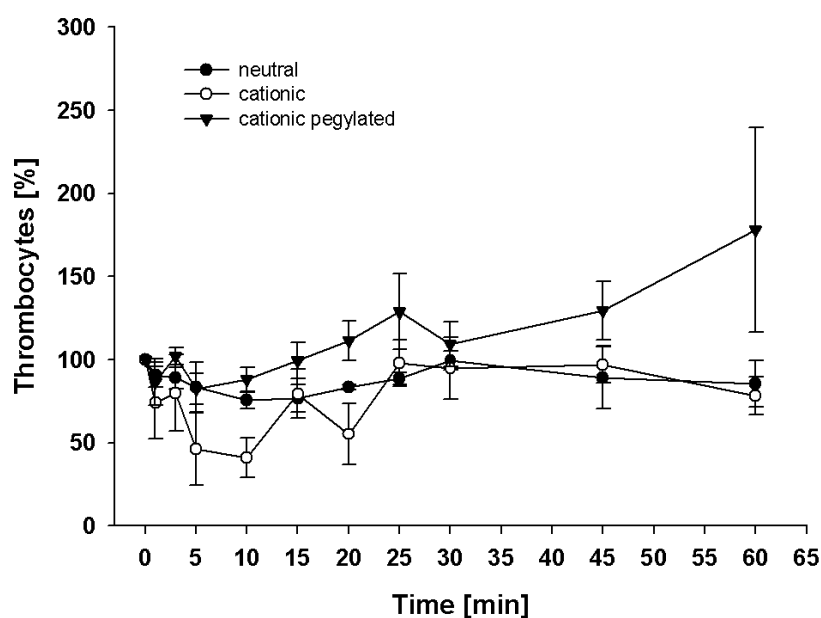
Figure 3.65

Thrombocytes concentration measured by coulter counter (n=3)

With these results, the influence of nanoparticles on the red blood cells had to be examined as well. Here we found out that the concentration of hemoglobin was also slightly reduced throughout the time of nanoparticle application. **Figure 3.66** shows how, again, the cationic gelatin nanoparticles have the greatest interaction potential with red blood cells, while neutral and pegylated gelatin nanoparticles only led to minor concentration changes. In contrast to the white blood cell and thrombocyte kinetics, a regeneration within the analysis time could not

be observed. The measured hemoglobin concentration, especially in the case of cationic nanoparticles, stayed low [Verma, A. K. et al. 2005].
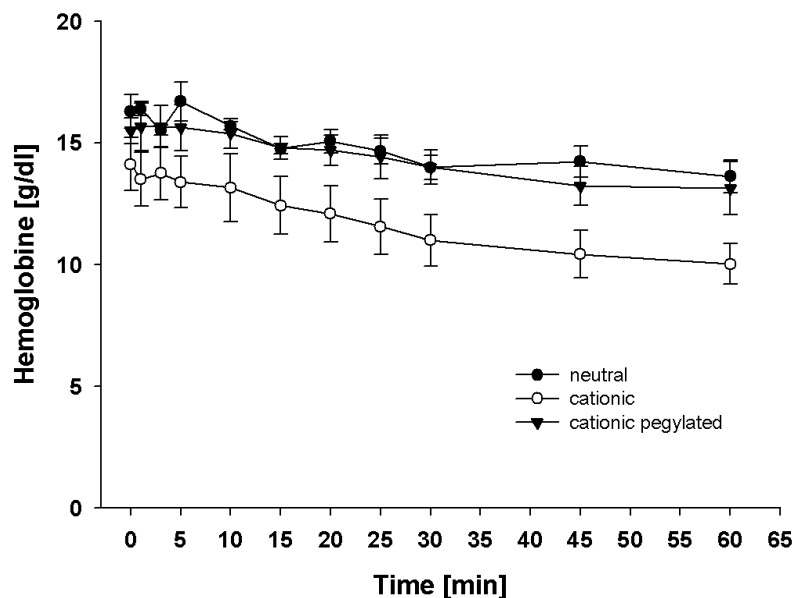
Figure 3.66

Hemoglobin concentration measured photometrically at different time points

Hence the nanoparticle – blood cell interaction was measured and we found out that indeed there is a massive decrease of white blood cells right after nanoparticle application. Interestingly this effect could be shown for all nanoparticle types and surface modifications. Yet there were differences in the regeneration of the white blood cells that suggest different interaction patterns and adhesion strengths of nanoparticles with those blood cells. Whether nanoparticles directly bind to the white blood cells or induce a general white blood cell aggregation and therefore reduction in the measured quantity can not be told, but it can explain the potential reason for the afore mentioned secondary nanoparticle peak. While the white blood cells regenerate over a time period of 60 minutes for all tested nanoparticle formulations, so does the concentration of detectable Tween coated nanoparticles. An explanation why only Tween coated cationic nanoparticles show the secondary concentration peak might be a protective effect against aggregation of surfactant coated nanoparticles compared to pure cationic nanoparticles. A comparable effect of blood cell interaction for the

tested nanoparticles was found for thrombocytes, while red blood cells did not show this effect. When correlating the cell count data with the available nanoparticle *in-vivo* data, we can clearly show how the interaction with the measured blood cells results in a decrease of available nanoparticle concentration within the approximate time span of 10-15 minutes. It is interesting how this effect correlates with the afore-examined white blood cell depletion. Neutral nanoparticles in our studies did not seem to influence the concentration of thrombocytes at all as seen in **Figure 3.65**. A possible explanation might be found in the different surface protein patterns of thrombocytes compared to white blood cells. Thrombocytes for example have collagen receptors, but only when activated. White blood cells however, due to their immune systemic nature show a permanent potential for nanoparticle interaction, as could be shown especially with cationic nanoparticles.

Whole body imaging

To complete the study, *in-vivo* experiments with differently coated and charged nanoparticles were conducted in mice and particle distribution was measured using far-infrared fluorescence camera read-out on extracted organs and anaesthetized mice. The analysis of the organs revealed a preferred and charge dependent accumulation of the nanoparticles inside the lung tissue and the liver. Especially the highly cationic DEAE-dextran modified gelatin nanoparticles showed a high affinity to the liver and the lung.
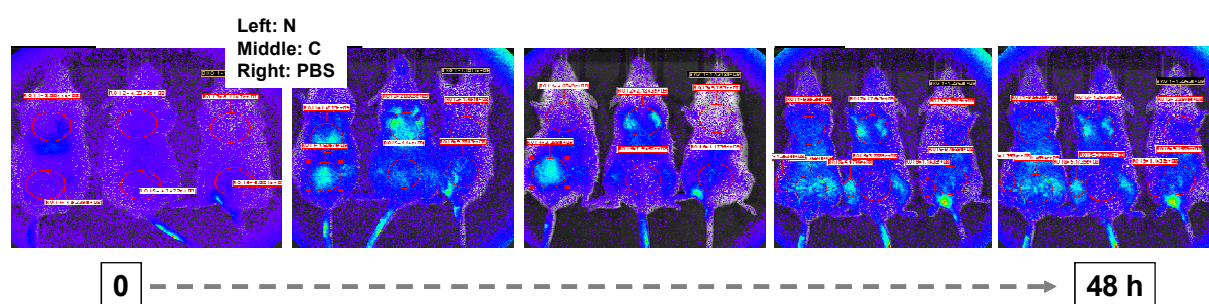
Figure 3.67

Whole body images of neutral (150 nm, PDI, 0.09, 2 mV) and cationic (270, PDI, 0.05, 37 mV) GNP applied in a concentration of 5 mg/kg *b.w.* Recordings were taken over 48 h.

The lower the surface charge of the nanoparticles was in the experiments, the lower was also the concentration in the investigated organs. The high concentrations of cationic nanoparticles could also be detected under live conditions for the liver and the lung areas, while the fluorescence emission in all other organs was too weak for the camera setup. In The data in **Figure 3.67** supports the hypothesis that accumulation and targeting of our nanoparticles to lung, liver and joints (potentially inflamed) is size and charge dependent. The critical size for less lung accumulation as tested across several nanoparticle batches was determined to be below 150 nm.
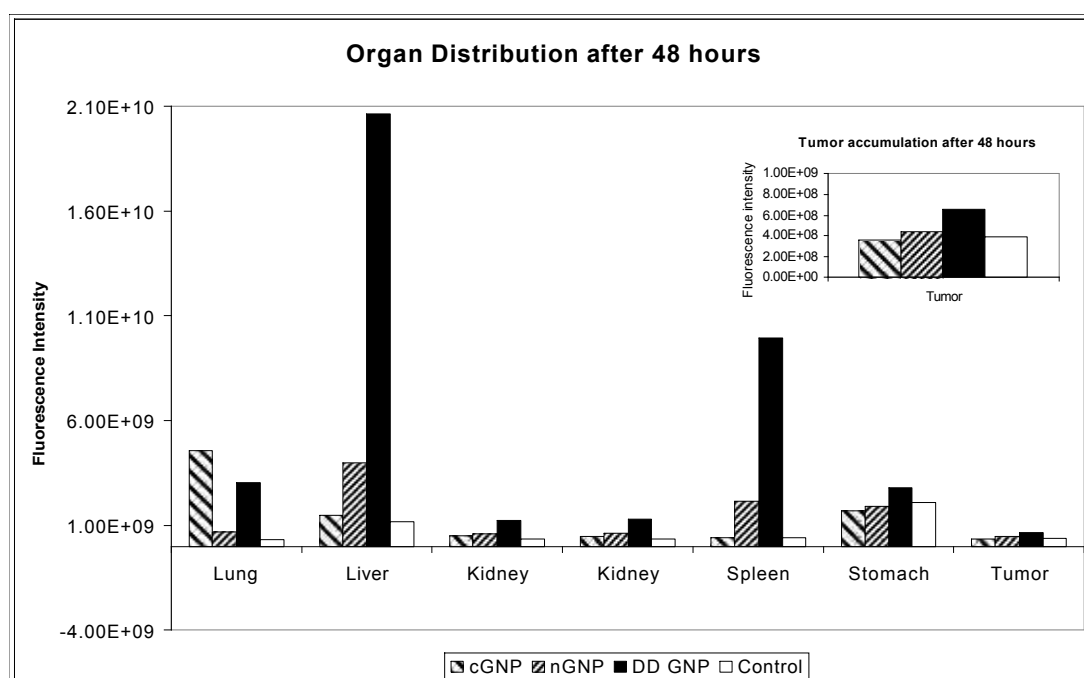
Figure 3.68

Organ distribution pattern and tumor accumulation of cationic, neutral and DD-GNP after 48 hours in the mouse model

Detailed tumor tissue analysis did show a discriminative accumulation of our nanoparticles within the tumor (**Figure 3.38**). In this case it was questionable whether those amounts of nanoparticles are sufficient for an effective therapeutic approach. Even if this might not be the case for normal small molecule drugs, in theory, it might be enough for therapies based on siRNA mediated RNA interference mechanisms, where small amounts of siRNA have a large impact.

3.12 In-vitro / in-vivo correlation

Basically the purpose of an *in-vitro in-vivo* correlation (IVIVC) is to demonstrate that a certain *in-vitro* approach can work as a valid surrogate for complex *in-vivo* studies. This may then reduce the number of expensive studies required for approval as well as be helpful for scale-up and post-approval changes. The United States Pharmacopoeia has defined the *in-vitro in-vivo* correlation as "the establishment of a relationship between a biological property or a parameter derived from a biological property from a certain formulation and a physiological property of the same formulation" [Leeson, L. J. 1995]. In our studies the first incident of *in-vitro in-vivo* correlation was within the fluorescence labeling studies (refer to 2.2.2 Fluorescence labeling). There we demonstrated the influence of different fluorophores and labeling techniques on the *ex-vivo* and *in-vivo* signal read-outs. High fluorescence signals, always sufficient for any *in-vitro* detection of the nanoparticles were well suitable for the conducted chamber slide preclinical studies. *In-vivo* however, as seen in the case of the hamster dorsal skin fold chamber and also in the mouse cremaster model, blood components and the technical setup prevented a high resolution fluorescence analysis of the nanoparticles. A correlation from the *in-vitro* model to the *in-vivo* whole body imaging approach shown in (3.11.4 Pharmacokinetics and whole body imaging) is also difficult since the fluorophore needed to pass a signal through the animal skin emits in the long wavelength spectrum which is more than 200 nm apart from the standard labeling wavelength. This holds especially true if we take into account different physicochemical properties of the nanoparticles for different fluorophores as demonstrated in a cooperation Broermann [Broermann, P. et al. 2008]. Nevertheless the *in-vitro in-vivo* correlation for our nanoparticles was successful for the newly developed cell culture flow model. Leaving the slight surface changes through the fluorophores aside, we were able to demonstrate a charge related cell interaction of the nanoparticle *in-vitro* and could confirm a similar behaviour later in all *in-vivo* models. A deeper analysis of the influence of shear stress and medium as well as vessel (channel) diameter in the *in-vitro* flow model are a needful addition to elucidate the nanoparticle fate *in-vivo*. Importantly, an incubation of nanoparticles under flow and at high FCS concentrations resulted in different cell interaction patterns than observed for "standard" static and low FCS conditions. As a result, nanoparticles showed less cell interaction *in-vivo* than what would have been expected from simulations in the static model compared to the near to reality results from the flow model.

3.13 Application of siRNA containing gelatin nanoparticles for gene delivery

The big advantage of targeted nanoparticles compared to other forms of drug and gene delivery rather than a pure localisation inside the tumor region, is the uptake into the cell [Bartlett, D. W. et al. 2007]. Only with the successful uptake of the carrier and its payload can our nanoparticles trigger the relevant RNAi mechanism. Hence for a successful RNA based therapy it is mandatory to effectively deliver the siRNA molecules into the cytoplasm of the cell without changing the morphology or viability of the cells to a large extent. From such a therapeutic point of view, nanoparticles loaded with reporter gene siRNA, *e.g.* luciferase siRNA (luc-siRNA) need to find their target cell first and in a second step enter the cell by an endocytotic and endolysosomal mechanism. The target cell can be an angiogenic endothelial cell or any tumor cell or cell in an inflamed tissue region.

Cholamine gelatin nanoparticles for gene silencing

In a first try, gelatin nanoparticles cationized with cholamine and loaded with either luc-siRNA or a control siRNA (mut-siRNA) (refer to 2.3.12 siRNA loading determination via ultra-violet-absorption) were examined for their gene silencing potential as previously described (refer to 2.6 siRNA mediated gene silencing and protein knock-down).

In 10 % (v/v) FCS medium 500 ng luc-siRNA loaded onto cationic nanoparticles (234 nm, PDI 0.005, +53 mV) at different ratios of 1:1, 2:1, 4:1, 8:1, 12:1, 16:1, 20:1 were not able to induce an RNAi mediated luciferase knock-down within the chosen time window (**Figure 3.69**). At this point we estimated that the nanoparticles were not taken up successfully by the cells due to a sub-optimal nanoparticle-cell interaction, potentially based on the low zeta potential of the cholamine gelatin nanoparticles. While the size of the nanoparticles with 210 nm (PDI 0.01) was in a range where other polymeric carriers would normally be taken up by cells as shown by Nguyen [Nguyen, J. et al. 2008] the cationization of the nanoparticles after loading with the siRNA molecules was most likely not sufficient to interact with the cell membrane long enough to get internalized into the endosome. We determined the charge with 41 mV after loading in MQ and with only 21 mV in the relevant transfection cell culture

medium. On the contrary however, internalization might after all have taken place with only the endosomal release not working.
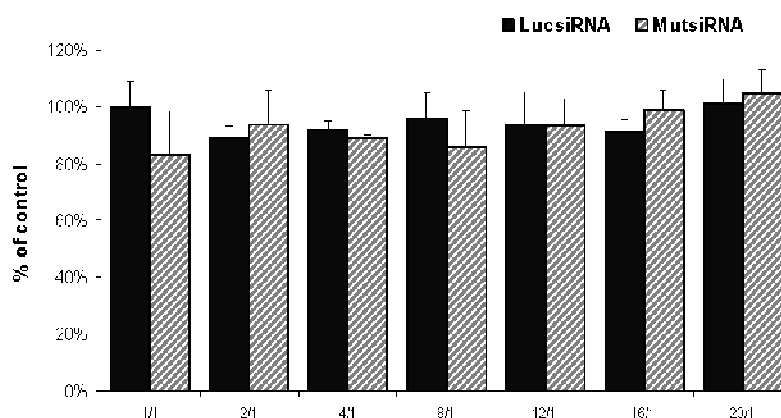
Figure 3.69

Gene silencing efficacy of the cholamine GNP loaded with luciferase siRNA revealed no statistically significant difference to the rates achieved with mut-siRNA.

The pH in the endosome is known to be acidic (~5). This might influence the knock-down through degradation of the siRNA inside the endosome. However, taken into account an effective protection of the siRNA by the inherent buffer capacity of the gelatin molecule, as proposed in literature, can elevate the pH in the lysosome again. A more basic pH level will then effectively diminish the activity of enzymes in the lysosome including nucleases [Seglen, P. O. 1983].

DEAE-dextran gelatin nanoparticles for gene silencing

Therefore in the following studies, the strong cationic nanoparticles were modified with the polysaccharide DEAE-dextran matrix and were examined. With the knowledge that DEAE-dextran was many times successfully used in transfecting DNA to bacterial and even mammalian cells [Schenborn, E. T. et al. 2000], our formulation with DEAE-dextran modified gelatin nanoparticles was loaded with 0.5 µg siRNA molecules as described above.

DEAE-dextran mediated transfection was first described by Vaheri [Vaheri, A. et al. 1965] using viral RNA and by McCutchan [McCutchan, J. H. et al. 1968] with DNA.

Figure 3.70

Gene silencing efficacy of the DEAE-dextran GNP loaded luciferase siRNA revealed no statistically significant difference to the rates achieved with mut-siRNA.

The percentage of luciferase knock-down in our experiment was again tested in the established luciferase assay and compared to DEAE-dextran modified gelatin nanoparticles loaded with a non-sense siRNA (mut-siRNA). We found out, that DEAE-dextran nanoparticles when loaded with 500 ng luc-siRNA or 500 ng control siRNA at different ratios (5:1 to 200:1) and incubated with the cells for 48 hours did not induce a significant luciferase knock-down (**Figure 3.70**). At a ratio of 20:1 the mean effect in luciferase signal was 90 % that of the control, for 40:1 an effect of 85 % was recorded and for 200:1 it was already at 40°%. Interestingly, we detected an increased interaction of the nanoparticles with cells, reflected in decreased cell viability at higher nanoparticle concentrations. This however shall not interrupt our further studies since for RNAi much less amounts of GNP then tested here will be needed. It is known that DEAE-dextran when used for transfection can only achieve a transient gene regulation [Gluzman, Y. 1981]. Yet in our experiment no knock-down could be observed throughout the whole incubation time indicating that the nanoparticles, which eventually were taken up by the cells, could not escape the endosomal trap. With the higher zeta potential of siRNA loaded DEAE-dextran nanoparticles (refer to 3.6 siRNA containing

gelatin nanoparticles (SICONs)) the nanoparticles would attach to the cell membrane as shown in the *in-vitro* experiments and from the discussion in 3.12 In-vitro / in-vivo correlation.

DEAE-dextran and cholamine gelatin nanoparticles for gene silencing

Since cationic charge of the cholamine modified gelatin nanoparticles as well as of those nanoparticles cationized solely with DEAE-dextran was still in the medium range of 25-35 mV we thought of pushing the boundaries of cationization even further. Some research groups have shown that a higher charge of their transfection reagent was directly related to the transfection efficacy [Takeuchi, K.-i. et al. 1996; Huang, Y.-Z. et al. 2006] and in many liposomal or basically lipid based transfection reagents a high net charge of the final nucleotide loaded formulation is centrally important. For this reason we decided to formulate dual modified highly cationic gelatin nanoparticles based on an incorporation of DEAE-dextran inside the nanoparticle core and a covalent cationic linking of cholamine to the free carboxy groups of the protein. Those nanoparticles could be formulated in a validated process resulting in homogeneous and monodispersly distributed nanoparticles in the lower size range of 170 – 280 nm as shown in 2.1.5 Formulation of diethyl-amino-ethanol-dextran and cholamine modified gelatin nanoparticles.

The novelty of this formulation was not only its initial high cationic charge (53 mV) but also the fact that loading with siRNA molecules over a wider nanoparticle to siRNA range would not decrease the charge dramatically anymore (**Figure 3.30**).

Hence, even after loading of high siRNA ratios in HEPES buffer or PBS a cationic charge of the nanoparticles was present. Compared to other studies [Chen, J. et al. 2007], where the charge of loaded methoxypolyethyleneglycol polylactic chitosan (MePEG-PLA-CS) and polylactic chitosan (PLA-CS) nanoparticles was in the range of 21 mV and 12 mV respectively the charge of our nanoparticles was even higher. Therefore the cell interaction and uptake probability at least in theory were maximized for this type of formulation.
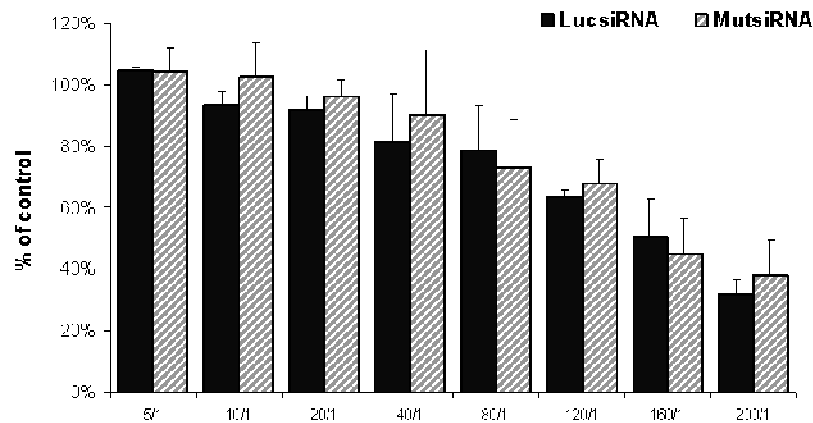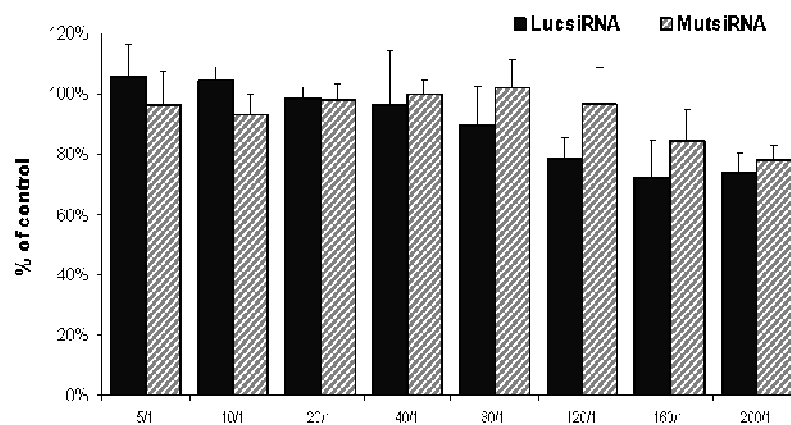
Figure 3.71

Knock-down efficacy of the cholamine DD-GNP loaded with luciferase siRNA revealed no statistically significant difference to the rates achieved with mut-siRNA but for 120:1 and 160:1 an effect was measured

This strongly cationic DEAE-dextran cholamine formulation was not able to transfer luc-siRNA into the chosen cell culture assay (**Figure 3.71**). Only at a ratio of 120:1 an indication of a 20 % knock-down was determined, as well as at a ratio of 160:1. A therapeutically useful RNAi should switch protein production nearly completely and lastingly off making further improvements to the transfection potential of the formulation mandatory. Many researchers have given the cationic charge in their nanoparticle formulations not a too close look due to postulated negative side effects related to the high charge. Our study data suggested that nanoparticles when formulated from gelatin with a high cationic charge still show high cell viability, which is needed for an ideal transfection candidate.

PEI modified DEAE-dextran gelatin nanoparticles for gene silencing

With this knowledge, our theoretic model developed into the direction where a missing endosomal escape of the gelatin nanoparticles became most likely. Endosomal release of most carriers is usually achieved by making use of a polyamine based proton sponge effect on the nanoparticle surface. Polyethylene imine (PEI) is widely used for endosmolytic effects. What needs to be stated is that PEI alone with siRNA cannot induce RNA interference. This was

confirmed by us at PEI:siRNA (w/w) ratios from 0,5:1to 2:1 up to concentrations of 4:1, where the highest cell toxicity was reached (**Figure 3.72**).
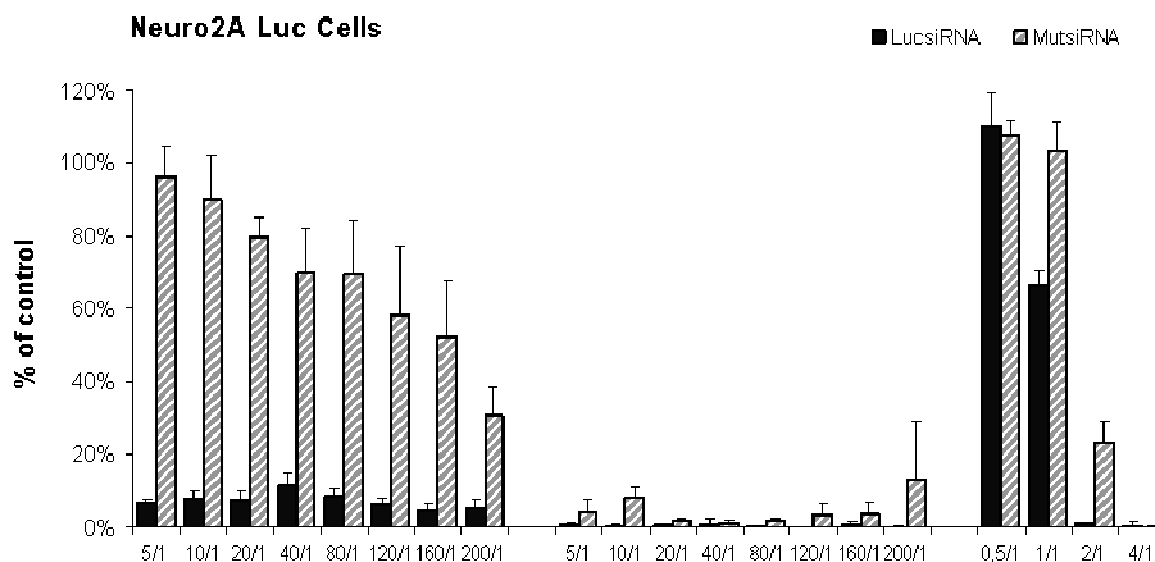
Figure 3.72

Knock-down assay with 0.5 µg PEI modified DEAE-dextran GNP (left), 1 µg PEI modified DEAE-dextran GNP (center) and PEI complexed siRNA (right) prepared in HBG

    Now in combination with the strongly cationic gelatin nanoparticles, PEI was able to induce a strong silencing effect. For this experiment the cholamine cationized DEAE-dextran gelatin nanoparticles were loaded with siRNA at different ratios as described above. To the negatively charged nucleotide coating of the nanoparticle surface PEI 25br was added to form a monolayer of this polyamine moiety around the nanoparticle shell. Those luc-siRNA nanoparticles when incubated with the cells showed an effective RNAi based protein knockdown over the whole incubation time. These results demonstrate that our earlier nanoparticle formulations were, when cationic enough for cell interaction, always entrapped inside the endosome preventing them from releasing their payload into the cytoplasm. Here we could show that the same nanoparticles, that when applied alone to the cells could not silence the genes at all, in combination with PEI 25br showed a maximum knock-down efficiency over the whole range of nanoparticle:siRNA ratios. For higher PEI concentrations of 1 µg in the formulation the cell viability decreased below 10 % indicating the maximum

tolerable dose of PEI for these *in-vitro* experiments. We were surprised that gelatin nanoparticles in this special case also seemed to protect the cells to a certain extent from the toxic influence of PEI 25br, which cannot be explained fully so far. Even at fifty times the amount of our nanoparticles applied to the cells compared to the PEI complex left a cell viability of approximately 30 % (**Figure 3.72**). At twenty times the amount of nanoparticles the viability was still at 72 % while for the PEI no cells survived the 48 hours incubation time. At the lowest nanoparticle amount tested, which was a ratio of 5:1 compared to a 4:1 ratio for the PEI polyplex our DEAE-dextran cholamine modified nanoparticles coated with PEI left the cells at an average of 100 % viability over 48 hours, tremendously protecting the cells from the negative PEI side effects.

Polyamine modified gelatin nanoparticles for gene silencing

The postulated proton sponge effect responsible for the effective endosomal release of our PEI formulation was also tested with tetra-ethylene-pentamine (TEPA) and spermidine modified SICONS. Within this formulation 50 % of the cholamine was substituted with either TEPA or spermidine and examined in the same way as the previous nanoparticle formulations (**Figure 3.73**). Neither of the two polyamine modifications was able to induce a sufficient proton-sponge effect or endosome rupture that would be sufficient for nanoparticle release to the cytoplasm. In detail, the TEPA modification lead to luciferase signals ranging from 98.29 % $\pm$ 12.17 % S.D. at 5:1 down to 58.62 % $\pm$ 25.24 % S.D. at 200:1. For the spermidine modification signals from 83.85 % $\pm$ 6.60 % S.D. at 10:1 down to 2.05 % $\pm$ 1.40 % S.D. at 200:1 were measured. Also, while TEPA modified nanoparticles showed a good cell viability over almost 90 % of the incubated GNP ratios, spermidine decreased the cell viability above a NP:siRNA ratio of 80:1 to 49.38 % $\pm$ 17.68 % S.D. and as low as 0.59 % $\pm$ 0.45% S.D. preventing the use of this formulation above this concentration.
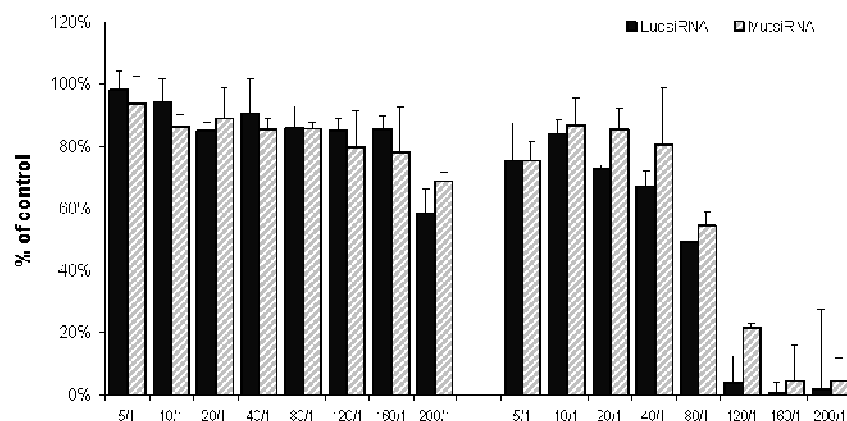
Figure 3.73

TEPA (left) and spermidine (right) modified cationic gelatin nanoparticles

Novel sandwich gelatin nanoparticles for gene silencing

Rounded up with the above PEI results, we were able to demonstrate that our siRNA containing gelatin nanoparticle systems (refer to 3.6 siRNA containing gelatin nanoparticles (SICONs)) generally and by their inherent properties do have the potential as both highly and stable loadable and also efficient RNA interference mediators. The only real obstacle that had to be overcome at this point in our research was how to induce an endosomolytic effects in the **SICON**s. In the end the most adequate solution was to alter the actual **SICON** formulation from a single nanoparticle system to novel sandwich like PEG-PLL-DMMel modified **SICON**s. With this novel carrier system that was developed and advanced by the research group of Professor Dr. Ernst Wagner at the University of Munich, we can use the high endosomolytic efficiency of Melittin peptide combined with the inherent positive properties of our gelatin nanoparticles. Only with the generosity of and in close cooperation with Professor Wagner and his team the above luciferase transfection results as well as the following Melittin experiments could be realized. At first the cells were treated with standard DEAE-dextran **SICON**s and the PEG-PLL-DMMel was added right afterwards to form endosmolytic sandwich nanoparticles. After the incubation time the cells were lysed and prepared for the luciferase assay. We could show a high knock-down rate again over all employed loading ratios (**Figure 3.74**). Based on our photometric studies that showed a sandwich complex formation between **SICON**s and PEG-PLL-DMMel (refer to 3.7 Sandwich

nanoparticle formulation with a Melittin construct) we postulate such a novel complex formation either in the endosome or in the first case right in the cell reaction chamber. In both cases the siRNA delivery and luciferase protein knock-down was successful. Compared to pure PEG-PLL-DMM as the "gold standard" for this type of gene silencing, our novel nanoparticles showed almost 50 % greater cell viability at similar carrier concentrations.
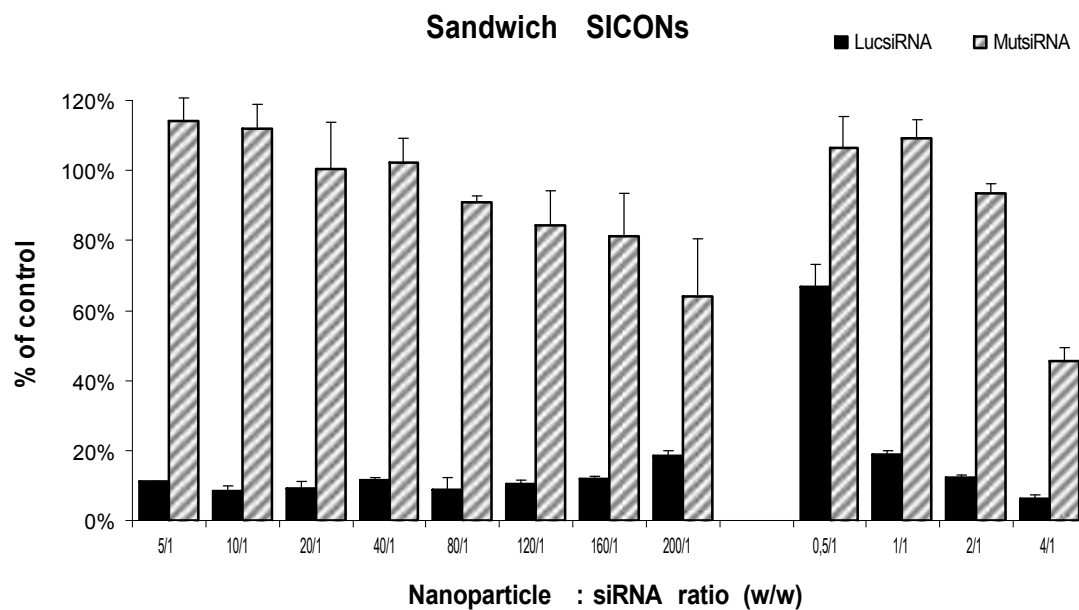
Figure 3.74

Knock-down assay PEG-PLL-DMMel modified DD-**SICON**s in HBG (left) and pure PEG-PLL-DMMel polyplex (right). **SICON**s show a high cell viability over all tested ratios.

MTT assay

The general high cell tolerability of our novel nanoparticles was finally examined in a separate MTT assay. The above results in viability from the transfection experiments could be confirmed. The nanoparticles up to a ratio of 160:1 had a median cell viability of above 80 % and only for a ratio of 200:1 dropped to approximately 74 % (**Figure 3.75**).
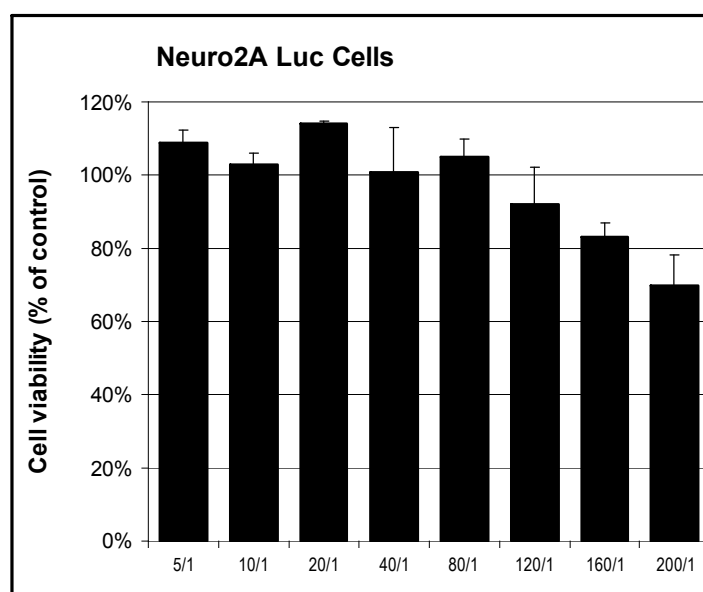
Figure 3.75

MTT test of CDD-GNP

In conclusion our final formulation approach with a Melittin construct on the nanoparticle surface was successful to induce an endosomal escape of the nanoparticles and release the siRNA into the cytoplasm where RNAi could take place. Compared to the pure Melittin construct as a polyplex the novel formulation had a higher cell viability over all tested concentrations.

4 Summary and Outlook

The recent progress in the potential therapeutic applications of siRNAs is owed largely to major breakthroughs in delivery. Even a systemic delivery of therapeutic amounts of anti-ApoB siRNAs in chimpanzees was recently accomplished by the use of bi-layer liposomes [Zimmermann, T. S. et al. 2006]. These important proofs of principle studies demonstrated that it is indeed safe and effective to systemically delivery therapeutically relevant doses of siRNAs to primates, paving the way for other future systemic applications of RNA.

In the present thesis, we formulated novel nanoparticles from the bio-tolerable protein gelatin and the cationic polysaccharide DEAE-dextran and demonstrated their potential for siRNA delivery. In this context, these and other materials like thiomers were at first characterized in terms of molecular weight to invent new formulation techniques for small and homogenous nanoparticles, which were then extensively tested for their potential as siRNA carriers. Especially Asymmetric flow field-flow fractionation and automatic microviscosimetry proved to be fast and reliable methods to screen nanoparticle excipients in a pre-formulation environment. With a close focus on later *in-vitro* and *in-vivo* fluorescence based studies we evaluated the labeling efficiency of various fluorescent dyes and their impact on the physicochemical properties of the nanoparticles. An optimum formulation for DEAE-dextran and cholamine modified gelatin nanoparticles was developed and enhanced with an endosomolytic moiety comprising a cationic backbone and a stabilized Melittin peptide for effective RNA interference. The final formulation with a Melittin modification was shown to induce an efficient protein knockdown of luciferase as a model protein and of VEGF-receptor as a therapeutic protein. At the same time the formulation prompted a higher cell tolerability than several gold standard siRNA transfection reagents like for example polyethylene imine. For the first time, gelatin nanoparticles from type A gelatin could be formulated with a sufficiently high cationic charge for siRNA loading and endothelium targeting and at the same time induce RNA interference *in-vitro* for a model and a therapeutic protein. In perspective, the targeting and transfection efficacies of siRNA loaded gelatin type A nanoparticles together with the newly introduced modifications comprising DEAE-dextran and PLL-PEG-DMMAn-Mel need to be demonstrated under *in-vivo* conditions as a final proof of concept. As a first step in this direction the pharmacokinetic distribution of the newly developed formulations was already analyzed in the mouse model, giving a promising outlook for further

clinical studies. In addition, hydrophobic, methylated, acetylated, and with various other surface modifications altered nanoparticles were formulated and characterized for their potential as siRNA carrier systems. The successful surface alterations were analysed by nuclear magnetic resonance spectroscopy and quasi elastic light scattering. The sum of these nanoparticles was further examined in a newly developed *in-vitro* flow model where we could simulate for the first time under near to realistic *in-vivo* conditions the nanoparticle cell interaction patterns. We could demonstrate differences in the nanoparticle behaviour among various nanoparticle excipients with discrepancies in the amount of interacting nanoparticles per cell and cell viability if either a static cell culture was used or the novel flow model. Cationic nanoparticles in most cases showed an increased endothelial cell attachment compared to hydrophobic and neutral nanoparticles whereas the low tolerability of polybutylcyanoacrylate nanoparticles in the static model was confirmed even under flow conditions.

Last but not least, we examined our nanoparticle formulations in several *in-vivo* models. At first, we elucidated the nanoparticle fate via concentration and size finding studies in the hamster dorsal skin fold chamber model. Compared to highly dosed and fluorescently labeled liposomal formulations, did the gelatin nanoparticles not show significantly strong signals within this model, which could be due to the narrow capillary bed in the observation area and a low fluorescence emission. Additional studies in the mouse cremaster model gave evidence of the potential of cationic gelatin nanoparticle to target inflamed endothelium tissue *in-vivo*. The antigen induced arthritis model in the mouse knee which was eventually used to compare the gelatin formulation loaded with siRNA to chitosan nanoparticles revealed an advantageous *in-vivo* stability or distribution homogeneity of the gelatin nanoparticles compared to the chitosan formulation. A correlation in terms of nanoparticle surface properties could be drawn from the *in-vitro* flow model to the *in-vivo* observations once again pointing out the relevance of thorough preclinical investigations of nanoparticles for further therapeutic use. Based on our development of a realistic nanoparticle observation model and based on the results from our *in-vivo* observations and gene silencing studies, we see the great potential of using nanoparticles for targeted systemic delivery of siRNA in order to treat the upcoming burdens of humanity and the toll for a longer lifetime like increasing incidents of cancer and all the vessel related diseases. Our nanoparticles can be formulated with most likely any therapeutically relevant siRNA and endothelial cell interaction studies in the flow model will allow forecasting the later *in-vivo* behaviour.

5 Final Conclusion

Goal of the presented doctoral thesis was to formulate advanced gelatin nanoparticles for the delivery of small oligonucleotides, especially siRNA. The intention then was to transfer the newly discovered principle of RNAi based protein knock-down to a protein based, biocompatible, biodegradable nanoparticles for in-vivo therapeutic applications.

For the characterization of the nanoparticles ex-vivo several physical, biochemical and laser based techniques were used.

In a first step, novel gelatin nanoparticle formulations were developed in order to alter their biological and physicochemical properties for an improved siRNA loading and new and efficient cell targeting properties. In this context, methylation, pegylation, acetylation, surfactant coatings and polysaccharide incorporation nanoformulations were developed and characterized.

Most importantly the development of new sandwich gelatin nanoparticles has to be highlighted. This novel nanoparticle carrier is based on a strong cationic gelatin polysaccharide matrix core that could be loaded successfully with siRNA in a layer around the central nanoparticle and then encapsulated with an endosmolytic peptide construct. We demonstrated that these gelatin sandwich nanoparticles do not only protect the siRNA from sudden load dumping in physiological media like many other nanoformulations but also efficiently overcome the endosomal trap to induce the sought for RNAi based protein knock-down.

Secondly we adapted a novel cell-flow model for our nanoparticle cell interaction studies. We demonstrated that the flow model can be used as an invaluable improvement for the preclinical evaluation of nanoformulations in an *in-vitro* or respectively near-to-physiological environment. Furthermore, we demonstrated the charge related targeting effects of gelatin and other nanoparticles to endothelium cells. We delivered a proof of principle that cationic gelatin nanoparticles are a potential therapeutic nanoparticle system for the targeting of endothelium and angiogenetic related diseases.

Next, the endothelium targeting properties and pharmacokinetic properties of gelatin nanoparticles were investigated in a hamster skin fold chamber and a mouse cremaster model. For the first time gelatin nanoparticles were monitored on the microvascular level. Nanoparticle size, charge and also surface coatings were found to play a major role in the nanoparticle half-life and endothelium attachment properties confirming the assumptions from the cell flow-model.

In summary, we improved gelatin nanoparticles to a carrier system for siRNA. In addition we could demonstrate their potential in the field of RNA interference, laying the basis for an anti-angiogenetic and tumor therapy. The transfer of a promising new preclinical *in-vitro* evaluation model with the potential to overcome static cell culture models into the field of nanoparticle research was an important for a better analytical understanding of the ins and outs of nanoscaled biopharmaceuticals like liposomes and antibodies.

In the near future of the 21st century siRNA loaded gelatin sandwich nanoparticles could be an option as new delivery systems in the field of biopharmacy.

Leuchtende Tage!
Nicht weinen, weil sie vorüber,
sondern lächeln, weil sie gewesen.

Rabindranâth Tagore
Nobelpreis für Literatur
1861 - 1941

References

Albini, A. et al. (1996). "The angiogenesis induced by HIV-1 Tat protein is mediated by the Flk-1/KDR receptor on vascular endothelial cells." <u>Nature Medicine</u> **2**(12): 1371-1375.

Algire, G. H. (1943). "An adaptation of the transparent chamber technique to the mouse." <u>Journal of the National Cancer Institute</u> **4**: 1-11.

Allémann, E. et al. (1993). "In vitro extended-release properties of drug-loaded poly(DL-lactic acid) nanoparticles produced by a salting-out procedure." <u>Pharmaceutical Research</u> **10**(12): 1732-1737.

Amarzguioui, M. et al. (2003). "Tolerance for mutations and chemical modifications in a siRNA." <u>Nucleic Acids Research</u> **31**(2): 589-595.

Amiji, M., Ed. (2004). <u>Polymeric gene delivery: principles and applications</u>. New York, Amiji, M.

Anna, R. et al. (2005). "Nanoparticle-induced platelet aggregation and vascular thrombosis." <u>British Journal of Pharmacology</u> **146**(6): 882-893.

Aouadi, M. et al. (2009). "Orally delivered siRNA targeting macrophage Map4k4 suppresses systemic inflammation." <u>Nature</u> **458**(7242): 1180-1184.

Arai, K. et al. (1968). "Toxicity of chitosan." <u>Bull Tokai Region Fish Lab</u> **56**.

Arnedo, A. et al. (2002). "Albumin nanoparticles as carriers for a phosphodiester oligonucleotide." <u>International Journal of Pharmaceutics</u> **244**: 59-72.

Asaishi, K. et al. (1981). "Quantitative analysis of micro-vascular structure and function in the amelanotic melanoma A-Mel-3." <u>Cancer Research</u> **41**(5): 1898-1904.

Aspden, T. et al. (1997). "The effect of chronic nasal application of chitosan solutions on cilia beat frequency in guinea pigs." International Journal of Pharmaceutics **153**: 137-146.

Augsten, C. (2008). Asymmetrische Fluß Feld-Fluß Fraktionierung in Verbindung mit Mehrwinkellichtstreudetektion – Eine neue bedeutende Methode der Pharmazeutischen Analytik zur Charakterisierung von Makromolekülen und Nanopartikeln. Biosciences. Halle-Wittenberg, Martin-Luther University. **Dr. rer. nat.:** 144.

Backer, M. V. et al. (2001). "Shiga-like toxin-VEGF fusion proteins are selectively cytotoxic to endothelial cells overexpressing VEGFR-2." Journal of Controlled Release **74**(1-3): 349-355.

Baez, S. (1973). "An open cremaster muscle preparation for the study of blood vessels by in vivo microscopy." Microvascular Research **5**: 384-394.

Bajpai, A. and Choubey, J. (2006). "Design of gelatin nanoparticles as swelling controlled delivery system for chloroquine phosphate." Journal of Materials Science: Materials in Medicine **17**: 345-358.

Baluk, P. et al. (2008). Cellular actions of angiogenesis inhibitors on blood vessels. Tumor Angiogenesis**:** 557-576.

Bartlett, D. W. et al. (2007). "Impact of tumor-specific targeting on the biodistribution and efficacy of siRNA nanoparticles measured by multimodality in vivo imaging." Proceedings of the National Academy of Sciences **104**(39): 15549-15554.

Bekeredjian, R. et al. (2007). "Ultrasound targeted microbubble destruction increases capillary permeability in hepatomas." Ultrasound in Medicine & Biology **33**(10): 1592-1598.

Berg van den, W. B. and Lent van, P. L. (1996). "The role of macrophages in chronic arthritis." Immunobiology **195**(4-5): 614-623.

178

Bernkop-Schnuerch, A. B. and Hopf, T. E. (2001). "Synthesis and in vitro evaluation of chitosan-thioglycolic acid conjugates." Scientia Pharmaceutica **69**: 109-118.

Bernkop-Schnuerch, A. B. et al. (2003). "Thiolated polymers – thiomers: modification of chitosan with 2-iminothiolane." International Journal of Pharmaceutics **260**: 229-237.

Bernkop-Schnürch, A. et al. (2006). "Development of a novel method for the preparation of submicron particles based on thiolated chitosan." European Journal of Pharmaceutics and Biopharmaceutics **63**(2): 166-172.

Berth, G. and Dautzenberg, H. (1998). "Solution behaviour of some selected polysaccharides studied preferentially by static light scattering." Recent Research Developments in Macromolecules **3**: 225-248.

Bodmeier, R. et al. (1989). "A novel approach to the oral delivery of micro- or nanoparticles." Pharmaceutical Research **6**: 413-417.

Bourquin, C. et al. (2008). "Targeting CpG oligonucleotides to the lymph node by nanoparticles elicits efficient antitumoral immunity." The Journal of Immunology **181**(5): 2990-2998.

Bowman, K. and Kam, W. L. (2006). "Chitosan nanoparticles for oral drug and gene delivery." International Journal of Nanomedicine **1**(2): 117-128.

Braasch, D. A. et al. (2003). "RNA interference in mammalian cells by chemically-modified RNA " Biochemistry **42**(26): 7967-7975.

Brahn, E. (1991). "Animal models of rheumatoid arthritis: clues to etiology and treatment." Clinical Orthopaedics: 42-53.

Branemark, P. L. et al. (1964). "Microcirculatory studies in man by high resolution vital microscopy." Angiology **15**: 329-332.

Brekken, R. A. et al. (2000). "Selective inhibition of vascular endothelial growth factor (VEGF) receptor 2 (KDR/Flk-1) activity by a monoclonal anti-VEGF antibody blocks tumor growth in mice." Cancer Research **60**(18): 5117-5124.

Bresnihan, B. (1999). "Pathogenesis of joint damage in rheumatoid arthritis." Journal of Rheumatology **26**: 717-719.

Brigger, I. et al. (2002). "Nanoparticles in cancer therapy and diagnosis." Advanced Drug Delivery Reviews **54**(5): 631-651.

Broermann, P. et al. (2008). Bringing light into the dark: influence of fluorescence labeling on protein nanoparticles for in-vivo use. EHRLICH II – 2nd World Conference on Magic Bullets. Nürnberg, Germany.

Brukner, I. and Tremblay, G. A. (2000). "Cellular proteins prevent antisense phosphorothioate oligonucleotide (SdT18) to target sense RNA (rA18): development of a new in vitro assay." Biochemistry **39**(37): 11463-11466.

Cafaggi, S. et al. (2007). "Preparation and evaluation of nanoparticles made of chitosan or N-trimethyl chitosan and a cisplatin-alginate complex." Journal of Controlled Release **121**(1-2): 110-123.

Calvo, P. et al. (1997). "Novel hydrophilic chitosan-polyethylene oxide nanoparticles as protein carriers." Journal of applied polymer science **63**(1): 125-132.

Carmeliet, P. (2005). "Angiogenesis in life, disease and medicine." Nature **438**(7070): 932-936.

Carpenter, J. F. et al. (2009). "Overlooking subvisible particles in therapeutic protein products: Gaps that may compromise product quality." Journal of Pharmaceutical Sciences **98**(4): 1201-1205.

Cascone, M. G. et al. (2002). "Gelatin nanoparticles produced by a simple W/O emulsion as delivery system for methotrexate." Journal of Materials Science: Materials in Medicine **13**(5): 523-526.

Chambers, E. and Mitragotri, S. (2007). "Long circulating nanoparticles via adhesion on red blood cells: mechanism and extended circulation." Experimental Biology and Medicine **232**(7): 958-966.

Chen, J. et al. (2007). "Preparation, characterization and transfection efficiency of cationic PEGylated PLA nanoparticles as gene delivery systems." Journal of Biotechnology **130**(2): 107-113.

Chiu, Y.-L. et al. (2004). "Visualizing a correlation between siRNA localization, cellular uptake, and RNAi in living cells." Chemistry & Biology **11**(8): 1165-1175.

Chiu, Y.-L. and Rana, T. M. (2002). "RNAi in human cells: basic structural and functional features of small interfering RNA." Molecular Cell **10**(3): 549-561.

Cho, Y. S. et al. (2001). "Antisense DNAs as multisite genomic modulators identified by DNA microarray." Proceedings of the National Academy of Sciences of the United States of America **98**(17): 9819-9823.

Chu, B. and Liu, T. (2000). "Characterization of nanoparticles by scattering techniques." Journal of Nanoparticle Research **2**(1): 29-41.

Clark, E. R. et al. (1930). "Recent modifications in the method of studying living cells and tissues in transparent chambers inserted in the rabbit's ear." Anatomical record **47**: 187-211.

Clark, P. R. and Hersh, E. M. (1999). "Cationic lipid-mediated gene transfer: current concepts." Current Opinion in Molecular Therapeutics **1**: 158-176.

Coester, C. (2000). Entwicklung peptidischer oberflächenmodifizierter nanopartikulärer Trägersysteme für Antisense-Wirkstoffe und präklinische Testung gegen HIV. Aachen, Shaker.

Coester, C. (2003). "Development of a new carrier system for oligonucleotides and plasmids based on gelatin nanoparticles." New Drugs(1): 14-17.

Coester, C. et al. (2006). Nanoparticles and method for the production thereof. Office, G. P. **WO002006021367A1**.

Coester, C. J. et al. (2000). "Gelatin nanoparticles by two step desolvation a new preparation method, surface modifications and cell uptake." Journal of Microencapsulation **17**: 187-193.

Cortesi, R. et al. (1999). "Dextran cross-linked gelatin microspheres as a drug delivery system." European Journal of Pharmaceutics and Biopharmaceutics **47**(2): 153-160.

Couvreur, P. et al. (1979). "Polycyanoacrylate nanocapsules as potential lysosomotropic carriers: preparation, morphological and absorptive properties." Journal of Pharmacy and Pharmacology **31**.

Couzin, J. (2002). "Breakthrough of the year: small RNAs make big splash." Science **298**(5602): 2296-2297.

Crommelin, D. J. and Schreier, A., Eds. (1994). Liposomes. Colloidal drug delivery systems. New York, Marcel Dekker.

Crooke, S. T. (2000). "Evaluating the mechanism of action of antiproliferative antisense drugs." Antisense and Nucleic Acid Drug Development **10**(2): 123-126.

Cui, Z. et al. (2006). "Lecithin-based cationic nanoparticles as a potential DNA delivery system." International Journal of Pharmaceutics **313**(1-2): 206-213.

Dalby, B. et al. (2004). "Advanced transfection with Lipofectamine 2000 reagent: primary neurons, siRNA, and high-throughput applications." Methods **33**(2): 95-103.

David, P. (1998). "Retroviral vectors and lentiviral vectors." Gene Therapy **5**: 1481-1487.

Decher, G. and Hong, J. D. (1991). "Buildup of ultrathin multilayer films by a self-assembly process. Consecutive adsorption of anionic and cationic bipolar amphiphiles on charged surfaces." Makromolare Chemie Macromol Symp **46**.

Dekker, R. J. et al. (2002). "Prolonged fluid shear stress induces a distinct set of endothelial cell genes, most specifically lung Kruppel-like factor (KLF2)." <u>Blood</u> **100**(5): 1689-1698.

Denli, A. M. and Hannon, G. J. (2003). "RNAi: an ever-growing puzzle." <u>Trends in Biochemical Sciences</u> **28**(4): 196-201.

Deol, P. and Khuller, G. K. (1997). "Lung specific stealth liposomes: stability, biodistribution and toxicity of liposomal antitubercular drugs in mice." <u>Biochimica et Biophysica Acta (BBA) - General Subjects</u> **1334**(2-3): 161-172.

DeWitt, N. (2005). "Angiogenesis." <u>Nature</u> **438**(7070): 931-931.

Dhaneshwar, S. et al. (2006). "Dextran: d promising macromolecular drug carrier." <u>Indian Journal of Pharmaceutical Sciences</u> **68**(6): 705-714.

Di Paolo, D. et al. (2008). "Drug delivery systems: application of liposomal anti-tumor agents to neuroectodermal cancer treatment " <u>Tumori</u> **94**(2).

Dorn, G. et al. (2004). "siRNA relieves chronic neuropathic pain." <u>Nucleic Acids Research</u> **32**(5).

Ehrenberg, M. S. et al. (2009). "The influence of protein adsorption on nanoparticle association with cultured endothelial cells." <u>Biomaterials</u> **30**(4): 603-610.

Eichhorn, M. E. et al. (2004). "Anti-vascular tumor therapy: recent advances, pitfalls and clinical perspectives." <u>Drug Resistance Updates</u> **7**(2): 125-138.

Einstein, A. (1910). "Theorie der Opaleszenz von homogenen Flüssigkeiten und Flüssigkeitsgemischen in der Nähe des kritischen Zustandes." <u>Annalen der Physik</u> **338**(16): 1275-1298.

El Ouahabi, A. et al. (1997). "The role of endosome destabilizing activity in the gene transfer process mediated by cationic lipids." <u>FEBS Letters</u> **414**(2): 187-192.

Elbashir, S. M. et al. (2001). "Duplexes of 21-nucleotide RNAs mediate RNA interference in cultured mammalian cells." Nature **411**(6836): 494-498.

Endrich, B. et al. (1980). "Technical report - a new chamber technique for microvascular studies in unanesthetized hamsters." Research in Experimental Medicine **177**(2): 125-134.

Evans, C. E. et al. (1999). "Cytotoxicity of cyanoacrylate adhesives to cultured tendon cells." The Journal of Hand Surgery: Journal of the British Society for Surgery of the Hand **24**(6): 658-661.

Ferber, D. (2001). "Gene therapy: safer and virus-free?" Science **294**(5547): 1638-1642.

Ferrara, N. (2002). "VEGF and the quest for tumour angiogenesis factors." Nat Rev Cancer **2**(10): 795-803.

Ferrara, N. and Kerbel, R. S. (2005). "Angiogenesis as a therapeutic target." Nature **438**(7070): 967-974.

Ferrari, M. (2005). "Cancer nanotechnology: opportunities and challenges." Nature Reviews Cancer **5**(3): 161-171.

Fire, A. et al. (1998). "Potent and specific genetic interference by double-stranded RNA in caenorhabditis elegans." Nature **391**(6669): 806-811.

Fisher, A. A. et al. (2002). "Evaluating the specificity of antisense oligonucleotide conjugates. a DNA array analysis." Journal of Biological Chemistry **277**(25): 22980-22984.

Flanagan, N. (2009). "Improving delivery of RNAi drugs."   Retrieved 12.07.2009, 2009, from http://www.genengnews.com/articles/chitem_print.aspx?aid=2758&chid=0.

Folkman, J. (1971). "Tumor angiogenesis: therapeutic implications." New England Journal of Medicine **285**(21).

Folkman, J. (1995). "Angiogenesis in cancer, vascular, rheumatoid and other disease." <u>Nature Medicine</u> **1**(1): 27-30.

Folkman, J. and Klagsbrun, M. (1987). "Angiogenic factors." <u>Science</u> **235**(4787): 442-447.

Fraunhofer, W. et al. (2004). "Asymmetrical flow field-flow fractionation and multiangle light scattering for analysis of gelatin nanoparticle drug carrier systems." <u>Analytical Chemistry</u> **76**(7): 1909-1920.

Fricker, G. and Miller, D. S. (2004). "Modulation of drug transporters at the blood-brain barrier." <u>Pharmacology</u> **70**(4): 169-176.

Gao, K. and Huang, L. (2008). "Nonviral methods for siRNA delivery." <u>Molecular Pharmaceutics</u> **6**(3): 651.

Gao, X. et al. (2004). "In vivo cancer targeting and imaging with semiconductor quantum dots." <u>Nature Biotech</u> **22**(8): 969-976.

Gao, X. et al. (2007). "Nonviral gene delivery: what we know and what is next." <u>The AAPS Journal</u> **9**(1).

Ge, Q. et al. (2004). "Inhibition of influenza virus production in virus-infected mice by RNA interference." <u>Proceedings of the National Academy of Sciences of the United States of America</u> **101**(23): 8676-8681.

Geisbert, Thomas W. et al. (2006). "Postexposure protection of guinea pigs against a lethal ebola virus challenge is conferred by RNA interference." <u>The Journal of Infectious Diseases</u> **193**(12): 1650-1657.

Ghazizadeh, S. et al. (1997). "Repression of retrovirus-mediated transgene expression by interferons: implications for gene therapy." <u>Journal of Virology</u> **71**(12): 9163-9169.

Gipps, E. M. et al. (1987). "The effects of polyalkylcyanoacrylate nanoparticles on human normal and malignant mesenchymal cells in vitro." <u>International Journal of Pharmaceutics</u> **40**(1-2): 23-31.

Glazer, A. N. et al., Eds. (1976). Chemical modification of proteins. Laboratory Techniques in Biochemistry and Molecular Biology. New York, American Elsevier Publishing Co., INC.

Gluzman, Y. (1981). "SV40-transformed simian cells support the replication of early SV40 mutants." Cell **23**(1): 175-182.

Goto, F. et al. (1993). "Synergistic effects of vascular endothelial growth factor and basic fibroblast growth factor on the proliferation and cord formation of bovine capillary endothelial cells within collagen gels." Laboratory Investigation **69**(5): 508-517.

Gragoudas, E. S. et al. (2004). "Pegaptanib for neovascular age-related macular degeneration." New England Journal of Medicine **351**(27): 2805-2816.

Greenberg, D. A. and Jin, K. (2005). "From angiogenesis to neuropathology." Nature **438**(7070): 954-959.

Greenblatt, M. and Shubik, P. (1967). "Hamster cheek pouch chamber." Cancer Bulletin **19**: 65-81.

Gref, R. et al. (2006). "New self-assembled nanogels based on host-guest interactions: Characterization and drug loading." Journal of Controlled Release **111**(3): 316-324.

Grislain, L. et al. (1983). "Pharmacokinetics and distribution of a biodegradable drug-carrier." International Journal of Pharmaceutics **15**(3): 335-345.

Gupta, P. K. and Hung, C. T. (1989). "Albumin microspheres II: applications in drug delivery." Journal of Microencapsulation **6**(4): 463 - 472.

Hammond, S. M. et al. (2000). "An RNA-directed nuclease mediates post-transcriptional gene silencing in Drosophila cells." Nature **404**(6775): 293-296.

Hammond, S. M. et al. (2001). "Post-transcriptional gene silencing by double-stranded RNA." Nature Reviews Genetics **2**(2): 110-119.

Hansch, A. et al. (1996). "Quantification of macrophages and granulocytes at the joint cartilage-pannus junction in rheumatoid arthritis." Zeitschrift für Rheumatologie **55**(6): 401-409.

Harris, E. D. (1990). "Rheumatoid arthritis. Pathophysiology and implications for therapy." New England Journal of Medicine **322**(18): 1277-1289.

Harris, S. S. and Giorgio, T. D. (2005). "Convective flow increases lipoplex delivery rate to in vitro cellular monolayers." Gene Therapy **12**: 512-520.

Hasegawa, S. et al. (2001). "Microtubule involvement in the intracellular dynamics for gene transfection mediated by cationic liposomes." Gene Therapy **8**: 1669-1673.

Hässig, A. and Stampfli, K. (1969). "Plasma substitutes past and present." Bibl Haematologica **33**.

Hesse, M. et al., Eds. (1984). Spektroskopische Methoden in der organischen Chemie. Stuttgart, Georg Thieme Verlag.

Hobbs, J. B. et al. (1976). "The pathogenesis of hypertensive vascular changes in the rat: microscopic and ultrastructural correlation in vivo." Clinical Science **51**: 71-75.

Hogrefe, R. I. (1999). "An antisense oligonucleotide primer." Antisense and Nucleic Acid Drug Development **9**: 351-357.

Horn, E. (2006). "Konkurrenz für Deckglas & Co. – Neue Methoden der Kombination von Zellkultur und Mikroskopie." Mikrokosmos **95**(3).

Hough, S. R. et al. (2003). "Why RNAi makes sense." Nature Biotech **21**(7): 731-732.

Hsu, J.-P. and Liu, B.-T. (1999). "Stability of colloidal dispersions: charge regulation/adsorption model." Langmuir **15**(16): 5219-5226.

Hu-Lieskovan, S. et al. (2005). "Sequence-specific knockdown of EWS-FLI1 by targeted, nonviral delivery of small interfering RNA inhibits tumor growth in a murine model of metastatic ewing's sarcoma." Cancer Research **65**(19): 8984-8992.

Huang, Y.-Z. et al. (2006). "Cationic liposomes modified with non-ionic surfactants as effective non-viral carrier for gene transfer." Colloids and Surfaces B: Biointerfaces **49**(2): 158-164.

Hurwitz, H. et al. (2004). "Bevacizumab plus irinotecan, fluorouracil, and leucovorin for metastatic colorectal cancer." New England Journal of Medicine **350**(23): 2335-2342.

Hutvagner, G. and Zamore, P. D. (2002). "A microRNA in a multiple-turnover RNAi enzyme complex." Science **297**(5589): 2056-2060.

Iler, R. K. (1966). "Multilayers of colloidal particles." Journal of Colloid and Interface Science **21**(6): 569-594.

Illum, L. (1998). "Chitosan and its use as a pharmaceutical excipient." Pharmaceutical Research **15**.

Illum, L. and Davis, M. E. (1987). "Targeting of colloidal particles to the bone marrow." Life Sciences **40**.

Illum, L. and Davis, S. S. (1984). "The organ uptake of intravenously administered colloidal particles can be altered using a non-ionic surfactant (Poloxamer 338)." FEBS Letters **167**(1): 79-82.

Ishida, T. et al. (2006). "Spleen plays an important role in the induction of accelerated blood clearance of PEGylated liposomes." Journal of Controlled Release **115**(3): 243-250.

Jabr-Milane, L. et al. (2008). "Multi-functional nanocarriers for targeted delivery of drugs and genes." Journal of Controlled Release **130**(2): 121-128.

Janas, J. et al. (2006). "Lentiviral delivery of RNAi in hippocampal neurons." Methods in Enzymology **406**: 593-605.

Jeffery, P. K. and Li, D. (1997). "Airway mucosa: secretory cells, mucus and mucin genes." European Respiratory Journal **10**(7): 1655-1662.

Karkkainen, M. J. et al. (2002). "Lymphatic endothelium: a new frontier of metastasis research." Nature Cell Biology **4**(1): E2-E5.

Kast, C. E. and Bernkop-Schnürch, A. (2001). "Thiolated polymers -- thiomers: development and in vitro evaluation of chitosan-thioglycolic acid conjugates." Biomaterials **22**(17): 2345-2352.

Katas, H. and Alpar, H. O. (2006). "Development and characterisation of chitosan nanoparticles for siRNA delivery." Journal of Controlled Release **115**(2): 216-225.

Kennerdell, J. R. and Carthew, R. W. (1998). "Use of dsRNA-mediated genetic interference to demonstrate that frizzled and frizzled 2 Act in the wingless pathway." Cell **95**(7): 1017-1026.

Kim, S. H. et al. (2006). "PEG conjugated VEGF siRNA for anti-angiogenic gene therapy." Journal of Controlled Release **116**(2): 123-129.

Kinne, R. W. et al. (2000). "Macrophages in rheumatoid arthritis." Arthritis Research **2**(3): 189 - 202.

Klein, T. (2008). AF4 membrane properties. Personal communication Schultes, S. Munich.

Kohn, D. B. et al. (2003). "Occurrence of leukaemia following gene therapy of X-linked SCID." Nature Reviews Cancer **3**(7): 477-488.

Kommareddy, S. and Amiji, M. (2007). "Biodistribution and pharmacokinetic analysis of long-circulating thiolated gelatin nanoparticles following systemic administration in breast cancer-bearing mice." Journal of Pharmaceutical Sciences **96**(2): 397-407.

Kommareddy, S. and Amiji, M. (2007). "Poly(ethylene glycol) modified thiolated gelatin nanoparticles for glutathione-responsive intracellular DNA delivery." Nanomedicine: the official journal of the American Academy of Nanomedicine **3**(1): 32-42.

Kosmala, J. D. et al. (2000). "Preparation of interpenetrating networks of gelatin and dextran as degradable biomaterials." Biomaterials **21**: 2019-2023.

Krasnici, S. et al. (2003). "Effect of the surface charge of liposomes on their uptake by angiogenic tumor vessels." International Journal of Cancer **105**(4): 561-567.

Kreuter, J. (1983). "Physicochemical characterization of polyacrylic nanoparticles." International Journal of Pharmaceutics **14**: 43-58.

Kreuter, J., Ed. (1994). Nanoparticles. Colloidal drug delivery systems. New York, Marcel Dekker.

Kuhn, S. H. et al. (1983). "Interaction of liposomes with human leukocytes in whole blood." Biochimica et Biophysica Acta (BBA) - Molecular Cell Research **762**(1): 119-127.

Kumar, P. et al. (2007). "Transvascular delivery of small interfering RNA to the central nervous system." Nature **448**(7149): 39-43.

Langer, K. et al. (2003). "Optimization of the preparation process for human serum albumin (HSA) nanoparticles." International Journal of Pharmaceutics **257**: 169-180.

Langer, R. (1990). "New methods of drug delivery." Science **249**(4976): 1527-1533.

Lappalainen, K. et al. (1997). "Intracellular distribution of oligonucleotides delivered by cationic liposomes: ight and electron microscopic study." Journal of Histochemistry and Cytochemistry **45**(2): 265-274.

Lechardeur, D. and Lukacs, G. L. (2002). "Intracellular barriers to non-viral gene transfer." Current Gene Therapy **2**: 183-194.

Lee, N. S. et al. (2002). "Expression of small interfering RNAs targeted against HIV-1 rev transcripts in human cells." Nature Biotech **20**(5): 500-505.

Leeson, L. J. (1995). "In vitro / in vivo correlations." Drug Information Journal **29**: 903-915.

Lehr, H. A. et al. (1993). "Dorsal skinfold chamber technique for intravital microscopy in nude mice." American Journal of Pathology **143**(4): 1055-1062.

Lewis, D. L. and Wolff, J. A. (2007). "Systemic siRNA delivery via hydrodynamic intravascular injection." Advanced Drug Delivery Reviews **59**(2-3): 115-123.

Li, J. K. et al. (1998). "Gelatin nanoencapsulation of protein/peptide drugs using an emulsifier-free emulsion method." Journal of Microencapsulation **15**(2): 163-172.

Li, S.-D. et al. (2008). "Efficient gene silencing in metastatic tumor by siRNA formulated in surface-modified nanoparticles." Journal of Controlled Release **126**(1): 77-84.

Li, S.-D. et al. (2008). "Efficient oncogene silencing and metastasis inhibition via systemic delivery of siRNA." Molecular Therapy **16**(5): 942-946.

Li, S. et al. (1999). "Dynamic changes in the characteristics of cationic lipidic vectors after exposure to mouse serum: implications for intravenous lipofection." Gene Therapy **6**(4): 585-594.

Li, W. and Szoka, F. (2007). "Lipid-based nanoparticles for nucleic acid delivery." Pharmaceutical Research **24**(3): 438-449.

Lin, W. et al. (1999). "Preparation and in vitro characterization of HSA-mPEG nanoparticles." International Journal of Pharmaceutics **189**(2): 161-170.

Löffler, G. et al., Eds. (2007). Biochemie und Pathobiochemie. Heidelberg, Springer Medizin Verlag.

Loretz, B. and Bernkop-Schnuerch, A. (2007). "In vitro cytotoxicity testing of non-thiolated and thiolated chitosan nanoparticles for oral gene delivery." Nanotoxicology **1**(2): 139 - 148.

Loretz, B. et al. (2007). "Role of sulfhydryl groups in transfection? a case study with chitosan-NAC nanoparticles." Bioconjugate Chemistry **18**: 1028-1035.

Lutsiak, M. E. C. et al. (2002). "Analysis of polyD,L-lactic-co-glycolic acid nanosphere uptake by human dendritic cells and macrophages in vitro." Pharmaceutical Research **19**: 1480-1487.

Mao, H.-Q. et al. (2001). "Chitosan-DNA nanoparticles as gene carriers: synthesis, characterization and transfection efficiency." Journal of Controlled Release **70**(3): 399-421.

Marty, J. J. et al. (1978). "Nanoparticles - a new colloidal drug delivery system." Pharmaceutica Acta Helvetiae **53**: 17–23.

Matsumoto, G. et al. (2006). "Cationized gelatin delivery of a plasmid DNA expressing small interference RNA for VEGF inhibits murine squamous cell carcinoma." Cancer Science **97**(4): 313-321.

Mayer, A. et al. (2008). "Hemocompatibility of various nanoparticles in human blood." Toxicology Letters **180**(Supplement 1): S223-S224.

McCutchan, J. H. and PAgano, J. S. (1968). "Enhancement of the infectivity of Simian virus 40 deoxyribonucleic acid with diethylaminoethyl-dextran." Journal of the National Cancer Institute **41**: 351-357.

McLean, J. W. et al. (1997). "Organ-specific endothelial cell uptake of cationic liposome-DNA complexes in mice." American Journal of Physiology - Heart and Circulatory Physiology **273**(1): H387-404.

McManus, M. T. and Sharp, P. A. (2002). "Gene silencing in mammals by small interfering RNAs." Nature Reviews Genetics **3**(10): 737-747.

McNamara, J. O. et al. (2006). "Cell type-specific delivery of siRNAs with aptamer-siRNA chimeras." Nature Biotech **24**(8): 1005-1015.

Medarova, Z. et al. (2007). "In vivo imaging of siRNA delivery and silencing in tumors." Nature Medicine **13**(3): 372-377.

Mello, C. C. and Conte, D. (2004). "Revealing the world of RNA interference." <u>Nature</u> **431**(7006): 338-342.

Meyer, K. et al. (1997). Manipulating the intracellular trafficking of nucleic acids. <u>Gene therapy for diseases of the lung</u>. Brigham, K. L. New York Marcel Dekker Inc**:** 135-180.

Meyer, M. et al. (2008). "Breathing life into polycations: functionalization with pH-responsive endosomolytic peptides and polyethylene glycol enables siRNA delivery." <u>Journal of the American Chemical Society</u> **130**(11): 3272-3273.

Moghimi, S. M. et al. (2001). "Long-circulating and target-specific nanoparticles: theory to practice." <u>Pharmacological Reviews</u> **53**(2): 283-318.

Monahan, P. E. et al. (2002). "Safety of adeno-associated virus gene therapy vectors: a current evaluation." <u>Expert Opinion on Drug Safety</u> **1**(1): 79-91.

Morris, K. V. and Rossi, J. J. (2006). "Lentivirus-mediated RNA interference therapy for human immunodeficiency virus type 1 infection." <u>Human Gene Therapy</u> **17**(5): 479-486.

Mueller, B. G. et al. (1996). "Albumin nanospheres as carriers for passive drug targeting: an optimized manufacturing technique." <u>Pharmaceutical Research</u> **13**: 32-37.

Mumper, R. J. et al. (1998). "Polymeric chitosan based vesicles for drug delivery." <u>Proceedings of the International Symposium on Controlled Release Bioactive Materials</u> **22**.

Murata, N. et al. (2008). "Anti-tumor effects of anti-VEGF siRNA encapsulated with PLGA microspheres in mice." <u>Journal of Controlled Release</u> **126**(3): 246-254.

Nahrendorf, M. et al. (2008). "Nanoparticle PET-CT imaging of macrophages in inflammatory atherosclerosis." <u>Circulation</u> **117**(3): 379-387.

Neumann, T. et al. (2003). "Tissue engineering of perfused microvessels." <u>Microvascular Research</u> **66**: 59-67.

Nguyen, J. et al. (2008). "Fast degrading polyesters as siRNA nano-carriers for pulmonary gene therapy." <u>Journal of Controlled Release</u> **132**(3): 243-251.

Novina, C. D. and Sharp, P. A. (2004). "The RNAi revolution." <u>Nature</u> **430**(6996): 161-164.

Nussbaum, C. (2008). Funktion von Thrombozyten bei antivaskulärer Tumortherapie durch Paclitaxel enkapsuliert in kationische Liposomen. <u>Department of Medicine</u>. Munich, LMU. **Doctor of Medicine:** 106.

Nykänen, A. et al. (2001). "ATP requirements and small interfering RNA structure in the RNA interference pathway." <u>Cell</u> **107**(3): 309-321.

Ohki, E. C. et al. (2001). "Improving the transfection efficiency of post-mitotic neurons." <u>Journal of Neuroscience Methods</u> **112**: 95-99.

Ohura, N. et al. (2003). "Global analysis of shear stress-responsive genes in vascular endothelial cells." <u>Journal of Atherosclerosis and Thrombosis</u> **10**(5): 304-313.

Ohya, Y. et al. (1994). "Release behavior of 5-fluorouracil from chitosan-gel nanospheres immobilizing 5-fluorouracil coated with polysaccharides and their cell specific cytotoxicity." <u>Journal of Macromolecular Science, Part A: Pure and Applied Chemistry</u> **31**(5): 629 - 642.

Owens, D. and Peppas, N. (2006). "Opsonization, biodistribution, and pharmacokinetics of polymeric nanoparticles." <u>International Journal of Pharmaceutics</u> **307**(1): 93-102.

Paciotti, G. F. et al. (2004). "Colloidal gold: a novel nanoparticle vector for tumor directed drug delivery." <u>Drug Delivery</u> **11**: 169-183.

Paddison, P. J. et al. (2002). "Stable suppression of gene expression by RNAi in mammalian cells." <u>Proceedings of the National Academy of Sciences of the United States of America</u> **99**(3): 1443-1448.

Park, K. (2007). "Nanotechnology: What it can do for drug delivery." Journal of Controlled Release **120**(1-2): 1-3.

Paroo, Z. and Corey, D. R. (2004). "Challenges for RNAi in vivo." Trends in Biotechnology **22**(8): 390-394.

Passirani, C. et al. (1998). "Long-circulating nanoparticles bearing heparin or dextran covalently bound to poly(methyl methacrylate)." Pharmaceutical Research **15**(7): 1046-1050.

Paul, C. P. et al. (2002). "Effective expression of small interfering RNA in human cells." Nature Biotech **20**(5): 505-508.

Perkel, J. M. (2007). "Life science technologies: therapeutic RNAi: delivering the future?" Retrieved 17.07.2009, 2009, from http://www.sciencemag.org/products/lst_20071102.dtl.

Pillé, J. Y. et al. (2006). "Intravenous delivery of anti-RhoA small interfering RNA loaded in nanoparticles of chitosan in mice: safety and efficacy in xenografted aggressive breast cancer." Human Gene Therapy **17**(10): 1019-1026.

Pirollo, K. F. et al. (2007). "Materializing the potential of small interfering RNA via a tumor-targeting nanodelivery system." Cancer Research **67**(7): 2938-2943.

Polnok, A. et al. (2004). "Influence of methylation process on the degree of quaternization of N-trimethyl chitosan chloride." European Journal of Pharmaceutics and Biopharmaceutics **57**(1): 77-83.

Porschke, D. (1991). "Nature of protamine-DNA complexes : A special type of ligand binding co-operativity." Journal of Molecular Biology **222**(2): 423-433.

Prakash, T. P. et al. (2005). "Positional effect of chemical modifications on short interference RNA activity in mammalian cells." Journal of Medicinal Chemistry **48**(13): 4247-4253.

Prior, B. M. et al. (2004). "What makes vessels grow with exercise training?" Journal of Applied Physiology **97**(3): 1119-1128.

Raedler, U. and Zantl, R. (2005). "Simulation von Blutgefäßen in Zellkultur-Biochips." Laborwelt **1**.

Raman, C. V. (1928). "A new radiation." Indian Journal of Physics **2**(1): 387-398.

Ramge, P. et al. (2000). "Polysorbate-80 coating enhances uptake of polybutylcyanoacrylate (PBCA)-nanoparticles by human and bovine primary brain capillary endothelial cells." European Journal of Neuroscience **12**(6): 1931-1940.

Rao, J. et al. (2007). "Fluorescence imaging in vivo: recent advances." Current Opinion in Biotechnology **18**(1): 17-25.

Reichel, C. A. (2008). Die Bedeutung des Adhäsionsmoleküls JAM-A sowie der Chemokinrezeptoren CCR1, -2 und -5 für die Rekrutierung von Leukozyten bei Entzündung und Ischämiereperfusion. Institut für Chirurgische Forschung. München, Ludwig-Maximilians-Universität. **Doctor of Medicine:** 147.

Remaut, K. et al. (2006). "Influence of plasmid DNA topology on the transfection properties of DOTAP/DOPE lipoplexes." Journal of Controlled Release **115**(3): 335-343.

Risau, W. (1997). "Mechanisms of angiogenesis." Nature **386**(6626): 671-674.

Roger, C. A. and Kevin, G. R. (1999). "Metabolic stability of glutaraldehyde cross-linked peptide DNA condensates." Journal of Pharmaceutical Sciences **88**(8): 739-746.

Roldo, M. et al. (2004). "Mucoadhesive thiolated chitosans as platforms for oral controlled drug delivery: synthesis and in vitro evaluation." European Journal of Pharmaceutics and Biopharmaceutics **57**(1): 115-121.

Rolland, A. (1989). "Blood clearance and organ distribution of intravenously administered polymethacrylic nanoparticles in mice." Journal of Pharmaceutical Sciences **78**(6): 481-484.

Rollins, S. A. et al. (1996). "Retroviral vector producer cell killing in human serum is mediated by natural antibody and complement: strategies for evading the humoral immune response." Human Gene Therapy **7**(5): 619-626.

Rothmeier, A. S. et al. (2009). "Investigation of the marine compound spongistatin 1 links the inhibition of PKC{alpha} translocation to nonmitotic effects of tubulin antagonism in angiogenesis." FASEB Journal **23**(4): 1127-1137.

Rubanyi, G. M., Ed. (2000). Angiogenesis in health and disease. New York - Basel, M. Dekker, Inc.

Ruiz, F. E. et al. (2001). "A clinical inflammatory syndrome attributable to aerosolized lipid DNA administration in cystic fibrosis." Human Gene Therapy **12**(7): 751-761.

Rumbaut, R. E. et al. (2006). "Endotoxin enhances microvascular thrombosis in mouse cremaster venules via a TLR4-dependent, neutrophil-independent mechanism." American Journal of Physiology - Heart and Circulatory Physiology **290**(4): H1671-1679.

Sandison, J. C. (1928). "The transparent chamber of the rabbit's ear giving a complete description of improved techniques of construction and introduction and general account of growth and behavior of living cells and tissues as seen with the microscope." American Journal of Anatomy **41**: 447-472.

Schenborn, E. T. and Goiffon, V. (2000). DEAE-dextran transfection of mammalian cultured cells. Transcription Factor Protocols**:** 147-153.

Scheule, R. K. (2000). "The role of CpG motifs in immunostimulation and gene therapy." Advanced Drug Delivery Reviews **44**: 119-134.

Schmitt-Sody, M. et al. (2003). "Quantitative assessment of angiogenesis in murine antigen-induced arthritis by intravital fluorescence microscopy." Journal of Vascular Research **40**(5): 460-466.

Schwick, H. G. and Heide, K. (1969). "Immunochemistry and immunology of collagen and gelatin." Bibl Haematologica **33**: 111-125.

Seglen, P. O. (1983). "Inhibitors of lysosomal function." Methods in Enzymology **96**: 737-764.

Shen, C. et al. (2003). "Gene silencing by adenovirus-delivered siRNA." FEBS Letters **539**: 111-114.

Shi, Y. (2003). "Mammalian RNAi for the masses." Trends in Genetics **19**: 9-12.

Shutava, T. G. et al. (2009). "Layer-by-layer-coated gelatin nanoparticles as a vehicle for delivery of natural polyphenols." ACS Nano.

Shyh-Dar, L. I. and Leaf, H. (2006). "Surface-modified LPD nanoparticles for tumor targeting." Annals of the New York Academy of Sciences **1082**(Oligonucleotide Therapeutics: First Annual Meeting of the Oligonucleotide Therapeutics Society): 1-8.

Simoes, S. et al. (1999). "Cationic liposomes as gene transfer vectors: Barriers to successful application in gene therapy." Current Opinion in Structural Biology **1**: 147-157.

Simon, J. et al. (2001). "Systemic macrophage activation in locally-induced experimental arthritis." Journal of Autoimmunity **17**(2): 127-136.

Skobe, M. et al. (1997). "Halting angiogenesis suppresses carcinoma cell invasion." Nature Medicine **3**(11): 1222-1227.

Sommerfeld, P. et al. (2000). "Long-term stability of PBCA nanoparticle suspensions." Journal of Microencapsulation **17**(1): 69-79.

Song, E. et al. (2005). "Antibody mediated in vivo delivery of small interfering RNAs via cell-surface receptors." Nature Biotech **23**(6): 709-717.

Soutschek, J. et al. (2004). "Therapeutic silencing of an endogenous gene by systemic administration of modified siRNAs." Nature **432**(7014): 173-178.

Spagnou, S. et al. (2004). "Lipidic carriers of siRNA: differences in the formulation, cellular uptake, and delivery with plasmid DNA " <u>Biochemistry</u> **43**(42): 13348-13356.

Stein, C. A. (1995). "Does antisense exist?" <u>Nature Medicine</u> **1**(11): 1119-1121.

Steinbauer, M. et al. (2000). "Characterization and prevention of phototoxic effects in intravital fluorescence microscopy in the hamster dorsal skinfold model." <u>Langenbeck's Archives of Surgery</u> **385**(4): 290-298.

Sugimoto, T. et al. (2003). "Synthesis of uniform anatase TiO2 nanoparticles by gel-sol method: 3. Formation process and size control." <u>Journal of Colloid and Interface Science</u> **259**(1): 43-52.

Takeuchi, K.-i. et al. (1996). "Effect of zeta potential of cationic liposomes containing cationic cholesterol derivatives on gene transfection." <u>FEBS Letters</u> **397**(2-3): 207-209.

Thepen, T. et al. (1994). "The role of alveolar macrophages in regulation of lung inflammation." <u>Annals of the New York Academy of Sciences</u> **725**(Cells and Cytokines in Lung Inflammation): 200-206.

Thorlacius, H. et al. (1997). "Cytokine-induced leukocyte rolling in mouse cremaster muscle arterioles in P-selectin dependent." <u>American Journal of Physiology - Heart and Circulatory Physiology</u> **272**(4): H1725-1729.

Tinkov, S. et al. (2009). "Microbubbles as ultrasound triggered drug carriers." <u>Journal of Pharmaceutical Sciences</u> **98**(6): 1935-1961.

Tomlinson, E. and Burger, J. J. (1987). "Monolithic albumin particles as drug carriers. In: L. Illum, J.G. McVie and E. Tomlinson (eds.), Wright, Bristol." <u>Polymers in Controlled Drug Delivery</u>: 25–48.

Truong-Le, V. L. et al. (1999). "Gene transfer by DNA-gelatin nanosphere." <u>Archives of Biochemistry and Biophysics</u> **361**(1).

Turner, J. L. et al. (2005). "Synthesis of gadolinium-labeled shell-crosslinked nanoparticles for magnetic resonance imaging applications." Advanced Functional Materials **15**(8): 1248-1254.

Ueda, A. et al. (2004). "Effect of shear stress on microvessel network formation of endothelial cells with in vitro three-dimensional model." American Journal of Physiology - Heart and Circulatory Physiology **287**(3): H994-1002.

Uyttendaele, H. et al. (1996). "Notch4/int-3, a mammary proto-oncogene, is an endothelial cell-specific mammalian Notch gene." Development **122**(7): 2251-2259.

Vaheri, A. and Pagano, J. S. (1965). "Infectious poliovirus RNA: a sensitive method of assay." Virology **27**(3): 434-436.

Vallhov, H. et al. (2006). "The importance of an endotoxin-free environment during the production of nanoparticles used in medical applications." Nano Letters **6**(8): 1682-1686.

van der Lubben, I. M. et al. (2001). "Chitosan microparticles for oral vaccination:: preparation, characterization and preliminary in vivo uptake studies in murine Peyer's patches." Biomaterials **22**(7): 687-694.

Verma, A. K. et al. (2005). "Release Kinetics from Bio-Polymeric Nanoparticles Encapsulating Protein Synthesis Inhibitor- Cycloheximide, for Possible Therapeutic Applications." Current Pharmaceutical Biotechnology **6**: 121-130.

Vink, H. and Duling, B. R. (1996). "Identification of distinct luminal domains for macromolecules, erythrocytes, and leukocytes within mammalian capillaries." Circulation Research **79**(3): 581-589.

Wan, W. K. et al. (2007). "Use of degradable and nondegradable nanomaterials for controlled release." Nanomedicine **2**: 483-509.

Wartlick, H. et al. (2004). "Tumour cell delivery of antisense oligonucleotides by human serum albumin nanoparticles." Journal of Controlled Release **96**(3): 483-495.

200

Weber, C. et al. (2000). "Desolvation process and surface characteristics of HSA-nanoparticles." International Journal of Pharmaceutics **196**(2): 197-200.

Wiethoff, C. and Middaugh, R. (2003). "Barriers to nonviral gene delivery." Journal of Pharmaceutical Sciences **92**(2): 203-217.

Wikipedia. (2009, 07.07.2009). "Angiogenesis." from http://en.wikipedia.org/w/index.php?title=Angiogenesis&oldid=300885718

Winter, R. and Noll, F., Eds. (1998). Methoden der Biophysikalischen Chemie. Stuttgart, B. G. Teubner.

Wisner, R. et al. (1996). "Characterization of normal and cancerous lymph nodes on indirect computed tomography lymphographic studies after interstitial injection of iodinated nanoparticles." Academic Radiology **3**: 257–260.

Wissmann, C. and Detmar, M. (2006). "Pathways targeting tumor lymphangiogenesis." Clinical Cancer Research **12**(23): 6865-6868.

Wolfrum, C. et al. (2007). "Mechanisms and optimization of in vivo delivery of lipophilic siRNAs." Nature Biotech **25**(10): 1149-1157.

Wyatt, P. J. (1993). "Light scattering and the absolute characterization of macromolecules." Analytica Chimica Acta **272**: 1-40.

Yeh, T. K. et al. (2005). "Formulating paclitaxel in nanoparticles alters its disposition." Pharmaceutical Research **22**(6): 867-874.

Yew, N. S. et al. (1999). "Contribution of plasmid DNA to inflammation in the lung after administration of cationic lipid:pDNA complexes." Human Gene Therapy **10**(2): 223-234.

Yongsheng, Y. et al. (2001). "Cross-linked low molecular weight glycopeptide-mediated gene delivery: Relationship between DNA metabolic stability and the level of transient gene expression in vivo." Journal of Pharmaceutical Sciences **90**(12): 2010-2022.

Zhang, X. et al. (2004). "Small interfering RNA targeting heme oxygenase-1 enhances ischemia-reperfusion-induced lung apoptosis." Journal of Biological Chemistry **279**(11): 10677-10684.

Zillies, J. and Coester, C. (2004). "Evaluating gelatin based nanoparticles as a carrier system for double stranded oligonucleotides." Journal of Pharmacy & Pharmaceutical Sciences **7**(4): 17-21.

Zillies, J. C. (2008). "Dissertation."

Zillies, J. C. et al. (2007). "Method for quantifying the PEGylation of gelatin nanoparticle drug carrier systems using asymmetrical flow field-flow fractionation and refractive index detection." Analytical Chemistry **79**(12): 4574-4580.

Zimmermann, T. S. et al. (2006). "RNAi-mediated gene silencing in non-human primates." Nature **441**(7089): 111-114.

zur Hausen, H. (1967). "Induction of specific chromosomal aberrations by adenovirus type 12 in human embryonic kidney cells." Journal of Virology **1**(6): 1174-1185.

Zwiorek, K. (2006). "Dissertation."

Zwiorek, K. et al. (2008). "Delivery by cationic gelatin nanoparticles strongly increases the immunostimulatory effects of CpG oligonucleotides." Pharmaceutical Research **25**(3): 551-562.

Zwiorek, K. et al. (2004). "Gelatin nanoparticles as a new and simple gene delivery system." Journal of Pharmacy & Pharmaceutical Sciences **7**(4): 22-28.

Publications

Original Papers

S. Schultes, A. Philipp, M. Ogris, G. Winter, E. Wagner, C. Coester
From endosomal escape with sandwich nanoparticles to RNA interference, Pharmaceutical Research, *to be submitted*

S. Schultes, K. Mathis, J. Zillies, K. Zwiorek, C. Coester, G. Winter
Analysis of prototype polymers and protein nanoparticles with asymmetrical flow field-flow fractionation, LCGC Europe 2009, **9**

Bihari P[1], Vippola M[2], **Schultes S**[3], Coester C[3], Tuomi T[4], Rehberg M[1], Krombach F[1]
Optimized dispersion of nanoparticles for biological in vitro and in vivo studies, Particle and Fibre Toxicology 2008, **5**:14; Impact Factor 5.11

Broermann P, **Schultes S**, Coester C
Bachelor Thesis, Modification, In Vitro and In Vivo Tests of Gelatin Nanoparticles as Drug Delivery Systems, Munich, November 2008

S. Schultes, K. Mathis, G. Winter, C. Coester
Novel hydrophobic prototype gelatins for nanoparticle preparation analyzed by AF4 and MALS; Proceedings to the 6th World Meeting on Pharmaceutics, Biopharmaceutics and Pharmaceutical Technology, Barcelona, Spain, April, 6th-10th 2008

S. Schultes, G. Winter, C. Coester
Simulated *in-vivo* endothelial cell adhesion of cationic polysaccharide-gelatin nanoparticles; Proceedings to the 6th World Meeting on Pharmaceutics, Biopharmaceutics and Pharmaceutical Technology, Barcelona, Spain, April, 6th-10th 2008

Application Notes

S. Schultes, K. Mathis, C. Coester, G. Winter
Automatic Microviscometry as a Tool for Fast Biopolymer Analysis Compared to AF4, www.anton-paar.com, 2008

Oral Presentations

Stephan Schultes, Alexander Philipp, Manfred Ogris, Gerhard Winter, Ernst Wagner, Conrad Coester; From Endosomal Escape with Sandwich Nanoparticles to RNA Interference, NanoBio: 3rd International Congress of Nanobiotechnology and Nanomedicine, San Francisco, USA, June 22nd – 24th 2009

S. Schultes
Feld-Fluss-Fraktionierung: Analytik in der Nanotechnologie, Seminar im Rahmen des Fortbildungsprogramms 2009 am Bayerischen Landesamt für Gesundheit und Lebensmittelsicherheit, Für GMP-/GCP-Inspektoren, Regierungsapotheker, Pharmazeuten, Naturwissenschaftler und Lebensmittelchemiker, Munich, April 20th 2009

S. Schultes

Feld-Fluss-Fraktionierung: ein neues Analyseverfahren zur Stabilitätsbeurteilung, Seminar im Rahmen der Weiterbildung der Bayerischen Landesapothekerkammer für die Gebiete Pharmazeutische Technologie und Pharmazeutische Analytik, Munich, March 24th 2009

Gerhard Winter with Conrad Coester, WF, SG, RL, KM, **Stephan Schultes**, JZ, KZ

The use of asymmetrical flow field flow fractionation (AF4) for the analysis of pharmaceutically relevant macromolecular systems. SCM-4 Fourth International Symposium on the Separation and Characterization of Natural and Synthetic Macromolecules, Rhône Congress Center, Amsterdam, January 28th - 30th 2009

S. Schultes, C. Coester

Simulated *in-vivo* Endothelial Cell Adhesion of Cationic Polysaccharide Gelatin Nanoparticles, DPHG Jahrestagung, Bonn, October 9th 2008

S. Schultes

Concept Presentation, 1st Progress Report, 2nd Progress Report

Department of Pharmacy, Pharmaceutical Technology and Biopharmacy, University of Munich, 2006, 2007, 2008

Poster Presentations

Stephan Schultes, Martin Eichhorn, Gerhard Winter, Conrad Coester

Simulated *in-vivo* Endothelial Cell Adhesion of Cationic Polysaccharide-Gelatin Nanoparticles, NanoBio: 3rd International Congress of Nanobiotechnology and Nanomedicine, San Francisco, USA, June 22nd – 24th 2009

Broermann P, **Schultes S**, Coester C

Bringing Light Into the Dark: Influence of Fluorescence Labeling on Protein Nanoparticles for *in-vivo* Use, EHRLICH II – 2nd World Conference on Magic Bullets, Nürnberg, Germany, October 3rd – 5th 2008

S. Schultes, K. Mathis, C. Coester

Hydrophobic prototype gelatins for Nanoparticle Preparation analysed by AF 4, DPHG Jahrestagung, Bonn, October 9th 2008

Bihari P[1], Vippola M[2], **Schultes S**[3], Coester C[3], Tuomi T[4], Rehberg M[1], Krombach F[1]

Optimized dispersion of nanoparticles for biological in vitro and in vivo studies, NANOTox 2nd International Conference, Zurich, Schweiz, September 7th – 10th 2008

S. Schultes, K. Mathis, G. Winter, C. Coester

Automatic microviscosimetry as a tool for fast biopolymer analysis compared to AF4, Interact Max Plank Society PhD Symposium, Munich, December 7th 2007

Curriculum Vitae

Stephan Johannes Baptist Schultes

Personal data:

Date of birth	November 14th, 1979
Place of birth	Dachau
Nationality	German

Professional experience:

Licensed pharmacist, Rosen Apotheke, Munich
Licensed pharmacist, St. Alto-Birgitten Apotheke, Altomünster

University education:

PhD thesis at the Department of Pharmaceutical Technology and Biopharmacy at the University of Munich

State Examination Pharmacy, LMU University of Munich 06/2006

Food Chemistry, Technical University of Munich

Internships:

Dronania Pharma GmbH, Bad Wörishofen
Delta-Apotheke, Dortmund
Hermes Pharma GmbH, Wolfratshausen
Pfizer Pharma AG, Karlsruhe and Freiburg
Rathaus-Apotheke, Schrobenhausen
Novartis Pharma AG, Munich
Phytovisions GmbH, Munich
Regulatory Affairs Institute LAT GmbH, Munich

High schools:

Deutschherren-Highschool, Aichach, Germany
Thomas B. Peddie School, Princeton, New Jersey, USA

Extracurricular activities:

       Lecturer for the Bavarian Pharmacists Chapter

       McKinsey Course „Case Studies in Strategic Management"

       Roland Berger Strategy Consultants – Workshop

       Science4Life Business Plan Workshop

       Qualification as Specialist in Pharmaceutical Technology

       Student at the University of Munich Entrepreneurship Center

       Associate Member of the European Qualified Person Association

       Member of the „Arbeitsgemeinschaft Pharmazeutische Technologie"

Scholarships and awards:

       Bavarian Research Foundation - Grant

       Medigene AG – Financial Support Grant

       Merit of Honor of the International Association of Nanotechnology

       Robert Hooke Award of the International Association of Nanotechnology